*SAND2019-9768 R*
*Unlimited Release*

**FEDERAL RADIOLOGICAL**
**MONITORING AND ASSESSMENT CENTER**

# FRMAC Gamma Spectroscopist Knowledge Guide

**August 2019**

Prepared by
Sandia National Laboratories
Albuquerque, New Mexico 87185 and Livermore, California 94550

Sandia National Laboratories is a multimission laboratory managed and operated by National Technology & Engineering Solutions of Sandia, LLC, a wholly owned subsidiary of Honeywell International Inc., for the U.S. Department of Energy's National Nuclear Security Administration under contract DE-NA0003525.

# FRMAC Gamma Spectroscopist Knowledge Guide

Author

Michael W. Enghauser, Skill Set Lead
FRMAC Gamma Spectroscopist
Sandia National Laboratories
Albuquerque, NM

Approved By

Arthur Shanks Jr., Technical Chairman
FRMAC Laboratory Analysis Working Group
Sandia National Laboratories
Albuquerque, NM

This work was supported by the U.S. Department of Energy, National Nuclear Security Administration Nevada Operations Office, under Contract No. DE-AC08-96NV11718.

FRMAC is an acronym for Federal Radiological Monitoring and Assessment Center.

## DISCLAIMER



## AVAILABILITY

Available for sale to the public, in paper, from:

U.S. Department of Commerce
National Technical Information Service
5285 Port Royal Road
Springfield, VA 22161
phone: 800.553.6847
fax: 703.605.6900
email: orders@ntis.gov
online ordering: http://www.ntis.gov/ordering.htm

Available electronically at http://www.osti.gov/bridge

Available for a processing fee to U.S. Department of Energy and its contractors, in paper, from:

U.S. Department of Energy
Office of Scientific and Technical Information
P.O. Box 62
Oak Ridge, TN 37831-0062
phone: 865.576.8401
fax: 865.576.5728
email: reports@adonis.osti.gov

Also available at the FRMAC website,
**http://www.nv.doe.gov/nationalsecurity/homelandsecurity/frmac/manuals.aspx**

## Acronyms and Abbreviations

| | |
|---|---|
| Ω | Solid angle |
| Ag | Chemical symbol for silver |
| Al | Chemical symbol for aluminum |
| ASPECT | Airborne Spectral Photometric Environmental Collection Technology |
| Au | Chemical symbol for gold |
| C | Chemical symbol for carbon |
| CFs | Correction Factors |
| $CH_2$ | Molecular formula for polyethylene (the most common type of plastic) |
| $C_6H_{10}O_5$ | Molecular formula for cellulose |
| CI | Confidence Interval |
| Cu | Chemical symbol for copper |
| DE | Double Escape |
| DOE | U.S. Department of Energy |
| EML | Environmental Measurements Laboratory |
| EPA | Environmental Protection Agency |
| ETNA | Efficiency Transfer for Radionuclide Activity |
| Fe | Chemical symbol for iron |
| FEP | Full-Energy Peak |
| FIDLER | Field Instrument for the Detection of Low-Energy Radiation |
| FOV | Field of View |
| FP | Fission Product |
| FRMAC | Federal Radiological Monitoring and Assessment Center |
| FWHM | Full Width at Half Maximum |
| GADRAS | Gamma Detector Response and Analysis Software |
| Ge | Chemical symbol for germanium |
| HASL | Health and Safety Laboratory |
| HEU | Highly Enriched Uranium |
| HPGe | High Purity Germanium |
| ID | Identification |
| ISOCS | In-Situ Object Calibration Software |
| keV | Kilo-electron Volt |
| $LaBr_3$ | Lanthanum bromide |
| LabSOCS | Laboratory Source-less Calibration Software |
| LANL | Los Alamos National Laboratory |
| Lc | Critical level |
| L/D | Length/Diameter |
| Ld | Detection limit |
| LLNL | Lawrence Livermore National Laboratories |
| MeV | Mega-electron Volt |
| MGA | Multi-Group Analysis |
| NaI | Sodium iodide |

| | |
|---|---|
| Ni | Chemical symbol for nickel |
| NIST | National Institute of Standards and Technology |
| NNSA/NSO | National Nuclear Security Administration/Nevada Site Office |
| NRC | U. S. Nuclear Regulatory Commission |
| ORIGEN | Oak Ridge Isotope Generation and Depletion |
| ORNL | Oak Ridge National Laboratory |
| Pb | Chemical symbol for lead |
| PUR/LTC | Pileup Rejection/Live Time Correction |
| Rn-220 | Thoron |
| Rn-222 | Radon |
| RSICC | Radiation Safety Information Computational Center |
| SE | Single Escape |
| $SiO_2$ | Molecular formula for silicon dioxide (primary component of glass) |
| SNL | Sandia National Laboratories |
| TCS | True/cascade Coincidence Summing |
| TIG | Tungsten Inert Gas |
| $UO_2$ | Molecular formula for uranium dioxide |

## Table of Contents

## Table of Appendices

# SECTION 1.0 INTRODUCTION

This knowledge guide was developed as a training and reference manual for Federal Radiological Monitoring and Assessment Center (FRMAC) gamma spectroscopists. The knowledge guide is geared towards applied High Purity Germanium (HPGe) gamma spectroscopy with an emphasis on examples. As such, the knowledge guide generally provides a limited but sufficient discussion of physics concepts. For more detailed information on the physics concepts discussed in this guide, please refer to the references listed.

# SECTION 2.0 INTERACTION OF GAMMA AND X-RADIATION WITH MATTER

## Table of Contents



## Figures



## Equations

## 2.1 Introduction

This entire section has been excerpted/adapted from Reference [3] with permission.

## 2.2 Photoelectric effect

Photoelectric absorption involves a photon interacting with a bound electron with all the photon's energy being absorbed in the process (Figure 2-1).

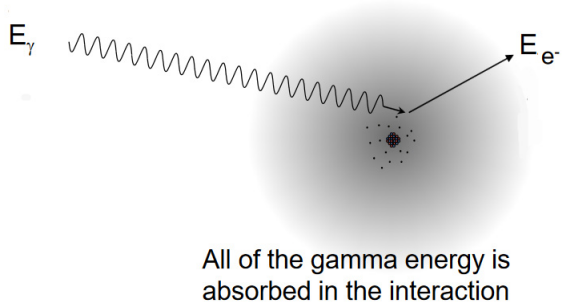


***Figure 2-1. Photoelectric effect. [1]***

The electron is ejected from the atom with an energy approximated by Equation 2-1.

**Equation 2-1. Photoelectric effect.**

$$E_e = E_\gamma - E_b$$

where $E_b$ represents the electron binding energy and $E_\gamma$ is the energy of the interacting photon, and $E_e$ is the energy of the ejected electron. The vacancy left by the ejected electron will typically result in x-ray emission but if the interaction takes place in bulk material both the electron and the x-ray will be absorbed. This results in all the photon energy being deposited near the interaction site.

## 2.3 Compton scattering

In the Compton Scattering process an incident photon scatters off an electron, normally in the outermost atomic electron shell of the absorbing material, transferring a portion of its energy and then reappears as a secondary photon with reduced energy. Figure 2-2 below describes the scattering interaction, where the electron at rest is at the vertex of the scattering interaction.

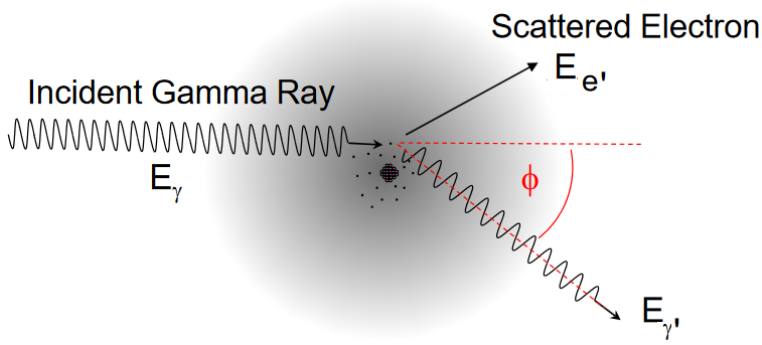


***Figure 2-2. Compton scattering. [1]***

This situation can be described, in terms of conservation of energy, using Equation 2-2.

**Equation 2-2. Compton scattering.**

$$E_\gamma + E_e = E_{\gamma'} + E_{e'}$$

where $E_\gamma$ represents the energy of the incoming gamma ray photon (hν), $E_e$ is the energy of the electron at rest ($m_0c^2$ = 0.511 MeV), $E_{\gamma'}$ ($h\nu'$) is the energy of the scattered gamma ray, $E_{e'}$ ($mc^2$) is the energy of the scattered electron and $\Phi$ is the angle of the scattered photon (0 to 180 degrees) relative to its original direction. Our analysis here ignores the small binding energy of the atomic electron involved in the scattering process. To conserve energy and momentum, the energies of the scattered photon and electron are related to the angles at which they are emitted. If we solve for the energy of the Compton-scattered gamma ray photon and the scattered electron we get the following solutions, based on this scattering geometry:

**Equation 2-3. Compton scattering: scattered gamma ray.**

$$E_{\gamma'} = \frac{E_\gamma}{1 + (E_\gamma/E_e)(1 - \cos\Phi)}$$

and

**Equation 2-4. Compton scattering: scattered electron.**

$$E_{e'} = E_\gamma \left\{ \frac{\left((E_\gamma/E_e)(1 - \cos\Phi)\right)}{\left(1 + (E_\gamma/E_e)(1 - \cos\Phi)\right)} \right\}$$

The probability of Compton scattering depends on the density of available electrons for the scattering interaction and increases linearly with the Z of the scattering medium.

## 2.4 Pair production

Pair production only becomes possible when the energy of the incident gamma radiation exceeds twice the rest mass of the electron (1.022 MeV). Even though the process is possible above this energy, this interaction does not occur to any significant extent until gamma ray energies reach several MeV. In this interaction, the incident gamma ray photon disappears within the vicinity of a nucleus and is replaced by an electron-positron pair. Any photon energy more than the 1.022 MeV required to form this pair goes into kinetic energy that is shared by the electron and positron. The positron slows down in the absorber material, annihilates with an electron, and two annihilation photons (0.511 MeV) are produced as secondary radiation products of the interaction, emitted approximately 180 degrees apart. There is no simple expression for the cross section for pair production, but it varies approximately as $Z^2$, increasing as Z increases.

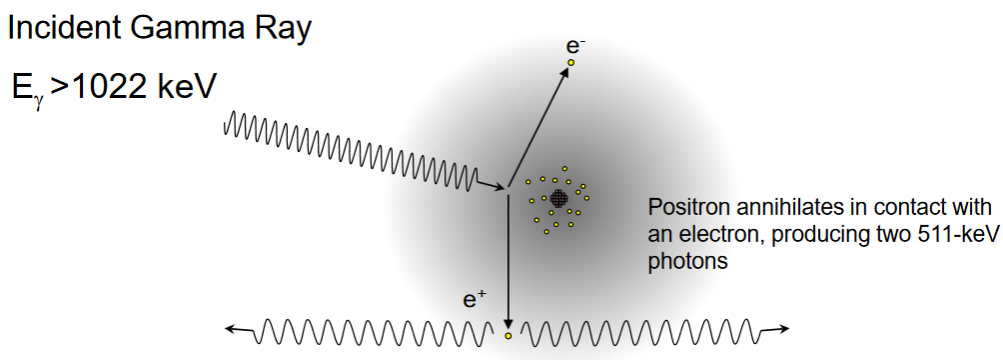


***Figure 2-3. Pair production. [1]***

## 2.5 Summary

For gamma ray detection, the three most important interaction processes are: photoelectric absorption; Compton scattering; and pair production. The relative probabilities of these processes for germanium varies as a function of gamma ray energy as illustrated in Figure 2-4. [2]

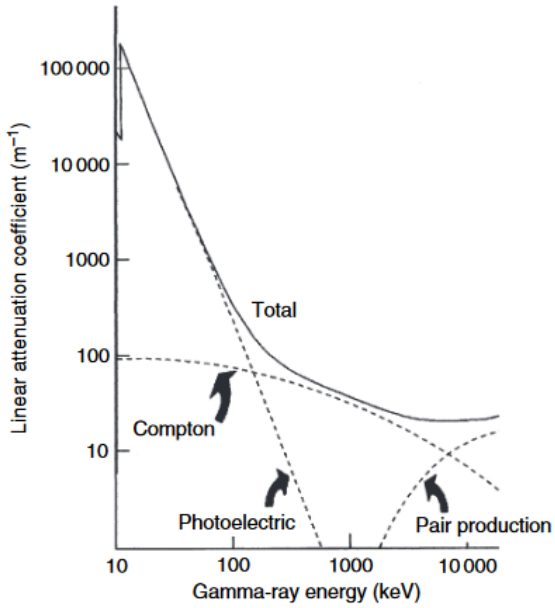


***Figure 2-4. Linear attenuation coefficient for germanium showing relative contributions from photoelectric absorption, Compton scattering, and pair production processes. [2]***

As one can see from Figure 2-4, photoelectric absorption is by far the most important contribution to the attenuation coefficient at low energies. Compton scattering is the most dominant component of the attenuation coefficient over a wide energy range, from a few hundred keV to about 5 MeV. Finally, pair production begins to contribute above 1.022 MeV but only becomes important above 3-4 MeV and dominates above energies about 6-7 MeV.

# SECTION 3.0 NATURALLY OCCURRING RADIOACTIVE RADIONUCLIDES

## Table of Contents



## Figures



## Tables

## 3.1 Introduction

The very long-lived radionuclides U-238, U-235, Th-232, and K-40 (formed during the creation of the earth) are present in soil, water, and air.

***Table 3-1. U-238, U-235, Th-232, and K-40 half-lives.***

| Nuclide | Half Life (years) |
|---|---|
| U-238 | 4.47E+09 |
| U-235 | 7.04E+08 |
| Th-232 | 1.41E+10 |
| K-40 | 1.25E+09 |

While K-40 has no radioactive decay products, U-238, U-235, and Th-232 decay sequentially to a series of radioactive decay products. Since U-238, U-235, and Th-232 are very long-lived radionuclides and the earth is roughly 4.5 billion years old, their decay products have reached secular equilibrium (discussed in SECTION 4.0) in undisturbed earth.

- Note: Geochemical processes can affect uranium and thorium ore deposits resulting in decay chain disequilibrium.

The U-238, U-235, Th-232, and K-40 decay chains and their primary gamma emissions are presented in Figures 3-1 through 3-4 and Tables 3-1 through 3-5, respectively.

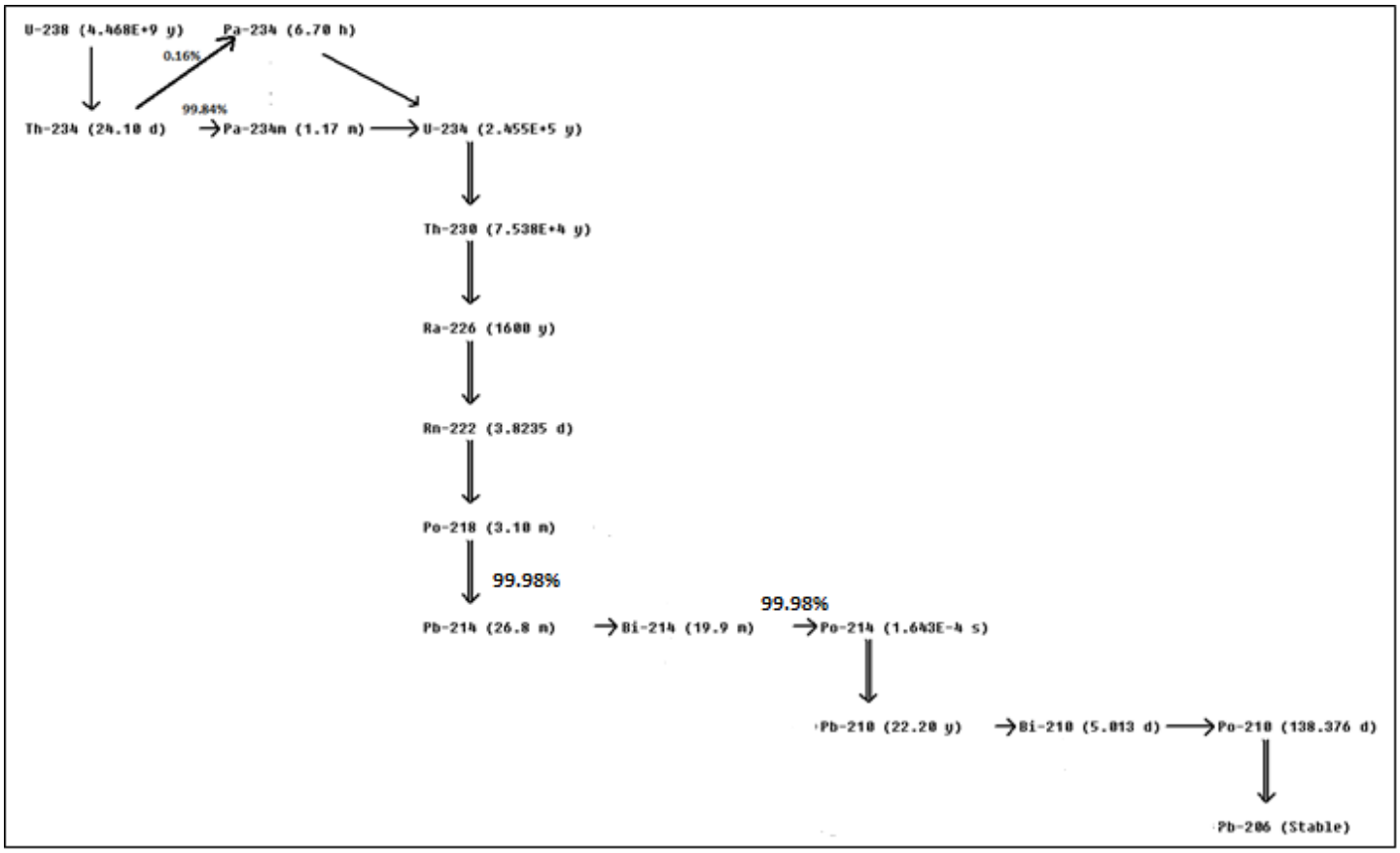


***Figure 3-1. Simplified U-238 decay chain. [4]***

***Table 3-2. Primary U-238 decay chain gamma emissions.***

| Emitter | Energy (keV) | Yield (gps/dps) |
|---|---|---|
| **Bi-214** | **609.3** | **4.61E-01** |
| **Pb-214/Bi-214** | **351.9** | **3.77E-01** |
| Pb-214 | 295.2 | 1.93E-01 |
| **Bi-214** | **1764.5** | **1.54E-01** |
| **Bi-214** | **1120.3** | **1.51E-01** |
| Pb-214 | 242.0 | 7.43E-02 |
| Bi-214 | 1238.1 | 5.79E-02 |
| **Th-234 x 2** | **92.6** | **5.58E-02** |
| Bi-214 | 2204.2 | 5.08E-02 |
| Bi-214 | 768.4 | 4.94E-02 |
| **Th-234** | **63.3** | **4.84E-02** |
| Bi-214 | 1377.7 | 4.00E-02 |
| Ra-226 | 186.2 | 3.59E-02 |
| Bi-214 | 934.1 | 3.08E-02 |
| Bi-214 | 2447.9 | 1.57E-02 |
| **Pa-234m** | **1001.0** | **8.36E-03** |
| **Pa-234m/Pa-234** | **766.4** | **2.94E-03** |

Primary gamma emissions are "**bolded**"

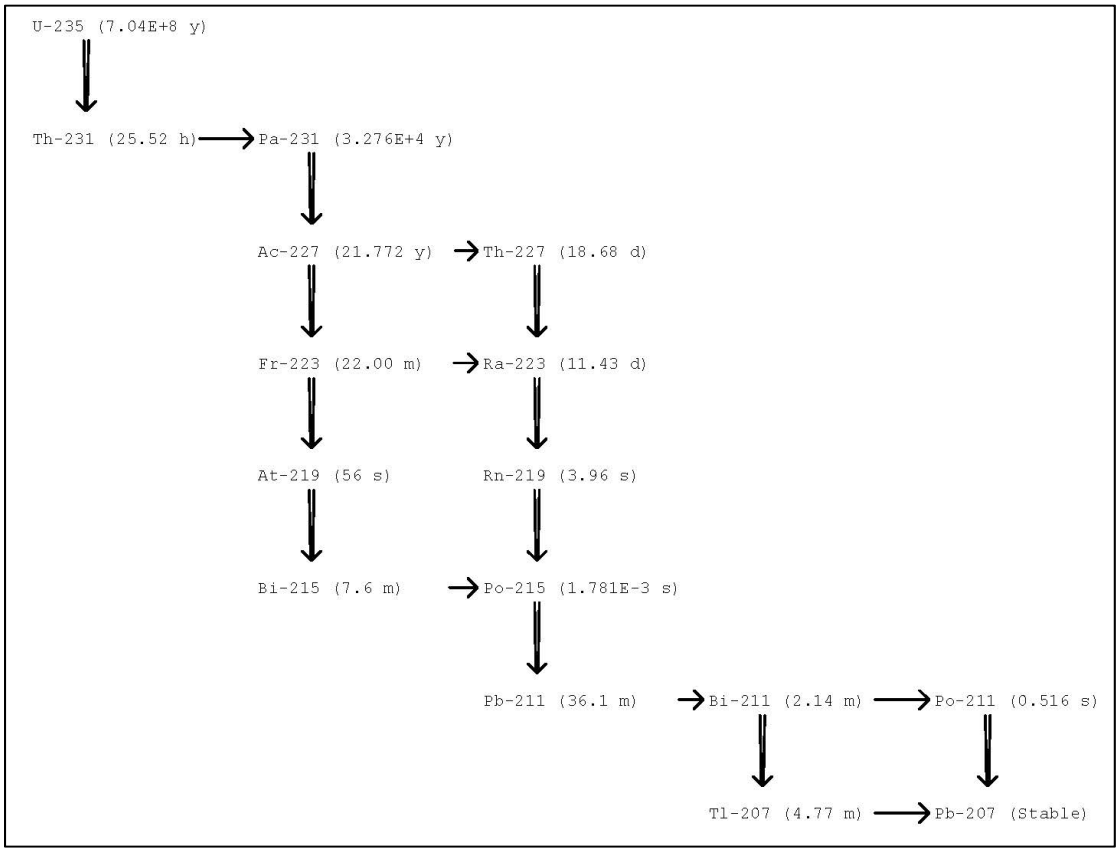


***Figure 3-2. U-235 decay chain. [4]***

***Table 3-3. Primary U-235 decay chain gamma emissions.***

| Emitter | Energy (keV) | Yield (gps/dps) |
|---|---|---|
| **U-235** | **185.7** | **5.72E-01** |
| **U-235** | **143.8** | **1.10E-01** |
| **U-235** | **163.3** | **5.08E-02** |
| **U-235** | **205.3** | **5.01E-02** |

Primary gamma emissions are "**bolded**"

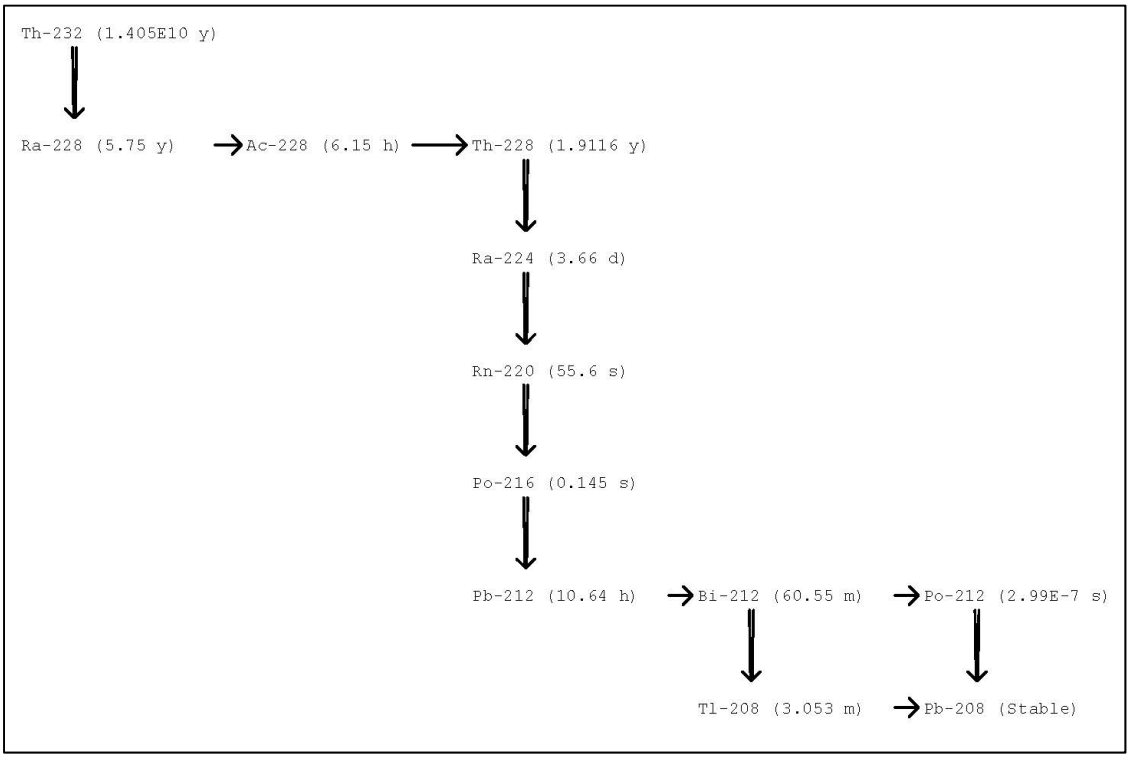


***Figure 3-3. Th-232 decay chain. [4]***

***Table 3-4. Primary Th-232 decay chain gamma emissions.***

| Emitter | Energy (keV) | Yield (gps/dps) |
|---|---|---|
| **Pb-212** | **238.6** | **4.33E-01** |
| **Tl-208** | **2614.5** | **3.56E-01** |
| **Tl-208/Ac-228** | **583.2** | **3.05E-01** |
| **Ac-228** | **911.2** | **2.58E-01** |
| **Ac-228** | **969.0** | **1.58E-01** |
| **Ac-228** | **338.3** | **1.13E-01** |
| **Bi-212/Ac-228** | **727.3** | **7.20E-02** |
| Tl-208 | 860.6 | 4.47E-02 |
| Ac-228 | 794.9 | 4.25E-02 |
| Ac-228 | 1588.2 | 3.22E-02 |

Tl-208: Yield includes the 35.94% branch from its parent radionuclide, Bi-212
Primary gamma emissions are "**bolded**"

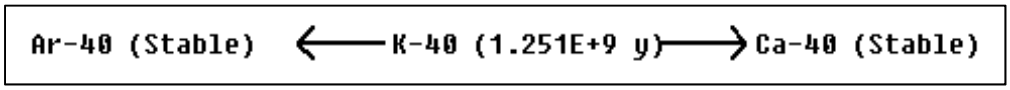


***Figure 3-4. K-40 decay chain. [4]***

***Table 3-5. Primary K-40 gamma emission.***

| Parent | Emitter | Energy (keV) | Yield (gps/dps) |
|---|---|---|---|
| **K-40** | **K-40** | **1460.8** | **1.07E-01** |

## 3.2 Typical soil background concentrations

Typical background soil activity concentrations are provided for the Th-232 decay series, U-238 decay series, U-235 decay series, and K-40 in Table 3-6.

***Table 3-6. Natural radioactivity in soil.***

| Nuclide / Decay Series | Typical soil concentration (pCi/g) | Typical soil concentration (ppm by mass or percent by mass) |
|---|---|---|
| Th-232 decay series | 1.1 | 10.00 ppm |
| U-238 decay series | 1.3 | 3.85 ppm |
| U-235 decay series | 0.06 | 0.55 ppm |
| K-40 | 11 | 1.47% |

Adapted from Reference [6]

## 3.3 Background spectral features

When reviewing background spectra measured with *unshielded* HPGe detectors (such as environmental in-situ gamma spectroscopy spectra), the 609.3 keV Ra-226 decay product full-energy peak area will generally be greater than the 583.2 keV Th-232 decay product full-energy peak area (Figure 3-5). In addition, the 1460.8 keV K-40 full-energy peak area will generally be several times greater than 2614.5 keV Th-232 decay product full-energy peak area (Figure 3-6).

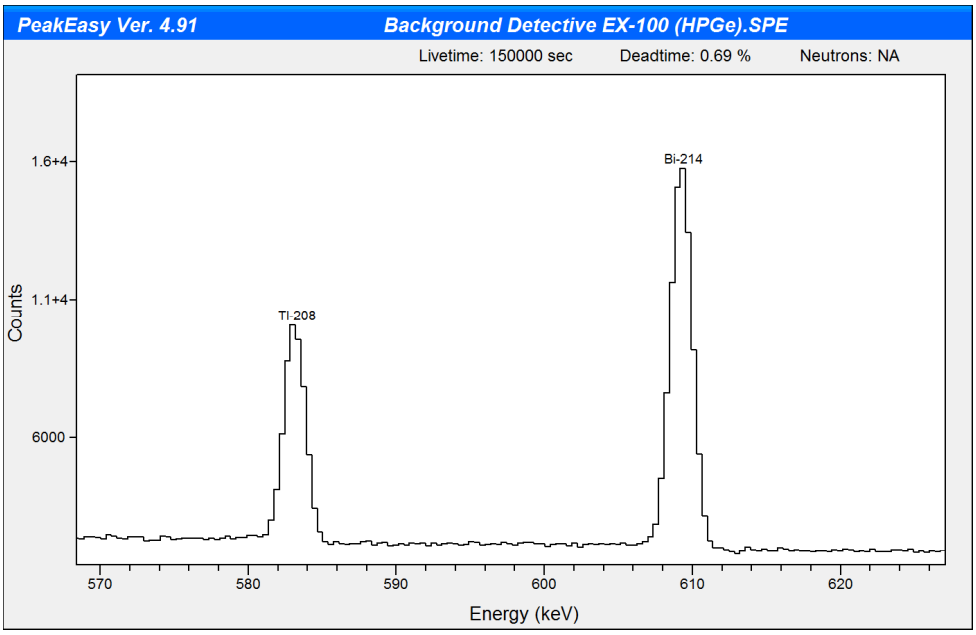


***Figure 3-5. Comparison of 583.2 keV Th-232 decay chain and 609.3 keV Ra-226 decay chain peaks in a background spectrum. Linear scale. [5]***

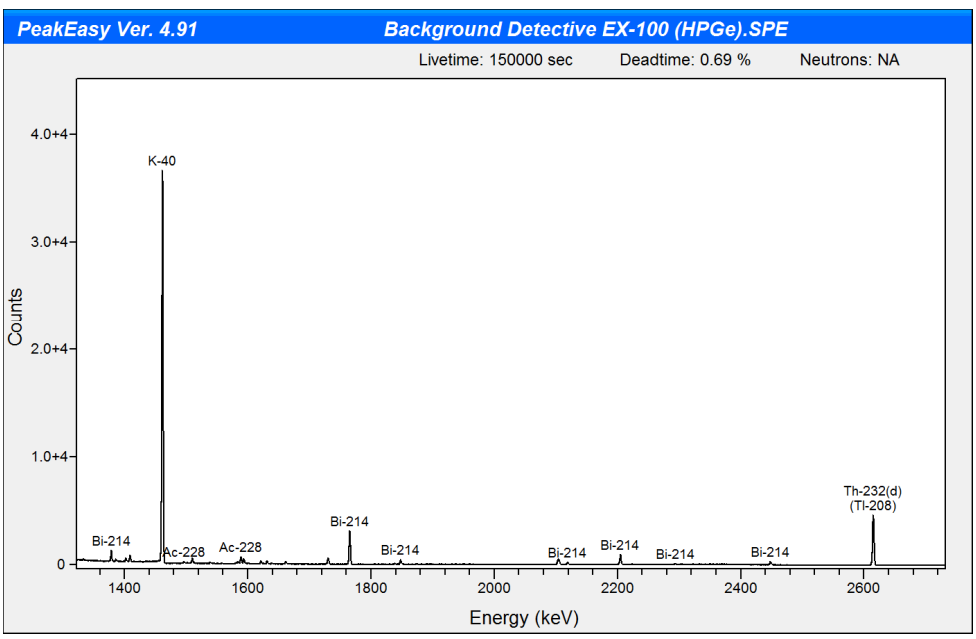


***Figure 3-6. Comparison of 1460.8 keV K-40 and 2614.5 keV Th-232 decay chain peaks in a background spectrum. Linear scale. [5]***

For detailed information on common gamma emissions found in background spectra, see Table 13.9 and Table D.1 in Reference [2].

## 3.4 Radon (Rn-222) and thoron (Rn-220)

It should be noted that radon (Rn-222), a noble gas produced from the decay of Ra-226 in the U-238 decay chain, can diffuse/escape during soil sample collection and preparation. Since the Ra-226 decay products (Pb-214 and Bi-214) follow Rn-222 decay and have gamma emissions with much higher yields than Ra-226, it may be necessary to seal sample containers and allow for in-growth of Rn-222 decay products (Rn-222 half-life = 3.8 days) to properly estimate the activity of Ra-226 using gamma spectroscopy. Typically, five Rn-222 half-lives or 19 days is sufficient to allow for in-growth of Rn-222 decay products.

- Note: When the Ra-226 186.2 keV gamma emission (with a moderate 3.59% yield is detected), the extent of Rn-222 escape can be evaluated by comparing the calculated Ra-226 decay product to Ra-226 activity ratio using the following full-energy peak pairs: 609.3 / 186.2 keV; 351.9 / 186.2 keV; 295.2 / 186.2 keV; and many others.

Thoron (Rn-220), a noble gas produced from the decay of Ra-224 in the Th-232 decay chain, can produce similar issues to radon (Rn-222) but is much less problematic due to its short half-life (Rn-220 half-life = 55.6 seconds).

## 3.5 Air filters

When large quantities of air are passed through filters, buildup of Pb-210 and Po-210 from the decay of Rn-222 and its decay products can be significant. Although Po-210 has gamma emissions with very low yields, Pb-210 has a 46.5 keV gamma emission with a moderate 4.1% yield which is semi-routinely detected by gamma spectroscopy on air filters. In addition, Be-7, a radionuclide produced in the earth's atmosphere by cosmic rays (Be-7 half-life = 53.2 days), can be detected on air filters at low activity concentrations by gamma spectroscopy.

# SECTION 4.0 RADIOACTIVE EQUILIBRIUM

## Table of Contents



## Figures



## Tables



## Equations

## 4.1 Introduction

When radioactive equilibrium is reached, the parent to decay product activity ratio is constant and both the parent and decay product decay with the half-life of the parent radionuclide.

## 4.2 Time to reach equilibrium

The time to reach radioactive equilibrium (transient or secular) is typically quoted as several half-lives (5 to 10) of the decay product. The following table displays the fraction of decay product equilibrium as function of the number of decay product half-lives (assuming no decay product activity is initially present).

| Number of Decay Product Half-Lives | Fraction of Equilibrium |
|---|---|
| 0 | 0.000 |
| 1 | 0.500 |
| 2 | 0.750 |
| 3 | 0.875 |
| 4 | 0.938 |
| 5 | 0.969 |
| 6 | 0.984 |
| 7 | 0.992 |
| 8 | 0.996 |
| 9 | 0.998 |
| 10 | 0.999 |

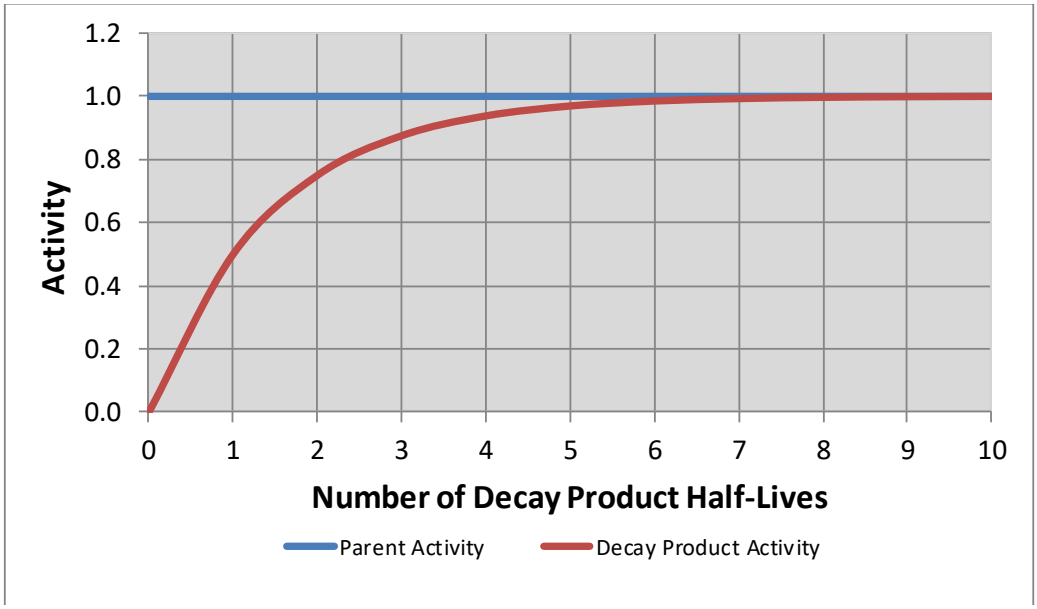


***Figure 4-1. Time to reach radioactive equilibrium example.***

## 4.3 Transient equilibrium

If the parent radionuclide's half-life is greater, but not much greater, than the half-life of the decay product, transient equilibrium is possible. Once transient equilibrium is reached, the decay product activity exceeds the parent radionuclide activity and both the parent and decay product decay with the half-life of the parent radionuclide.

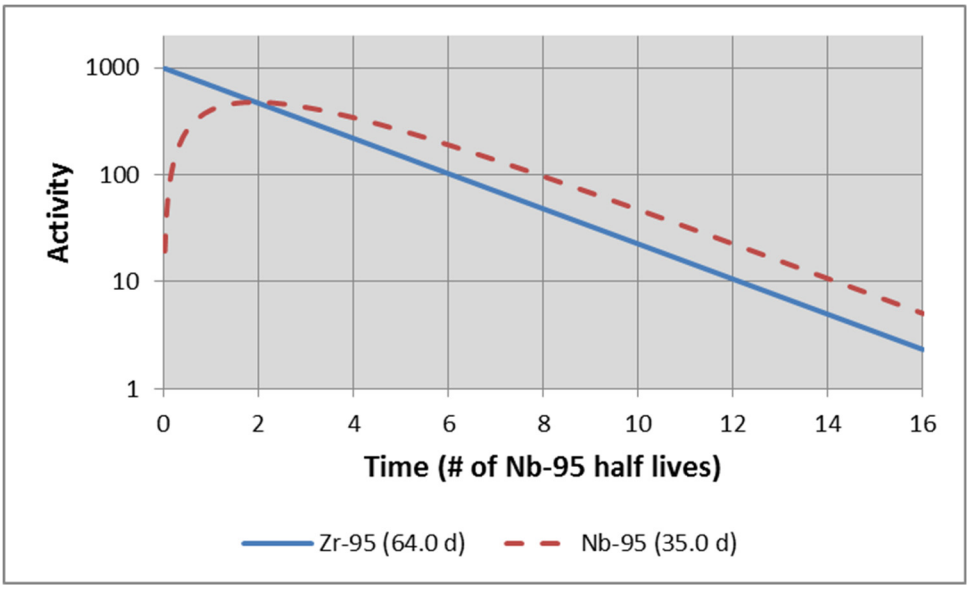


***Figure 4-2. Example of transient equilibrium for Zr-95 and its decay product Nb-95.***

## 4.4 Secular equilibrium

If the parent radionuclide's half-life is much greater than the half-life of the decay product, secular equilibrium is possible. Once secular equilibrium is reached, the decay product and parent radionuclide activity are equal and both the parent and decay product decay with the half-life of the parent radionuclide.

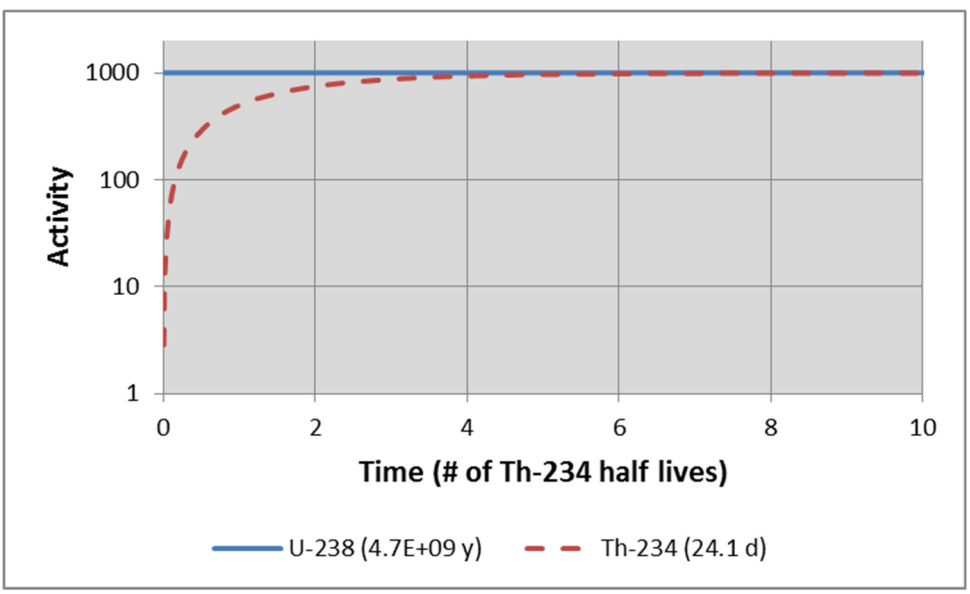


***Figure 4-3. Example of secular equilibrium for U-238 and its decay product Th-234.***

- Note: For decay chains, if the parent radionuclide's half-life is much greater than the half-lives of the decay products, the time to reach secular equilibrium can generally be estimated using the half-life of the longest-lived decay product in the chain.

## 4.5 No equilibrium

If the half-life of the parent radionuclide is less than the half-life of the decay product, no equilibrium is possible. The decay product activity will simply increase from zero, reach a maximum, and decay at a rate largely dependent on its half-life.

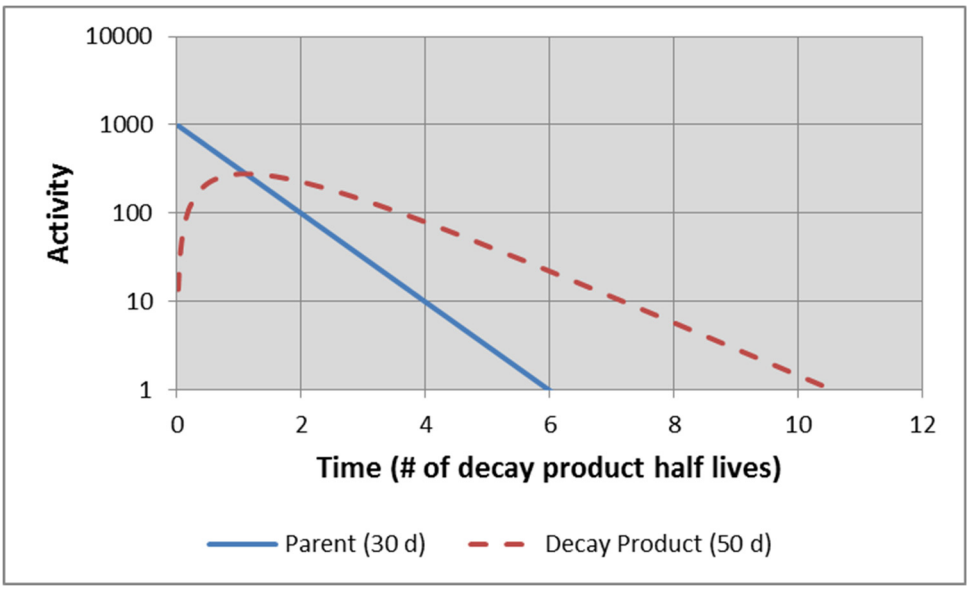


***Figure 4-4. Generic example of no equilibrium.***

## 4.6 Equation or decay product in-growth

If no decay product activity is initially present, Equation 4-1 can be used to determine decay product activity from parent radionuclide radioactive decay.

**Equation 4-1. Equation for decay product in-growth.**

$$A_D = B \cdot A_{P_0} \cdot \left(\frac{\lambda_D}{\lambda_D - \lambda_P}\right) \cdot \left(e^{-\lambda_P \cdot t} - e^{-\lambda_D \cdot t}\right)$$

Where:
$A_D$ = Decay product radionuclide activity;
$B$ = Branching ratio;
$A_{P_0}$ = Parent radionuclide initial activity;
$\lambda_D$ = Decay product radionuclide decay constant (days$^{-1}$);
$\lambda_P$ = Parent radionuclide decay constant (days$^{-1}$);
$t$ = Time (days).

For situations requiring complex decay chain activity determinations, applications such as NRC Rad Toolbox, MicroShield, and Interspec, described in *Appendix C. Software/applications of Potential Interest*, can be used.

## 4.7 Time since last chemical separation determinations (chronology)

The decay product in-growth equation provided above (Equation 4-1) can be used with gamma spectroscopy results for suitable parent/decay product radionuclides to estimate the time since last chemical separation (commonly referred to as "age"). Optionally, "Time since last chemical separation (age) determination tables" are provided in *Appendix B. Time Since Last Chemical Separation (age) Tables* for several suitable parent/decay product radionuclides.

For material "age" determinations, it is generally assumed that no decay product activity is present immediately following chemical separation (aka, 100% chemical separation). However, when all the decay product activity is not removed during the chemical separation process, the spectroscopist should be aware that the "age" calculated will be biased high.

### *4.7.1 Example*

An Am-241:Be-9(α,nγ)C-12 source is measured by gamma spectroscopy. Estimate the time since last chemical separation using the information provided below.

**Am-241 (Half-life = 433.2 y) -> Np-237 (Half-life = 2.14E+06 y) -> Pa-233 (Half-life = 27.0 d)**

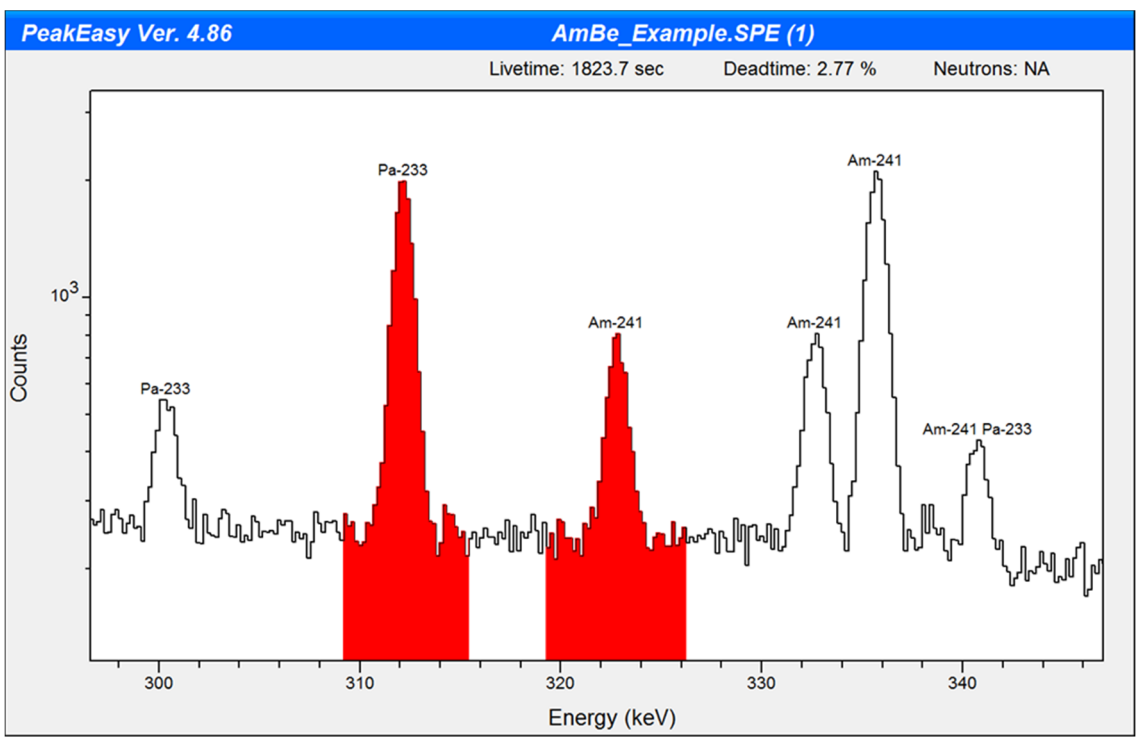


***Figure 4-5. Am-241:Be source example spectrum.***

***Table 4-1. Relevant information for AmBe source example.***

| Nuclide | Energy (keV) | Yield (gps/dps) | Net Area (counts) | Net Area / Yield |
|---|---|---|---|---|
| Am-241 | 322.5 | 1.52E-06 | 3583 | 2.36E+09 |
| Pa-233 | 312.2 | 3.86E-01 | 11222 | 2.91E+04 |

Np-237/Am-241 activity ratio estimate = 2.91E+04 / 2.36E+09 = 1.2E-05.

Since the gamma emissions are close in energy, the efficiencies can be assumed to be the same for the 312.2 and 322.5 keV gamma emissions from Pa-233 and Am-241, respectively. Next, the full-energy peak areas are divided by their respective gamma emission yields to calculate a Pa-233/Am-241 activity ratio of 1.2E-05. Using the calculated Pa-233/Am-241 activity ratio and assuming no Np-237 is present following the last chemical separation, the "age" is estimated at 36 years using Equation 4-1 or *Appendix B. Time Since Last Chemical Separation (age) Tables*.

## 4.8 Time since fission irradiation using Zr-95/Nb-95 full-energy peak pairs

For short fission irradiations, the time since irradiation can be estimated using Zr-95/Nb-95 gamma spectroscopy results. This is possible since the individual neutron induced fission product yield for Nb-95 is very low relative to Zr-95 and the fission products generated that decay to Zr-95 (precursors) have very short half-lives (see Table 4-2). Accordingly, the amount of Nb-95 at the end of short irradiations is orders of magnitude lower than Zr-95 and can be ignored. This allows Equation 4-1 to be used in conjunction with Zr-95/Nb-95 full-energy peak areas, yields, and full-energy peak efficiencies to calculate the time since fission irradiation.

***Table 4-2. U-235 thermal fission product yields for mass number 95. [7]***

| Nuclide | t1/2 | Ind. Yield | Cum. Yield |
|---|---|---|---|
| 95Kr | 0.78 s | 7.19E-03 | 7.19E-03 |
| 95Rb | 0.377s | 7.64E-01 | 7.70E-01 |
| 95Sr | 25.1s | 4.54E+00 | 5.27E+00 |
| 95Y | 10.3 m | 1.11E+00 | 6.38E+00 |
| 95Zr | 64.02d | 1.27E-01 | 6.50E+00 |
| 95Nb-m | 3.61 d | 2.48E-05 | 6.51E-02 |
| 95Nb | 34.97d | 1.06E-04 | 6.50E+00 |
| 95Mo | stable | 4.94E-10 | 6.50E+00 |

### *4.8.1 Example*

Assuming a short fission irradiation time, estimate the time since irradiation using the information provided below.

**Zr-95 (Half-life = 64.0 d, Branching Ration (BR) = 0.9892) -> Nb-95 (Half-life = 35.0 d)**
**Zr-95 (Half-life = 64.0 d, BR 0.0108) -> Nb-95m (Half-life = 3.6 d, BR 0.944) → Nb-95 (Half-life = 35.0 d)**

***Table 4-3. Relevant information for Zr-95/Nb-95 example.***

| Nuclide | Energy (keV) | Yield (gps/dps) | Net Area (counts) | Net Area / Yield | Relative Activity |
|---|---|---|---|---|---|
| Zr-95 | 756.7 | 5.44E-01 | 57750 | 1.06E+05 | 1.00E+00 |
| Nb-95 | 765.8 | 9.98E-01 | 42846 | 4.29E+04 | 4.04E-01 |

Full-energy peak efficiencies are assumed to be the same since the gamma emissions are very close in energy.

Using the calculated Nb-95/Zr-95 activity ratio of 4.04E-01 in conjunction with Equation 4-1 or *Appendix B. Time Since Last Chemical Separation (age) Tables,* the time since irradiation is estimated at 22.5 days prior to gamma spectroscopy analysis.

- Note: The known time since fission irradiation was 22.1 days.

# SECTION 5.0 DETECTOR RESOLUTION, SOLID ANGLE, DETECTOR EFFICIENCY, AND CALIBRATION

## Table of Contents



## Figures



## Tables



## Equations

## 5.1 Detector resolution

The Full Width Half Maximum (FWHM) is the most commonly cited value of detector resolution. The FHWM is defined as the full width of the peak at one-half the maximum height. Alternatively, the FWHM may be quoted as a percentage by dividing the FWHM value in keV by the full-energy peak photon energy in keV. For Gaussian-shaped peaks, the FWHM is related to the sigma (σ) or half-width used in the Gaussian distribution equation (see Equation 5-1).

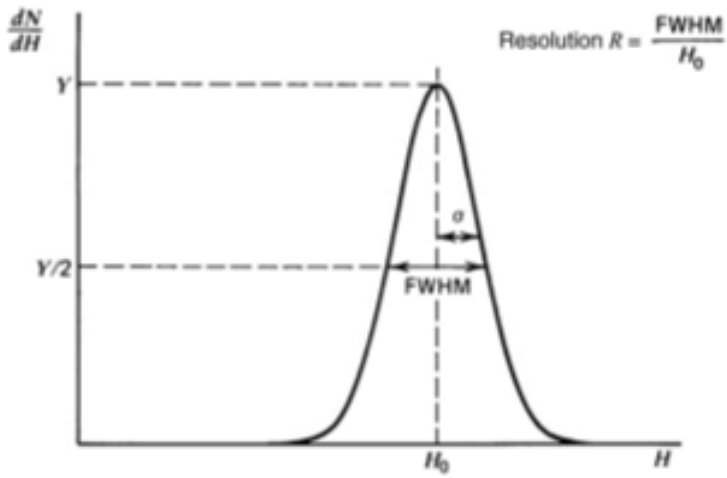


***Figure 5-1. FWHM representation. [8]***

**Equation 5-1. FWHM Gaussian distribution equation.**

$$\boldsymbol{FWHM = 2 \cdot \sqrt{2 \cdot ln2} \cdot \sigma \approx 2.3548 \cdot \sigma}$$

Typical FWHM values for sodium iodide (NaI), lanthanum bromide (LaBr3), and HPGe detectors at 661.7 keV are roughly 8%, 3.5%, and 0.3%, respectively. To illustrate the importance of resolution on the ability to distinguish full-energy peaks, Zr-95/Nb-95 spectra for NaI, LaBr3, and HPGe detectors are shown in Figure 5-2.

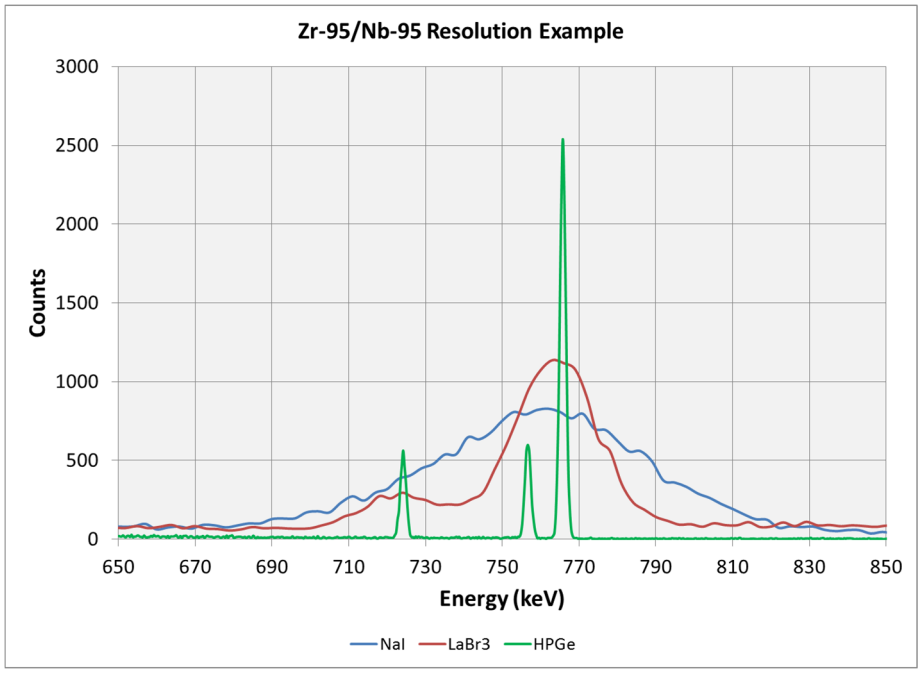


***Figure 5-2. Detector resolution example comparing Zr-95/Nb-95 spectra for NaI, $LaBr_3$, and HPGe detectors. Note: Zr-95 gamma emissions at 724.2 and 756.7 keV; Nb-95 gamma emission at 765.8 keV.***

Although the absolute FWHM value in keV increases with energy, the FWHM percentage decreases with energy as shown in Table 5-1.

***Table 5-1. Example HPGe FHWM in keV and % as a function of gamma emission energy for a mulitinuclide calibration source.***

| Centroid (keV) | Net Area Counts | Net Area Uncertainty | FWHM (keV) | FWHM (%) |
|---|---|---|---|---|
| 88.2 | 32853 | 207 | 1.07 | 1.22% |
| 122.2 | 17439 | 161 | 1.07 | 0.88% |
| 166.0 | 18518 | 161 | 1.11 | 0.67% |
| 279.4 | 11533 | 124 | 1.18 | 0.42% |
| 391.9 | 14328 | 130 | 1.28 | 0.33% |
| 661.8 | 11694 | 117 | 1.47 | 0.22% |
| 898.2 | 19418 | 145 | 1.62 | 0.18% |
| 1173.4 | 15396 | 127 | 1.82 | 0.16% |
| 1332.7 | 13760 | 120 | 1.86 | 0.14% |
| 1836.4 | 12698 | 113 | 2.18 | 0.12% |

## 5.2 Detector resolution calibration

Detector resolution calibrations are commonly performed for HPGe detector systems. These calibrations are used by peak fitting routines to determine peak widths and estimate full-energy peak areas. Accordingly, square root quadratic (best) and regular quadratic (good) equations (Equation 5-2 and Equation 5-3, respectively) are generally used to fit the measured detector resolution as a function of energy [2]. Please note that the current detector resolution calibration equation used by CANBERRA Industries (Equation 5-4) is not a square root or regular quadratic and generally results in poorer fits to the FWHM data.

**Equation 5-2. FWHM square root quadratic equation.**

$$\boldsymbol{FWHM = \sqrt{a + b \cdot E + c \cdot E^2}}$$

**Equation 5-3. FWHM quadratic equation.**

$$\boldsymbol{FWHM = a + b \cdot E + c \cdot E^2}$$

**Equation 5-4. CANBERRA Industries FWHM equation.**

$$\boldsymbol{FWHM = a + b \cdot \sqrt{E}}$$

Where:
$a$, $b$, and $c$ = Curve fit coefficients
$E$ = Energy.

## 5.3 Solid angle

In practical terms, the solid angle subtended by a detector from a source (G = Ω / 4π) is the "ratio of particles striking the detector to those emitted by the source" [10]. For a point source on-axis with a circular detector face, the solid angle (Ω) can be calculated using Equation 5-5.

**Equation 5-5. Solid angle equation for a point source on-axis with a circular detector face.**

$$\boldsymbol{\Omega = 2\pi \cdot \left(\frac{1 - d}{\sqrt{d^2 + r^2}}\right)}$$

Where:

$\Omega$ = Solid angle (steradians);
$d$ = Distance between the source and the detector face;
$r$ = Detector radius.

When the radiation source to the detector distance is 3 times or greater than the longest detector and source dimension, the solid angle ($\Omega$) can be approximated for an on-axis source by dividing the area of the detector face by the square of the source to detector face distance.

For more complex source and/or detector geometries, the calculation of the solid angle can be difficult. For more information on solid angle, see Section 8.2 Geometry Effects in Measurement and Detection of Radiation in Reference [10]. In addition, the Radiation Safety Information Computational Center (RSICC) computer code SACALC is useful for complex solid angle calculations and can be used calculate the average solid angle subtended by a detector for various geometries, displacements, and rotations.

## 5.4 Detector efficiency

Efficiency is typically described as absolute or intrinsic. The *absolute efficiency* is defined as the number of photons detected divided by the number of photons emitted from the source. Similarly, the *intrinsic efficiency* is defined as the number of photons detected divided by the number of photons incident on the detector. The *intrinsic full-energy peak efficiency* "depends primarily on the detector material, the incident gamma ray energy, and the physical thickness of the detector in the direction of the incident radiation" [11]. Absolute and intrinsic efficiency can be related using Equation 5-6.

**Equation 5-6. Absolute efficiency equation.**

$$\boldsymbol{\varepsilon_a = \varepsilon_i \cdot \frac{\Omega}{4\pi}}$$

Where:
$\varepsilon_a$ = Absolute efficiency;
$\varepsilon_i$ = Intrinsic efficiency;
$\Omega$ = Solid angle.

## 5.5 Detector efficiency calibration

Laboratory gamma spectroscopy system efficiency calibrations are typically determined by measuring a source constructed with several radionuclides of known energy and activity that span the energy range of interest in a geometry that is as close as possible to the unknown sources. For example, since soil and water samples are commonly placed in a Marinelli sampling container (Figure 5-3), efficiency calibration sources using materials with similar attenuation properties as the samples are fabricated using the same size Marinelli container.

***Figure 5-3. Photo of Marinelli container. [9]***

Following measurement of the calibration source, polynomial equations like Equation 5-7 are used to fit the measured full-energy peak efficiency as a function of energy.

**Equation 5-7. LN(X) LN(Y) polynomial curve fit equation.**

$$\boldsymbol{\varepsilon = \exp\left[\sum_{i=0}^{7} a_i \cdot \ln(E)^i\right]}$$

Where:
$\varepsilon$ = Efficiency (counts/gamma);
$E$ = Energy (keV);
$a_i$ = Curve fit coefficients.

In some instances, it may not be possible to use a known counting geometry when measuring a sample. When it is necessary to measure a sample in a non-standard counting geometry, the efficiency for a known counting geometry that is most like the measured counting geometry should be used. When this is done, the spectroscopist should have a general understanding of the effect on the results. Alternatively, software, such as the source modeling and quantitative spectral analysis software, listed in *Appendix C. Software/applications of Potential Interest*, may be used to model the sample geometry/media and/or detector for analysis of samples in non-standard counting geometries.

### *5.5.1 Example*

Assume a 2-inch diameter air filter is measured on the surface of the 60-mm diameter x 50-mm deep HPGe detector with a 1.5 cm offset (Figure 5-4).

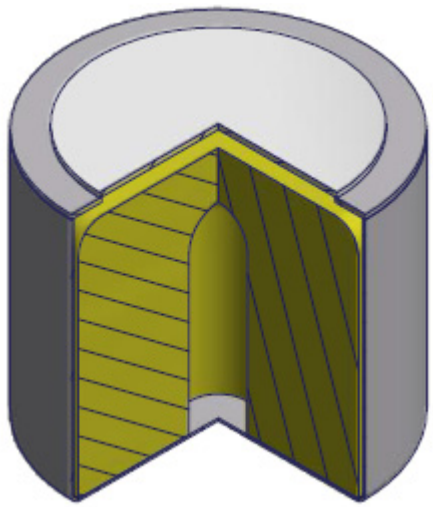

***Figure 5-4. Measurement geometry: HPGe detector with 2-inch diameter radioactive air filter on-contact.***

The most similar efficiency available for use by the lab is a point source counted on the surface of the detector (Figure 5-5).

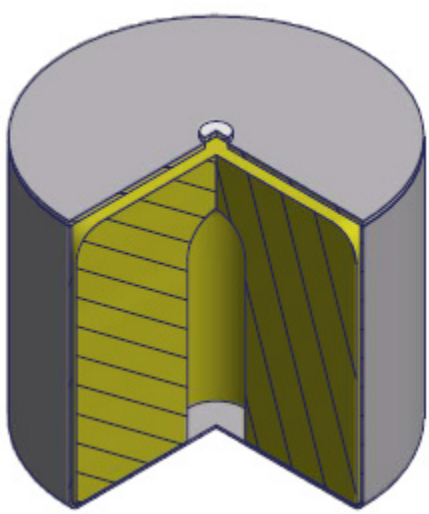

***Figure 5-5. Calibration geometry: HPGe detector with a radioactive point source on-contact.***

If the point source counting geometry is used for efficiency correction, will the reported results for Cd-109 at 88.0 keV be over or underestimated?

### *5.5.2 Example solution*

The solid angle is better for a point source than a 2-inch diameter air filter counted on the surface of the detector. In addition, the average path length in germanium (Ge) for photons emitted from a point source counted on the surface of the detector will be longer than the average path length in Ge for photons emitted from a 2-inch diameter air filter counted on the surface of the detector. Therefore, the reported results will be underestimated.

# SECTION 6.0 COMMON SPECTRAL FEATURES AND EFFECTS

## Table of Contents



## Figures

## Tables



## Equations

## 6.1 Introduction

Example spectra, with additional discussion, for each of the spectral features/effects listed below is provided in this section:

- Compton edge
- Backscatter peak
- Single escape peak
- Double escape peak
- Characteristic x-ray peak
- Germanium characteristic x-ray escape peak
- Summation peaks
- Shielding effects
- Neutron interactions on germanium

## 6.2 Compton edge and backscatter peak

The Compton edge is produced in spectra when photons enter the detector and Compton scatter at 180 degrees (see SECTION 2.0). This interaction represents the most energy that can be deposited in the detector by a single Compton scatter. Backscatter peaks are generated in spectra when photons outside the detector are scattered at 180 degrees and deposit all their energy in the detector.

The energy of the backscatter peak and Compton edge can be calculated using Equation 6-1 and Equation 6-2, respectively. Based on Equation 6-1 and Equation 6-2, the energy of the Compton edge will exceed the backscatter peak energy when the incident gamma ray energy is greater than 255.5 keV (half the rest energy of an electron).

**Equation 6-1. Backscatter peak energy.**

$$\boldsymbol{E_{bs} = \frac{E_\gamma}{1 + \left(2 \cdot E_\gamma / 511\ keV\right)}}$$

Where:
$E_{bs}$ = Energy of the backscatter peak (keV).
$E_\gamma$ = Energy of the incoming gamma (keV);

**Equation 6-2. Compton edge energy.**

$$E_{ce} = E_{\gamma} - E_{bs}$$

Where:
$E_{ce}$ = Energy of the Compton edge (keV).
$E_{\gamma}$ = Energy of the incoming gamma (keV);
$E_{bs}$ = Energy of the backscatter peak (keV).

Figure 6-1 and Figure 6-2 show Cs-137 and Cr-51 spectra, respectively, with the backscatter peak, Compton edge, and full-energy peak labeled.

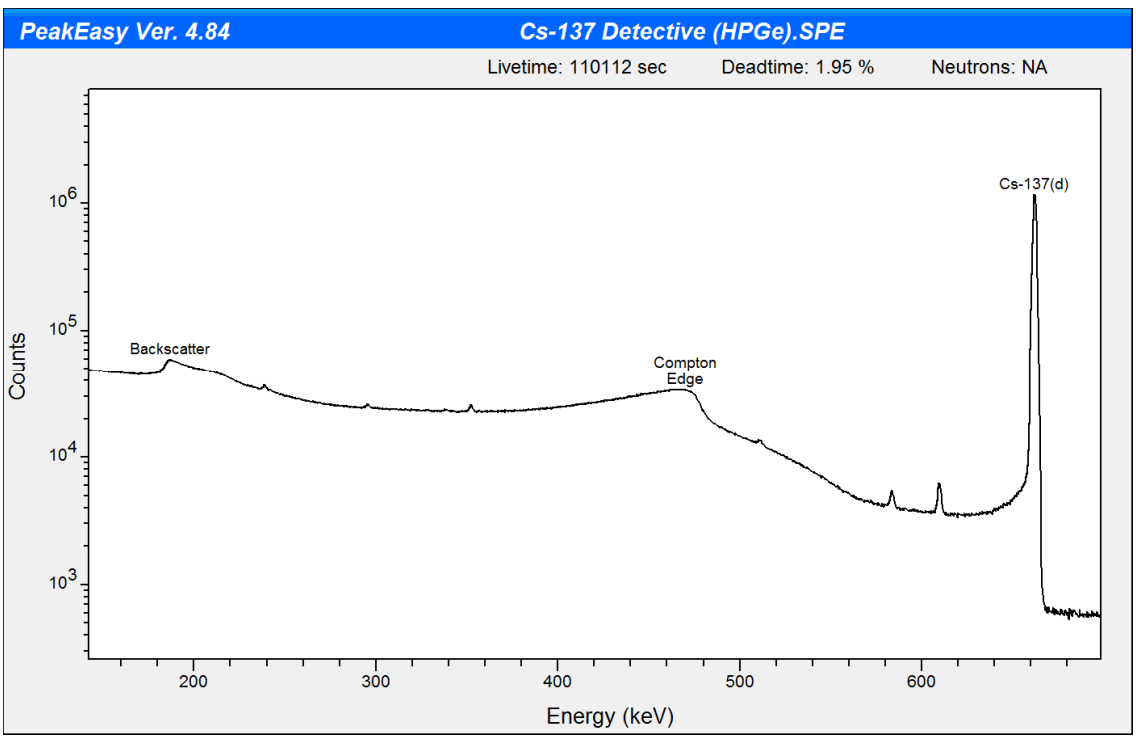


***Figure 6-1. Compton edge (477.3 keV) and backscatter peak (184.3 keV) from Cs-137 (661.7 keV). [5]***

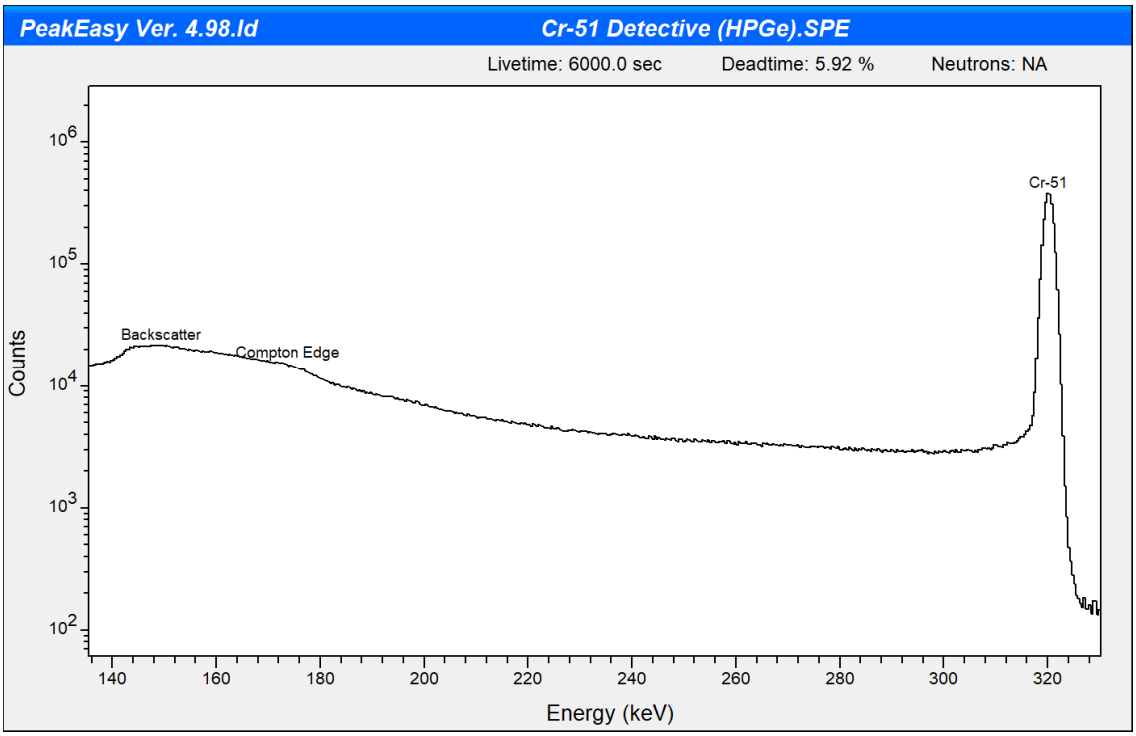


***Figure 6-2. Compton edge (178.0 keV) and backscatter peak (142.1 keV) from Cr-51 (320.1 keV). [6]***

Lastly, Compton scattering in the detector at less than 180 degrees and photons backscattered at less than 180 degrees can produce counts between the backscatter peak and Compton edge. Alternatively, Compton scatter or multiple Compton scatters can occur in the detector followed by the photoelectric effect to generate a full-energy count.

## 6.3 Single and double escape peaks

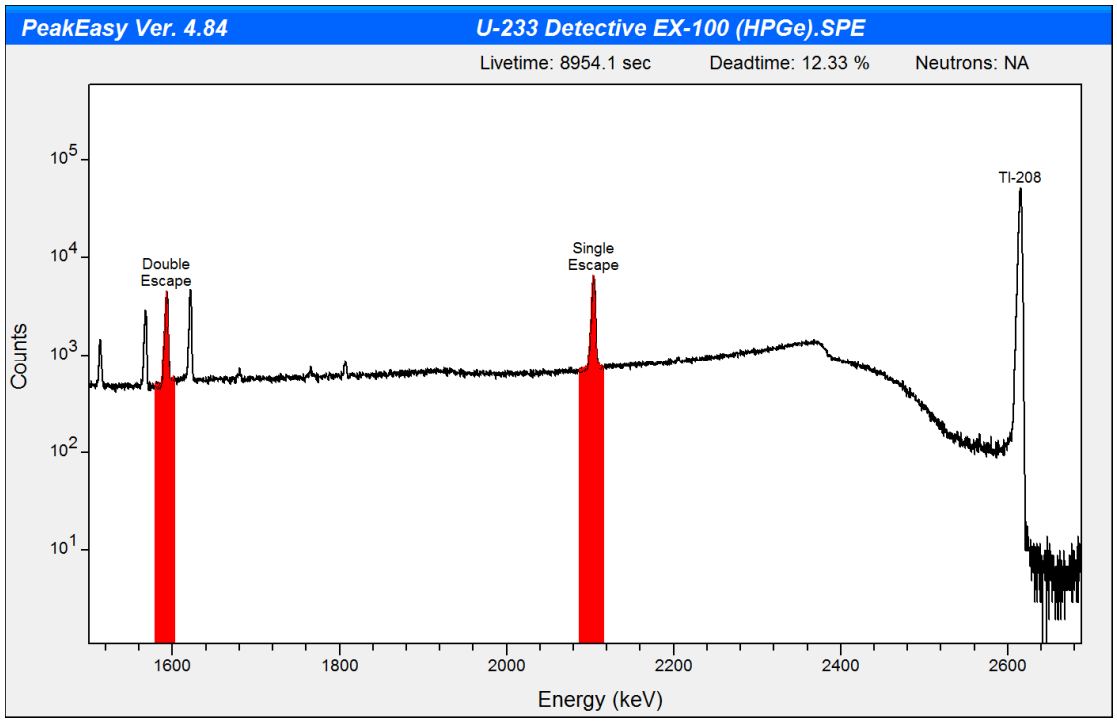


***Figure 6-3. Single (2103.5 keV) and double escape (1592.5 keV) peaks from Tl-208 (2614.5 keV). [5]***

Single and double escape peaks are generated in the spectrum when one or both 511 keV annihilation photons generated escape the detector without interaction. Accordingly, single and double escape peaks are located 511 keV and 1022 keV, respectively, below the full-energy peak. Lastly, single and double escape peaks are wider than a gamma ray of the same energy due to the Doppler broadening that can occur during the annihilation process (see SECTION 16.0 for more information on Doppler broadening).

### *6.3.1 Escape probability as a function of detector volume*

In a tiny detector, the pair of 511 keV annihilation photons generated escape the detector without interaction and only double escape peaks are present in the spectrum. In a huge detector, the pair of 511 keV annihilation photons generated do not escape and no escape peaks are present in the spectrum. Since single and double escape peaks are primarily dependent on detector volume, smaller volume detectors exhibit higher double escape to single escape peak area ratios than larger volume detectors. To a smaller extent, the double escape to single escape peak area ratio for a detector depends on detector geometry.

### *6.3.2 Example*

Using the background spectra and information provided in Figure 6-4, Figure 6-5, and ***Table*** 6-1, compare the 2614.5 keV full-energy peak double escape (DE) to single escape (SE) peak area ratios for an ORTEC Detective (50-mm diameter x 33-mm deep) and ORTEC Detective-100 (65-mm diameter x 50-mm deep). Does the smaller volume detector (ORTEC Detective) exhibit higher double escape to single escape peak area ratios than larger volume detector (ORTEC Detective-100)?

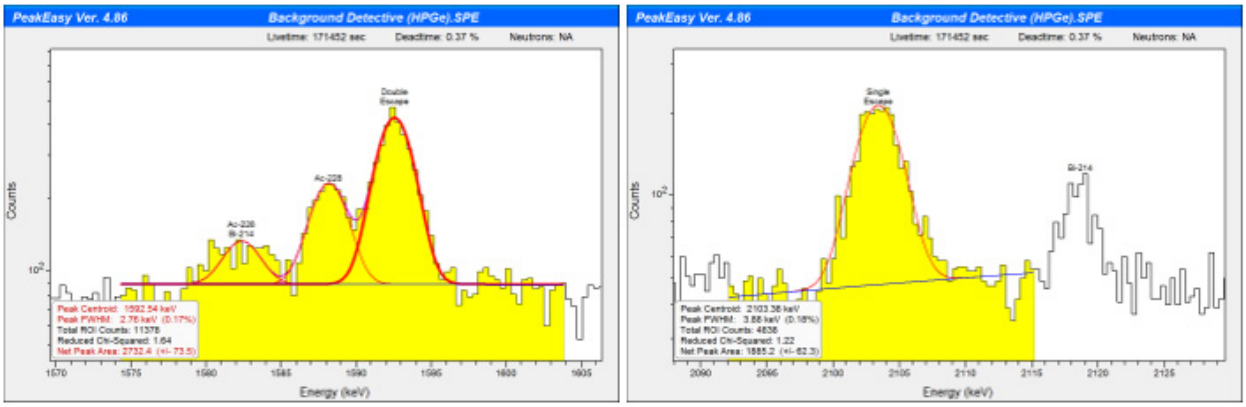


***Figure 6-4. ORTEC Detective 2614.5 keV double and single escape peak areas. [5]***

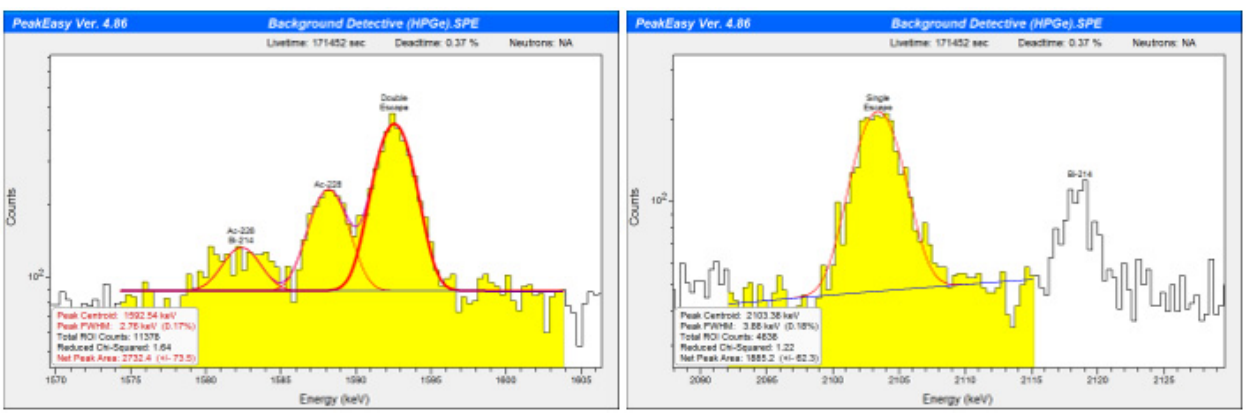


***Figure 6-5. ORTEC Detective-100 2614.5 keV double and single escape peak areas. [5]***

***Table 6-1. Calculated double to single escape full-energy peak area ratios.***

| Detector | HPGe Crystal Dimensions | Double Escape/Single Escape Peak Area Ratio |
|---|---|---|
| ORTEC Detective | 50-mm diameter x 33-mm deep | 2732.4 / 1885.2 = 1.45 |
| ORTEC Detective-100 | 65-mm diameter x 50-mm deep | 2985.5 / 5033.1 = 0.59 |

## 6.4 Characteristic x-ray peaks

### *6.4.1 Characteristic x-rays from induced x-ray fluorescence*

X-ray fluorescence results from the ionization of atoms, for which the excited state returns to the ground state emitting x-ray photons characteristic of the element that was ionized.

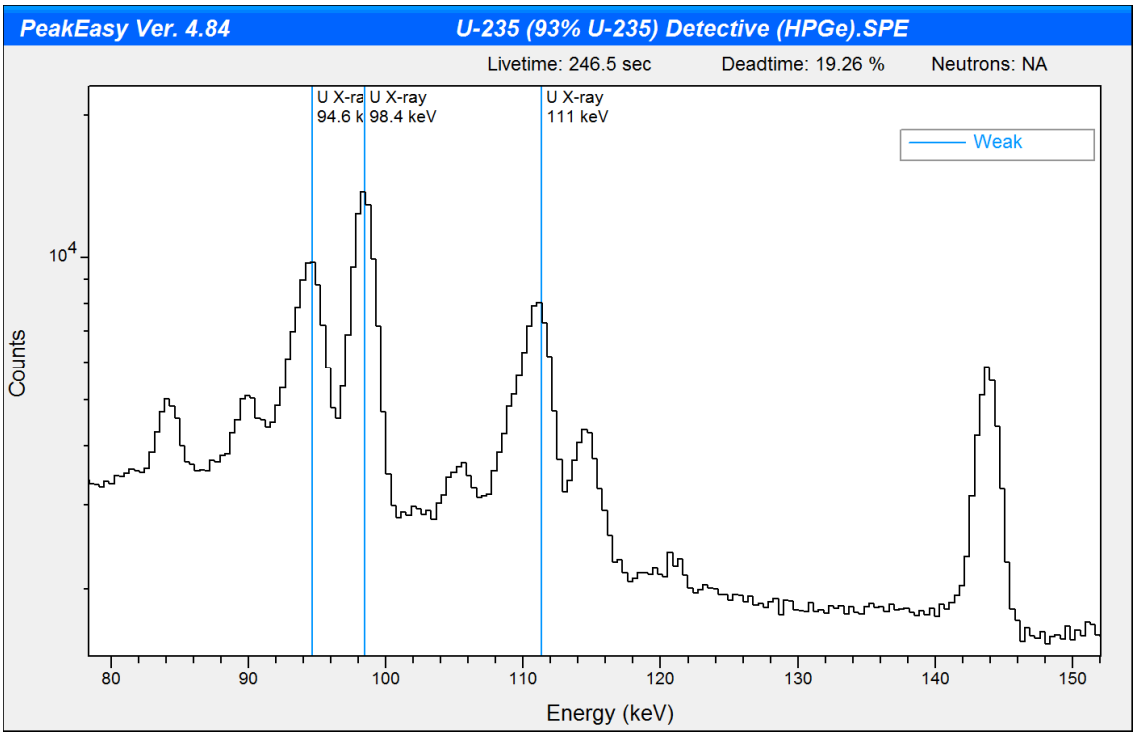


***Figure 6-6. Highly enriched uranium (HEU) with uranium (U) x-rays from self-induced x-ray fluorescence. [5]***

### *6.4.2 Characteristic x-rays from internal conversion*

Following radioactive decay, a decay product in an excited state is formed. Generally, the excited state emits a photon to returns to ground state. Alternatively, an orbital electron can be ejected to return to ground state (internal conversion). Following internal conversion, outer orbital electrons fill the lower energy levels producing characteristic x-rays. These x-rays are characteristic of the decay product element. The ratio of internal conversion electrons to gamma emission photons is known as the internal conversion coefficient.

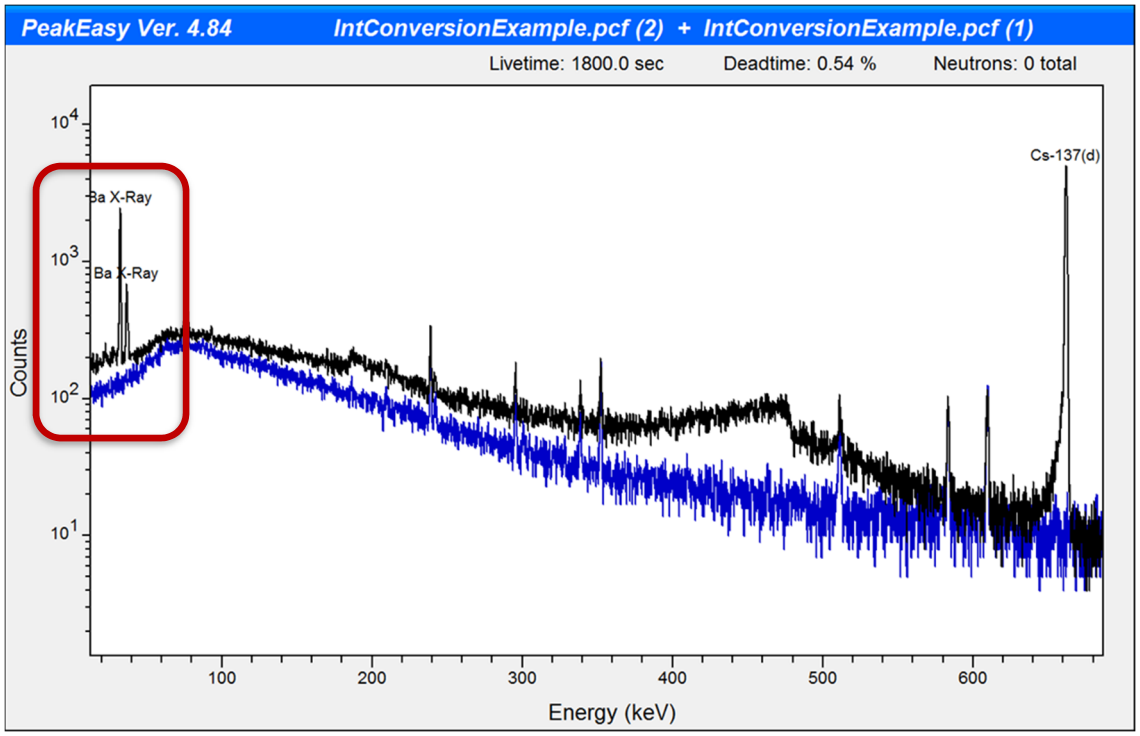


***Figure 6-7. Unshielded Cs-137 with characteristic Ba x-rays. Note: Cs-137 decays by beta emission to the excited state of Ba-137m which generates characteristic Ba x-rays via the internal conversion process. The internal conversion coefficient for Ba-137m is 11%.***

### *6.4.3 Parent and decay product element characteristic x-rays*

High-Z materials have high internal conversion coefficients which, as discussed, generate x-rays that are characteristic of the decay product element. In addition, high-mass or high-concentration radioactive samples produce self-induced x-ray fluorescence generating x-rays that are characteristic of the element that was ionized. [12]

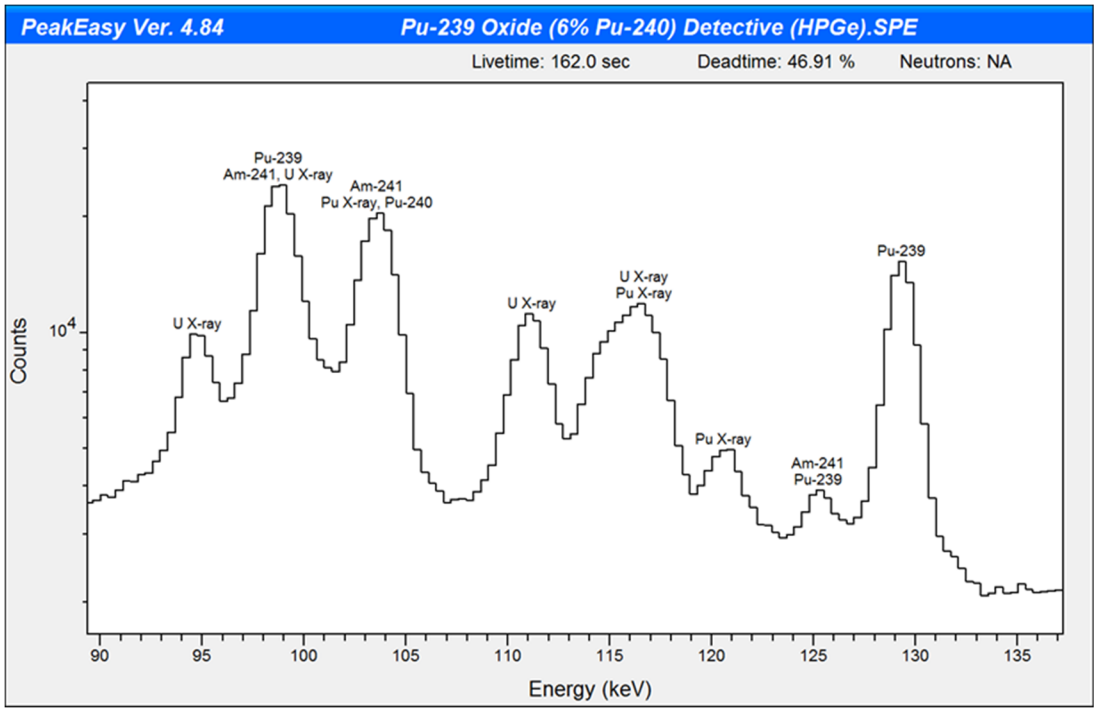


***Figure 6-8. Low burn-up plutonium (Pu) with parent (Pu) and decay product (U) element characteristic x-rays. [5]***

### *6.4.4 Characteristic x-rays found in ORTEC Detective and CANBERRA Falcon-5000 spectra*

For the ORTEC Detective series of detectors, spectroscopists should be aware that gold (Au) characteristic x-rays are commonly detected due to the presence of gold plating in the detector. In addition, for the CANBERRA Falcon-5000, it is not uncommon to detect lead (Pb) and silver (Ag) characteristic x-rays due to the presence of lead and silver plating in the detector. Example spectra with ORTEC Detective and CANBERRA Falcon characteristic x-rays are provided in Figures 6-4 through 6-6.

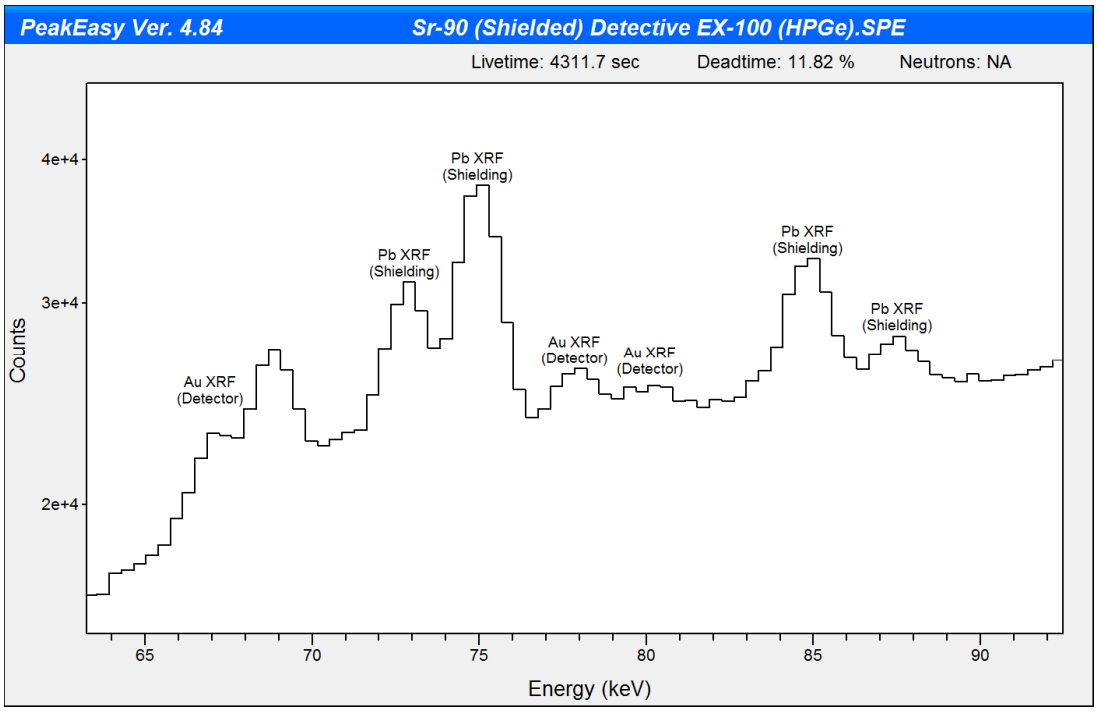


***Figure 6-9. Characteristic Pb x-rays from lead shielding and Au x-rays from gold plating present in ORTEC Detective detectors. Linear scale. [5]***

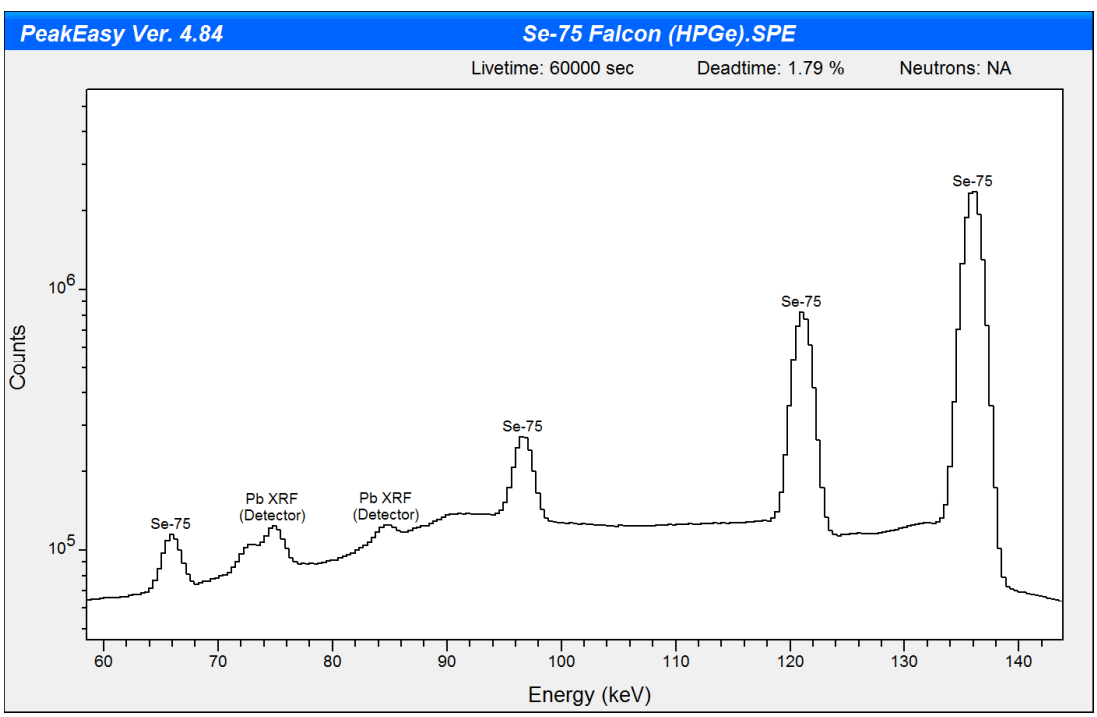


***Figure 6-10. Presence of Pb x-rays due to presence of lead in CANBERRA Falcon-5000 detectors. [5]***

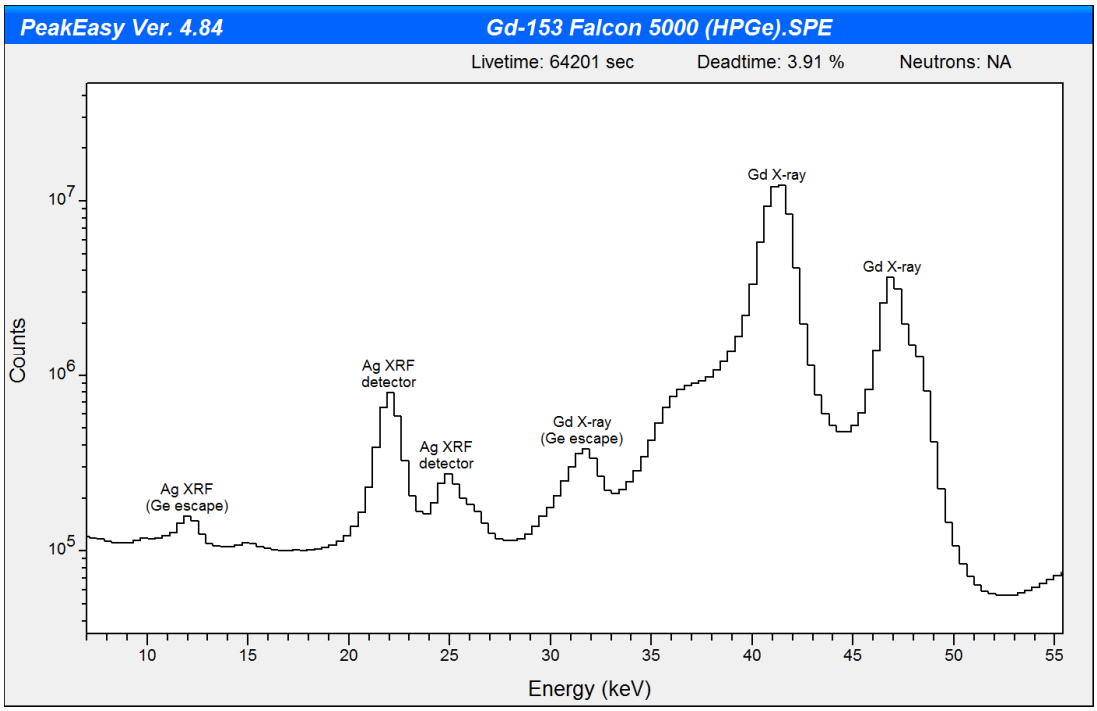


***Figure 6-11. Presence of Ag x-rays due to silver plating present in CANBERRA Falcon-5000 detectors. [5]***

## 6.5 Germanium characteristic x-ray escape peaks

Germanium (Ge) characteristic x-ray escape peaks can occur if low energy gamma rays (generally < 80 keV) are present and the detector has a large surface-to-volume ratio. Germanium Kα and Kβ characteristic x-ray escape peaks occur 9.9 and 11.0 keV below the full-energy peak, respectively.

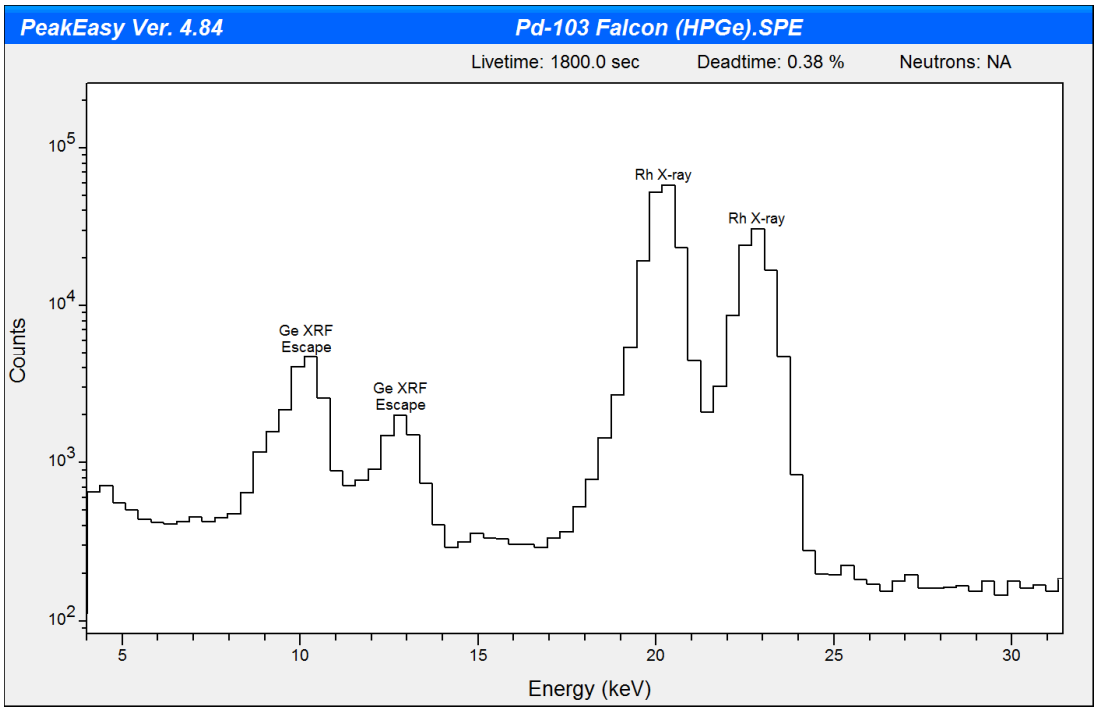


***Figure 6-12. Germanium x-ray escape peaks at 10.2 and 9.1 keV from 20.1 keV Pd-103 emission and at 12.8 and 11.7 keV from 22.7 keV Pd-103 emission. [5]***

## 6.6 Summation peaks

Summation peaks are produced due to random/chance coincidence (also known as pile-up) and true/cascade coincidence.

### *6.6.1 Random/chance coincidence (pile-up)*

Random/chance coincidence occurs when two or more photons are detected within the pulse processing time of the gamma spectroscopy system resulting in events being recorded in incorrect channels. It is a function of the square of the counting rate and the amplifier pulse width [13]. Accordingly, random/chance coincidence can be reduced by moving the sample further from the detector or shielding the sample or detector to reduce the count rate. Alternatively, the amplifier time constant can be decreased which reduces the duration of the amplifier pulses but increases incomplete charge collection resulting in poorer energy resolution.

To reduce random/chance coincidence, current gamma spectroscopy systems contain digital amplifiers with pile-up rejection which use timing circuitry to discard random/chance coincidence events resulting in lower background continuum and better resolution. When a gamma spectroscopy system is inspecting and processing a detected input pulse, the system is inactive (dead) to processing incoming events. Therefore, “dead time” must be accounted for to determine the correct measurement live time.

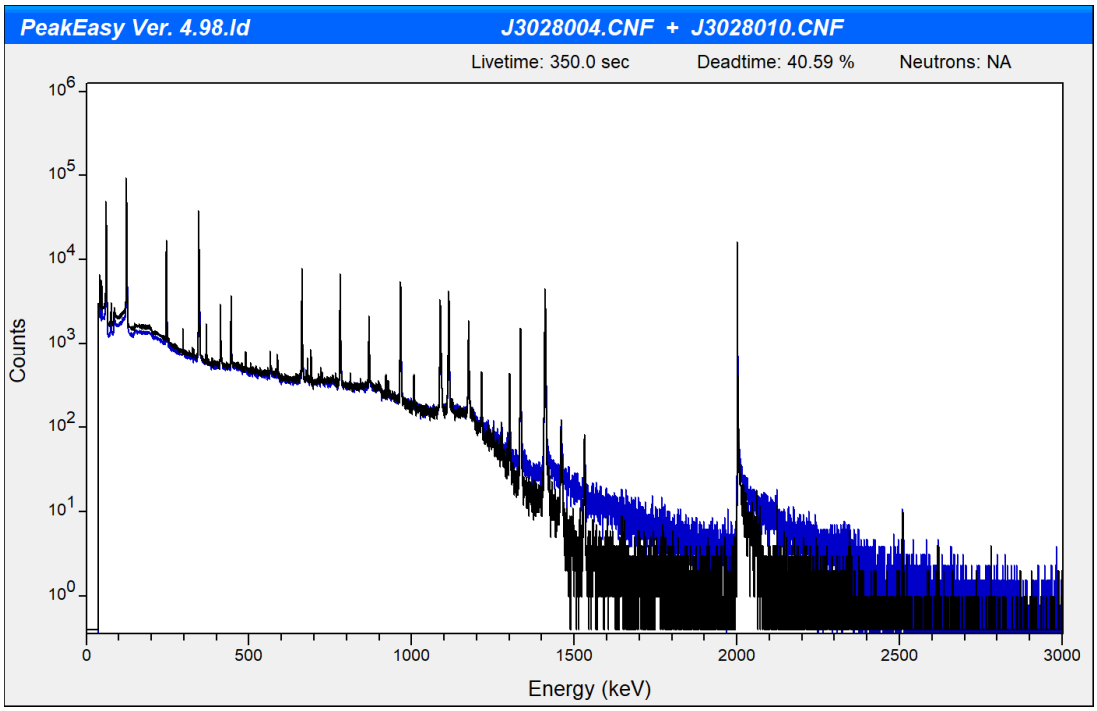


***Figure 6-13. Same counting geometry measured with (black) and without (blue) pileup rejection on.***

If it is necessary to evaluate the accuracy of the pileup rejection/live time correction (PUR/LTC) for a gamma spectroscopy system, the two-source method can be used. This involves measurement of a reference source which generates multiple full-energy peaks over the energy range of interest, such as Eu-152, Th-232, or U-232, at minimal dead time to establish reference full-energy peak count rates as a function of energy. Without moving the reference source, an additional source, such as Cs-137, is added and measured at several distances to generate dead times over the range of interest. Lastly, the reference peak count rates at minimal dead time are divided by the reference peak count rates at the various dead times measured to determine the pulse-pileup correction factor as a function of dead time/count rate and energy.

### 6.6.2 True/cascade coincidence

True/cascade coincidence occurs when two or more photons emitted from the same decay are detected within the pulse processing time of the gamma spectroscopy system. True/cascade coincidence can result from gamma-gamma, gamma-x-ray (x-rays generated following internal conversion or electron capture), and gamma-annihilation photon coincidence. It is a function of the detection efficiency (counting geometry and detector) and the radionuclide's decay scheme (not a function of the overall count rate). Therefore, true/cascade coincidence can be reduced by moving the sample further from the detector to reduce the solid angle (Ω). Typically, true/cascade coincidence causes counts to be lost from the full-energy peaks, but it can also cause addition to full-energy peaks dependent on the radionuclide's decay scheme. Common radionuclides susceptible to true/cascade coincidence are Co-60 (see Figure 6-14), Y-88, Eu-152, Eu-154, Sb-125, Cs-134, and Ba-133 (see Figure 6-15).

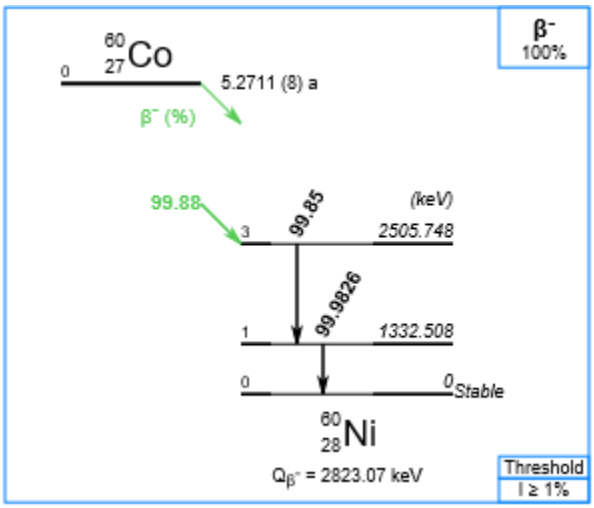


***Figure 6-14. Co-60 decay scheme. Note: Following the 1173.2 keV photon emission (2505.7 - 1332.5 keV), the 1332.5 keV photon is emitted almost simultaneously (Energy level lifetime = 0.713 picoseconds).***

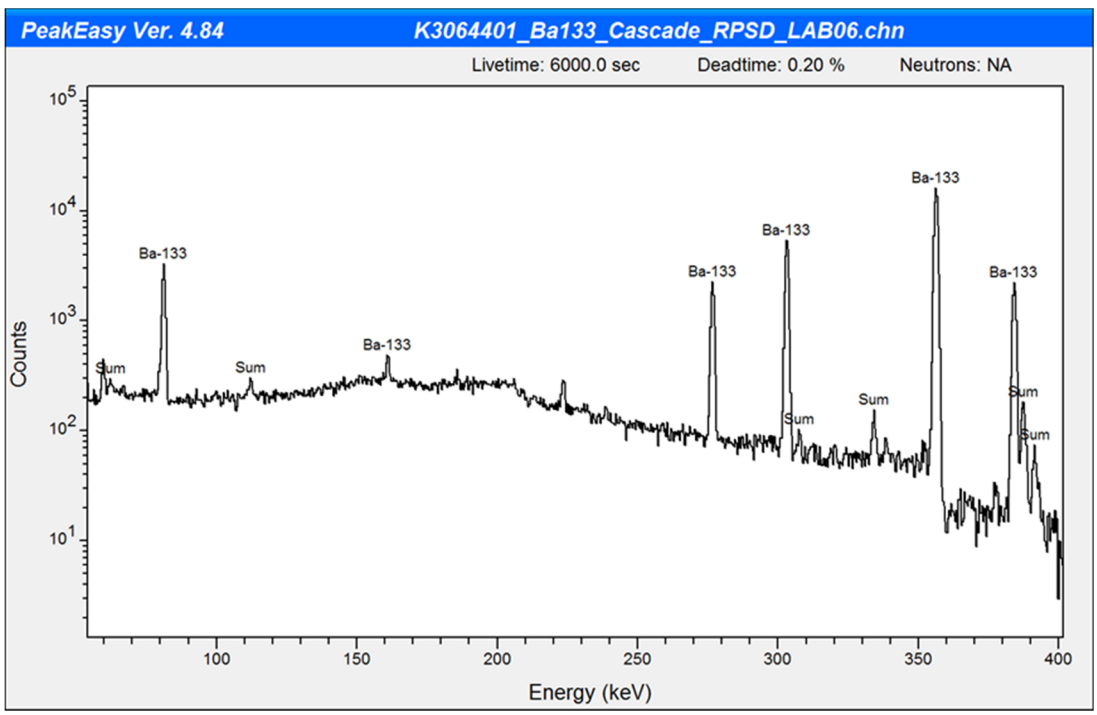


***Figure 6-15. Ba-133 measurement with true/cascade coincidence sum peaks identified.***

Since true/cascade coincidence summing (TCS) corrections are generally complicated, alternative solutions to avoid TCS corrections include reporting results for gamma emissions that are coincidence or near coincidence free, using calibration and sample radionuclide(s) that are the same (so that true/cascade coincidence summing is identical for the calibration standard and sample), or simply

moving the calibration position further from the detector (at the cost of increasing detection limits). When alternative solutions can't be used, true/cascade coincidence summing corrections must generally be made using TCS software applications, see *Appendix C. Software/applications of Potential Interest*.

- Note: As a rule of thumb, true/cascade coincidence summing corrections are generally recommended for sample to detector geometries with a solid angle (Ω) greater than 0.05 steradians [14].
- Note: For efficiency calibrations utilizing small sample to detector distances and radionuclides susceptible to true/cascade coincidence (such as Co-60, Y-88, Eu-152, and Ba-133), the activities reported for coincidence or near coincidence free radionuclides will be too high if no true/cascade coincidence corrections are made to the efficiency calibration curve prior to use.
- Note: For close sample to detector geometries requiring TCS corrections, use of n-type or extended range HPGe may make analysis more difficult relative to a standard coaxial p-type HPGe due to additional gamma/x-ray true coincidence. In addition, standard coaxial p-type HPGe true coincidence corrections may be more accurate since n-type or extended range HPGe true coincidence corrections may need to rely on efficiencies at x-ray energies which may not be as well-known or understood.
- Note: The TCS correction factor for a near calibration distance can be measured/estimated by calculating the ratio of the measured activities at a far distance (where no TCS correction is needed) to the measured activities at the near distance (where TCS correction is needed). This method assumes pulse pileup, dead-time, and non-uniform activity/geometry effects can be ignored. [15]

For reference purposes, calculated true coincidence correction factors for a point source on-contact with a "typical" standard and extended range coaxial HPGe are provided in True Coincidence Correction Factors for an On-contact Point Source. Lastly, a point source on-contact with the detector face represents the "worst case" true/cascade coincidence scenario.

## 6.7 Shielding effects

Shielding a radioactive source affects full-energy peak intensities and scattering in gamma ray spectra. When shielding is added, the signal from low energy gamma emissions is reduced relative to high energy gamma emissions. If shielding is sufficiently large, low energy full-energy peaks can be eliminated from the spectrum. Accordingly, for a single radionuclide with multiple gamma emissions, if high yield, high energy gamma emissions are detected but high yield, low energy gamma emissions are not detected (or significantly reduced) then the item is shielded.

Figure 6-16 provides an example of how the appearance of the spectrum can dramatically change with shielding. In the example, $LaBr_3$ spectra for an unshielded and heavily shielded Ir-192 source are plotted together. As shown, the heavily shielded Ir-192 source spectrum has little or no signal from the high yield, lower energy gamma emissions at 317 and 466 keV. Furthermore, the source intensity for the heavily shielded Ir-192 source is sufficiently large that low yield, high energy gamma emissions are now readily identified in the spectrum at 885, 1061, and 1378 keV.

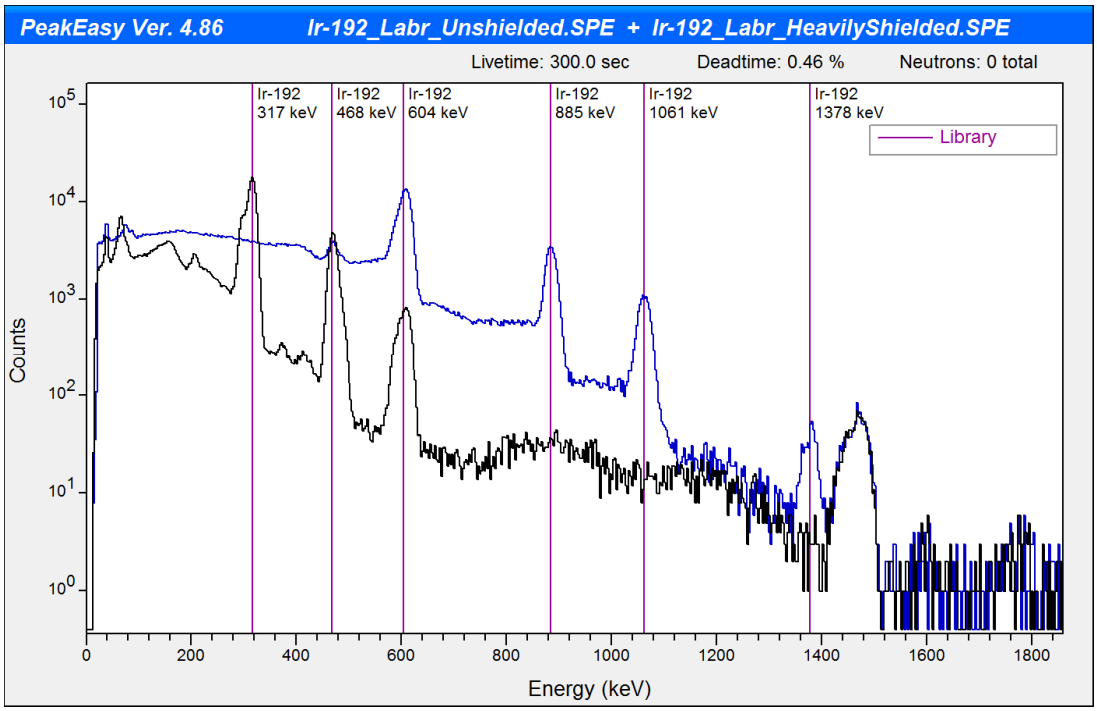


***Figure 6-16. $LaBr_3$ spectra, Ir-192_Unshielded (black), Ir-192_HeavilyShielded (blue).***

In addition to full-energy peak intensities changes, shielding affects the scattering observed in spectra. When scattering occurs, the continuum is elevated in the spectrum which limits the ability to detect low and mid energy gamma emissions. For example, consider a multilayered shield consisting of water and lead. If the water is placed before the lead, the scatter radiation from the water is more readily absorbed as it passes through the lead, and the overall scatter through the shield is small. If the lead were placed first, the subsequent scatter of radiation in the water more readily reaches the detector and the overall scatter is larger.

To demonstrate how the order of shielding affects the appearance of the spectrum, Figure 6-17 is provided. In this example, the same Ir-192 source is measured behind iron and polyethylene shielding twice. For each measurement, both shields are present, but the order is reversed. In the first measurement, the iron shield is closest to the source and in the second measurement the polyethylene shield is closest to the source. Since the same thickness of iron and polyethylene shielding is used for both measurements, the full-energy peak intensities in the spectra are the same but the scattering pattern is very different. As expected, the measurement with the iron shield closest to the source and the polyethylene on the outside has elevated scatter relative to measurement with the polyethylene shield closest to the source and the iron on the outside. In fact, the continuum has been elevated to the point that detection of low and mid energy gamma emissions has been eliminated or reduced.

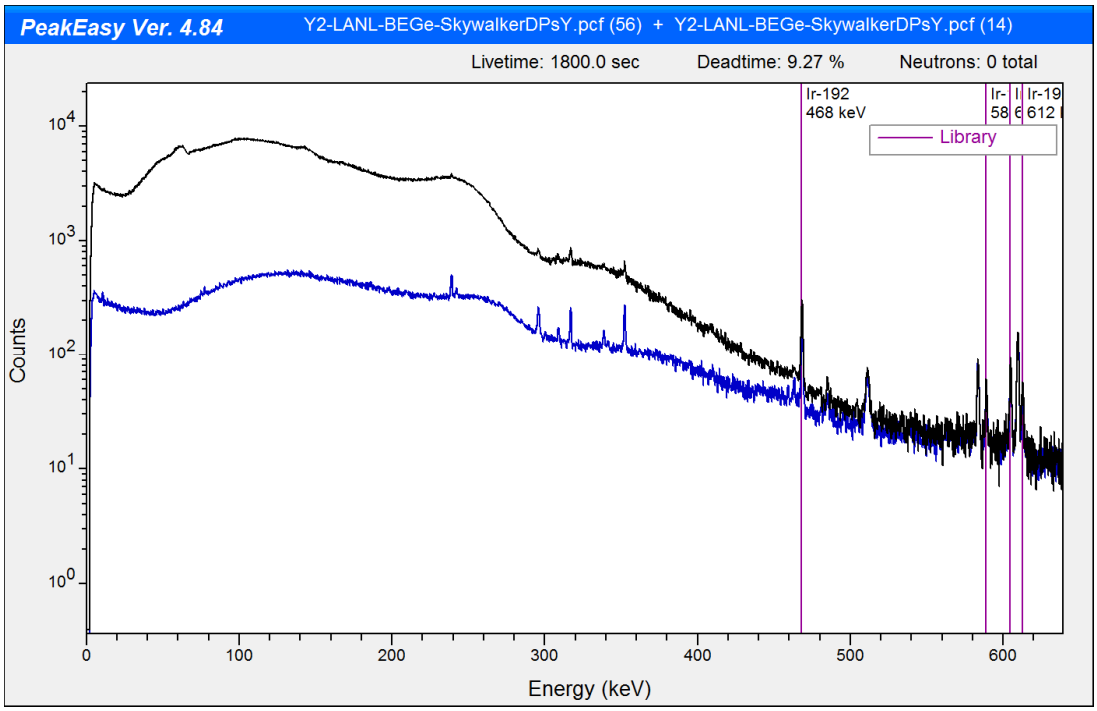


***Figure 6-17. HPGe spectra, Ir-192_Fe-9.366-cm_PE-5.239-cm (black), Ir-192_PE-5.239-cm_Fe-9.366-cm (blue).***

To illustrate the effect of nearby materials on portable gamma assays, Figure 6-18 is provided. During the first measurement (black), the detector is placed 1-meter above the floor in the center of the room. During the second measurement (blue), the detector is placed on the floor in the corner of the room near wall surfaces. As expected, additional scatter off the floor and nearby room surfaces elevates the amount of continuum seen in the second measurement.

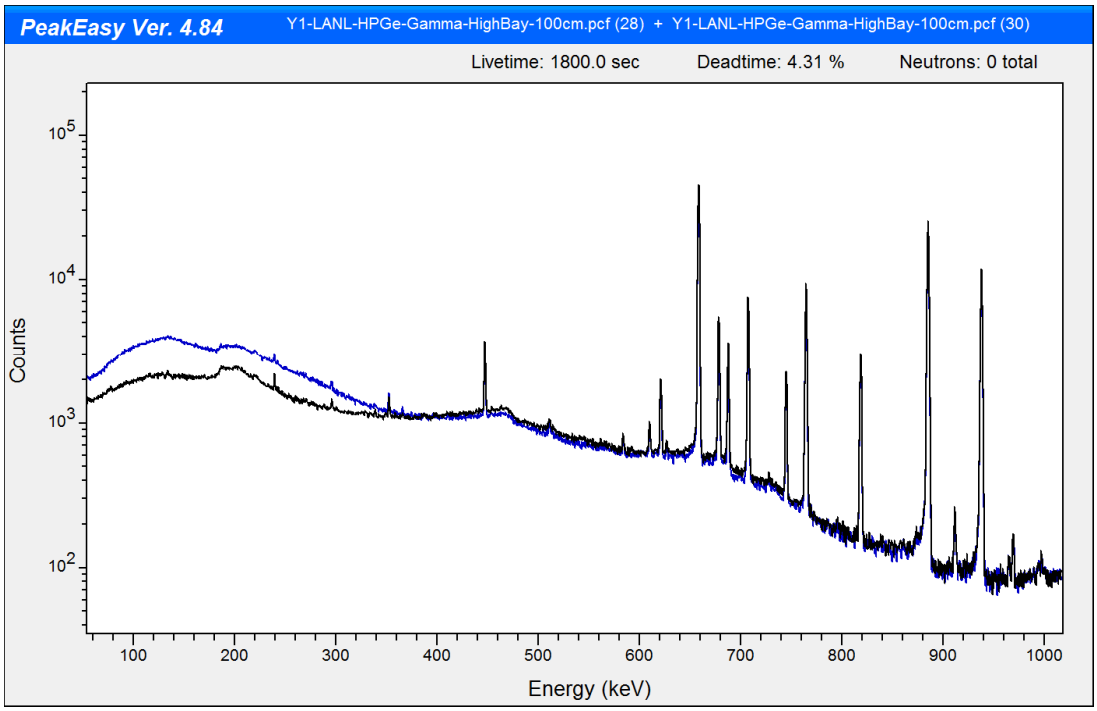


***Figure 6-18. HPGe spectra, Ag-110m_Unshielded (black), Ag-110m_Unshielded_HighScatter (blue).***

## 6.8 Neutron interactions on germanium

Fast neutron inelastic scatter interactions on germanium can produce "ski-slope" or "saw tooth" peak structures in HPGe spectra (Figure 6-19). The asymmetric peak structures are one sided "because the recoiling Ge atom is inside the detector, and thus all of the recoil energy is added to the transition energy regardless of the direction of the recoil." [16]

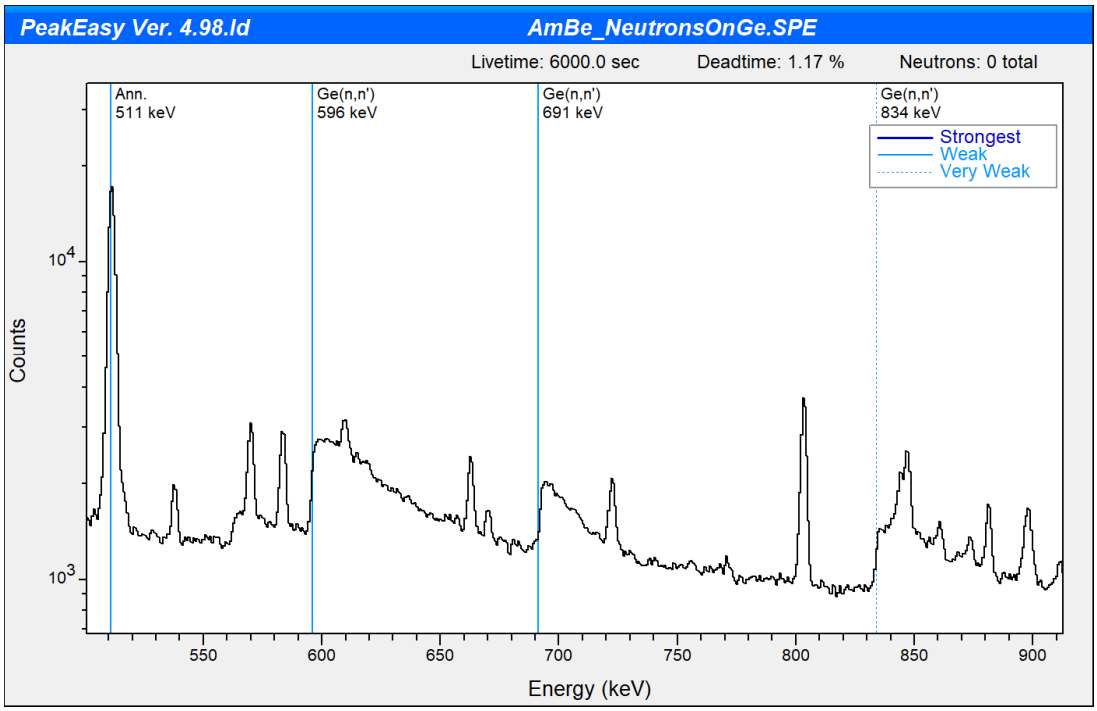


***Figure 6-19. Fast neutron inelastic scatter interactions on germanium at 596.0, 691.3, and 834.0 keV.***

In addition, full-energy peaks may be observed in HPGe spectra from germanium thermal neutron capture reactions (Figure 6-20).

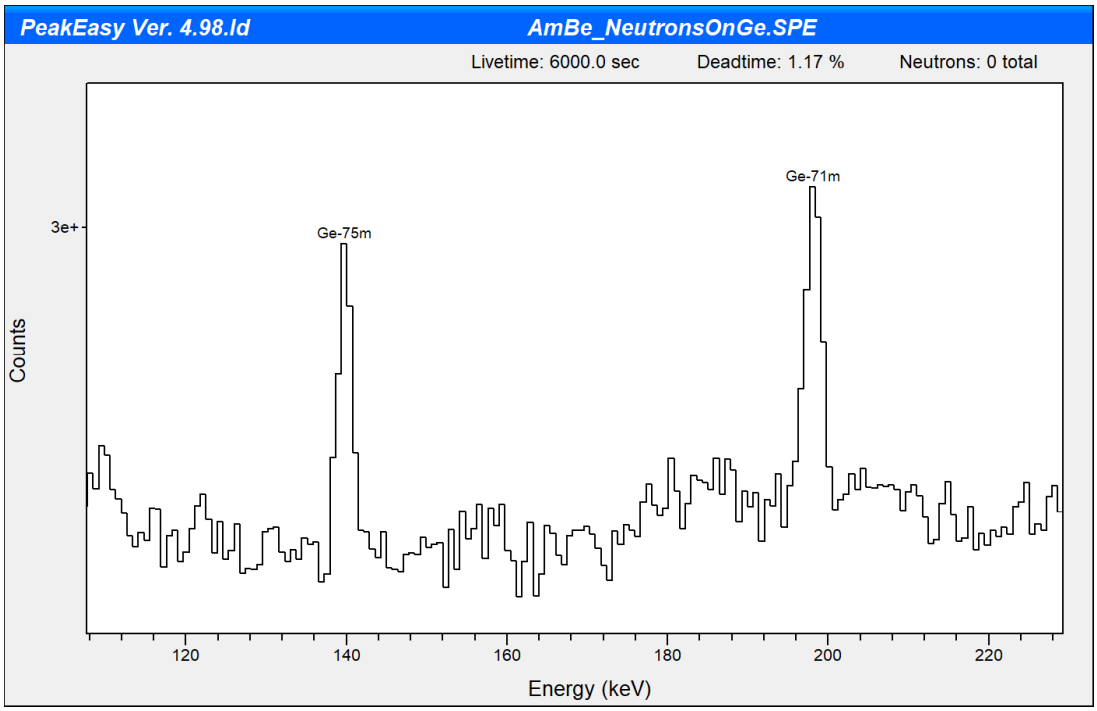


***Figure 6-20. Germanium thermal neutron capture full-energy peaks at 139.7 keV from Ge-74(n,γ)Ge-75m and 198.4 keV from (Ge-70(n,γ)Ge-71m.***

These germanium neutron interactions can be observed in spectra associated with measurement of neutron sources or measurements conducted with long count times (which allow detection of neutrons interactions on germanium from cosmic radiation).

For more detailed information on neutron interactions on germanium, please refer to Section 13.4.6 in Reference [2] and References [16] and [17].

# SECTION 7.0 DECISION LIMITS, STATISTICAL INTERVALS, ERROR PROPAGATION, AND GENERAL COUNTING STATISTICS CONCEPTS

## Table of Contents



## Figures



## Tables



## Equations

## 7.1 Basics

Using Poisson statistics, the variance is equal to the mean and the standard deviation is equal to the square root of the mean.

### *7.1.1 Example*

A radioactive sample is counted for 3 minutes and 55 counts are recorded. Calculate the count rate (CR) and standard deviation (σ)?

CR = 55 counts / 3 minutes = 18.3 cpm

σ = (55 counts)$^{1/2}$ / 3 minutes = 2.5 cpm

## 7.2 Decision limits

The critical level (Lc) and detection limit (Ld) are commonly used decision limits. The critical level (Lc) is used to determine whether the counts or activity *measured* are significant and the detection limit (Ld) is used to determine the minimum number of counts or minimum activity needed to be confident of detection in a sample with similar properties.

## 7.3 Decision limit equations

**Equation 7-1. Decision limit background.**

$$\boldsymbol{B = C_B \cdot T_s}$$

**Equation 7-2. Critical level.**

$$\boldsymbol{Lc = k \cdot \sqrt{2 \cdot B} = 1.645 \cdot \sqrt{2 \cdot B} \approx 2.33 \cdot \sqrt{B}}$$

**Equation 7-3. Detection limit.**

$$\boldsymbol{Ld = 2 \cdot Lc = 4.66 \cdot \sqrt{B}}$$

Where:
$B$ = Background (counts);
$C_B$ = Background count rate (counts per second);
$T_s$ = Live time (seconds);
$Lc$ = Critical level (counts);
$k$ = Confidence level and 1.645 represents a one-sided 95% confidence level;
$Ld$ = Detection limit (counts).

- Note: Background is equal to $2.38 \cdot FWHM$ where $2.38 \cdot FWHM$ is the coverage factor for 99.5% of the whole full-energy peak area.

Based on review of the critical level (Lc) and detection limit (Ld) equations, count rate and activity decision limits decrease with the square root of count time assuming a constant background. Therefore, increasing the count time by a factor or four will reduce the decision limit by a factor of two.

### 7.3.1 Example

A background sample of 500-grams of water is collected in a container and measured for 600-seconds with an ORTEC Detective EX-100 at 5-cm from the detector face (Figure 7-1). Estimate the detection limit (Ld) for Ag-110m at 657.8 keV given the following information.

- The absolute full-energy peak (FEP) efficiency at 657.8 keV is 9.25E-03 counts / gamma
- The full width at half maximum (FWHM) at 657.8 keV is ≈ 1.75 keV.
- The Ag-110m gamma yield at 657.8 keV is 0.94 gammas/disintegration.

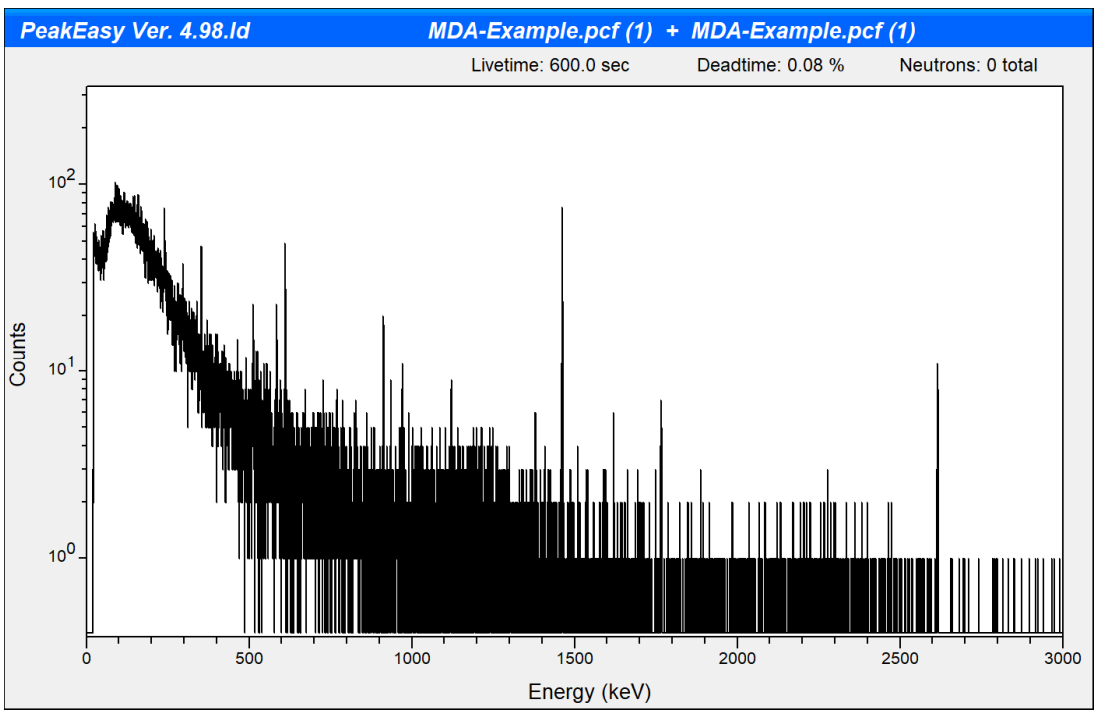


***Figure 7-1. Background water sample spectrum.***

Calculated detection limit (Ld): Counts

- Using a typical EX-100 FWHM at 657.8 keV of ≈ 1.75 keV, the background ROI (2.38 FWHM) is 655.7 keV to 659.7 keV which corresponds to ≈ 26 counts (Figure 7-2).
- $Ld = 4.66 \times (26 \text{ counts})^{1/2} = 23.8$ counts

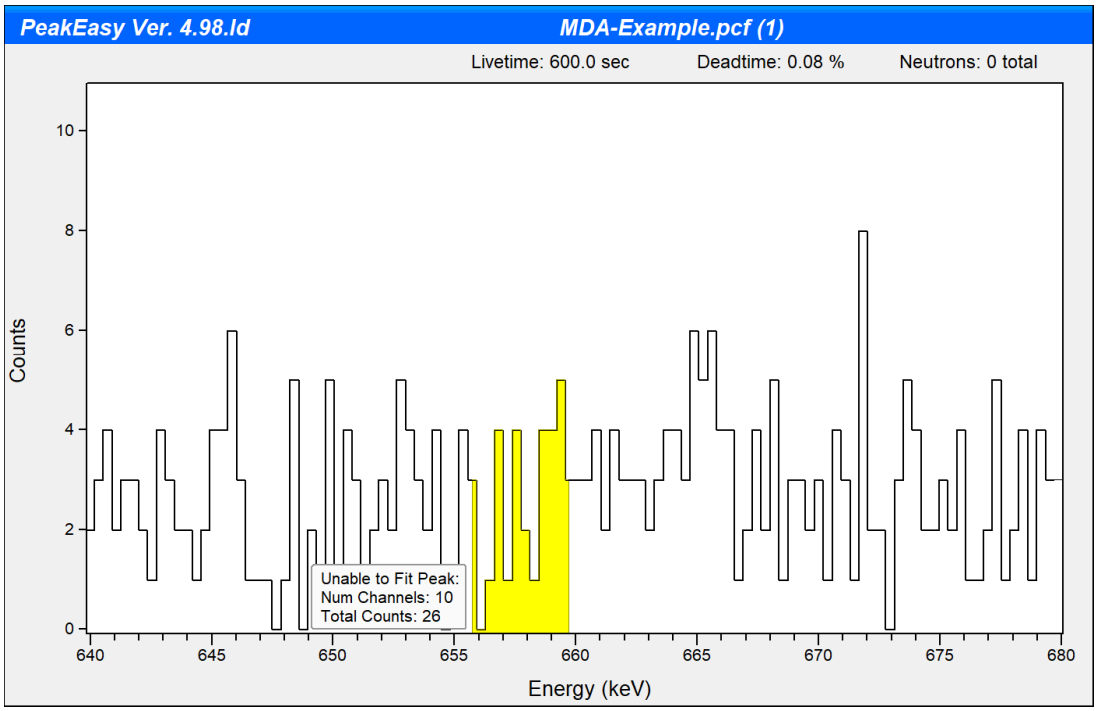


***Figure 7-2. 657.8 keV background water sample spectrum ROI determination.***

Calculated detection limit (Ld): Converted to activity

- Ld = (23.8 counts / 600 seconds) × (gammas / 9.25E-03 counts) × (disintegration / 0.94 gammas) / (3.7E+01 nCi/Bq) = 0.12 nCi
- Ld converted to activity = 0.12 nCi

The spectrum in Figure 7-3 includes the addition of 0.12 nCi Ag-110m to the background sample spectrum using the Gamma Detector Response and Analysis Software (GADRAS) synthetic spectrum inject tool.

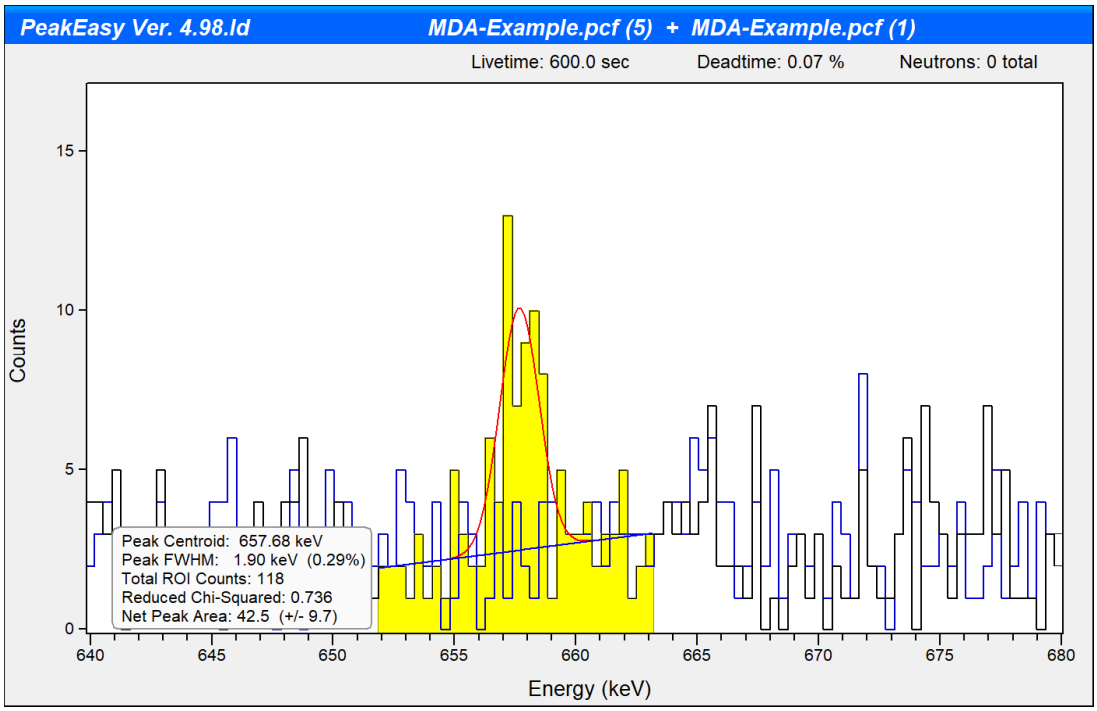


***Figure 7-3. Addition of 0.12 nCi Ag-110m to the background water sample spectrum using GADRAS.***

## 7.4 Statistical intervals and decision limit reporting

If a derived confidence interval contains zero, there is insufficient evidence to conclude that the sample result is above background. Conversely, if the derived confidence interval is above zero, there is sufficient evidence to conclude that the sample result is above background.

Accordingly, if the sample counts, count rate, or activity measured are greater than the critical level (Lc), the result is considered positive and the two-sided confidence interval should be reported. If the sample counts, count rate, or activity measured are less than the critical level (Lc), there is insufficient evidence to conclude that the sample result is above zero and the result should be reported as less than the calculated critical level (Lc).

### *7.4.1 Example A*

Ba-133 is measured 2.1 pCi/g ± 0.9 pCi/g at 1-sigma. How should the measurement result be reported using a two-sided 95% confidence interval (see Table 7-1).

***Table 7-1. Relationship between uncertainty (sigma) and 2-sided confidence interval coverage.***

| Sigma | 2-Sided CI Coverage |
|---|---|
| 1.000 | 68.3% |
| 1.282 | 80.0% |
| 1.645 | 90.0% |
| 1.960 | 95.0% |
| 2.000 | 95.4% |
| 3.000 | 99.7% |

- Since 1.96-sigma corresponds to a two-sided 95% confidence interval, the confidence interval exceeds zero (0.3, 3.9) and Ba-133 is reported as 2.1 pCi/g ± 0.9 pCi/g.

### *7.4.2 Example B*

Co-57 is measured 1.5 pCi/g ± 0.8 pCi/g at 1-sigma. How should the measurement result be reported using a two-sided 95% confidence interval?

- Since 1.96-sigma corresponds to a two-sided 95% confidence interval, the confidence interval contains zero (-0.1, 3.1) and Co-57 is reported as < 3.1 pCi/g with 95% confidence.

For more information on decision limits, a good overview can be found in *Chapter 5* of Reference [2].

## 7.5 Error propagation

Gamma spectroscopists commonly use measurements results in conjunction with reference values to determine some quantity of interest. Since measurements results and reference values both have uncertainty associated with them, it is necessary for the spectroscopist to properly propagate these uncertainties to estimate the uncertainty for the quantity of interest.

When uncertainties are uncorrelated and random, uncertainties can be added using the square root of the sum of squares (aka, quadrature).

For standard error propagation involving addition or subtraction, the uncertainties add in quadrature as shown in Example C. [18]

### *7.5.1 Example C*

Given
$X \pm \Delta X = 5.0 \pm 1.5$
$Y \pm \Delta Y = 10.0 \pm 5.1$

Calculate $Z = X + Y$ and $\Delta Z = (\Delta X^2 + \Delta Y^2)^{1/2}$

$Z = 5.0 + 10.0 = 15.0$
$\Delta Z = (1.5^2 + 5.1^2)^{1/2} = 5.32$
$Z \pm \Delta Z = 15.0 \pm 5.32$

For standard error propagation involving multiplication or division, the fractional uncertainties add in quadrature as shown in Example D. [18]

### 7.5.2 Example D

Given
$X \pm \Delta X = 5.0 \pm 1.5$
$Y \pm \Delta Y = 10.0 \pm 5.1$

Calculate $Z = X \bullet Y$ and $\Delta Z / Z = [(\Delta X / X)^2 + (\Delta Y / Y)^2]^{1/2}$

$Z = 5.0 \bullet 10.0 = 50.00$
$\Delta Z / Z = [(1.5 / 5.0)^2 + (5.1 / 10.0)^2]^{1/2} = 0.592$
$Z \pm \Delta Z = 50.00 \pm 29.58$

To further simplify error propagation calculations, relative uncertainties are often added in quadrature to derive the relative uncertainty in the overall quantity of interest.

### 7.5.3 Example E

Assuming the following 1-sigma uncertainties associated with a gamma spectroscopy measurement, calculate the uncertainty associated with the measured activity in percent.

| Uncertainty Component Description | Uncertainty Component ID | 1-sigma uncertainty |
|---|---|---|
| Full-energy peak area | B | 10.00% |
| Efficiency calibration | C | 5.00% |
| Gamma yield | D | 0.33% |

$\Delta A / A = [ (\Delta B / B )^2 + (\Delta C / C )^2 + (\Delta D / D )^2 ]^{1/2}$
$\Delta A / A = [ (10.00\%)^2 + (5.00\%)^2 + (0.33\%)^2]^{1/2} = 11.2\ \%$

# SECTION 8.0 TYPICAL NUCLEAR REACTOR INVENTORIES

## Table of Contents



## Tables



## Equations

## 8.1 Introduction

FRMAC gamma spectroscopists should have a general understanding of fission product yield terminology and typical nuclear reactor inventories.

## 8.2 Fission product yield

Fission product yields are reported as independent or cumulative. The *independent fission yield* is the number of atoms of a specific radionuclide produced directly by a fission event (not via radioactive decay of the precursors) and the *cumulative fission yield* is the total number of atoms of a specific radionuclide produced directly by a fission event and via decay of precursors [19].

Detailed information for independent and cumulative fission yields as a function of neutron spectrum energy and fissionable nuclear material can be found in the in the *FRMAC Gamma Spectroscopist Electronic Library / FP_Yields*.

## 8.3 Fission product activity determination [20]

When fissions occur at a constant rate and when neutron absorption reactions in the fission product and its precursors can be neglected, the activity of a radionuclide with short-lived precursors can be evaluated using Equation 8-1.

**Equation 8-1. Fission product activity equation.**

$$\boldsymbol{A = F \cdot y \cdot (1 - \lambda \cdot t_r) \cdot e^{-\lambda \cdot t_c}}$$

Where:
$A$ = Radionuclide activity, Bq;
$F$ = Fission rate, fissions/second;
$y$ = Cumulative fission yield, atoms/fission;
$\lambda$ = Decay constant, seconds$^{-1}$;
$t_r$ = Irradiation time, seconds;
$t_c$ = Cooling time, seconds.

For complex scenarios, the RSICC computer code Oak Ridge Isotope Generation and Depletion (ORIGEN) is commonly used to perform radionuclide kinetics modeling of irradiated reactor fuels to predict radionuclide inventories post irradiation.

## 8.4 Activation product activity determination [21]

When neutron capture occurs at a constant rate (neutron fluence rate is constant) and when neutron capture reactions by the activation product can be neglected, the activity of an activation product can be evaluated using Equation 8-2. When performing activation product activity estimates, the two neutron energies of importance (thermal and resonance) should both be evaluated and summed.

**Equation 8-2. Activation product activity equation.**

$$\boldsymbol{A = N \cdot \Phi \cdot \sigma \left(1 - e^{-\lambda \cdot t_r}\right) \cdot e^{-\lambda \cdot t_c}}$$

Where:
$A$ = Activation product activity, Bq;
$N$ = Number of target radionuclide atoms, atoms;
$\Phi$ = Neutron fluence rate, neutrons per $cm^2$ • second;
$\sigma$ = Neutron capture cross section of the target radionuclide, $cm^2$;
$\lambda$ = Decay constant of the activation product, $seconds^{-1}$;
$t_r$ = Irradiation time, seconds;
$t_c$ = Cooling time, seconds.

## 8.5 Typical nuclear reactor inventories

Nuclear reactor inventories contain nuclear material, fission products, activation products, transuranic radionuclides, and tritium. The inventories can vary widely and are dependent on the nuclear material irradiated, the neutron spectrum energy, the irradiation history (length and power), and the time since removal. In addition, volatile (such as I-129 and I-131) and semi-volatile radionuclides (such as Cs-134, Cs-137, Ru-103, Ru-106, Te-125m, Te-127m, Te-129m) are subject to losses during sample collection, handling, and radiochemical processing [22].

Regardless, summary tables of typical fission and activation products, generated from neutron activation of the reactor coolant and impurities in the reactor coolant, are provided below.

- Note: Radionuclides with very low gamma emission yields or no gamma emissions are presented in red font.

***Table 8-1. Typical nuclear reactor long-lived fission products.***

| Parent Nuclide | Half Life T1/2 | Energy (keV) | Yield (gps/dps) | Thermal U-235 Cumulative FY (%) |
|---|---|---|---|---|
| Ce-141 | 32.51 d | 145.4 | 4.83E-01 | 5.850 |
| Ce-144 | 284.91 d | 133.5 | 1.11E-01 | 5.500 |
| Cs-134* | 2.06 y | 604.7 | 9.76E-01 | NA* |
| Cs-137 | 30.17 y | 661.7 | 8.47E-01 | 6.190 |
| Eu-155 | 4.76 y | 86.5 | 3.07E-01 | 0.032 |
| Pm-147 | 2.62 y | 121.2 | 2.85E-05 | 2.250 |
| Ru-103 | 39.26 d | 497.1 | 9.10E-01 | 3.030 |
| Ru-106 | 373.59 d | 511.9 | 2.04E-01 | 0.402 |
| Sb-125* | 2.76 y | 427.9 | 2.98E-01 | 0.034 |
| Te-125m* | 57.40 d | 109.3 | 2.74E-03 | 0.0077 |
| Sr-90 / Y-90* | 29.10 y / 2.67 d | --- | --- | 5.780 / 5.780 |
| Te-127m | 109.00 d | 57.6 | 5.02E-03 | 0.025 |
| Te-129m | 33.60 d | 695.9 | 3.07E-02 | 0.090 |
| Zr-95* | 64.03 d | 756.7 | 5.44E-01 | 6.500 |
| Nb-95* | 34.99 d | 765.8 | 9.98E-01 | 6.500 |

Adapted from Reference [23].
Cs-134 is produced from long nuclear reactor irradiations: Xe-133 (Half-life = 5.2 d, 6.70 FP-yield) → Cs-133(n,γ)Cs-134
Sb-125 → Te-125m activity ratio at transient equilibrium equals 1/0.245
Zr-95 → Nb-95 activity ratio at transient equilibrium equals 1/2.205
Sr-90 and Y-90 are pure beta emitters

***Table 8-2. Typical nuclear reactor noble gas and halogen products.***

| Parent Nuclide | Half Life T1/2 | Gamma Energy (keV) | Yield (gps/dps) | Thermal U-235 Cumulative FY (%) |
|---|---|---|---|---|
| Kr-85 | 10.78 y | 514.0 | 4.34E-03 | 0.283 |
| Kr-85m | 4.48 h | 151.2 | 7.50E-01 | 1.290 |
| Kr-87 | 76.30 m | 402.6 | 4.96E-01 | 2.560 |
| Kr-88 | 2.84 h | 2392.1 | 3.46E-01 | 3.550 |
| Kr-89 | 3.15 m | 220.9 | 2.01E-01 | 4.510 |
| Xe-133 | 5.25 d | 81.0 | 3.80E-01 | 6.700 |
| Xe-133m | 2.19 d | 233.2 | 1.00E-01 | 0.189 |
| Xe-135 | 9.14 h | 249.8 | 9.00E-01 | 6.540 |
| Xe-137 | 3.82 m | 455.5 | 3.12E-01 | 6.130 |
| Xe-138 | 14.08 m | 258.4 | 3.15E-01 | 6.300 |
| I-131 | 8.02 d | 364.5 | 8.17E-01 | 2.890 |
| I-132 | 2.30 h | 667.7 | 9.87E-01 | 4.310 |
| I-133 | 20.80 h | 529.9 | 8.70E-01 | 6.700 |
| I-134 | 52.50 m | 847.0 | 9.54E-01 | 7.830 |
| I-135 | 6.57 h | 1260.4 | 2.87E-01 | 6.280 |

Adapted from Reference [23].

***Table 8-3. Typical nuclear reactor coolant activation products.***

| Parent Nuclide | Half Life T1/2 | Energy (keV) | Yield (gps/dps) | Activation Reaction | Abundance (%) | Thermal X-Section (b) | Epithermal X-Section (b) | Fast X-Section (b) |
|---|---|---|---|---|---|---|---|---|
| Cr-51 | 27.70 d | 320.1 | 9.92E-02 | Cr-50(n,γ) | 4.35 | 16.00 | 0.68 | --- |
| Mn-54 | 312.03 d | 834.8 | 1.00E+00 | Fe-54(n,p) | 5.80 | --- | --- | 0.11 |
| Mn-56 | 2.58 h | 846.8 | 9.89E-01 | Mn-55(n,γ) | 100.00 | 13.30 | 1.13 | --- |
| Fe-55 | 2.74 y | 126.0 | 1.28E-09 | Fe-54(n,γ) | 5.80 | 2.50 | 0.10 | --- |
| Fe-59 | 44.50 d | 1099.3 | 5.65E-01 | Fe-58(n,γ) | 0.30 | 1.14 | 0.10 | --- |
| Co-58 | 70.86 d | 810.8 | 9.95E-01 | Ni-58(n,p) | 68.30 | --- | --- | 0.15 |
| Co-60 | 5.27 y | 1332.5 | 1.00E+00 | Co-59(n,γ) | 100.00 | 37.50 | 6.05 | --- |
| Ni-63* | 100.10 y | --- | --- | Ni-62(n,γ) | 3.60 | 14.60 | 0.77 | --- |
| Ni-65 | 2.52 h | 1481.8 | 2.36E-01 | Ni-64(n,γ) | 0.90 | 1.50 | 0.07 | --- |
| Cu-64 | 12.70 h | 1345.8 | 4.73E-03 | Cu-63(n,γ) | 69.20 | 4.40 | 0.40 | --- |
| Zn-65 | 244.06 d | 1115.5 | 5.06E-01 | Zn-64(n,γ) | 48.60 | 0.82 | 0.15 | --- |
| As-76 | 1.08 d | 559.1 | 4.50E-01 | As-75(n,γ) | 100.00 | 4.40 | 5.08 | --- |
| Zr-95 | 64.03 d | 756.7 | 5.44E-01 | Zr-94(n,γ) | 17.40 | 0.08 | 0.03 | --- |
| Ag-110m | 249.95 d | 657.8 | 9.43E-01 | Ag-109(n,γ) | 47.17 | 4.70 | --- | --- |
| Sn-113 | 115.09 d | 391.7 | 6.49E-01 | Sn-112(n,γ) | 1.01 | 0.71 | 2.20 | --- |

Adapted from Reference [23].
Ni-63 is a pure beta emitter

## 8.6 Decay correction to a reference date

It is commonly requested that fission product results be decay corrected to some specified reference date. For fission products with decay products in equilibrium at the decay correction date requested, proper assessment can generally be made by assigning the parent half-life to the decay product and performing decay correction using Equation 8-3.

**Equation 8-3. Radioactive decay equation.**

$$A = A_0 \cdot e^{-\lambda \cdot t}$$

Where:
$A$ = Radionuclide activity at time t;
$A_0$ = Radionuclide initial activity;
$\lambda$ = Radionuclide decay constant (days$^{-1}$);
$t$ = Time (days).

For fission products with decay products not in equilibrium at the decay correction date requested, additional information concerning the activity relationship of the parent and decay product is needed. For example, estimates of the parent and decay product activities at the time of a nuclear power plant release may be available. Alternatively, a second count may be performed, and results compared with

the first count to potentially provide useful information on the parent to decay product activity relationship.

Table 8-4 presents useful information on several fission product parent-decay product pairs commonly encountered including the decay product to parent equilibrium activity ratio and the approximate time to reach equilibrium. In addition, Table 8-5 lists the primary gamma emission from each parent-decay product pair presented in Table 8-4.

***Table 8-4. Fission product parent-decay product pairs commonly encountered.***

| Parent/Decay Product | Decay Product to Parent Equilibrium Activity Ratio | Approx. Equilibrium Time (Set to 5 half-lives / 96.9% equilibrium) |
|---|---|---|
| Te-132 (3.2 d) → I-132 (2.3 h) | 1.031 | 11.5 h |
| Ba-140 (12.8 d) → La-140 (1.7 d) | 1.151 | 8.4 d |
| Ce-144 (284.9 d) → Pr-144 (17.3 m) | 1.000 | 86.4 m |
| Mo-99 (65.9 h) → Tc-99m (6.0 h) | 0.965 | 30.1 h |
| Ru-106 (373.6 d) → Rh-106 (29.8 s) | 1.000 | 149.0 s |
| Zr-95 (64.0 d) → Nb-95 (35.0 d) | 2.205 | 175.0 d |
| Zr-95 (64.0 d) → Nb-95m (3.6 d) | 0.0120 | 18.1 d |

Mo-99 (65.9 h, BR = 0.8773) → Tc-99m (6.0 h)
Zr-95 (64.0 d, BR 0.0108) -> Nb-95m (3.6 d, BR 0.944)

***Table 8-5. Fission product parent-decay product pairs primary gamma emissions.***

| Nuclide | Energy (keV) | Yield (gps/dps) |
|---|---|---|
| Te-132 | 228.2 | 8.80E-01 |
| I-132 | 667.7 | 9.87E-01 |
| Ba-140 | 537.3 | 2.44E-01 |
| La-140 | 1596.2 | 9.54E-01 |
| Ce-144 | 133.5 | 1.11E-01 |
| Pr-144 | 696.5 | 1.34E-02 |

| Nuclide | Energy (keV) | Yield (gps/dps) |
|---|---|---|
| Mo-99 | 739.5 | 1.21E-01 |
| Tc-99m | 140.5 | 8.91E-01 |
| Ru-106 | --- | --- |
| Rh-106 | 511.9 | 2.04E-01 |
| Zr-95 | 756.7 | 5.44E-01 |
| Nb-95 | 765.8 | 9.98E-01 |
| Nb-95m | 235.7 | 2.44E-01 |

# SECTION 9.0 SELF-ATTENUATION AND INFINITE THICKNESS

## Table of Contents



## Figures



## Tables

## 9.1 Introduction

Dense materials (uranium, thorium, plutonium, neptunium, americium, etc.) are very good at self-attenuating their gamma emissions. Therefore, high yield, low energy gamma emissions may be significantly reduced or not detected in gamma spectroscopy measurements performed on dense materials. If high yield, low energy gamma emissions are detected from dense materials, such as the 92.6 and 63.3 keV gamma emissions from the U-238 decay chain, then the material is likely unshielded or lightly shielded.

When dense radioactive materials reach infinite thickness (the thickness needed to reduce transmission to 0.1%), the outer layers of the dense radioactive material essentially shield all gamma emissions from inner layers of the dense radioactive material. This eliminates the ability to perform accurate activity and/or mass estimates unless additional information is known about the sample geometry and/or composition. However, in some instances, it may be possible to provide surface area estimates from gamma ray spectra.

For reference purposes, Table 9-1 presents thicknesses for 1% and 0.1% transmission for primary emissions from U-235, U-238, U-232, and Pu-239 in uranium and plutonium metal, respectively.

***Table 9-1. Thicknesses for 1% and 0.1% transmission for primary emissions from U-235, U-238, U-232, and Pu-239.***

| Decay Chain Parent radionuclide | Gamma Energy (keV) | Density (g/cc) | 1% Transmission Thickness (mm) | 0.1% Transmission Thickness (mm) |
|---|---|---|---|---|
| U-235 | 185.7 | 18.70 | 1.6 | 2.4 |
| U-238 | 1001.0 | 18.70 | 32.6 | 48.8 |
| U-232 | 583.2 | 18.70 | 16.7 | 25 |
| U-232 | 2614.5 | 18.70 | 54.7 | 82 |
| Pu-239 | 129.3 | 19.65 | 0.62 | 0.94 |
| Pu-239 | 413.7 | 19.65 | 8.4 | 12.6 |

- Note: For self-attenuation correction equations for slabs and spheres, see SECTION 16.0.

### *9.1.1 Example*

Consider the following dense radioactive material scenario shown in Figure 9-1. In this scenario, the uranium is sufficiently thick in both samples that infinite thickness has been established for U-235 low energy emissions. Accordingly, the spectra collected from the samples will be essentially the same for low energy emissions (see Figure 9-2).

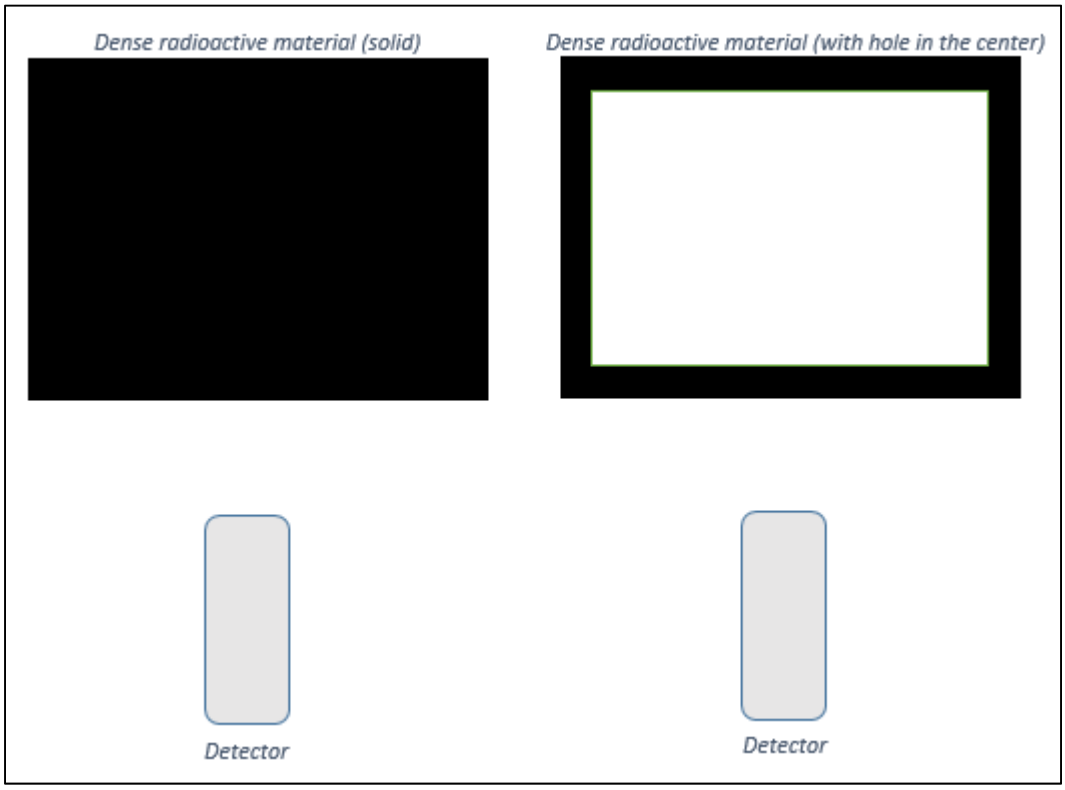


***Figure 9-1. 5 x 5 x 5-cm rectangular volume of uranium without hole (2369-g) and with hole (642-g).***

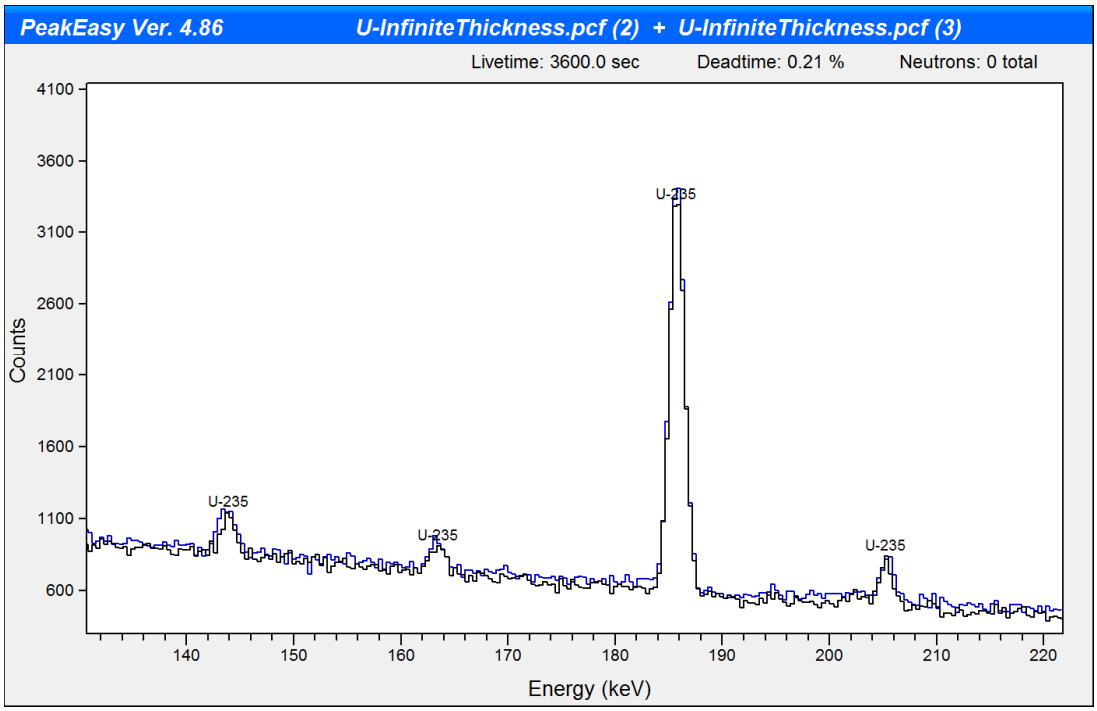


***Figure 9-2. Spectra of 5 x 5 x 5-cm rectangular volume of uranium without hole (2369-g) Dark blue, and with hole (642-g), Black.***

# SECTION 10.0 DIFFERENTIAL ATTENUATION PEAK ANALYSIS

## Table of Contents



## Figures



## Tables

## 10.1 Introduction

Differential peak analysis utilizes the difference in attenuation suffered by gamma rays of different energies from the same radionuclide to estimate the effective matrix density and thickness. To assist in understanding the concept of differential attenuation analysis, the following example is presented.

- Note: Attenuation correction equations for shield and self-attenuation can be found in SECTION 16.0.

### *10.1.1 Example*

A 1000 second measurement with an ORTEC Detective EX-100 is performed on an Eu-152 source of unknown activity in a steel container of unknown thickness at 25-cm from the detector endcap to the center of the container (see the spectrum presented in Figure 10-1). Assuming the Eu-152 source is in the center of the container; estimate the thickness of steel and the Eu-152 activity.

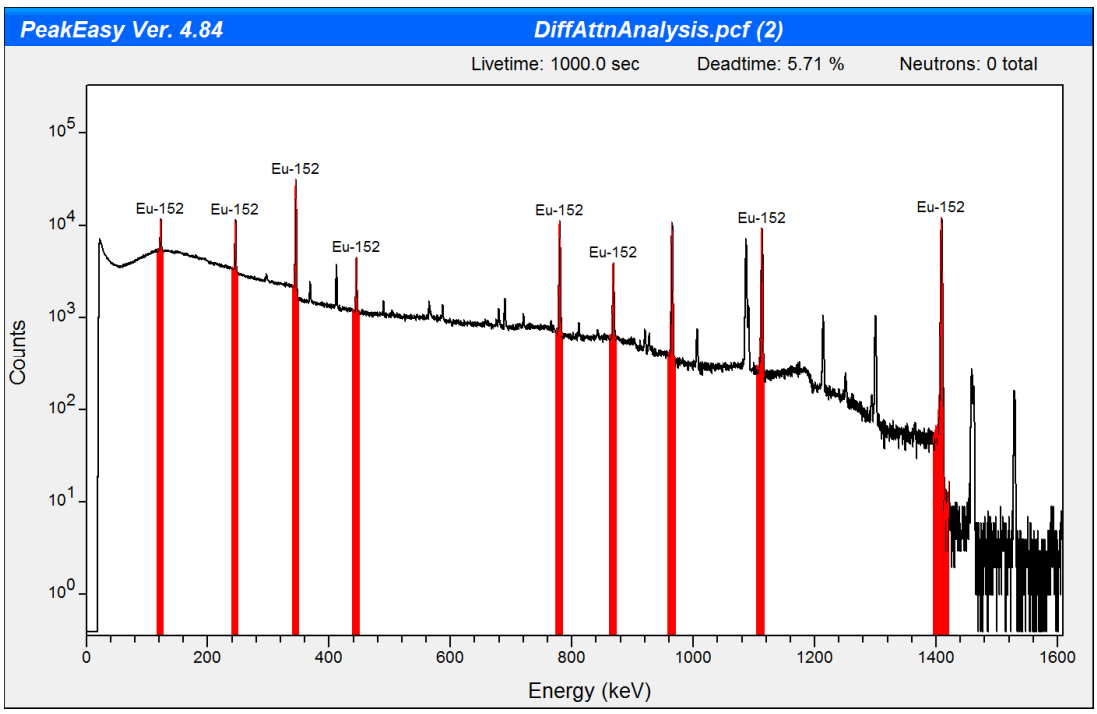


***Figure 10-1. Differential attenuation peak analysis example: Shielded Eu-152 spectrum.***

Assuming the thickness of steel is 1-cm and 3-cm, respectively, the following activities presented in Table 10-1 are calculated.

***Table 10-1. Differential attenuation full-energy peak analysis example: Shielded Eu-152 calculations not optimized.***

| | | | 1-cm Fe | 3-cm Fe |
|---|---|---|---|---|
| Nuclide | Energy (keV) | Net Area (counts) | Activity (µCi) | Activity (µCi) |
| Eu-152 | 244.7 | 41088 | 23 | 164 |
| Eu-152 | 344.3 | 151578 | 25 | 126 |
| Eu-152 | 444.0 | 17336 | 27 | 109 |
| Eu-152 | 778.9 | 56889 | 27 | 79 |
| Eu-152 | 867.4 | 18300 | 28 | 77 |
| Eu-152 | 964.1 | 61214 | 29 | 75 |
| Eu-152 | 1112.1 | 54758 | 30 | 74 |
| Eu-152 | 1408.0 | 79696 | 33 | 73 |

Based on differential attenuation analysis, 1-cm provides too little attenuation, since estimated activities are increasing with energy, and 3-cm provides too much attenuation, since estimated activities are decreasing with energy. Accordingly, the thickness of steel is optimized until the calculated activities at the different energies are approximately equal (Table 10-2).

***Table 10-2. Differential attenuation full-energy peak analysis example: Shielded Eu-152 calculations optimized.***

| | | | 1.7-cm Fe |
|---|---|---|---|
| Nuclide | Energy (keV) | Net Area (counts) | Activity (µCi) |
| Eu-152 | 244.7 | 41088 | 46 |
| Eu-152 | 344.3 | 151578 | 45 |
| Eu-152 | 444.0 | 17336 | 43 |
| Eu-152 | 778.9 | 56889 | 39 |
| Eu-152 | 867.4 | 18300 | 40 |
| Eu-152 | 964.1 | 61214 | 40 |
| Eu-152 | 1112.1 | 54758 | 41 |
| Eu-152 | 1408.0 | 79696 | 44 |

Actual Eu-152 activity = 50 µCi, Thickness of the iron container = 1.9-cm

- Note: Calculations were performed with SimpleMass.xls, a Los Alamos National Laboratory (LANL) EXCEL and Visual Basic application for full-energy peak analysis of shielded and unshielded point sources.

## 10.2 Additional information

As shown in Figure 10-2, normalized mass attenuation coefficients values are nearly independent of material between 150 and 3000 keV for several common materials including: aluminum (Al), carbon (C), concrete, water, cellulose ($C_6H_{10}O_5$), plastics ($CH_2$), glass ($SiO_2$), soil, and air.

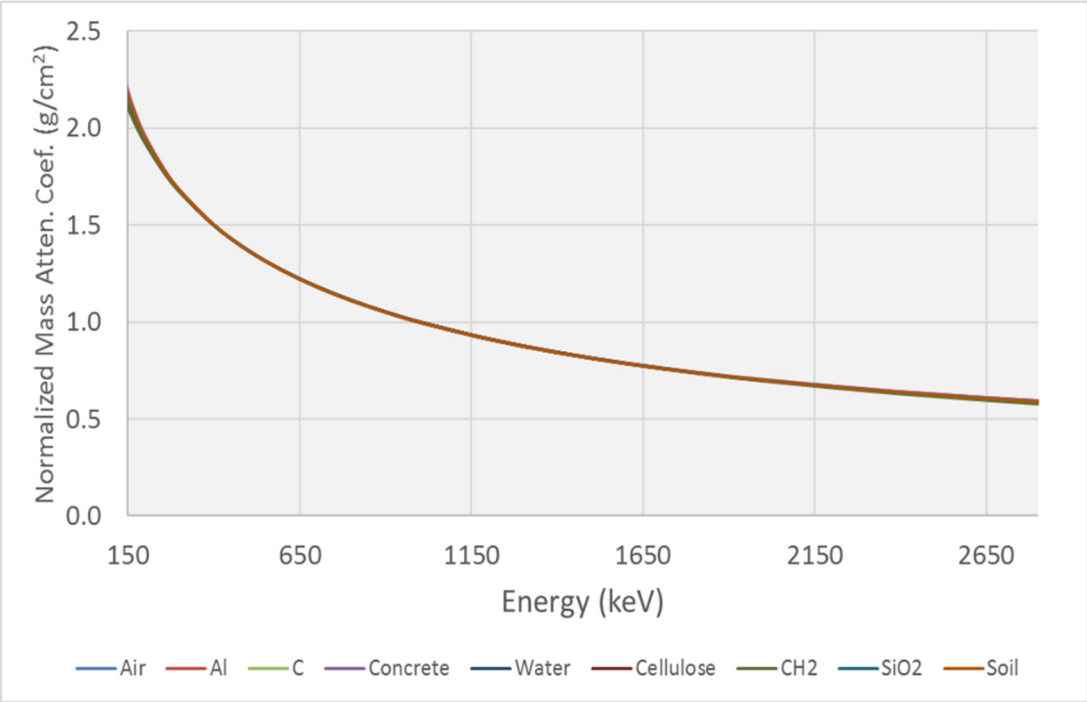


***Figure 10-2. Mass attenuation coefficients normalized to 1 MeV for each material (150 to 2800 keV).***

Between roughly 500 to 2000 keV, iron (Fe), copper (Cu), and nickel (Ni) can be added to the list (see Figure 10-3).

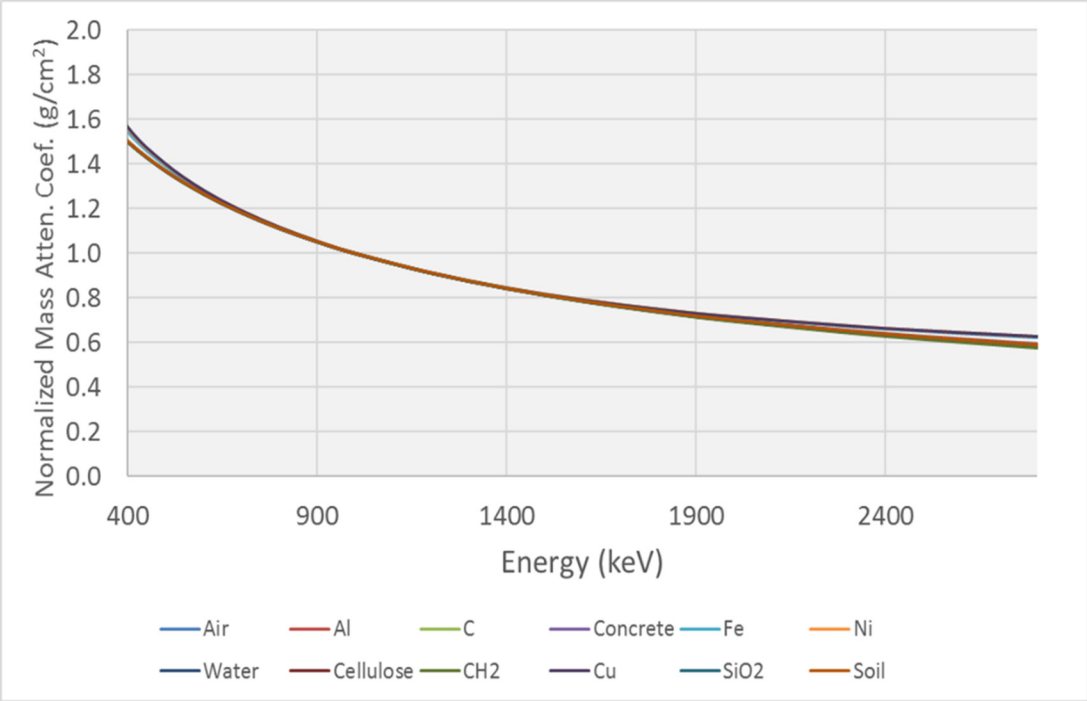


***Figure 10-3. Mass attenuation coefficients normalized to 1 MeV for each material (400 to 2800 keV).***

In these instances, the "correct" activity can be estimated, but not the "correct" shield thickness, using the "wrong" material (see Table 10-3).

***Table 10-3. Eu-152 activity estimates optimized using various shield materials.***

| Material | Activity Estimate (µCi) | % Error |
|---|---|---|
| Fe | 45 | -10% |
| Al | 49 | -2% |
| Concrete | 48 | -4% |
| Water | 49 | -3% |
| Cellulose | 49 | -2% |
| $CH_2$ | 50 | 0% |
| $SiO_2$ | 48 | -4% |
| Soil | 48 | -4% |
| Air | 50 | 0% |
| Cu | 43 | -14% |
| Ni | 45 | -10% |

Actual Eu-152 activity = 50 µCi, Thickness of the iron container = 1.9-cm
Eu-152 activity estimates performed using the following gamma emissions: 444.0, 778.9, 867.4, 964.1, 1112.1, 1408.0 keV

# SECTION 11.0 ENVIRONMENTAL IN-SITU GAMMA SPECTROSCOPY [24]

## Table of Contents



## Figures



## Tables



## Equations

## 11.1 Introduction

In-situ gamma spectroscopy is used for rapid assessment of environmental radioactive contamination or environmental radioactivity including radionuclide specific quantification. Typically, measurements utilize a downward facing HPGe detector at a height of 1-meter above the ground.

***Figure 11-1. ORTEC Detective HPGe in-situ gamma spectroscopy measurement.***

## 11.2 Radionuclide depth distribution models

In general, three different radionuclide depth distributions are used to model environmental radioactivity.

- Surface: Radioactivity is uniformly distributed on the surface of the ground.
- Uniform: Radioactivity is uniformly distributed in the soil as a function of depth.
- Exponential: Radioactivity is exponentially distributed in the soil as a function of depth (Equation 11-1).

**Equation 11-1. Exponential radionuclide depth distribution equation.**

$$S_z = S_0 \cdot e^{-\frac{\alpha}{\rho}\cdot\rho\cdot z}$$

Where:
$S_z$ = Activity at depth z;
$S_o$= Activity at the surface;
$\frac{\alpha}{\rho}$ = Depth distribution parameter ($cm^2/g$);
$\rho$ = Density of the soil ($g/cm^3$);
$z$ = Soil depth (cm).

As shown in Equation 11-1, the exponential model is defined using the *mass depth* (relaxation mass per unit area or 1/(α/ρ)), which depends upon the *relaxation length* (1/α) and the density (ρ) of the soil. The *relaxation length* (1/α) is equivalent to the soil depth at which 63.2% of the activity is contained above. Therefore, small relaxation lengths represent radioactivity deposited near the soil surface and large relaxation lengths represent radioactivity distributed further into the soil.

- Note: For exponential model results, the activity concentration reported represents the activity per unit surface area for the entire column of soil.
- Note: For radionuclides which emit multiple gamma emissions over a broad energy range, differential attenuation may be used to infer or estimate the exponential radionuclide depth distribution *relaxation length* (1/α).

### *11.2.1 Example*

A *relaxation length* (1/α) of 10-cm indicates that the radioactivity has penetrated the soil to the extent that 63.2% of the activity is contained within the first 10-cm of soil.

## 11.3 Detector field of view

The detector field of view (FOV) is defined as the circular radius corresponding to 95% contribution of the unattenuated gamma flux. The FOV as a function of photon energy and radionuclide depth distribution for measurements conducted at 1-meter above the ground is shown in Table 11-1.

***Table 11-1. Radial detector field of view as a function of photon energy and radionuclide depth distribution at 1-meter.***

| 1/α | Surface (0) | 0.1 | 1 | 1.25 | 2 | 3 | 5 | 10 | 12.5 | 15 | Uniform (∞) |
|---|---|---|---|---|---|---|---|---|---|---|---|
| α/ρ | ∞ | 6.25 | 0.625 | 0.5 | 0.3125 | 0.2083 | 0.125 | 0.0625 | 0.05 | 0.0417 | 0 |

| Energy (keV) | FOV (m) | FOV (m) | FOV (m) | FOV (m) | FOV (m) | FOV (m) | FOV (m) | FOV (m) | FOV (m) | FOV (m) | FOV (m) |
|---|---|---|---|---|---|---|---|---|---|---|---|
| 60 | 55.9 | 32.6 | 17.5 | 16.6 | 15.0 | 14.0 | 13.0 | 12.0 | 11.7 | 11.4 | 11.1 |
| 80 | 60.6 | 36.8 | 19.4 | 18.3 | 16.4 | 15.2 | 13.9 | 12.7 | 12.4 | 12.1 | 11.4 |
| 100 | 63.8 | 39.4 | 20.6 | 19.4 | 17.3 | 15.9 | 14.5 | 13.2 | 12.8 | 12.5 | 11.6 |
| 150 | 70.2 | 43.8 | 22.5 | 21.1 | 18.7 | 17.0 | 15.4 | 13.9 | 13.4 | 13.1 | 11.9 |
| 200 | 75.6 | 47.2 | 24.0 | 22.4 | 19.7 | 17.9 | 16.1 | 14.4 | 13.9 | 13.6 | 12.1 |
| 300 | 85.2 | 53.1 | 26.4 | 24.6 | 21.5 | 19.3 | 17.2 | 15.2 | 14.7 | 14.3 | 12.4 |
| 400 | 93.5 | 58.1 | 28.4 | 26.5 | 23.0 | 20.5 | 18.2 | 15.9 | 15.4 | 14.9 | 12.7 |
| 500 | 101.1 | 62.6 | 30.3 | 28.1 | 24.3 | 21.6 | 19.0 | 16.5 | 15.9 | 15.5 | 12.9 |
| 600 | 108.1 | 66.8 | 32.0 | 29.6 | 25.5 | 22.6 | 19.8 | 17.1 | 16.4 | 15.9 | 13.0 |
| 800 | 120.8 | 74.5 | 35.0 | 32.4 | 27.6 | 24.3 | 21.1 | 18.0 | 17.3 | 16.7 | 13.3 |
| 1000 | 132.5 | 81.4 | 37.7 | 34.8 | 29.6 | 25.9 | 22.3 | 18.9 | 18.0 | 17.4 | 13.5 |
| 1200 | 143.2 | 87.9 | 40.3 | 37.1 | 31.3 | 27.3 | 23.4 | 19.6 | 18.7 | 18.0 | 13.7 |
| 1400 | 153.4 | 94.1 | 42.6 | 39.2 | 33.0 | 28.7 | 24.4 | 20.3 | 19.3 | 18.6 | 13.8 |
| 1600 | 162.9 | 99.9 | 44.8 | 41.2 | 34.5 | 29.9 | 25.3 | 20.9 | 19.9 | 19.1 | 13.9 |
| 2000 | 180.7 | 110.5 | 48.9 | 44.8 | 37.3 | 32.1 | 27.0 | 22.1 | 20.9 | 20.0 | 14.1 |
| 2400 | 197.0 | 120.3 | 52.5 | 48.0 | 39.8 | 34.1 | 28.5 | 23.1 | 21.8 | 20.8 | 14.3 |
| 2800 | 211.4 | 128.9 | 55.7 | 50.9 | 42.0 | 35.9 | 29.8 | 24.0 | 22.6 | 21.5 | 14.4 |

1/α = Relaxation Length (cm)
α/ρ = Source depth parameter ($cm^2/g$)

Similarly, the FOV at 1-meter for surface and uniform radionuclide distributions are shown in Figure 11-2 and Figure 11-3, respectively, for gamma emissions at 100, 500, 1000, and 2000 keV.

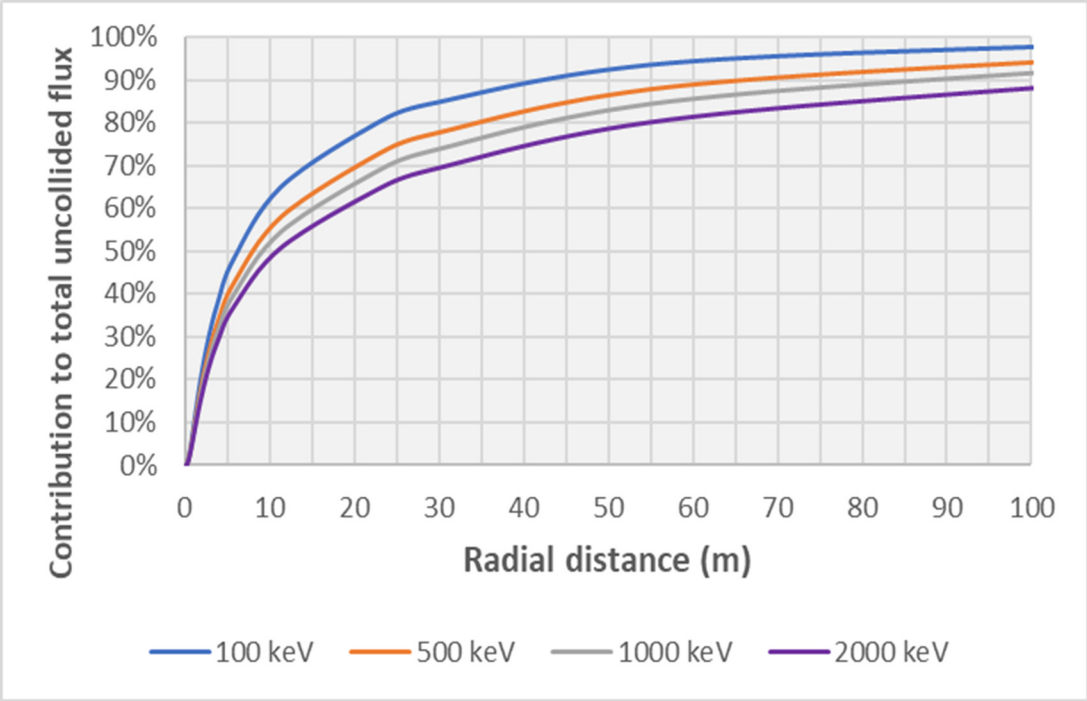


***Figure 11-2. Field of view at 1-meter: Surface radionuclide distribution.***

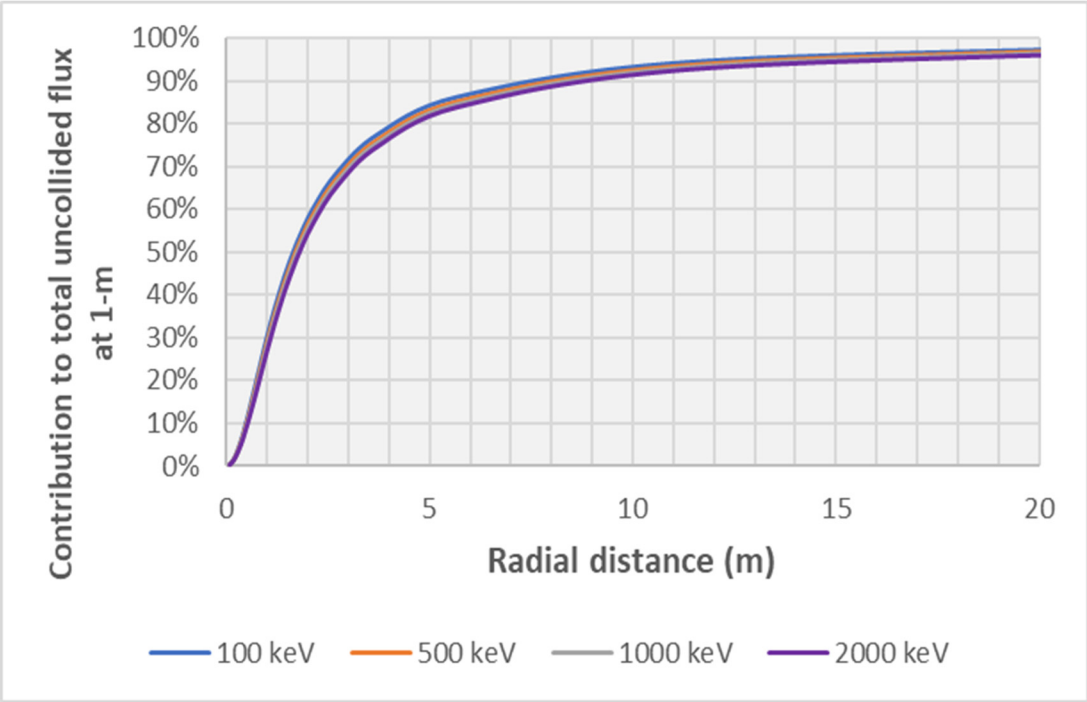


***Figure 11-3. Field of view at 1-meter: Uniform radionuclide depth distribution.***

## 11.4 Theory / methodology

The Environmental Measurements Laboratory (EML), formerly Health and Safety Laboratory (HASL), established the following methodology in the 1960s/1970s [25] [26] which is commonly used today.

**Equation 11-2. Environmental in-situ gamma spectroscopy equation.**

$$\frac{N_f}{A} = \left(\frac{N_0}{\Phi}\right) \cdot \left(\frac{N_f}{N_0}\right) \cdot \left(\frac{\Phi}{A}\right)$$

Where:

$\frac{\Phi}{A}$= Detector full-energy peak (FEP) count rate per unit concentration for a given radionuclide depth distribution = cps / (Bq/cm$^2$) or cps / (Bq/g)

$\frac{N_0}{\Phi}$ = Detector FEP efficiency at normal incidence = cps / (γ/cm$^2$ • s)

- Requires measurement of "bare" calibration sources or a "bare" multinuclide calibration source that spans the energy range of interest.
- This is the "traditional" absolute efficiency divided by $4\pi \cdot r^2$, where r is the distance to the effective detector crystal center.

$\frac{N_f}{N_0}$ = Detector FEP efficiency angular correction factor for a given radionuclide depth distribution = Unitless

- Dependent on detector angular response and geometry (radionuclide depth distribution and measurement height).
- Requires measurement of "bare" calibration sources or a "bare" multinuclide calibration source that span the energy range of interest as a function of angle. Typically, 0, 15, 30, 45, 60, 75, and 90 degrees are used to determine the relative response to normal incidence (0 degrees).
- Requires determination of the relative unattenuated gamma flux as a function of angle for the chosen radionuclide depth distribution and measurement height.
- In lieu of performing measurements and calculating $N_f$ / $N_o$, pre-calculated tables at 1-meter have been published.

$\frac{\Phi}{A}$ = Unattenuated gamma flux at the detector per unit concentration for a given radionuclide depth distribution = (γ/cm$^2$ • s) / (Bq/cm$^2$) or (γ/cm$^2$ • s) / (Bq/g)

- Determination of Φ / A using 1st order exponential integral series expansion equations [27].

**Exponential**

$$\frac{\Phi}{A} = \frac{1}{2} S_0 \left\{ E_1(\mu_a h) - e^{\frac{\mu_a h}{\mu L}} E_1 \left[ \left( 1 + \frac{1}{\mu L} \right) \mu_a h \right] \right\}$$

**Uniform**

$$\frac{\Phi}{A} = \frac{1}{2} S_v \frac{\mu_a}{\mu} \left[ \frac{1}{\mu_a h} e^{-\mu_a h} - E_1(\mu_a h) \right]$$

**Plane**

$$\frac{\Phi}{A} = \frac{1}{2} S_0 E_1(\mu_a h)$$

**The function $E_1(x)$ is the 1st order exponential integral**

$$E_1(x) = \int_x^{\infty} \frac{e^{-t}}{t} dt \approx -\gamma - \ln x - \sum_{n=1}^{\infty} \frac{(-1)^n x^n}{n n!}, \gamma = 0.5772156649 \ldots$$

Where $S_o$ = Activity in soil column (Bq/m$^2$); $S_v$ = Uniform activity concentration (Bq/kg); $\mu_a$ = linear attenuation coefficient for air (1/cm); μ = linear attenuation coefficient for soil (1/cm); $L$ = relaxation length (cm); $h$ = Detector height (cm).

## 11.5 Use of pre-calculate $N_f$ / $N_o$ tables

Angular correction factors at 1-meter from 300 to 2500 keV as a function of HPGe crystal length/diameter (L/D) ratio (0.5 to 1.3), radionuclide depth distribution (surface or uniform), and detector orientation (downward or upward facing) have been published in Reference [28]. See *Appendix E. Nf / No, pre-calculated tables for downward facing HPGe detector at 1-meter,* reproduced from Reference [28].

Since $N_f$ / $N_o$ did not vary significantly for the two bounding radionuclide depth distributions (surface or uniform) at 1-meter, pre-calculated tables for $N_f$ / $N_o$ at 1-meter are semi-routinely to routinely used in environmental in-situ gamma spectroscopy calculations to simplify the process. However, pre-calculated table values should not be used under the following circumstances:

- Extrapolating pre-calculated table values for $N_f$ / $N_o$ at 1-meter for gamma emissions much below 300 keV is generally not recommended. In particular, the detector angular response can be very sensitive to the detector mounting cup / end cap materials and thicknesses for gamma emissions below 125 keV.

- Since pre-calculated table values for $N_f$ / $N_o$ are not available for distances other than 1-meter, pre-calculated tables for $N_f$ / $N_o$ should not be extrapolated to distances that are not close to 1-meter.

## 11.6 Common sources of error

- Incorrect radionuclide depth distribution modeled.
- Obstacles in the field of view (such as large structures or trees).
- Non-uniform surfaces in the field of view (such as roads, surfaces that are sloped – hill side, surface irregularities – ground roughness).
- Non-uniform radioactivity distribution (vertically or horizontally).
- Poor calibration measurements.
- Poor FEP counting statistics.
- Soil composition differences and use of low energy gamma emissions below roughly 100 to 125 keV (see Figure 11-4).

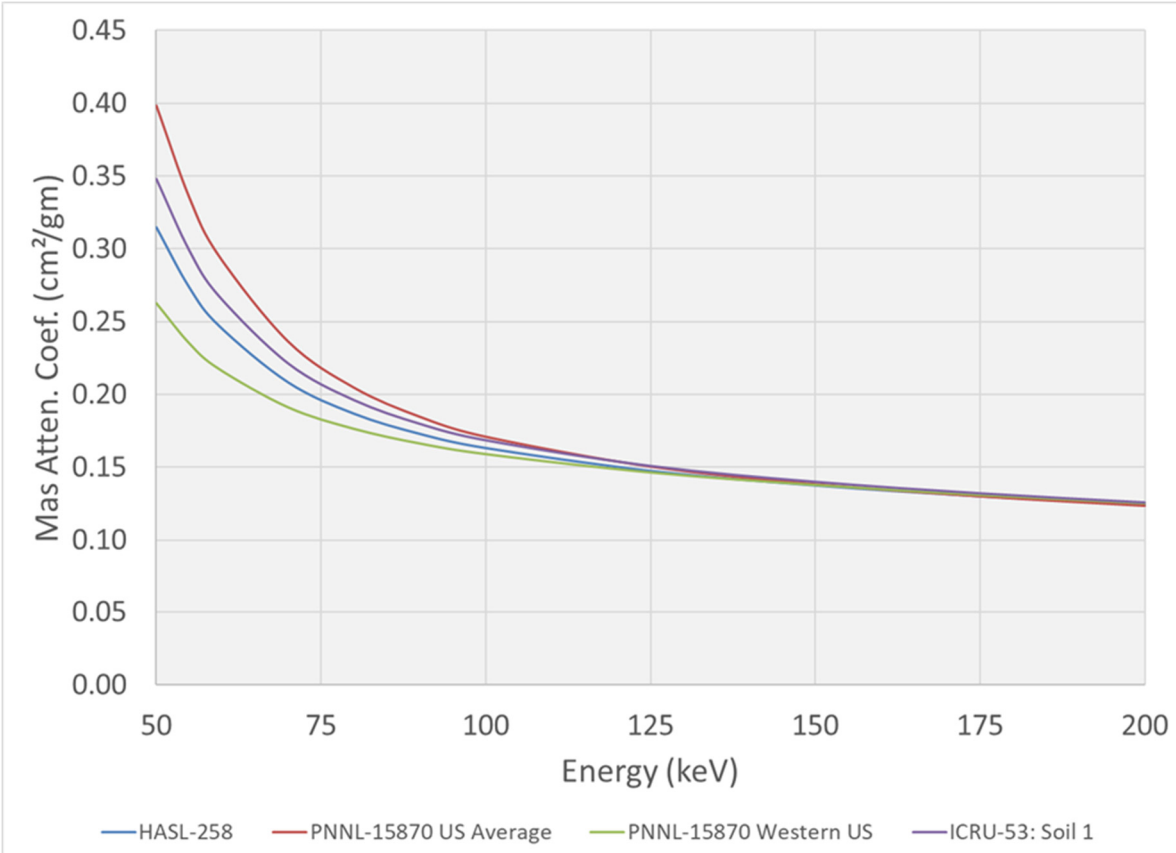


***Figure 11-4. Plot of mass attenuation coefficients for four different soil compositions.***

## 11.7 Alternative method for surface radionuclide distribution at 1-meter

In-situ surface activity concentration estimates for measurements performed at 1-meter can be made using full-energy peak areas and the absolute detector efficiency for a point source at 1-meter with correction factors (CFs) for geometry, air attenuation, and detector angular response as follows:

- Estimate the unattenuated point source activity at 1-meter.
- Multiply by the geometry CF of 7.889E+03 which corrects the point source activity at 1-meter to a 300-meter radius disk source activity at 1-meter without attenuation.

  Note: For a 2800 keV photon, nearly 97.5% of the unattenuated gamma flux at the detector face comes from within a 300-m radius.
- Multiply by the air attenuation CF to account for the air attenuation associated with a 300-meter radius disk source at 1-meter (Table 11-2).

- Divide by the FEP efficiency angular CF published in Reference [28] to correct for detector angular response. Alternatively use *Appendix E. Nf / No, pre-calculated tables for downward facing HPGe detector at 1-meter,* reproduced from Reference [28].
- Divide by the surface area of a 300-meter radius disk (2.827E+05 $m^2$) to calculate the activity per unit surface area.

***Table 11-2. Air attenuation CF table for a 300-meter radius disk source.***

| Energy (keV) | Air Attenuation CF |
|---|---|
| 60 | 1.73 |
| 80 | 1.68 |
| 100 | 1.65 |
| 150 | 1.60 |
| 200 | 1.56 |
| 300 | 1.51 |
| 400 | 1.46 |
| 600 | 1.41 |
| 800 | 1.37 |
| 1000 | 1.34 |
| 1200 | 1.31 |
| 1600 | 1.27 |
| 2000 | 1.25 |
| 2800 | 1.21 |

### 11.7.1 Example

- Calculated Cs-137 (661.7 keV) point source activity at 1-meter = 195 µCi
- Geometry CF = 7.889E+03
- Air attenuation CF = 1.395
- FEP efficiency angular CF (Detector L/D = 0.6) = 0.85
- Surface area of a 300-meter radius disk = 2.827E+05 $m^2$

Estimated in-situ activity concentration for surface radionuclide distribution at 1-meter = 195 µCi • 7.889E+03 • 1.395 / 0.85 / 2.827E+05 $m^2$ = 8.9 µCi/$m^2$

## 11.8 Applications

For gamma spectroscopists who don't want to perform detector angular response measurements and/or don't have the knowledge to perform gamma transport calculations, a measurement distance of 1-meter with pre-calculated table values, the alternate method for surface radionuclide distributions at 1-meter described above (if applicable), or a software program which incorporates the detector response with gamma transport calculations must be used.

For additional information on environmental in-situ gamma spectroscopy applications, see *Appendix C. Software/applications of Potential Interest*.

## 11.9 Additional information

For additional detailed information related to environmental in-situ gamma spectroscopy, see Reference [24] or the in-situ gamma spectroscopy references in the *FRMAC Gamma Spectroscopist Electronic Library / InSitu*.

# SECTION 12.0 URANIUM GAMMA SPECTROSCOPY [29]

## Table of Contents



## Figures

## Tables

## 12.1 Uranium mining, milling, conversion, and isotopic enrichment

Uranium ore is mined from the ground as $U_3O_8$ and subsequently milled to produce yellowcake. Following uranium mining and milling, which removes non-uranium radionuclides, the yellowcake is converted to uranium hexafluoride ($UF_6$) for isotopic enrichment.

***Table 12-1. Typical uranium concentrations. Adapted from Reference [31].***

| Description | Concentration (ppm U by mass) | Concentration (percent U by mass) |
|---|---|---|
| Very high-grade ore (Canada) | 200,000 | 20% |
| High-grade ore | 20,000 | 2% |
| Low-grade ore | 1,000 | 0.10% |
| Very low-grade ore* (Namibia) | 100 | 0.01% |
| Granite | 3 to 5 | 0.0003% to 0.0005% |
| Sedimentary rock | 2 to 3 | 0.0002% to 0.0003% |
| Earth's continental crust (Average) | 2.8 | 0.00028% |
| Seawater | 0.003 | 0.0000003% |

The primary methods used on an industrial scale to commercially enrich uranium are gaseous diffusion and gas centrifuge. Due to the high energy consumption/electricity requirements, gaseous diffusion is currently being phased out by gas centrifuge technology.

## 12.2 Chemically processed uranium

As discussed, chemically processed uranium removes non-uranium radionuclides (see Figure 3-1). This includes Ra-226 and its readily detectable gamma emitting decay products. Therefore, spectra for chemically processed uranium will not contain Ra-226 or its decay products due to the long half-lives of U-234 and Th-230, which precede Ra-226 in the U-238 decay chain, and effectively eliminate the in-growth of Ra-226.

## 12.3 Typical uranium isotopic mass and activity percentages

Uranium is commonly categorized by U-235 mass fraction as shown in Table 12-2.

***Table 12-2. Uranium categories by U-235 mass fraction.***

| Category | U-235 Mass % |
|---|---|
| Depleted uranium | U-235 < 0.711% |
| Natural uranium | U-235 = 0.711% |
| Low enriched uranium (LEU) | 20% > U-235 > 0.711% |
| High enriched uranium (HEU) | U-235 >= 20% |

For reference purposes, typical uranium isotopic mass and activity fractions are presented in Table 12-3 and Table 12-4, respectively.

***Table 12-3. Typical uranium mass percentages.***

| Nuclide | Depleted Uranium Mass % | Natural Uranium Mass % | 3% Enriched Mass % | 93.3% Enriched Mass % |
|---|---|---|---|---|
| U-238 | 99.7995% | 99.2830% | 96.9732% | 5.8308% |
| U-235 | 0.1995% | 0.7115% | 3.0000% | 93.3000% |
| U-234 | 0.0010% | 0.0055% | 0.0268% | 0.8692% |

***Table 12-4. Typical uranium activity percentages.***

| Nuclide | Depleted Uranium Activity % | Natural Uranium Activity % | 3% Enriched Activity % | 93.3% Enriched Activity % |
|---|---|---|---|---|
| U-238 | 84.039% | 48.260% | 15.858% | 0.035% |
| U-235 | 1.080% | 2.223% | 3.153% | 3.592% |
| U-234 | 14.900% | 49.510% | 80.989% | 96.373% |

Depleted uranium: Typical U-238/U-235 activity ratio 50:1 to 80:1.
Natural uranium: Typical U-238/U-235 activity ratio 22:1.

Although not listed in Table 12-3 and Table 12-4, U-232, U-233, and U-236 are produced during reactor irradiation and are present in uranium that has been reprocessed. In addition, FRMAC gamma spectroscopists should be aware that typical uranium enrichment processes (gaseous diffusion and gas centrifuge) enrich the lighter uranium isotopes (U-232, U-233, U-234, U-235) more readily than the heavier uranium isotopes (U-236, U-238).

Lastly, U-238/U-235 activity ratios as a function of U-235 mass percent are presented in Figure 12-1.

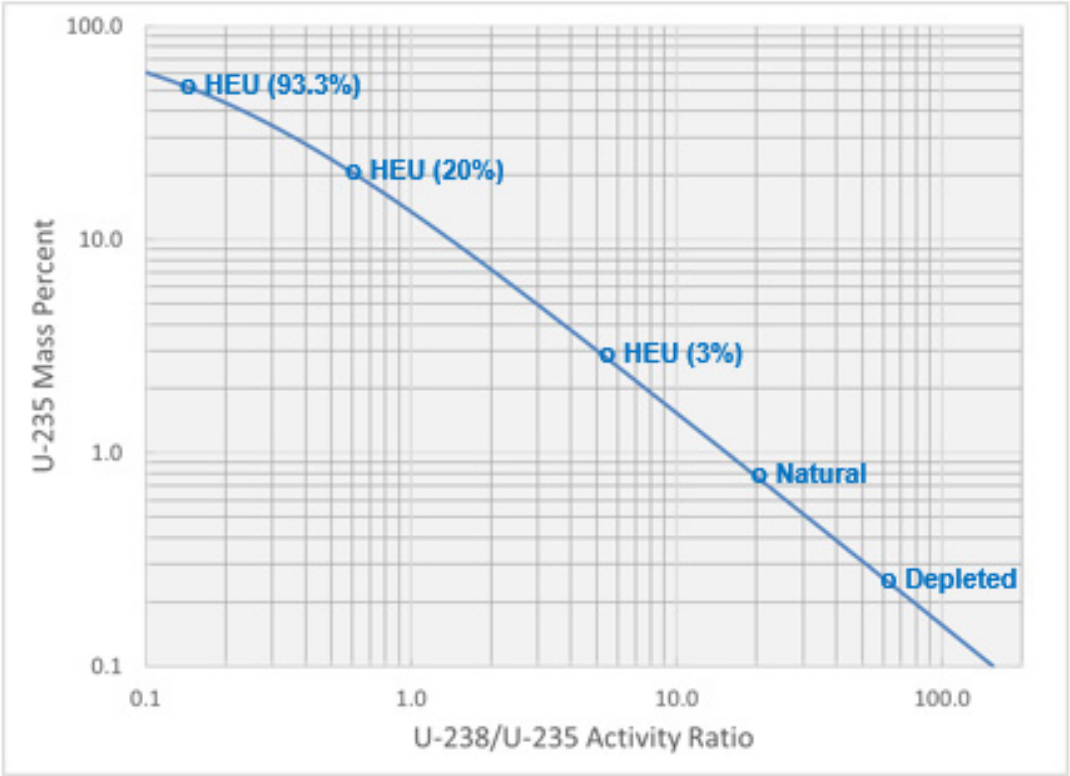


*Figure 12-1. U-238/U-235 activity ratios as a function of U-235 mass percent. Adapted from [31].*

## 12.4 U-238 decay chain with useful emissions for analysis

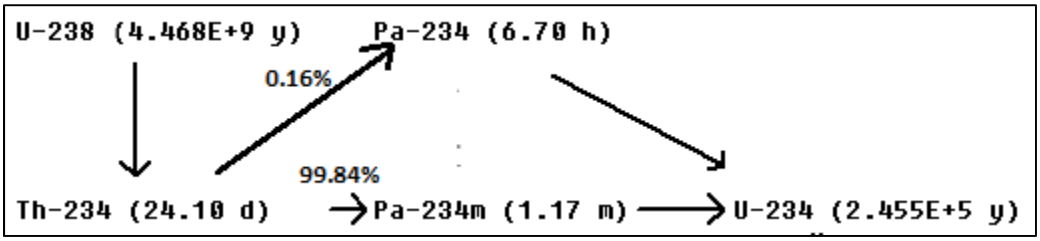


*Figure 12-2. U-238 decay chain. Note: 90% U-238 decay chain equilibrium with Th-234, Pa-234m, and Pa-234 takes roughly 79.9 days. [6]*

*Table 12-5. U-238 decay chain gamma emissions of interest.*

| Parent | Emitter | Energy (keV) | Yield (gps/dps) |
|---|---|---|---|
| **U-238+** | **Th-234** | **63.3** | **4.84E-02** |
| **U-238+** | **Th-234 x 2** | **92.6** | **5.58E-02** |
| **U-238+** | **Pa-234m** | **258.3** | **7.27E-04** |
| U-238+ | Pa-234 x 2 | 569.3 | 1.90E-04 |
| U-238+ | Pa-234m/Pa-234 | 742.8 | 8.32E-04 |
| **U-238+** | **Pa-234m/Pa-234** | **766.4** | **2.94E-03** |
| U-238+ | Pa-234m/Pa-234 | 786.3 | 5.03E-04 |
| U-238+ | Pa-234/Pa-234m | 946.0 | 3.13E-04 |
| **U-238+** | **Pa-234m** | **1001.0** | **8.36E-03** |
| **U-238+** | **Pa-234m/Pa-234** | **1737.7** | **2.12E-04** |
| **U-238+** | **Pa-234m** | **1831.3** | **1.72E-04** |

U-238+ represents U-238 in equilibrium with its decay products (Th-234, Pa-234m, and Pa-234)
U-238+ (Pa-234): Yield includes the 0.16% branch from its parent radionuclide, Th-234
U-238+ (Pa-234m): Yield includes the 99.84% branch from its parent radionuclide, Th-234
Primary gamma emissions are "**bolded**"

## 12.5 U-235 decay chain with useful emissions for analysis

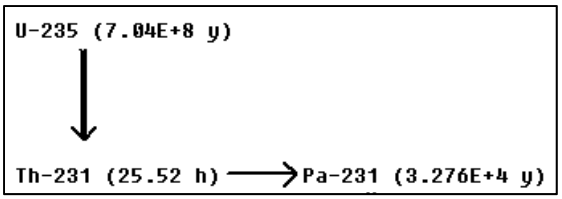


*Figure 12-3. U-235 decay chain. Note: 90% U-235 decay chain equilibrium with Th-231 takes roughly 3.5 days. [6]*

*Table 12-6. U-235 decay chain gamma emissions of interest.*

| Parent | Emitter | Energy (keV) | Yield (gps/dps) |
|---|---|---|---|
| **U-235** | **U-235** | **185.7** | **5.72E-01** |
| **U-235** | **U-235** | **143.8** | **1.10E-01** |
| **U-235** | **U-235** | **163.3** | **5.08E-02** |
| **U-235** | **U-235** | **205.3** | **5.01E-02** |

Primary gamma emissions are "**bolded**"

## 12.6 U-232 decay chain with useful emissions for analysis

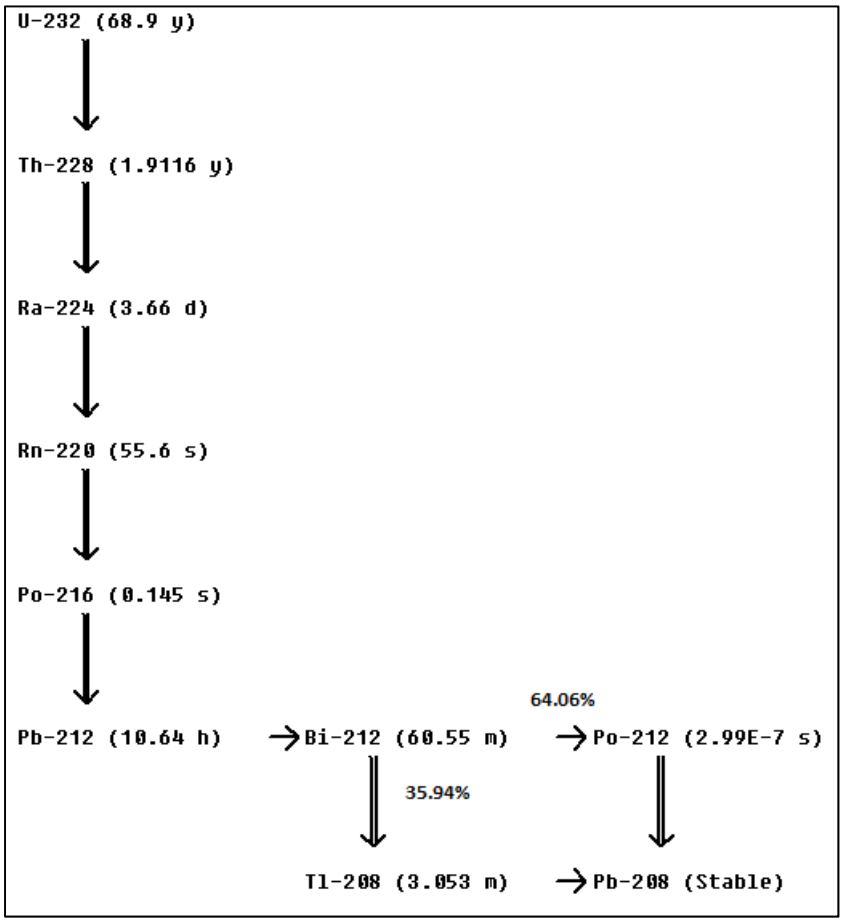


***Figure 12-4. U-232 decay chain. Note: 90% U-232 → Th-228 equilibrium takes roughly 6.3 years; 90% Th-228 decay chain equilibrium takes roughly 12.2 days. [6]***

***Table 12-7. U-232 decay chain gamma emissions of interest.***

| Parent | Emitter | Energy (keV) | Yield (gps/dps) |
|---|---|---|---|
| **U-232+** | **Pb-212** | **238.6** | **4.33E-01** |
| **U-232+** | **Tl-208** | **2614.5** | **3.56E-01** |
| **U-232+** | **Tl-208** | **583.2** | **3.04E-01** |
| **U-232+** | **Bi-212** | **727.3** | **6.58E-02** |
| **U-232+** | **Tl-208** | **860.6** | **4.47E-02** |
| **U-232+** | **Bi-212** | **1620.5** | **1.49E-02** |

U-232+ represents U-232 in equilibrium with its decay products
U-232+ (Tl-208): Yield includes the 35.94% branch from its parent radionuclide, Bi-212
Primary gamma emissions are "**bolded**"

Although U-232 is not readily detectable by gamma spectroscopy, U-232 decay product emissions are detectable in highly enriched uranium (HEU).

## 12.7 U-234 and U-236 decay chains with useful emissions for analysis

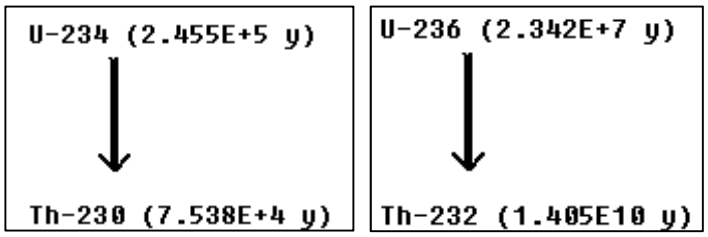


***Figure 12-5. U-234 and u-236 decay chains. [6]***

***Table 12-8. U-234 decay chain gamma emissions of interest.***

| Parent | Emitter | Energy (keV) | Yield (gps/dps) |
|---|---|---|---|
| U-234 | U-234 | 53.2 | 1.23E-03 |
| **U-234** | **U-234** | **120.9** | **3.97E-04** |

Primary gamma emissions are "**bolded**"

It should be noted that U-234 gamma emissions are easily shielded, and their yields are low. In addition, U-236 is not readily detectable by gamma spectroscopy.

## 12.8 Uranium associated x-rays emissions

Uranium characteristic x-rays from induced x-ray fluorescence are presented in Table 12-9

***Table 12-9. Uranium characteristic x-rays.***

| Element | Shell | Energy (keV) | Intensity per vacancy |
|---|---|---|---|
| U X-ray | Kα1 | 98.4 | 4.52E-01 |
| U X-ray | Kα2 | 94.7 | 2.82E-01 |

Thorium characteristic x-rays produced when outer orbital electrons fill the lower energy levels following uranium decay and internal conversion are shown in Table 12-10.

***Table 12-10. Thorium characteristic x-rays.***

| Element | Shell | Energy (keV) | Intensity per vacancy |
|---|---|---|---|
| Th X-ray | Kα1 | 93.4 | 4.60E-01 |
| Th X-ray | Kα2 | 90.0 | 2.82E-01 |

## 12.9 Chemically processed uranium gamma spectroscopy notes

- The U-238 gamma emissions listed in Table 12-5 are from Th-234, Pa-234m, and Pa-234. Unless the age of the uranium is known, equilibrium must be established between U-238 and Th-234, Pa-234m, and Pa-234 (roughly 80 days is needed for 90% equilibrium) for accurate U-238 quantification and uranium isotopic analysis. If equilibrium is assumed yet U-238 decay series equilibrium has not been reached, the assessed uranium enrichment will be biased high.

- U-235 low energy emissions (143.8, 163.3, 185.7, and 205.3 keV) are easier to shield than higher energy emissions from U-238 decay chain products (258.3, 742.8, 766.4, and 1001.0 keV). Therefore, if shield and/or self-attenuation corrections are not made for uranium samples experiencing attenuation, the high energy gamma emissions from U-238 decay chain products can dominate the gamma ray spectrum and the assessed uranium enrichment will be biased low.

- Although present in trace amounts, U-232 decay product emissions (238.6, 583.2, 727.3, 860.6, and 2614.5 keV) are commonly detectable in HEU gamma ray spectra and are very useful for HEU isotopic determinations.

- If the age of the uranium is unknown, equilibrium must be established between U-232 and its decay products (roughly 6.3 years is needed for 90% equilibrium) for accurate U-232 quantification.

- In uranium hexafluoride ($UF_6$) cylinders containing HEU, it is common to detect F-19(α,nγ)Na-22 (half-life = 2.6 y) gamma emissions at 1274.5 keV.

## 12.10 Uranium isotopic determinations

Uranium isotopic assessments are generally performed using relative efficiency curves. SECTION 14.0 provides a detailed overview of relative efficiency curves including examples using uranium gamma emissions between 120 and 1010 keV.

If only "rough" uranium isotopic determinations are needed, the following methods may provide useful information.

- <u>To estimate the minimum U-235 mass fraction</u>, use the detector efficiency curve without attenuation correction in conjunction with applicable yields and the following U-238/U-235 full-energy peak areas: 1001.0 / 185.7 keV or 258.3 / 185.7 keV.

- <u>To estimate the maximum U-235 mass fraction</u>, use the detector efficiency curve without attenuation correction in conjunction with applicable yields and the following U-238/U-235 full-energy peak areas: 92.6 / 185.7 keV or 63.3 / 185.7 keV.

### *12.10.1 Additional notes*

- The common fission product pair Zr-95/Nb-95 (765.8, 756.7, and 724.2 keV) can complicate assessment of uranium isotopic assessments due to interference with the 766.4 keV U-238 decay chain product emission.

- For uranium isotopic assessments in the 89 to 99 keV region of interest, additional information can be found in *Chapter 7.4.2* of Reference [33].

## 12.11 U-233 gamma spectroscopy

Although far less common than depleted, natural, and enriched uranium, FRMAC gamma spectroscopists should have a general understanding of U-233 production and U-233 gamma spectroscopy analysis methods.

U-233 is not found naturally and is bred from Th-232.

**Th-232 + n → Th-233**
**Th-233 → (Half-life = 22.2-min, beta) → Pa-233**
**Pa-233 → (Half-life = 27.0-day, beta) → U-233**

During production of U-233, U-232 is also produced from the following two reactions.

**Th-232 + n → Th-231 + 2n (~0.01 barns$_{thermal}$)**
**Th-230 (which is present in thorium) + n → Th-231 (23 barns$_{thermal}$)**

Followed by

**Th-231 → (Half-life = 25.5-hr, beta) → Pa-231**
**Pa-231 + n → Pa-232 (210 barns$_{thermal}$)**
**Pa-232 → (Half-life = 1.31-day, beta) → U-232**

## 12.12 U-233 decay chain with useful emissions for analysis

Figure 12-6 and Table 12-11 present the U-233 decay chain and useful gamma emissions for analysis, respectively.

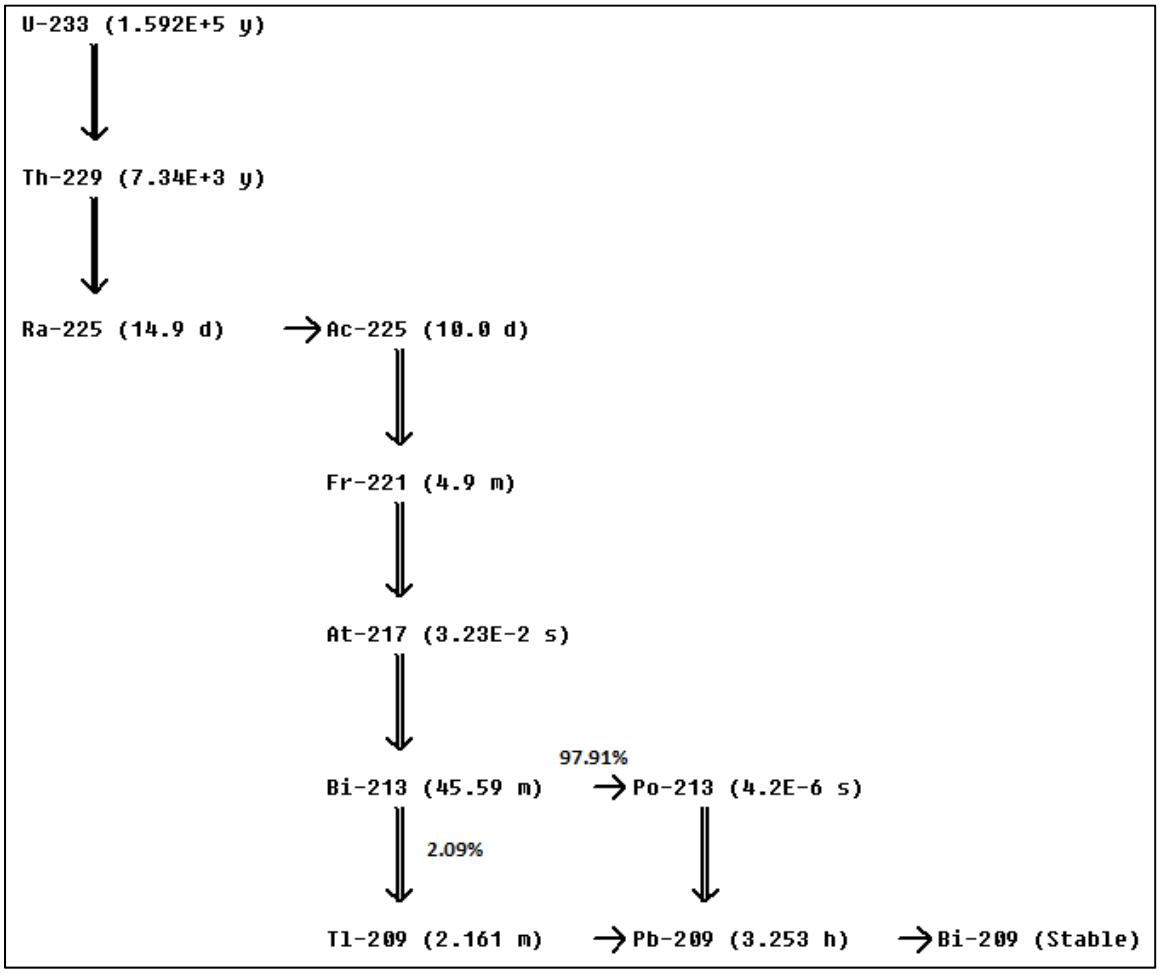


***Figure 12-6. U-233 decay chain. Note: 90% Th-229 decay chain equilibrium occurs at roughly 70 days. [6]***

***Table 12-11. U-233 decay chain gamma emissions of interest.***

| Parent | Emitter | Energy (keV) | Yield (gps/dps) |
|---|---|---|---|
| **U-233** | **U-233** | **317.2** | **7.76E-05** |

| Parent | Emitter | Energy (keV) | Yield (gps/dps) |
|---|---|---|---|
| Th-229+ | Bi-213 | 440.5 | 2.61E-01 |
| Th-229+ | Fr-211/Th-229 | 218.2 | 1.18E-01 |
| Th-229+ | Th-229 | 193.5 | 4.40E-02 |
| Th-229+ | Th-229 | 210.9 | 2.80E-02 |
| **Th-229+** | **Tl-209** | **1567.1** | **2.09E-02** |
| **Th-229+** | **Tl-209** | **465.1** | **2.03E-02** |

Th-229+ (Bi-213): Yield includes the 99.988% branch from its parent radionuclide, At-217
Th-229+ (Tl-209): Yield includes the 2.09% branch from its parent radionuclide, Bi-213
Primary gamma emissions are "**bolded**"

## 12.13 U-233 gamma spectroscopy notes

- For aged U-233, the gamma ray spectrum is dominated by U-232 decay product emissions from trace amounts of U-232 present with the U-233.
- Due to its low yield, the U-233 317.2 keV gamma emission is difficult to detect. However, when U-233 is aged and U-232 is present at lower levels, U-233 may be identified via primary Th-229 decay product emissions at 440.5 and 1567.1 keV.
- If U-233 or Th-229 decay product emissions are not detectable, U-233 spectra will be solely consistent with U-232 decay product emissions.
- The amount of U-233 can only be determined if it is detectable (317.2 keV) or Th-229 decay product emissions are detectable and the time since last chemical separation (age) is known.
- If U-233 and Th-229 decay product emissions are detectable, the age of the U-233 can be determined.
- If only Th-229 decay product emissions are detectable, the minimum U-233 age can be determined using the detectable Th-229 decay product emissions in conjunction with the U-233 detection limit.

## 12.14 U-232/Th-228 versus Th-232 decay chain spectra

Since the U-232/Th-228 and Th-232 decay chains are very similar (see Figure 12-7), it is not surprising that U-232/Th-228 and Th-232 decay chain spectra are also very similar (see Figure 12-8). However, Th-232 decay chain spectra contain readily detectable Ac-228 emissions (338.3, 911.2, and 969.0 keV) that are not present in U-232/Th-228 decay chain spectra (see Figure 12-9 and Figure 12-10).

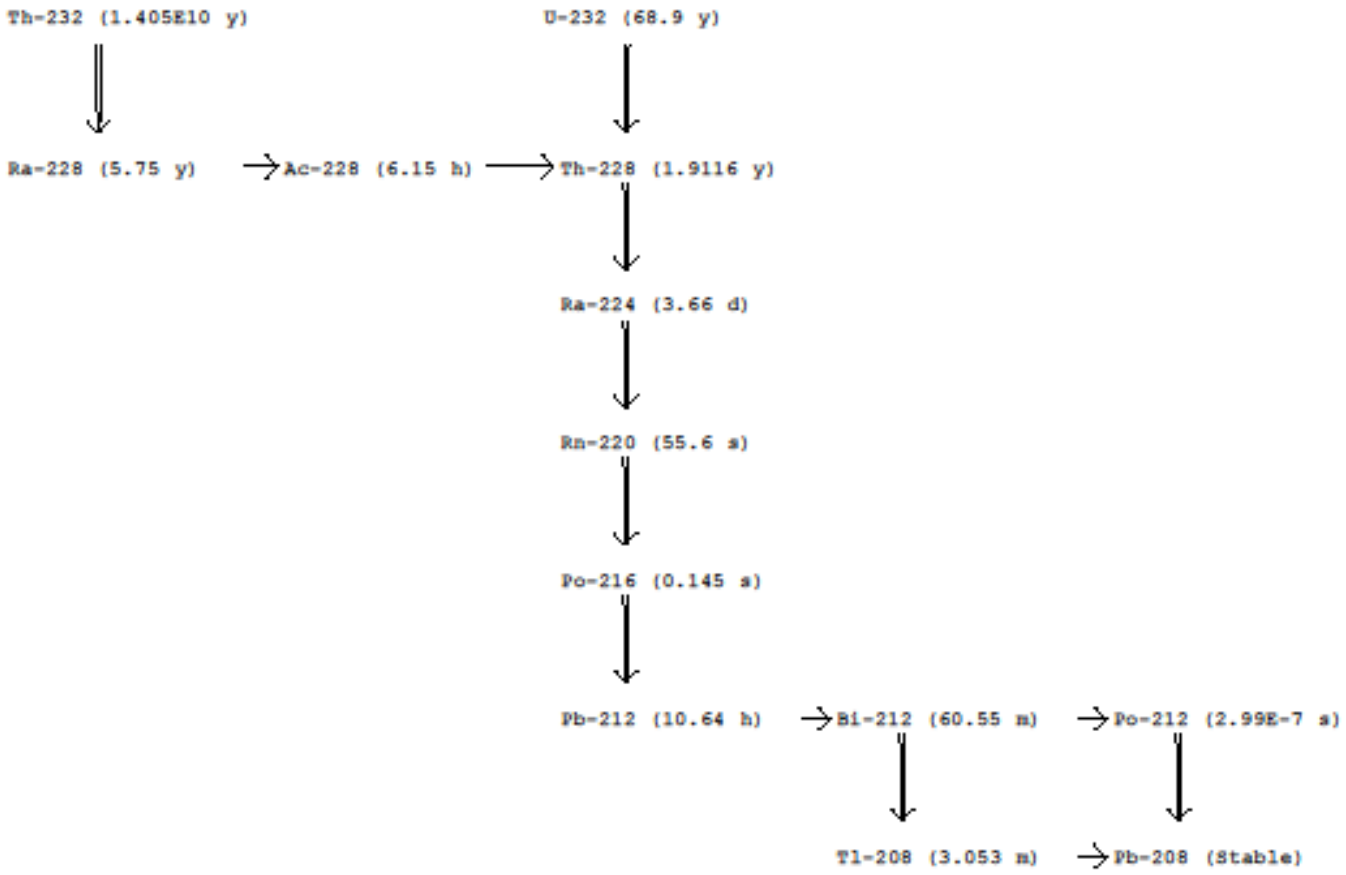


***Figure 12-7. Th-232 and U-232 decay chains. [6]***

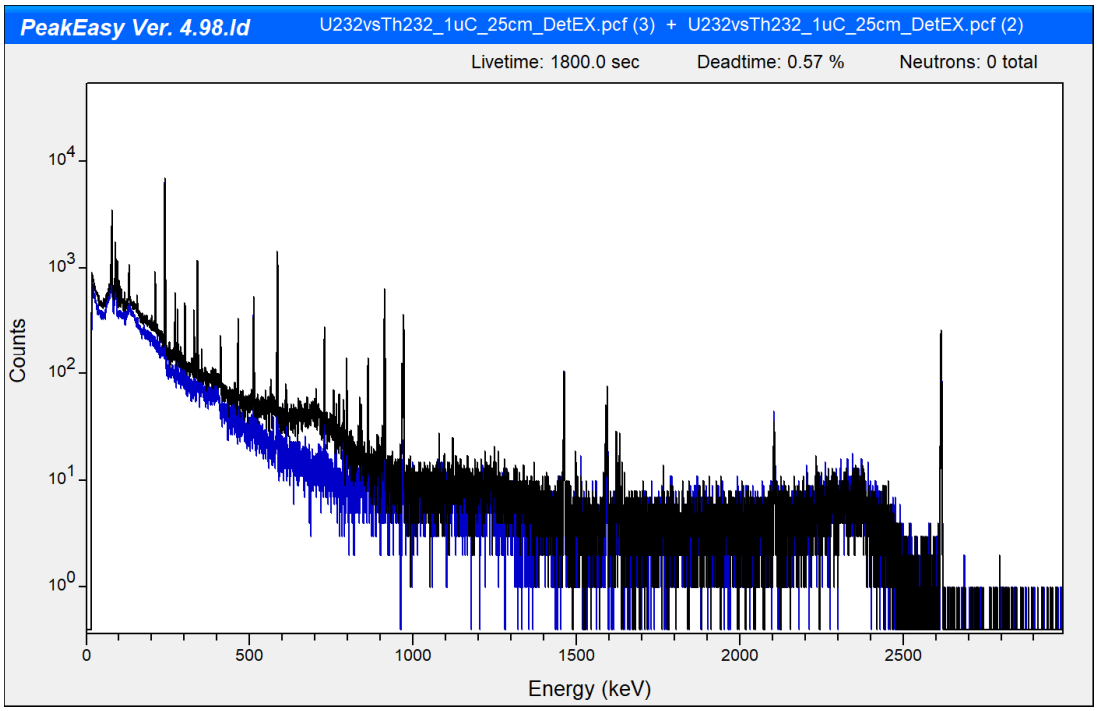


***Figure 12-8. Th-232 (black) and U-232 (blue) decay chain spectra.***

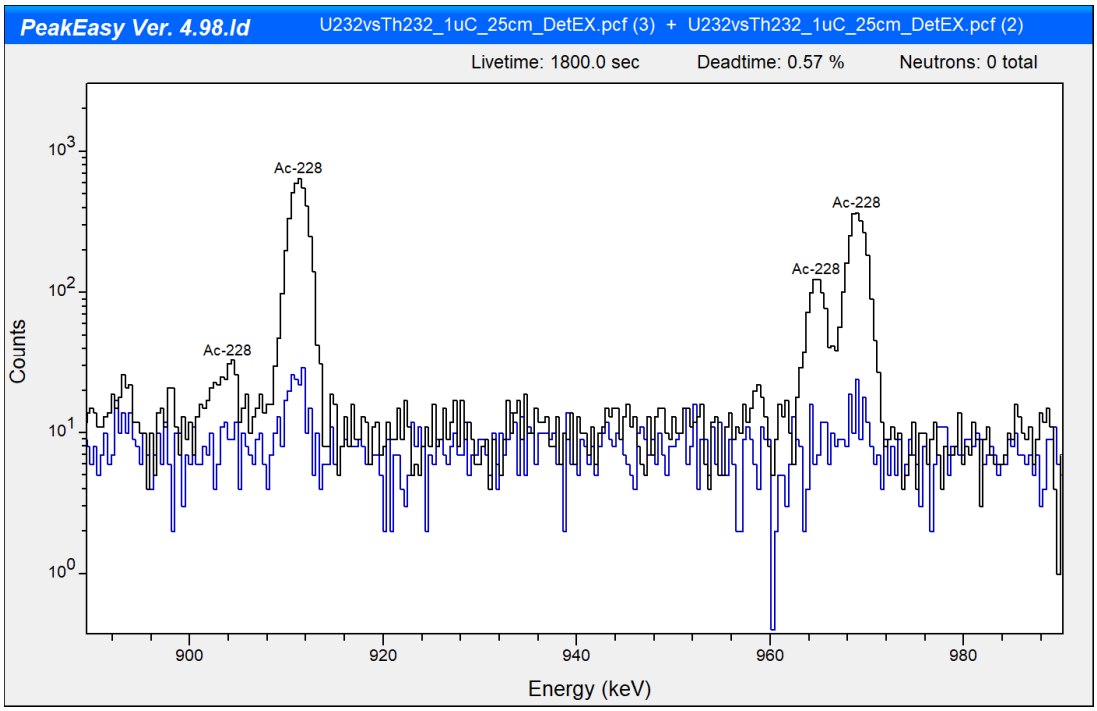


***Figure 12-9. Th-232 (black) and U-232 (blue) decay chain spectra (911 and 969 keV ROI).***

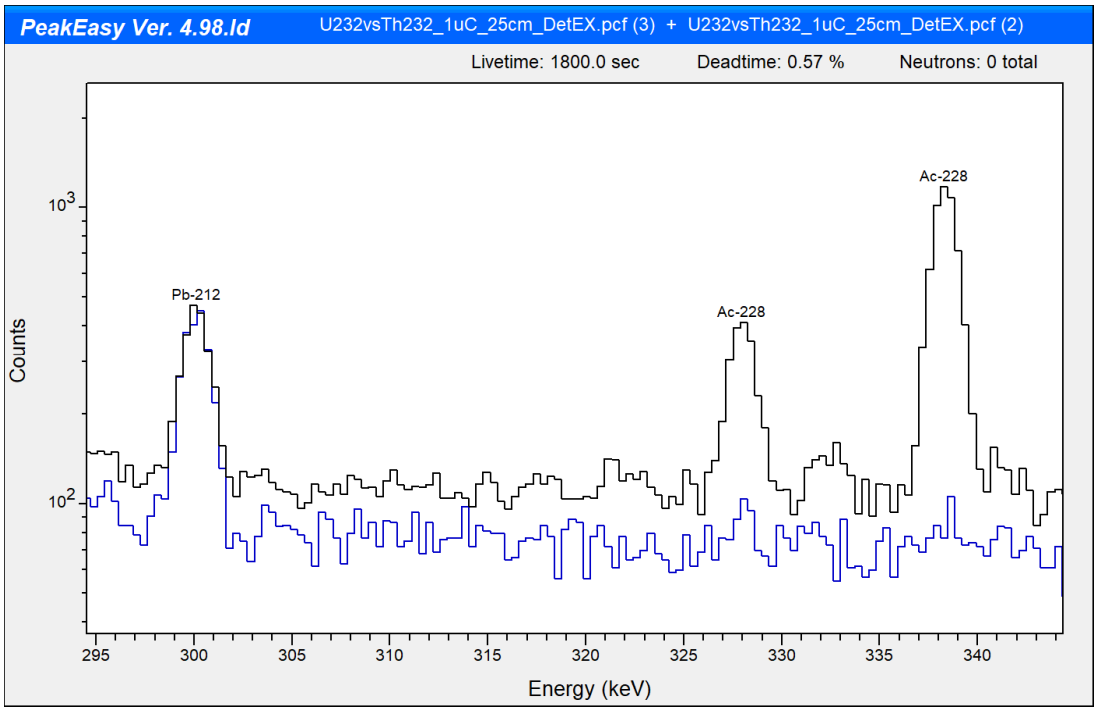


***Figure 12-10. Th-232 (black) and U-232 (blue) decay chain spectra (328 and 338 keV ROI).***

### *12.14.1 Th-232 decay chain equilibrium check*

A good practice is to check the Tl-208 (Th-232 and Th-228 decay product) to Ac-228 (Th-232 decay product) activity ratio using the 860.6 keV (Tl-208) and 911.2 keV (Ac-228) full-energy peaks (if present). If the Tl-208 to Ac-228 activity ratio is above 1.0 and statistically significant, the gamma spectroscopist should consider the possibility of that Th-232 has not reached equilibrium and/or the presence of U-232/Th-228. If the activity ratio is below 1.0 and statistically significant, the spectroscopist should consider the possibility that Th-232 has not reached equilibrium (see Chemically processed natural thorium in **SECTION 16.0** for further discussion).

## 12.15 Uranium ore gamma spectroscopy

Uranium ore, uranium that has not been chemically processed, will contain U-238 and Ra-226 decay chain emissions. Accordingly, uranium ore gamma ray spectra are dominated by Ra-226 decay chain emissions (see Table 12-12) and are very similar to Ra-226 decay chain spectra (see Figure 12-11).

*Table 12-12. Ra-226 decay chain gamma emissions of interest.*

| Parent | Emitter | Energy (keV) | Yield (gps/dps) |
|---|---|---|---|
| **Ra-226+** | **Bi-214** | **609.3** | **4.61E-01** |
| **Ra-226+** | **Pb-214/Bi-214** | **351.9** | **3.77E-01** |
| Ra-226+ | Pb-214 | 295.2 | 1.93E-01 |
| **Ra-226+** | **Bi-214** | **1764.5** | **1.54E-01** |
| **Ra-226+** | **Bi-214** | **1120.3** | **1.51E-01** |
| Ra-226+ | Pb-214 | 242.0 | 7.43E-02 |
| Ra-226+ | Bi-214 | 1238.1 | 5.79E-02 |
| Ra-226+ | Bi-214 | 2204.2 | 5.08E-02 |
| Ra-226+ | Bi-214 | 768.4 | 4.94E-02 |
| Ra-226+ | Bi-214 | 1377.7 | 4.00E-02 |
| Ra-226+ | Ra-226 | 186.2 | 3.59E-02 |
| Ra-226+ | Bi-214 | 934.1 | 3.08E-02 |
| Ra-226+ | Bi-214 | 2447.9 | 1.57E-02 |

Ra-226+ represents Ra-226 in equilibrium with its decay products
Primary gamma emissions are "**bolded**"

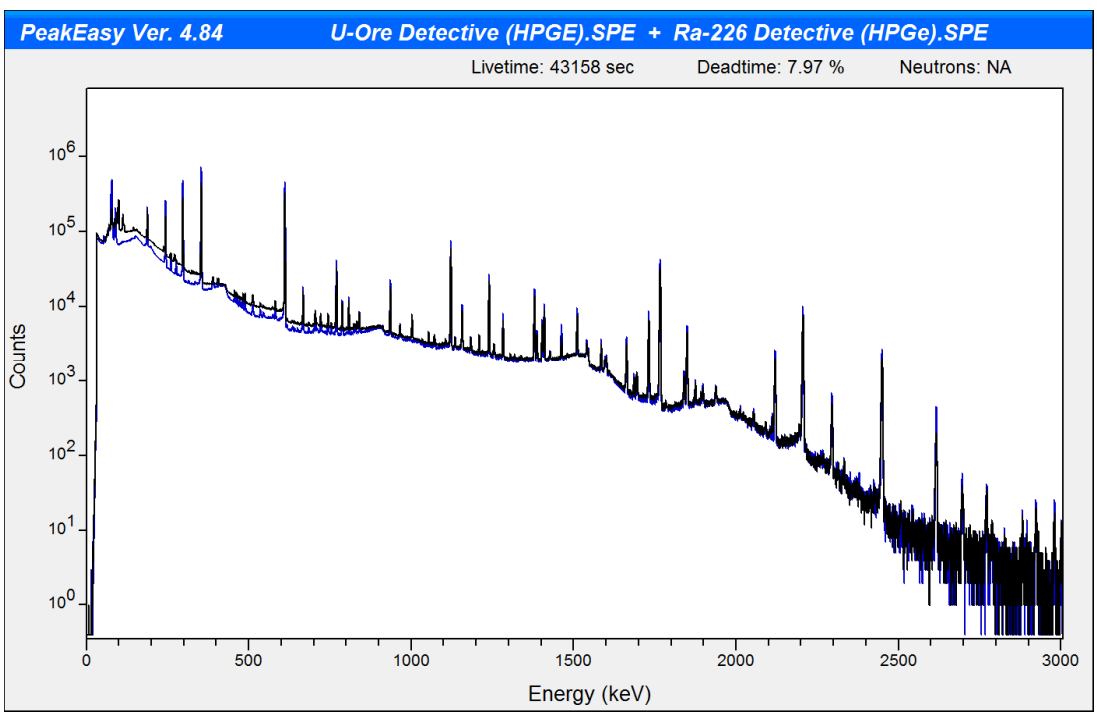


*Figure 12-11. Ra-226 (blue) versus uranium ore (black). [7]*

Uranium ore spectra may be identifiable from Ra-226 decay chain spectra if uranium x-rays (98.4 and 94.6 keV), U-238 decay product emissions (92.6, 63.3, 1001.0 keV), or U-235 emissions (143.8, 163.3,

205.3 keV) are detectable (see Figure 12-12 and Figure 12-13). However, correct identification may be difficult for shielded sources, spectra collected with low resolution detectors, or spectra collected with poor counting statistics.

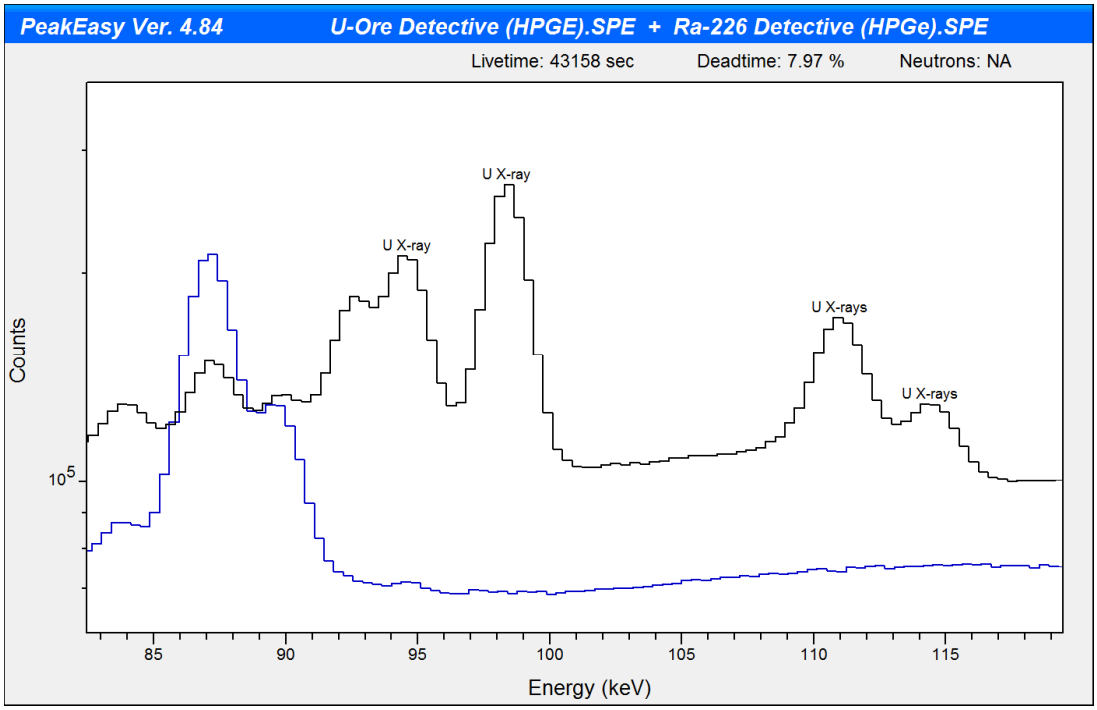


***Figure 12-12. Presence of U X-rays in U-ore spectrum. Ra-226 (blue) versus uranium ore (black). [7]***

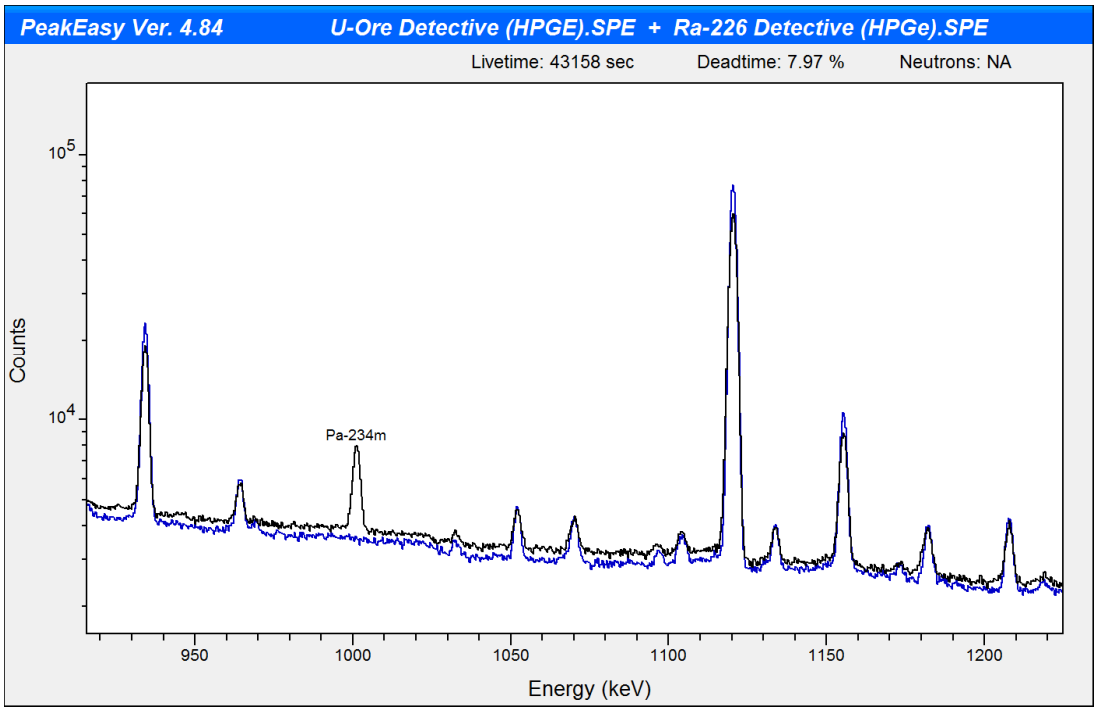


***Figure 12-13. Presence of 1001.0 keV emission from Pa-234m in U-ore spectrum. Ra-226 (blue) versus uranium ore (black). [7]***

### *12.15.1 186 keV full-energy peak interference*

Gamma spectroscopists should be cognizant that the primary U-235 emission at 185.7 keV experiences significant interference with the 186.2 keV Ra-226 emission. For natural uranium ore, Ra-226 and U-235 contribute 58% and 42% to the 186 keV full-energy peak, respectively.

### *12.15.2 Uranium ore equilibrium check*

Disequilibrium between the U-238 and Ra-226 decay chains can occur when radon (Rn-222), a noble gas produced from the decay of Ra-226, diffuses/escapes from the uranium ore. The extent of disequilibrium can be evaluated by comparing the calculated Ra-226 decay product to U-238 decay chain activity ratio using the following full-energy peak pairs (if present): 1120.3 / 1001.0 keV and 934.1 / 1001.0 keV.

If the Ra-226 decay product to U-238 decay chain activity ratio is very low, additional U-238 may be present or the uranium ore may have been chemically processed incompletely.

# SECTION 13.0 PLUTONIUM GAMMA SPECTROSCOPY [34]

## Table of Contents



## Figures



## Tables

## 13.1 Plutonium production, typical isotopic mass percentages, and typical isotopic activity percentages

A plutonium production reactor irradiates U-238, then processes it to chemically remove the plutonium isotopes.

- Note: Pu-239 is produced by neutron capture in U-238 followed by two beta decays.

**U-238 (4.5E+09 y) + n → U-239 (23.5 m) → Np-239 (2.4 d) → Pu-239 (24,100 y)**

The longer the exposure time in the reactor (higher burnup), the more Pu-238, Pu-240, Pu-241, and Pu-242 are produced relative to Pu-239. In addition, Pu-241 increases more rapidly than Pu-240 as burnup increases. Following chemical separation, Am-241 builds-in from the decay of Pu-241 (half-life = 14.4 y).

For reference purposes, typical plutonium isotopic mass and activity fractions for low and high-burnup plutonium as well as heat source plutonium are presented in Table 13-1 and Table 13-2, respectively.

***Table 13-1. Typical isotopic plutonium type mass percentages. [35] [36]***

Initial mass percentages

| Nuclide | Low-burnup Mass % | High-burnup Mass % | Heat Source Mass % |
|---|---|---|---|
| Pu-238 | 0.010% | 1.500% | 83.890% |
| Pu-239 | 93.780% | 58.100% | 13.800% |
| Pu-240 | 6.000% | 24.100% | 1.900% |
| Pu-241 | 0.200% | 11.400% | 0.320% |
| Pu-242 | 0.020% | 4.900% | 0.090% |
| Am-241 | 0.000% | 0.000% | 0.000% |

Decay corrected activity percentages at 20 years

| Nuclide | Low-burnup Mass % | High-burnup Mass % | Heat Source Mass % |
|---|---|---|---|
| Pu-238 | 0.009% | 1.286% | 81.652% |
| Pu-239 | 93.783% | 58.319% | 15.723% |
| Pu-240 | 5.991% | 24.154% | 2.161% |
| Pu-241 | 0.076% | 4.357% | 0.139% |
| Pu-242 | 0.020% | 4.921% | 0.103% |
| Am-241 | 0.122% | 6.962% | 0.222% |

***Table 13-2. Typical isotopic plutonium type activity percentages. [35] [36]***

Initial mass percentages

| Nuclide | Low-burnup Activity % | High-burnup Activity % | Heat Source Activity % |
|---|---|---|---|
| Pu-238 | 0.611% | 2.118% | 97.664% |
| Pu-239 | 20.761% | 0.297% | 0.058% |
| Pu-240 | 4.858% | 0.451% | 0.029% |
| Pu-241 | 73.770% | 97.133% | 2.248% |
| Pu-242 | 0.000% | 0.002% | 0.000% |
| Am-241 | 0.000% | 0.000% | 0.000% |

Decay corrected activity percentages at 20 years

| Nuclide | Low-burnup Activity % | High-burnup Activity % | Heat Source Activity % |
|---|---|---|---|
| Pu-238 | 0.937% | 4.358% | 98.828% |
| Pu-239 | 37.262% | 0.716% | 0.069% |
| Pu-240 | 8.707% | 1.084% | 0.035% |
| Pu-241 | 50.419% | 89.110% | 1.014% |
| Pu-242 | 0.001% | 0.004% | 0.000% |
| Am-241 | 2.675% | 4.727% | 0.054% |

## 13.2 Additional notes

1) When reporting Am-241 mass fractions, the convention is to report the mass fraction of Am-241 relative to the total amount of plutonium mass present (Am-241 mass/total Pu mass).
2) Pu-236 is present in trace quantities in plutonium. Although Pu-236 and U-232 are not readily detectable by gamma spectroscopy, Th-228 decay product gamma emissions can be detected in some aged plutonium spectra.

   **Pu-236 (2.9 y) → U-232 (72.0 y) → Th-228 (1.9 y)**

3) When the measured Pu-239/Pu-240 mass ratio is less than 5, do not simply use the measured Pu-240/(Pu-239 + Pu-240) mass fraction to estimate the Pu-240 mass fraction in the plutonium. To better estimate the Pu-240 mass fraction, corrections should be made for the contributions from other plutonium isotopes (Pu-238, Pu-241, Pu-242) present. Correlations are commonly used to account for Pu-242 since it is essentially undetectable by gamma spectroscopy. See *Chapter 2* of Reference [14] for more information.
4) Plutonium is a dense, high Z material and therefore very good at self-attenuating its gamma emissions. Therefore, high yield, low energy gamma emissions may be significantly reduced or not detected.
5) For unshielded plutonium samples, consider the use of Cd-Cu or Sn-Cu graded shielding (discussed in SECTION 16.0) to eliminate/reduce Am-241 59.5 keV gamma emissions in the spectrum. This may allow closer sample to detector distances to be used (reducing detection limits and increasing higher energy emission count rates) as well as reducing "coincidence" summing with other photon emissions.

## 13.3 Useful plutonium gamma emissions for analysis

Useful plutonium gamma emissions for analysis can be found in *Appendix A. Gamma and X-Rays of Interest.*

## 13.4 Plutonium isotopic determinations

Plutonium isotopic assessments are generally performed using relative efficiency curves with numerous peak interference corrections. These interferences affect Pu-240 peak area determinations making accurate assessment of plutonium burn-up difficult. Accordingly, relative efficiency isotopic software programs such as Fixed-Energy Response-Function Analysis with Multiple Efficiency (FRAM) and Multi-Group Analysis (MGA) are commonly used (see SECTION 16.0 for additional information on relative efficiency curves).

Above 100 keV, the four primary regions of interest used for plutonium isotopic assessments are: 160 keV; 208 keV; 332/336 keV; and 640 keV. Only two of the four regions of interest, 160 keV and 640 keV, can be used for direct measurement of both Pu-239 and Pu-240.

A brief discussion of each region of interest above 100 keV is provided below with example spectra for 20-year-old, low-burnup plutonium (6.0% by weight Pu-240) and 20-year-old, high-burnup plutonium (18.0% by weight Pu-240).

- Note: For plutonium isotopic assessments at or below the 100 keV region, see *Chapter 8.3* of Reference [33].

### *13.4.1 160 keV region of interest*

The 160 keV ROI primary gamma emissions are presented in Table 13-3

***Table 13-3. 160 keV ROI plutonium gamma emissions of interest.***

| Energy (keV) | Yield (gps/dps) | Nuclide |
|---|---|---|
| 160.0 | 6.54E-08 | Pu-241 |
| 160.2 | 6.20E-08 | Pu-239 |
| 160.3 | 4.02E-06 | Pu-240 |
| 161.5 | 1.23E-06 | Pu-239 |
| 164.6 | 4.56E-07 | U-237 |
| 164.7 | 6.67E-07 | Am-241 |
| **169.6** | **1.73E-06** | **Am-241** |
| **171.4** | **1.10E-06** | **Pu-239** |

U-237: Yield includes the 2.45E-03% branch from its parent radionuclide, Pu-241
Gamma emissions that are "**bolded**" can be treated as interference free.

As shown in Figure 13-1 and Figure 13-2, the Pu-240 160.3 keV emission has strong interferences from Pu-241 at 160.0 keV and Pu-239 at 160.2 keV. If high dead times and large amounts of Am-241 present, then random sum peaks from Am-241 (59.5 keV with 99.0 and 103.0 keV) can further complicate assessment.

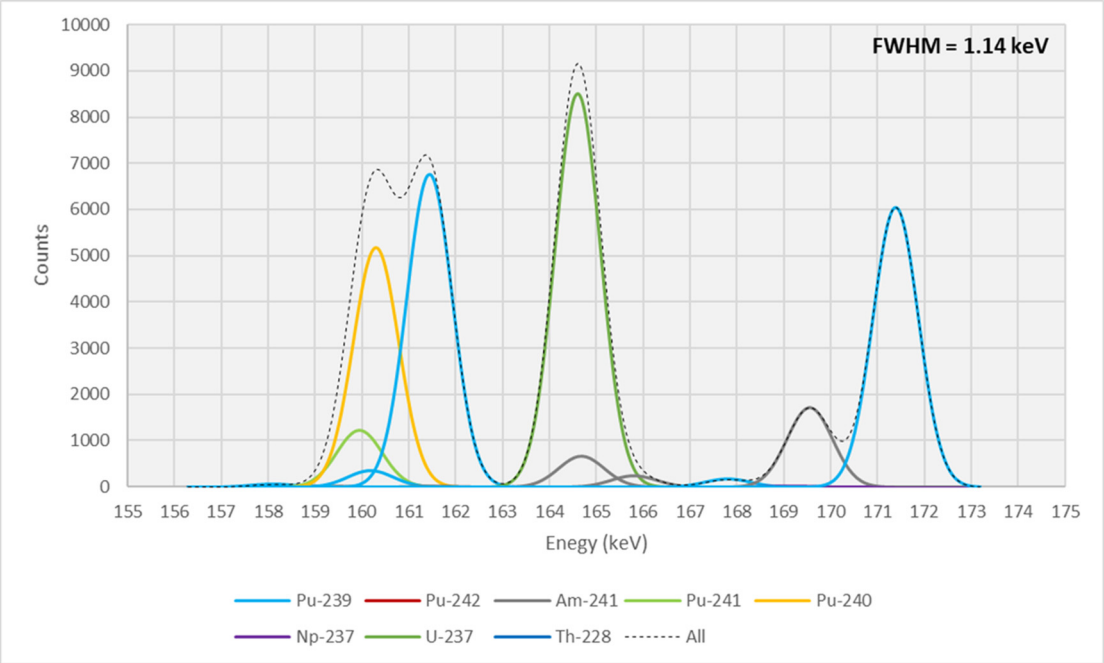


***Figure 13-1. 160 keV ROI example spectrum for 20-year-old, low-burnup plutonium (6.0% Pu-240). Linear scale.***

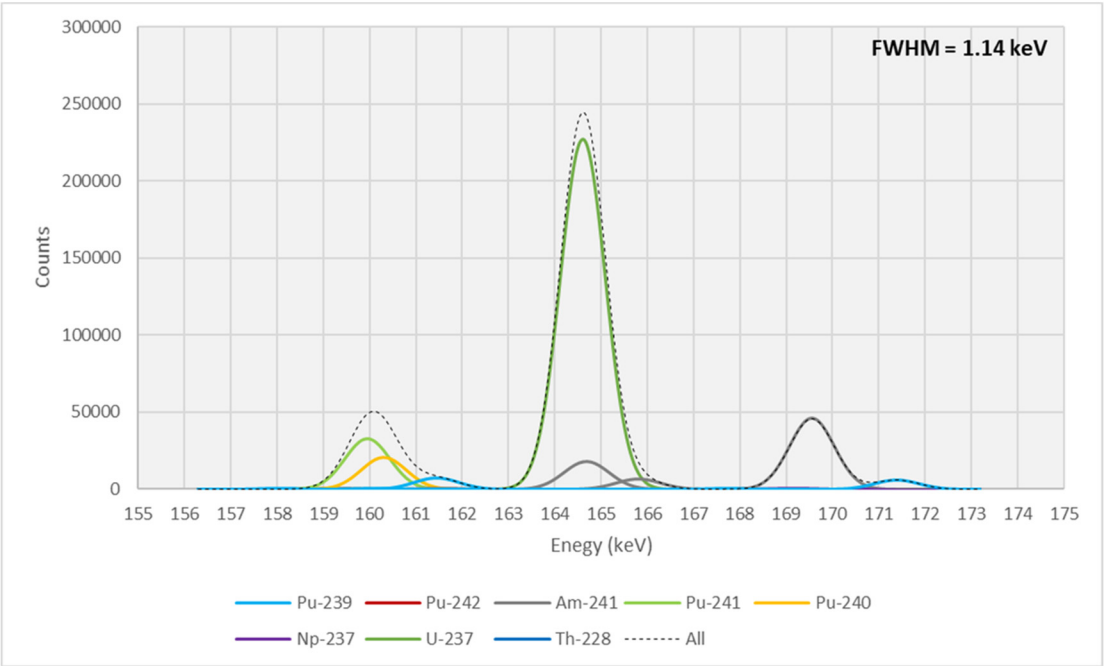


***Figure 13-2. 160 keV ROI example spectrum for 20-year-old, high-burnup plutonium (18.0% Pu-240). Linear scale.***

### *13.4.2 208 keV region of interest*

The 208 keV ROI primary gamma emissions are presented in Table 13-4.

***Table 13-4. 208 keV ROI plutonium gamma emissions of interest.***

| Energy (keV) | Yield (gps/dps) | Nuclide |
|---|---|---|
| **195.7** | **1.07E-06** | **Pu-239** |
| **203.6** | **5.69E-06** | **Pu-239** |
| 208.0 | 5.19E-06 | U-237 |
| 208.0 | 7.91E-06 | Am-241 |

U-237: Yield includes the 2.45E-03% branch from its parent radionuclide, Pu-241
Gamma emissions that are "**bolded**" can be treated as interference free.

As shown in Table 13-4, both Am-241 and U-237 contribute to the 208 keV full-energy peak. The relative contribution from Am-241 and U-237 to the 208.0 keV peak area as a function of time since last chemical separation is presented in Figure 13-3.

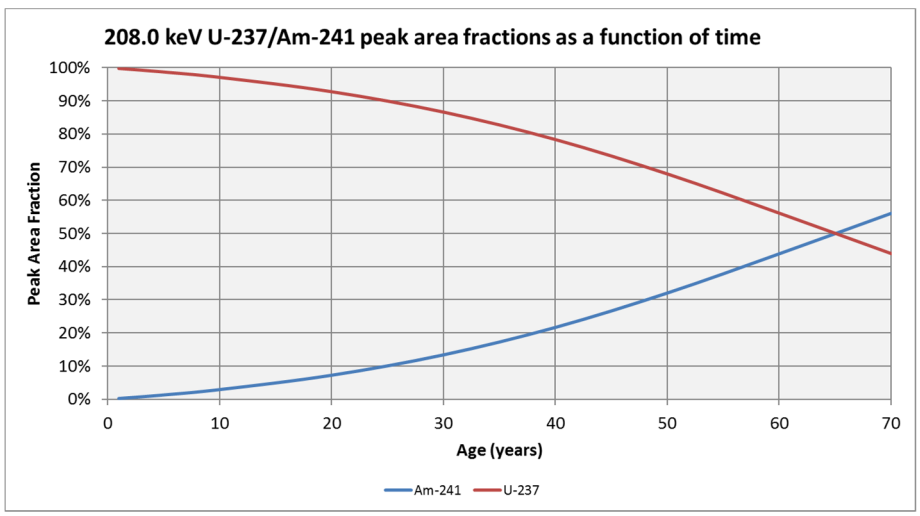


***Figure 13-3. 208.0 keV peak area contributions from Am-241/U-237 as a function of time.***

For reference purposes, example spectra for 20-year-old, low-burnup plutonium (6.0% Pu-240) and 20-year-old, high-burnup plutonium (18.0% Pu-240) are presented in Figure 13-4 and Figure 13-5, respectively.

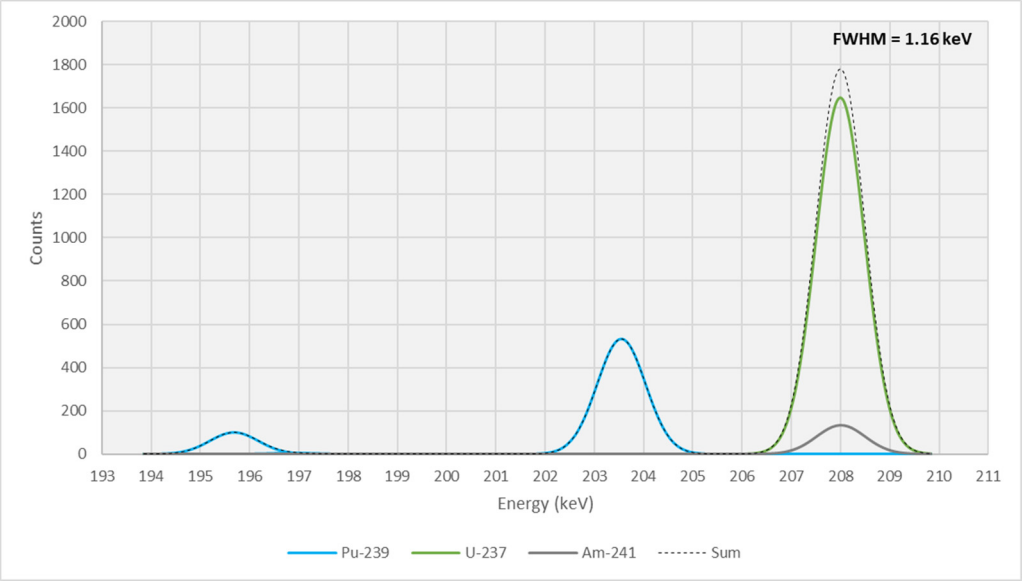


***Figure 13-4. 208 keV ROI example spectrum for 20-year-old, low-burnup plutonium (6.0% Pu-240). Linear scale.***

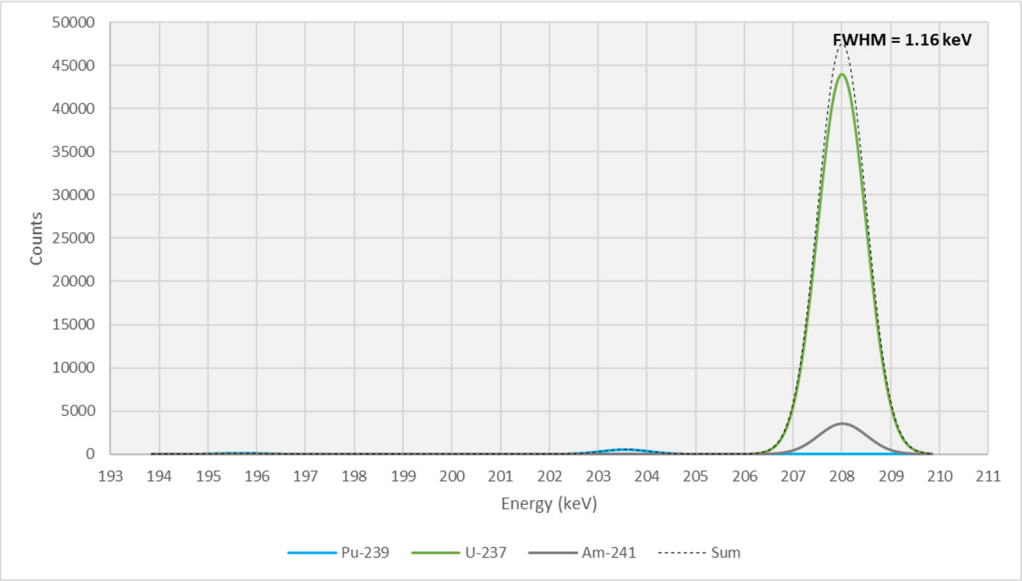


***Figure 13-5. 208 keV ROI example spectrum for 20-year-old, high-burnup plutonium (18.0% Pu-240). Linear scale.***

### *13.4.3 332/336 keV region of interest*

The 332/336 keV ROI primary gamma emissions are presented in Table 13-5.

***Table 13-5. 332/336 keV ROI plutonium gamma emissions of interest.***

| Energy (keV) | Yield (gps/dps) | Nuclide |
|---|---|---|
| 332.4 | 1.49E-06 | Am-241 |
| 332.4 | 2.94E-07 | U-237 |
| 332.8 | 4.94E-06 | Pu-239 |
| 335.4 | 4.96E-06 | Am-241 |
| 335.4 | 2.33E-08 | U-237 |
| 336.1 | 1.12E-06 | Pu-239 |
| **345.0** | **6.06E-06** | **Pu-239** |

U-237: Yield includes the 2.45E-03% branch from its parent radionuclide, Pu-241
Gamma emissions that are "**bolded**" can be treated as interference free.

Example spectra for 20-year-old, low-burnup plutonium (6.0% Pu-240) and 20-year-old, high-burnup plutonium (18.0% Pu-240) are presented in Figure 13-6 and Figure 13-7, respectively.

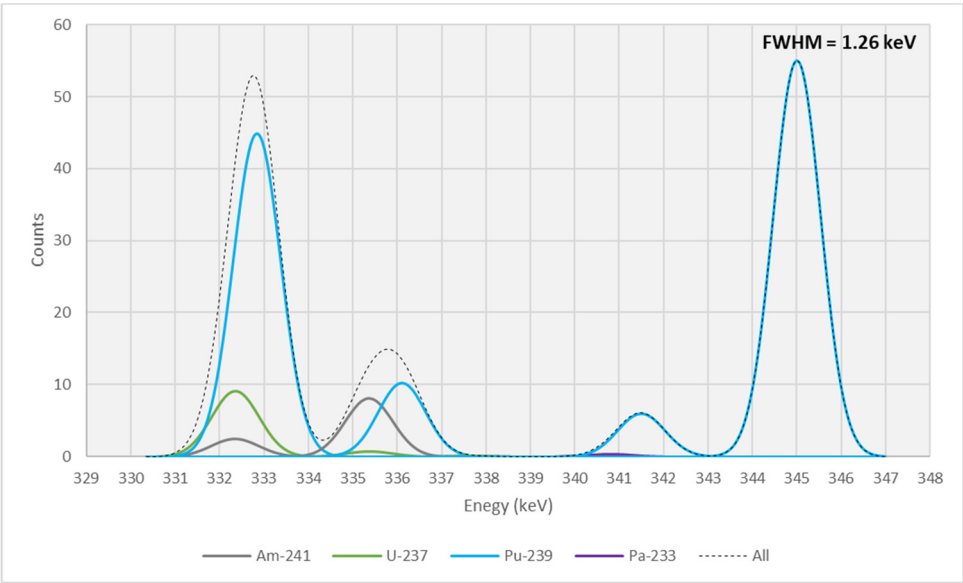


***Figure 13-6. 332/336 keV ROI example spectrum for 20-year-old, low-burnup plutonium (6.0% Pu-240). Linear scale.***

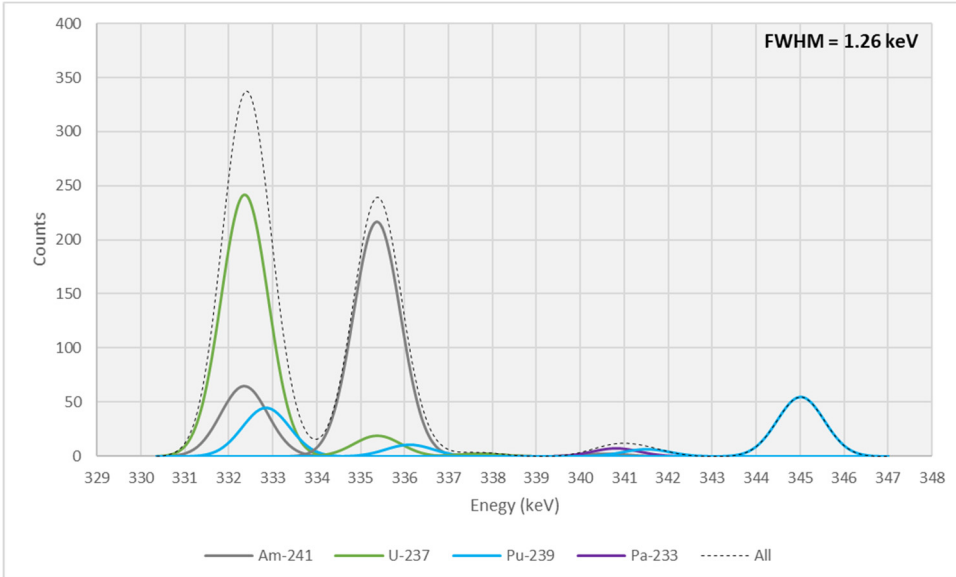


***Figure 13-7. 332/336 keV ROI example spectrum for 20-year-old, high-burnup plutonium (18.0% Pu-240). Linear scale.***

- Note: With good counting statistics, it is possible to strip the Pu-239 contribution from 332 and 336 keV complexes and solve for the Pu-241/U-237 and Am-241 peak areas to determine the time since last chemical separation.

### *13.4.4 640 keV region of interest*

The 640 keV ROI primary gamma emissions are presented in Table 13-6.

***Table 13-6. 640 keV ROI plutonium gamma emissions of interest.***

| Energy (keV) | Yield (gps/dps) | Nuclide |
|---|---|---|
| **637.8** | **2.56E-08** | **Pu-239** |
| 640.0 | 8.70E-08 | Pu-239 |
| 641.5 | 7.10E-08 | Am-241 |
| 642.4 | 1.30E-07 | Pu-240 |
| **645.9** | **1.52E-07** | **Pu-239** |
| 653.0 | 3.77E-07 | Am-241 |
| **658.9** | **9.70E-08** | **Pu-239** |
| **662.4** | **3.64E-06** | **Am-241** |
| **722.0** | **1.96E-06** | **Am-241** |

Gamma emissions that are "**bolded**" can be treated as interference free.

As shown in Figure 13-8 and Figure 13-9, the Pu-240 642.4 keV emission has interference from Am-241 at 641.5 keV for high burn-up and/or aged samples.

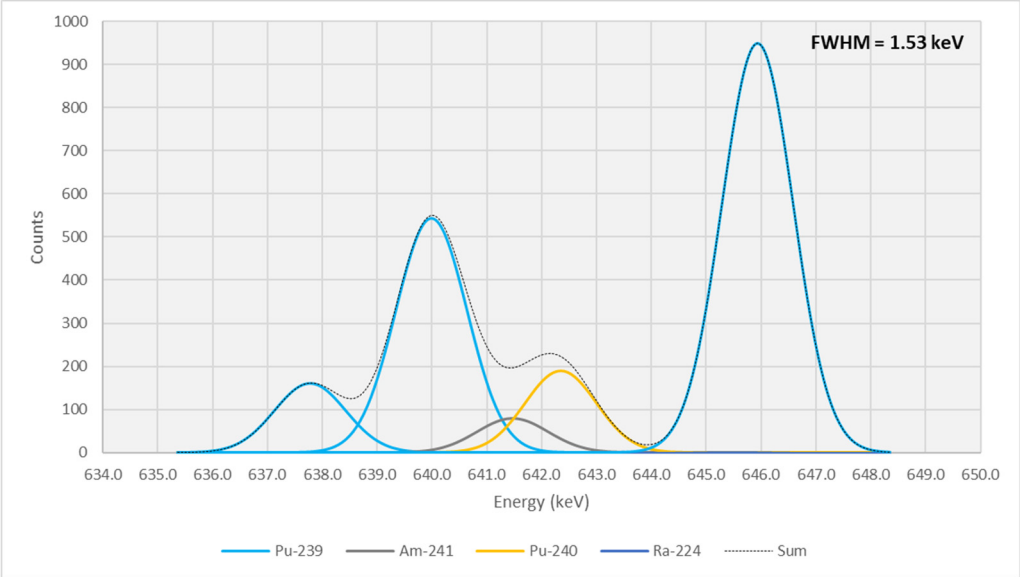


***Figure 13-8. 640 keV ROI example spectrum for 20-year-old, low-burnup plutonium (6.0% Pu-240). Linear scale.***

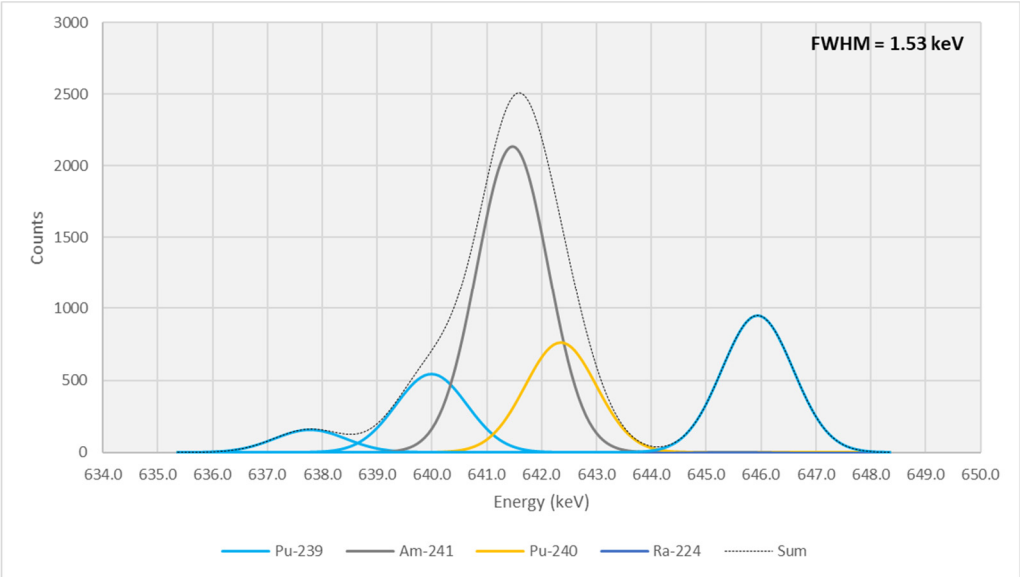


***Figure 13-9. 640 keV ROI example spectrum for 20-year-old, high-burnup plutonium (18.0% Pu-240). Linear scale.***

- Note: If the 662.4 keV peak area exceeds the 722.0 keV peak area by more than a factor of 2, the material has likely been irradiated and Cs-137 (661.7 keV) is likely present.

## 13.5 Plutonium time since last chemical separation determinations

The time since last chemical separation can be estimated by examining the decay of Pu-241 into Am-241/U-237.

**Pu-241 (14.35 y, BR = 0.99998) → Am-241 (433.2 y) → Np-237 (2.14E+06 y) → Pa-233 (27.0 d)**
**Pu-241 (14.35 y, BR = 0.0000245) → U-237 (6.8 d) → Np-237 (2.14E+06 y) → Pa-233 (27.0 d)**

Although there are many Am-241 gamma emissions that can be used, there are limited "useable" Pu-241 and/or U-237 gamma emissions above 100 keV.

***Table 13-7. "Useable" Pu-241 and/or U-237 gamma emissions for estimating the time since last chemical separation for plutonium.***

| Nuclide | Energy (keV) | Yield (gps/dps) |
|---|---|---|
| U-237 | 208.0 | 5.19E-06 |
| **Pu-241** | **148.6** | **1.86E-06** |
| U-237 | 332.4 | 2.94E-07 |

U-237: Yield includes the 2.45E-03% branch from its parent radionuclide, Pu-241
Gamma emissions that are "**bolded**" can be treated as interference free.

Regardless of what gamma emissions are used, interference corrections for Pu-241/U-237 and/or Am-241 are necessary. Accordingly, the time since last chemical separation can be estimated using closely spaced Am-241/Pu-239 peak pairs and the Pu-241/Am-241 activity ratio as follows.

Estimate the Pu-239/Am-241 activity ratio, using one of the following regions containing closely spaced Am-241/Pu-239 peak pairs (Table 13-8).

***Table 13-8. Am-241/Pu-239 peak pairs for estimating the time since last chemical separation for plutonium.***

| Nuclide | Energy (keV) | Yield (gps/dps) |
|---|---|---|
| Pu-239 | 124.5 | 6.81E-07 |
| Pu-239 | 125.2 | 5.63E-07 |
| Am-241 | 125.3 | 4.08E-05 |
| **Pu-239** | **129.3** | **6.31E-05** |

| Nuclide | Energy (keV) | Yield (gps/dps) |
|---|---|---|
| **Pu-239** | **658.9** | **9.70E-08** |
| **Am-241** | **662.4** | **3.64E-06** |

| Nuclide | Energy (keV) | Yield (gps/dps) |
|---|---|---|
| **Am-241** | **419.3** | **2.87E-07** |
| **Pu-239** | **413.7** | **1.47E-05** |

| Nuclide | Energy (keV) | Yield (gps/dps) |
|---|---|---|
| **Pu-239** | **718.0** | **2.80E-08** |
| **Am-241** | **722.0** | **1.96E-06** |

- Gamma emissions that are "**bolded**" can be treated as interference free. Accordingly, the 659/662, 718/722, and 414/419 keV regions are interference free.
- To estimate the Am-241 125.3 keV peak area, the 125 keV Pu-239 peak area contribution must be stripped using the 129.3 keV Pu-239 peak.
- If the Am-241 662.4 keV emission is being used, check the Am-241 662.4 and 722.0 keV peak area ratios for reasonableness to determine if Cs-137 is present.

Use the 208 keV region of interest to determine the Pu-241/Am-241 activity ratio as follows. Using the Pu-239 203.6 keV peak, strip the Am-241 contribution from the 208.0 keV peak using the previously estimated Pu-239/Am-241 activity ratio and determine the U-237 (Pu-241) peak area. Determine the Pu-241/Am-241 activity ratio and solve for time using Equation 2-1 or *Appendix B. Time Since Last Chemical Separation (age) Tables*.

- Note: Other regions that can be used to determine time since last chemical separation include the 332/336/345 keV region of interest and the 144/146/149 keV region of interest.

## 13.6 Additional information

The PeakEasy Library "Plutonium" folder contains useful reference spectra as a function of burn-up, shielding, and detector resolution.

For additional information related to plutonium gamma spectroscopy, please review Reference [14], [33], and [34].

# SECTION 14.0 RELATIVE EFFICIENCY CURVES [37]

## Table of Contents



## Figures



## Tables

## 14.1 Introduction

Relative efficiency curves are the fundamental basis of uranium and plutonium isotopic software programs such as FRAM developed by Los Alamos National Laboratory (LANL) and MGA developed by Lawrence Livermore National Laboratory (LLNL).

Relative efficiency curves are used to determine radionuclide activity ratios or radionuclide mass ratios (not absolute activity or mass). The benefit of relative efficiency curves is that they require no measurement of calibration sources and "self-correct" for geometry and attenuation (shield attenuation and self-attenuation).

## 14.2 Closely spaced full-energy peak pairs

When full-energy peaks from two different radionuclides are very close in energy the relative detection efficiency is essentially the same. As such, the relative activity of the radionuclides can be well estimated by taking the ratio of the net full-energy peak counts divided by the yield of each radionuclide.

### *14.2.1 Example*

A measurement of a high burnup plutonium sample with an ORTEC Detective is performed. Estimate the Am-241 to Pu-239 activity ratio using the closely spaced full-energy peak pairs of Am-241 and Pu-239 at 419.3 and 413.7 keV, respectively.

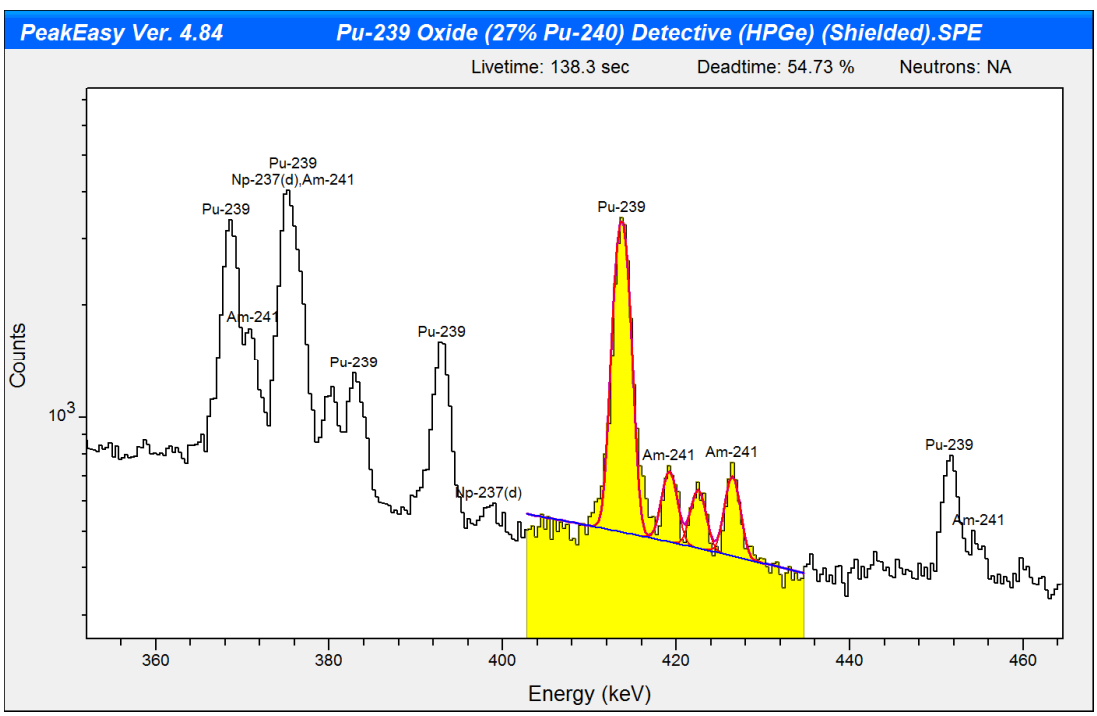


***Figure 14-1. High burnup plutonium sample spectrum. [7]***

For each gamma emission (419.3 and 413.7 keV), the net full-energy peak area (counts) is divided by the yield as shown in Table 14-1 and the ratio of these values is calculated to estimate a relative Am-241 to Pu-239 activity of 4.37.

***Table 14-1. High burnup plutonium sample relative activity determination.***

| Nuclide | Energy (keV) | Yield (gps/dps) | Net Area (counts) | Net Area / Yield | Relative Activity |
|---|---|---|---|---|---|
| Am-241 | 419.3 | 2.87E-07 | 1410 | 4.91E+09 | 4.37E+00 |
| Pu-239 | 413.7 | 1.47E-05 | 16529 | 1.12E+09 | 1.00E+00 |

## 14.3 Relative efficiency curve shapes

The shape of the relative efficiency curve is based on the detector efficiency, item geometry, shield attenuation, and self-attenuation. Accordingly, changes in detector efficiency, item geometry, shield attenuation, and self-attenuation are reflected by changes in the shape of the relative efficiency curve. Figure 14-2 displays an example of relative efficiency curves (shapes) as a function of uranium dioxide ($UO_2$) mass and shielding.

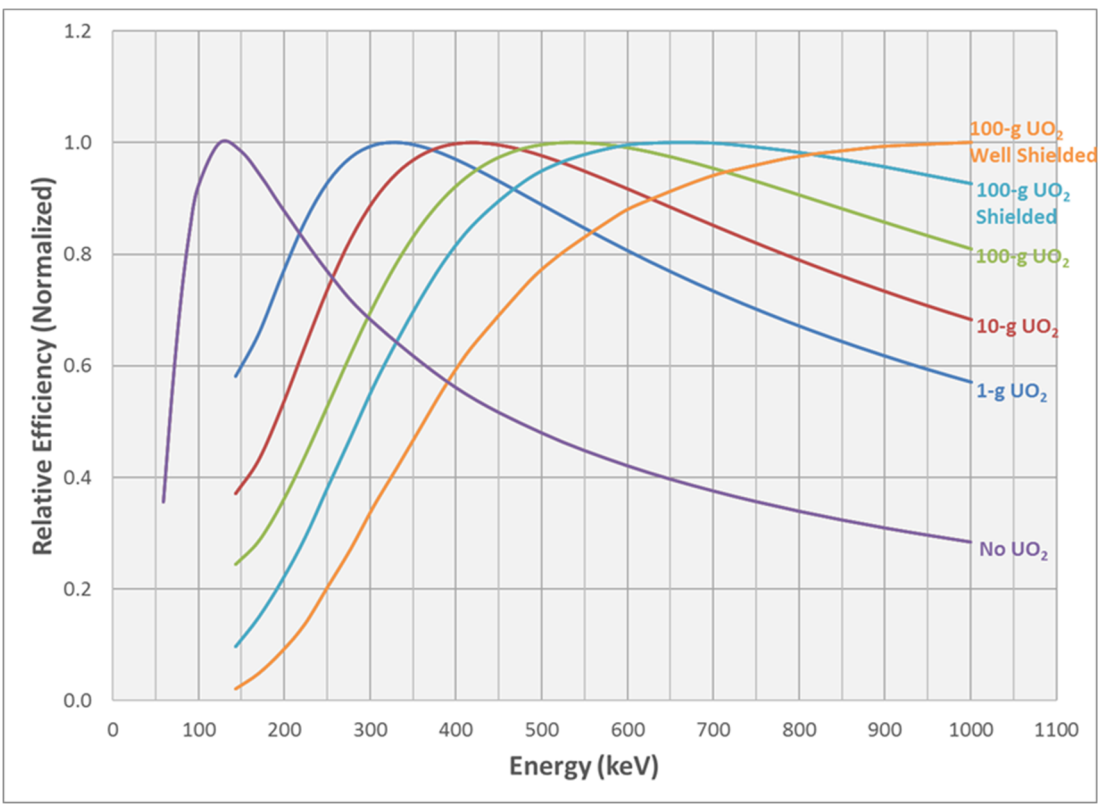


***Figure 14-2. Relative efficiency curves as a function of $UO_2$ mass and shielding.***

## 14.4 Relative efficiency curve generation

To generate an effective relative efficiency curve, it is necessary to have a radionuclide with full-energy peaks that span the energy range of interest or multiple radionuclides with full-energy peaks with sufficient overlapping or nearly overlapping energy ranges for the energy range of

interest. In addition, the isotopic composition throughout the sample must be the same for a relative efficiency curve to be valid.

### *14.4.1 Example A: Low enriched uranium sample*

An example of the relative efficiency curve generation process for an ORTEC Detective measurement of a known low enriched uranium sample is presented for illustrative purposes.

- Note: A similar process would generally be used for analysis of other depleted, natural, and low enriched uranium samples. An example of the relative efficiency curve generation process for measurements of highly enriched uranium samples is presented in Example B.

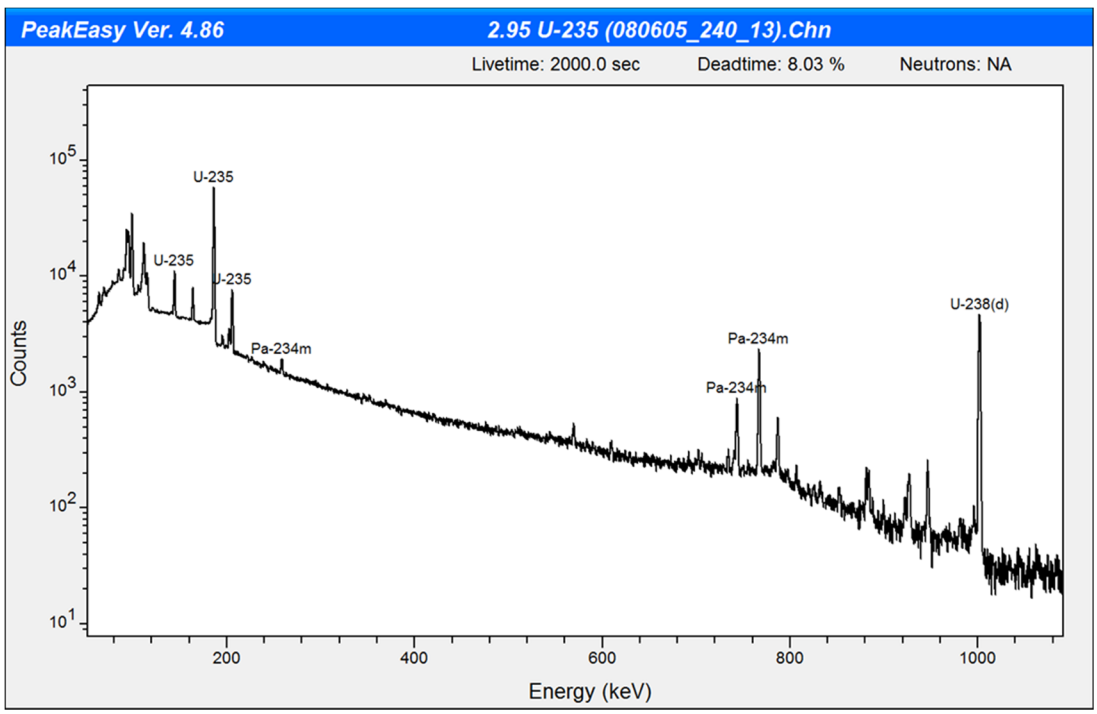


***Figure 14-3. Example A: Spectrum of low enriched uranium standard.***

1) For a selected radionuclide, divide the net full-energy peak counts by the yield for each gamma emission.

***Table 14-2. Example A: Relative efficiency curve generation (U-235): Step 1.***

| Nuclide | Energy (keV) | Yield (gps/dps) | Net Area (counts) | Net Area / Yield |
|---|---|---|---|---|
| U-235 | 143.8 | 1.10E-01 | 27974 | 2.54E+05 |
| U-235 | 163.3 | 5.05E-02 | 16719 | 3.31E+05 |
| U-235 | 185.7 | 5.70E-01 | 238763 | 4.19E+05 |
| U-235 | 205.3 | 5.03E-02 | 23549 | 4.68E+05 |

2) For the selected radionuclide, normalize the results using one of the selected radionuclide gamma emissions. Note: It is recommended that a high energy emission with good counting statistics be used when possible.

***Table 14-3. Example A: Relative efficiency curve generation (U-235): Step 2.***

| Nuclide | Energy (keV) | Yield (gps/dps) | Net Area (counts) | Net Area / Yield | Measured Relative Eff. |
|---|---|---|---|---|---|
| U-235 | 143.8 | 1.10E-01 | 27974 | 2.54E+05 | 0.6071 |
| U-235 | 163.3 | 5.05E-02 | 16719 | 3.31E+05 | 0.7904 |
| U-235 | 185.7 | 5.70E-01 | 238763 | 4.19E+05 | 1.0000 |
| U-235 | 205.3 | 5.03E-02 | 23549 | 4.68E+05 | 1.1177 |

Results normalized to the U-235 185.7 keV emission.

3) Plot the measured relative efficiency.

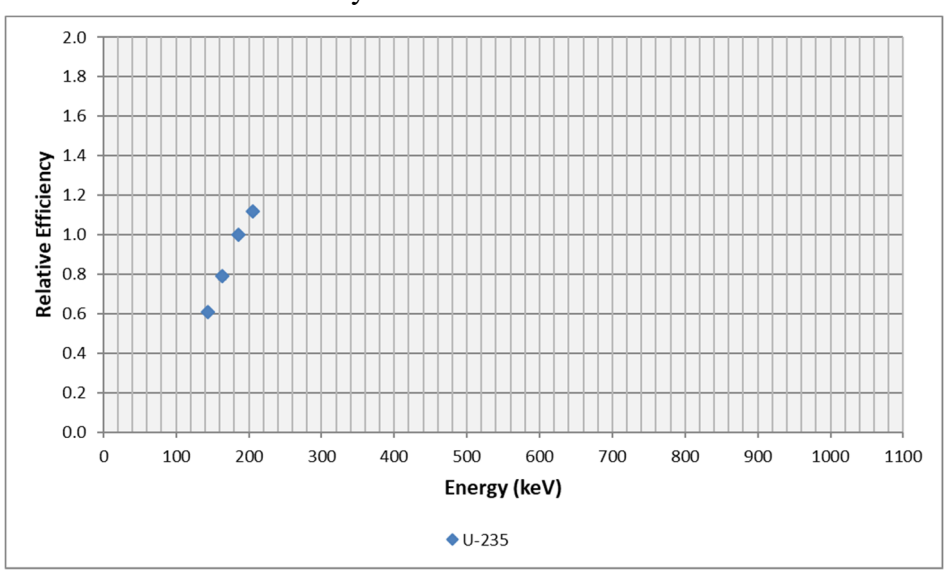


***Figure 14-4. Example A: Plot of measured relative efficiency (U-235): Step 3.***

4) Perform steps 1, 2, and 3 on remaining radionuclides.

***Table 14-4. Example A: Relative efficiency curve generation (U-238+): Step 1.***

| Nuclide | Energy (keV) | Yield (gps/dps) | Net Area (counts) | Net Area / Yield |
|---|---|---|---|---|
| U-238+ | 258.3 | 7.54E-04 | 2285 | 3.03E+06 |
| U-238+ | 766.4 | 3.07E-03 | 11561 | 3.76E+06 |
| U-238+ | 1001.0 | 8.37E-03 | 26372 | 3.15E+06 |

***Table 14-5. Example A: Relative efficiency curve generation (U-238+): Step 2.***

| Nuclide | Energy (keV) | Yield (gps/dps) | Net Area (counts) | Net Area / Yield | Measured Relative Eff. |
|---|---|---|---|---|---|
| U-238+ | 258.3 | 7.54E-04 | 2285 | 3.03E+06 | 0.9619 |
| U-238+ | 766.4 | 3.07E-03 | 11561 | 3.76E+06 | 1.1938 |
| U-238+ | 1001.0 | 8.37E-03 | 26372 | 3.15E+06 | 1.0000 |

Results normalized to the U-238+ 1001.0 keV emission.

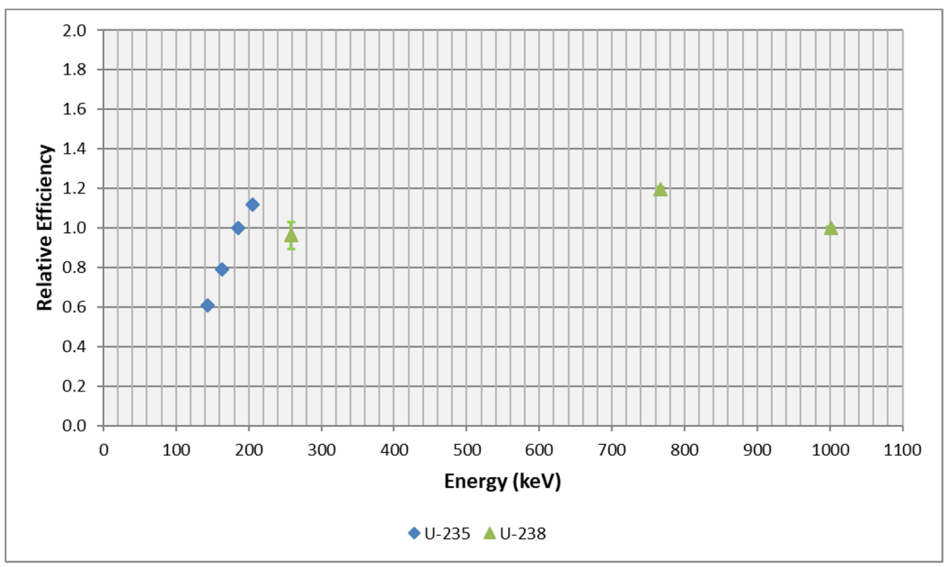


***Figure 14-5. Example A: Plot of measured relative efficiency without U-238+ activity scaling.***

Scale radionuclide efficiencies relative to the first selected radionuclide until a good fit is obtained.

- Note: The 258.3 keV U-238 peak is very important for depleted, natural, and low enriched uranium isotopic assessments and is used to link to the low energy U-235 emissions to the high energy U-238 emissions.

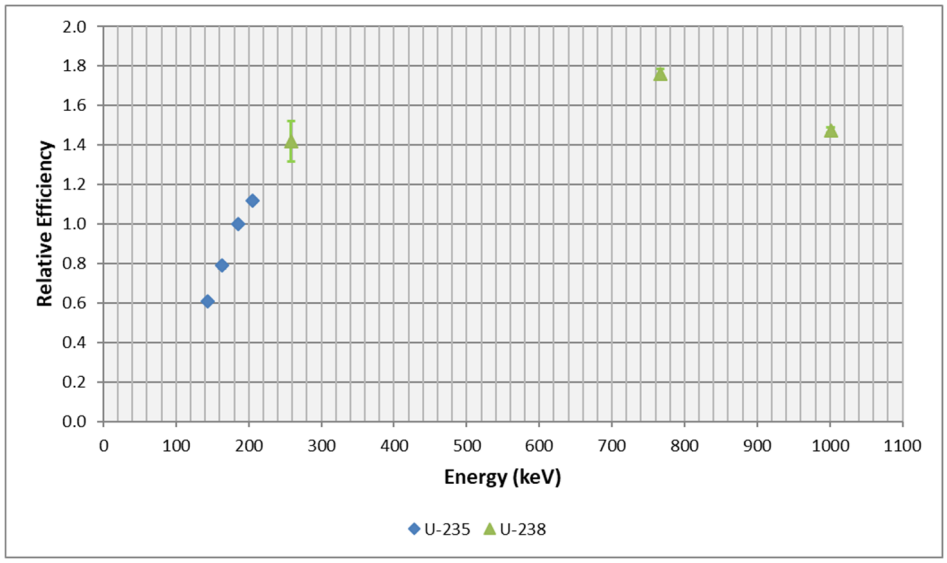


***Figure 14-6. Example A: Plot of measured relative efficiency with U-238+ activity scaling.***

Curve-fit the data to determine the relative efficiency as a function of energy.

$$\varepsilon_{rel} = 1.327\text{E+01} - 1.166\text{E+01} \cdot \ln E + 2.842\text{E+00} \cdot \ln(E)^2 - 2.027\text{E-01} \cdot \ln(E)^3$$

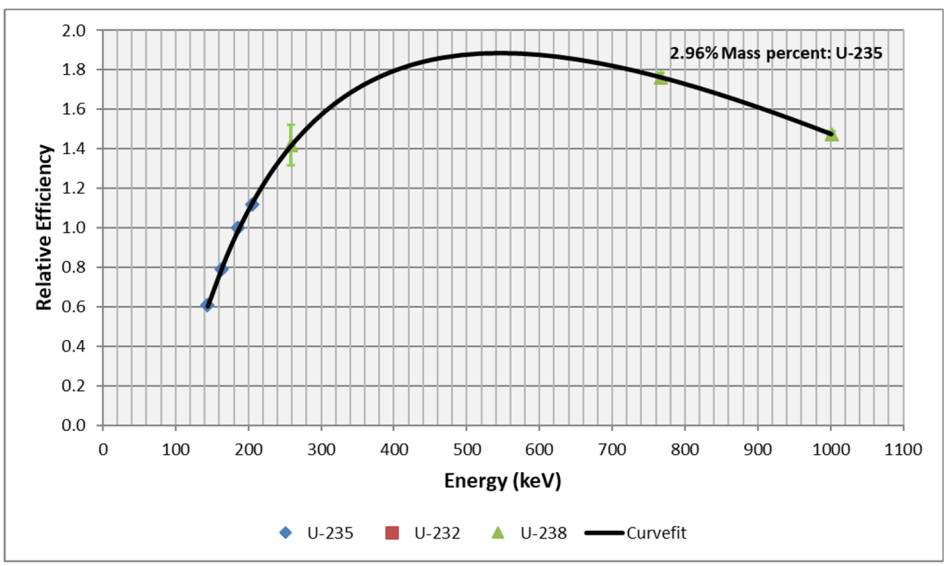


***Figure 14-7. Example A: Plot of relative efficiency curve-fit. Note: Actual 2.95% mass percent U-235. Analysis performed using SNL_Relative_Eff_Uiso.xlsb.***

Utilize the curve-fit to determine relative efficiencies and activities for other radionuclides present, as needed.

### *14.4.2 Example B: Highly enriched uranium sample*

An example of the relative efficiency curve generation process for an ORTEC Detective measurement of a known highly enriched uranium sample is presented for illustrative purposes.

- Note: For highly enriched uranium samples, U-232 emissions (238.6, 583.2, 727.3, and 860.6 keV) are commonly used to bridge the gap in the relative efficiency curve between the U-235 low energy emissions (143.8, 163.3, 185.7, and 205.3 keV) and the U-238 high energy emissions (742.8, 766.4, and 1001.0 keV).

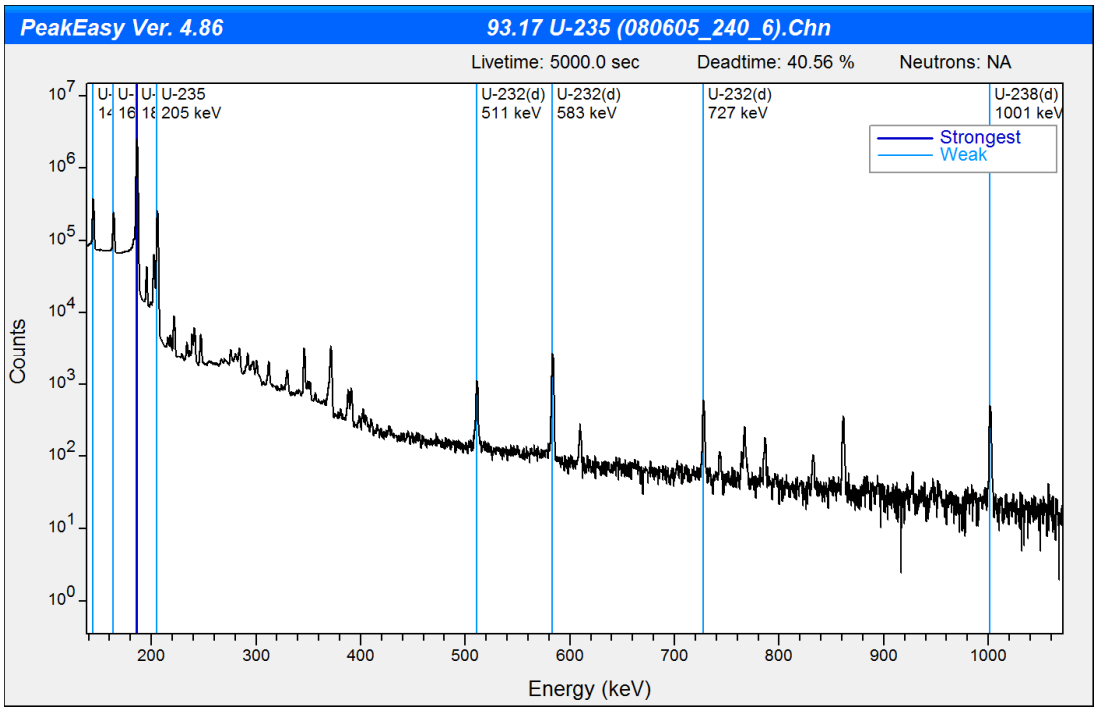


*Figure 14-8. Example B: Spectrum of highly enriched uranium standard.*

*Table 14-6. Example B: Relative efficiency curve generation (U-235).*

| Nuclide | Energy (keV) | Yield (gps/dps) | Net Area (counts) | Net Area / Yield | Measured Relative Eff. |
|---|---|---|---|---|---|
| U-235 | 143.8 | 1.10E-01 | 1282939 | 1.17E+07 | 0.6001 |
| U-235 | 163.3 | 5.05E-02 | 785728 | 1.56E+07 | 0.8006 |
| U-235 | 185.7 | 5.70E-01 | 11077932 | 1.94E+07 | 1.0000 |
| U-235 | 205.3 | 5.03E-02 | 1138432 | 2.26E+07 | 1.1645 |

Results normalized to the U-235 185.7 keV emission.

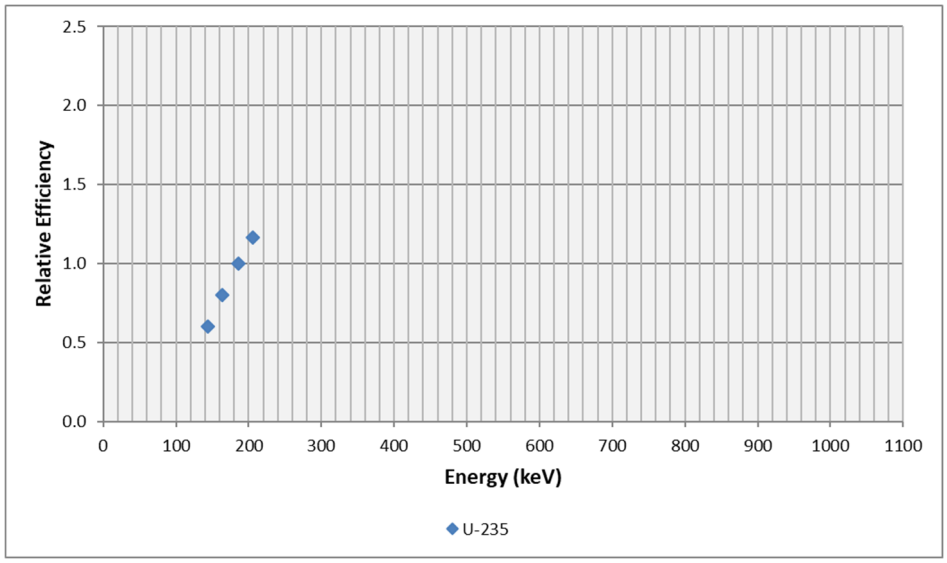


***Figure 14-9. Example B: Plot of measured relative efficiency (U-235).***

***Table 14-7. Example B: Relative efficiency curve generation (U-232+).***

| Nuclide | Energy (keV) | Yield (gps/dps) | Net Area (counts) | Net Area / Yield | Measured Relative Eff. |
|---|---|---|---|---|---|
| U-232+ | 238.6 | 4.80E-01 | 14899 | 3.10E+04 | 0.6468 |
| U-232+ | 583.2 | 3.06E-01 | 14685 | 4.80E+04 | 1.0000 |
| U-232+ | 727.3 | 6.76E-02 | 2964 | 4.38E+04 | 0.9136 |
| U-232+ | 860.6 | 4.60E-02 | 1808 | 3.93E+04 | 0.8190 |

Results normalized to the U-232+ 583.2 keV emission.

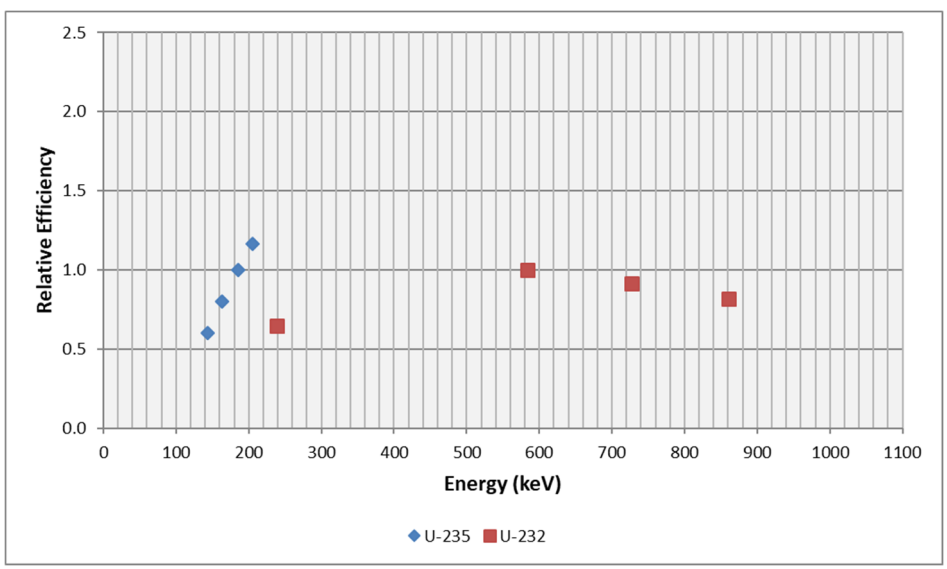


***Figure 14-10. Example B: Plot of measured relative efficiency without U-232+ activity scaling.***

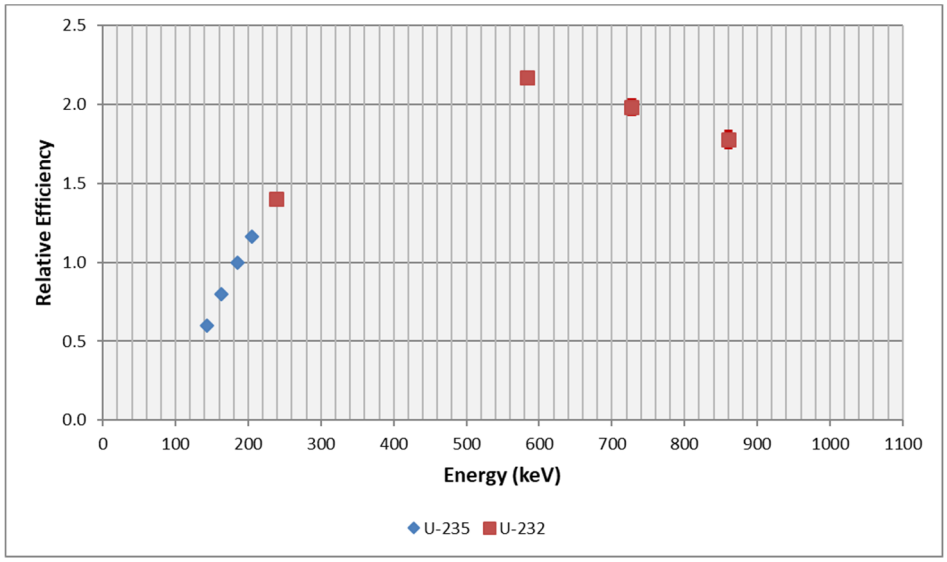


***Figure 14-11. Example B: Plot of measured relative efficiency with U-232+ activity scaling.***

***Table 14-8. Example B: Relative efficiency curve generation (U-238+).***

| Nuclide | Energy (keV) | Yield (gps/dps) | Net Area (counts) | Net Area / Yield | Measured Relative Eff. |
|---|---|---|---|---|---|
| U-238+ | 766.4 | 3.07E-03 | 1365 | 4.44E+05 | 1.3939 |
| U-238+ | 1001.0 | 8.37E-03 | 2667 | 3.19E+05 | 1.0000 |

Results normalized to the U-238+ 1001.0 keV emission.

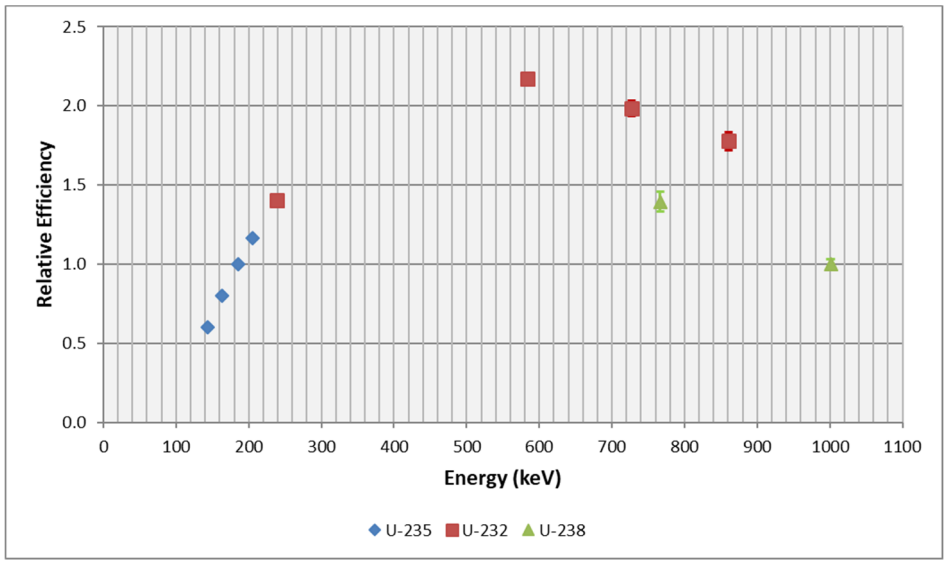


***Figure 14-12. Example B: Plot of measured relative efficiency without U-238+ activity scaling.***

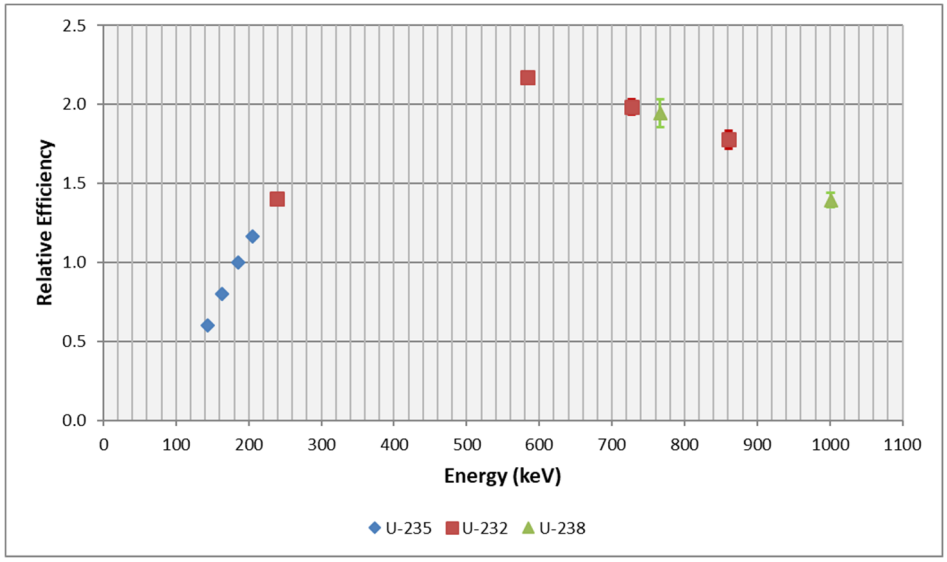


***Figure 14-13. Example B: Plot of measured relative efficiency with U-238+ activity scaling.***

Curve-fit the data to determine the relative efficiency as a function of energy.

$$\varepsilon_{rel} = 7.222\text{E+01} - 4.364\text{E+01} \cdot \ln E + 8.570\text{E+00} \cdot \ln(E)^2 - 5.408\text{E-01} \cdot \ln(E)^3$$

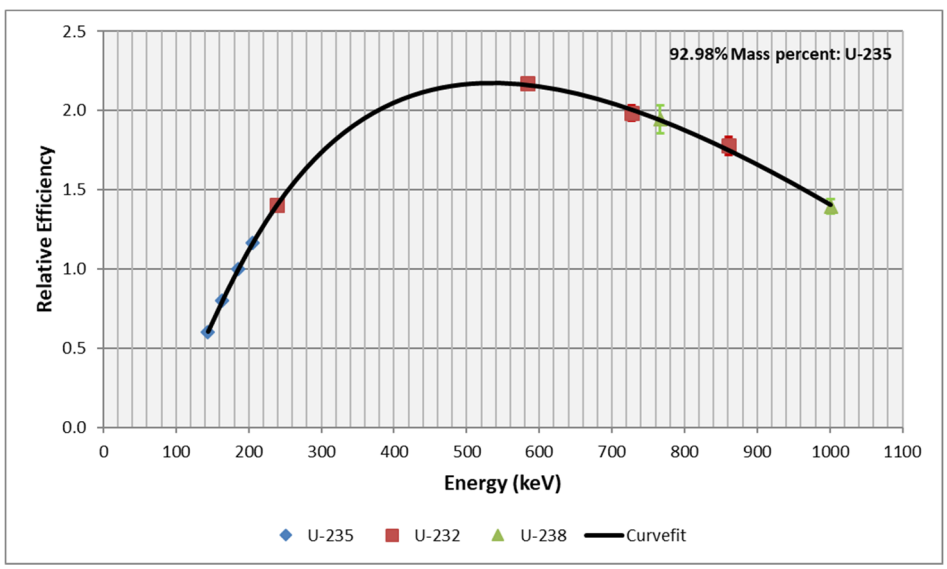


***Figure 14-14. Example B: Plot of relative efficiency curve-fit. Note: Actual 93.17% mass percent U-235. Analysis performed using SNL_Relative_Eff_Uiso.xlsb.***

## 14.5 Additional notes

- Counting statistics determine the ability to obtain precise results.
- Review full-energy peak fits for reasonableness.
- Review the spectrum for interferences.
- If U-232 is used in the relative efficiency curve, it might be necessary to perform proper background subtraction to accurately determine U-232 full-energy peak areas.
- Use of a relative efficiency curve does not correct for coincidence summing effects. Per Reference [38], "Coincidence summing effects are present in low-enriched uranium measurements analyzed in the 120-1001 keV energy range. The 258-keV gamma ray from the U-238 daughter Pa-234m is particularly affected." In addition, Reference [38] states "Coincidence summing is not recognized to be a problem with plutonium measurements."
- Another common definition for relative efficiency is the efficiency of the detector at 1332.5 keV to that of a 3-inch x 3-inch NaI gamma-radiation detector at 25-cm from the detector endcap which is quoted as $1.2 \times 10^{-3}$ counts per gamma for a point source. Therefore, relative efficiency values greater than 100% can be encountered when working with large or very large germanium detectors.

# SECTION 15.0 ROUTINE PERFORMANCE CHECKS

## Table of Contents

## 15.1 Introduction

A complete treatment of performance check measurements is beyond the scope of this document. Only key aspects of routine performance check measurements for instruments that record gamma ray energy spectra are described below. For additional information on performance checks and control chart generation, please see Reference [39] and/or Section 15.4 of Reference [4].

Source performance checks and background performance checks should be performed on a routine basis to verify that the detector system is operating properly. The frequency of performance checks should be based on the goals and objectives for the measurements being performed as well as the characteristics of the detector system.

## 15.2 Source performance checks

To ensure that the energy and efficiency calibration of a detector system is stable, performance check source measurements are commonly used to monitor full-energy peak location, resolution, and efficiency. Since performance checks compare relative values at a given energy, the performance check source does not need to be calibrated or National Institute of Standards and Technology (NIST) traceable. However, the performance check source should have a long half-life and be of sufficient source strength to provide well-defined full-energy peaks (at least 10,000 net counts in the full-energy peaks used) within a short count period over the energy range of interest. In addition, the source position should be reproducible so that efficiency performance checks are valid.

When circumstances preclude collection of a source performance check, the acquired background and sample spectrum should be reviewed shortly after collection to ensure full-energy peak locations and widths at low and high energy are consistent with the energy and resolution calibration. As soon as reasonable following acquisition of the background and sample spectrum, a source performance check should be performed to support the validity of the measurement results. Source performance checks are generally recommended to be performed each day or at a minimum, each week that measurements are collected.

## 15.3 Source performance check control charts

Each time a source performance check measurement is performed, the full-energy peaks should be analyzed with the software program routinely used. To evaluate changes in performance with respect to time, the peak locations, areas, and widths should be recorded on a control chart or data file and compared with the results of the previous performance check measurements. Control charts utilize a measure of central tendency (mean, median, etc.) and dispersion (sigma, range, etc.) to allow detection of patterns or unusual data trends. The measures of central tendency and dispersion used in control charts, as well as the criteria used to establish warning and action limits, should be documented.

Control charts should be constructed using individual and/or grouped measurement results with limits consistent with the goals and objectives for the measurements being performed. To determine limits for detector systems without a sufficient operational history, it is desirable to collect many measurements over a short time period utilizing several operators at various times of the day.

## 15.4 Background performance checks

In addition to performance checks that utilize a source, collection and monitoring of background spectra at a designated location should be considered if other radioactive sources are used near the detector or if there is a potential for detector assembly contamination during the test campaign. These measurements are made to verify consistent instrument performance and should not be confused with the background measurements that are made in conjunction with the measurements being performed. Background performance checks should be conducted with the same frequency as the source performance checks.

Ra-226 and Th-232 decay chains before radon and thoron, respectively, can be considered constant. However, due to routine changes in environmental conditions that affect the amount of radon and thoron in the air and soil, the natural gamma ray background for Ra-226 and Th-232 decay chains below radon and thoron, respectively, cannot be considered a constant and should not be used when comparing background spectra.

## 15.5 Background performance check control charts

If the background spectra are reviewed and monitored as outlined above, construction of background performance check control charts as a check of performance is not necessary.

# SECTION 16.0 MISCELLANEOUS

## Table of Contents



## Figures



## Tables

## Equations

## 16.1 Mean free path

The mean free path is the average distance a gamma ray travels in the absorber before interacting; it is also the absorber thickness that produces a transmission of 1/e, or 0.37, which is equal to 1 / linear attenuation coefficient.

## 16.2 Absorption edge

The absorption edge is a sudden increase in the attenuation coefficient of photons occurring at a photon energy just above the binding energy of the shell electron of the atoms interacting with the photons. A photon having an energy just above the binding energy of the electron is therefore more likely to be absorbed than a photon having an energy just below this binding energy (see Figure 16-1).

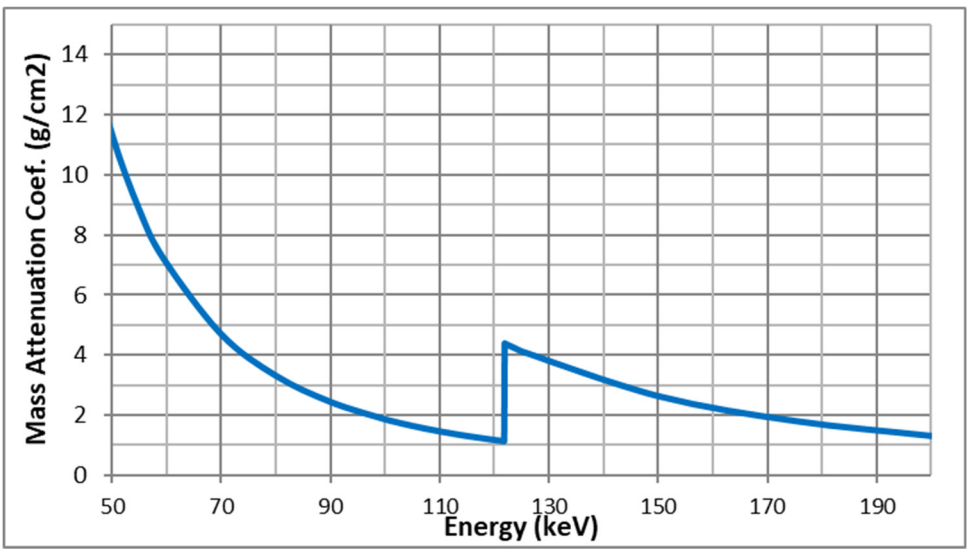


***Figure 16-1. Mass attenuation coefficient as a function of energy for plutonium with absorption edge at 121.8 keV [40].***

## 16.3 Inverse square law

Inverse square law: Radiation intensity decreases with the square of the distance from a point source.

If the distance from a radiation source is at least three times the longest dimension of the source, the source can be treated as a point source and the inverse square law will give the correct answer within a percent.

## 16.4 Decay during the count correction equation

For short-lived radionuclides measured with long count times (count times exceeding a few percent of the radionuclides half-life), the count rate should be corrected for radioactive decay during the count using Equation 16-1. When applied, the count rate is corrected to the start of the count. In lieu of using Equation 16-1, the table provided in *Appendix F. Decay During the Count Correction Factors* can be used.

**Equation 16-1. Correction factor equation for decay during the count.**

$$F_c = \frac{\lambda \cdot t}{1 - e^{-\lambda \cdot t}}$$

Where:
$F_C$ = Decay during the count correction factor (unitless);
$\lambda$ = Radionuclide decay constant (seconds $^{-1}$);
$t$ = Count time (seconds).

## 16.5 Attenuation correction equations

Gamma ray transmission through a shield can be calculated using Equation 16-2.

**Equation 16-2. Shield attenuation equation. [33]**

$$I = I_0 \cdot e^{\frac{\mu}{\rho} \cdot \rho x} = I_0 \cdot e^{-\mu \cdot x}$$

Where:
$I$ = Gamma ray intensity with shielding in place;
$I_0$ = Gamma ray intensity without shielding in place;
μ = Linear attenuation coefficient (cm$^{-1}$);
$\frac{\mu}{\rho}$ = Mass attenuation coefficient (cm$^2$/g)
$\rho$ = Density (g/cm$^3$);
$\rho x$ = Mass or density thickness (g/cm$^2$);
$x$ = Shield thickness (cm).

Self-attenuation transmission for an infinite slab source and spherical source can be calculated using Equation 16-3 and Equation 16-4, respectively.

**Equation 16-3. Infinite slab source self-attenuation transmission equation. [33]**

$$T_{slab} = \frac{1}{\mu x} \cdot (1 - e^{-\mu x})$$

Where:
$T_{slab}$ = Transmission (unitless);
μ = Linear attenuation coefficient (cm$^{-1}$);
$x$ = Slab thickness normal to the detector (cm).

**Equation 16-4. Spherical source self-attenuation transmission equation. [33]**

$$\boldsymbol{T_{sphere} = \left[\left(\frac{3}{2\mu D}\right) \cdot \left[\left(1 - \frac{2}{\mu D^2} + e^{-\mu D} \cdot \left(\frac{2}{\mu D} + \frac{2}{\mu D^2}\right)\right)\right]\right]^{-1}}$$

Where:
$T_{sphere}$ = Transmission (unitless);
$\mu$ = Linear attenuation coefficient ($cm^{-1}$);
$D$ = Sphere diameter (cm).

## 16.6 Chemically processed natural thorium

### *16.6.1 Th-228 to Th-232 activity ratio determinations and time since last chemical separation estimates*

When thorium ores are mined and processed, Th-232 and Th-228, present in the Th-232 decay chain (see Figure 3-3) in secular equilibrium, will remain in the chemically separated natural thorium. Due to the presence of Th-228 following chemical separation and Th-232 not being readily detectable by gamma spectroscopy, Th-228 to Th-232 activity ratio determinations by gamma spectroscopy can become complicated. Accordingly, Figure 16-2 and Figure 16-3 are provided to assist gamma spectroscopists with proper Th-228 to Th-232 activity ratio determinations as well as time since last chemical separation estimates.

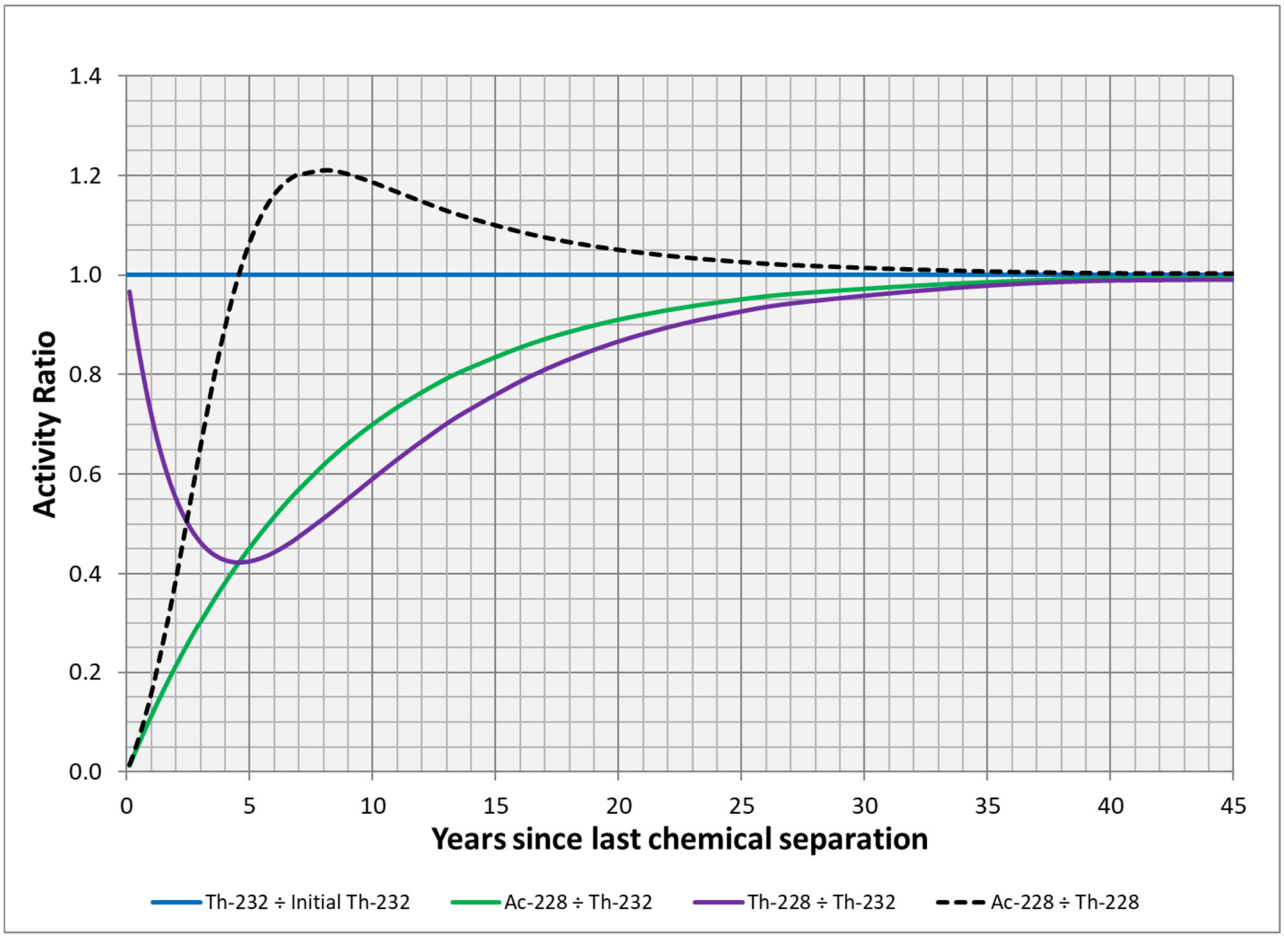


***Figure 16-2. Activity ratio following separation of Th-232 and Th-228: <u>0.1 to 45 years</u>.***

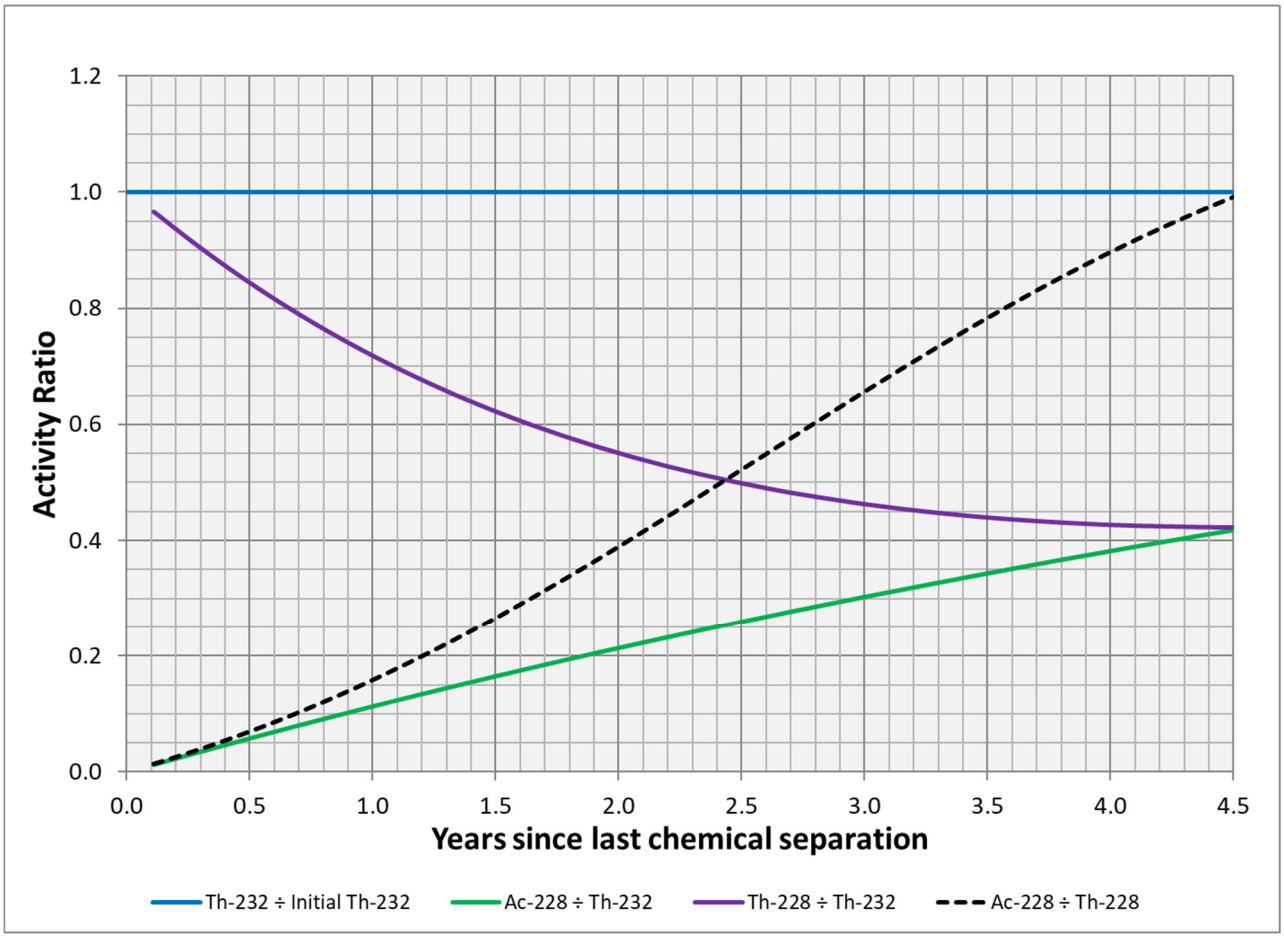


***Figure 16-3. Activity ratio following separation of Th-232 and Th-228: 0.1 to 4.5 years.***

### *16.6.2 Th-232 time since last chemical separation and activity estimate example*

A chemically processed natural thorium sample is measured by gamma spectroscopy. Estimate the time since last chemical separation and Th-232 activity using the gamma spectroscopy results presented in Table 16-1.

***Table 16-1. Relevant information for Th-232 age and activity estimate example.***

| Nuclide | Energy (keV) | Yield (gps/dps) | Activity (Bq) |
|---|---|---|---|
| Tl-208 (Th-228) | 860.6 | 4.47E-02 | 9405.2 |
| Ac-228 | 911.2 | 2.58E-01 | 3336.4 |

Tl-208 (Th-228): Yield includes the 35.94% branch from its parent nuclide, Bi-212 per ICRP Publication 107.

The measured Ac-228 to Th-228 activity ratio is 3336.4 Bq / 9405.2 Bq or 0.355 which corresponds to a time since last chemical separation estimate of 1.9 years using the black dashed line in Figure 16-3.

Additionally, the Th-232 activity can be estimated using the Ac-228 result and the Ac-228 to Th-232 activity correction factor (green line) from Figure 16-3 (3336.4 Bq / 0.20 = 16.7 kBq). Alternatively, the Th-232 activity can be estimated using the Th-228 result and the Th-228 to Th-232 activity correction factor (purple line) from Figure 16-3 (9405.2 Bq / 0.55 = 17.1 kBq).

### *16.6.3 Presence of Th-230*

As members of the U-238 decay chain (see Figure 3-1), Th-234 (half-life = 24.1 days) and Th-230 (half-life = 7.7E+04 years), are found in natural uranium. If natural uranium is present when thorium ores are mined and chemically processed, Th-234 and Th-230 from the U-238 decay chain as well as Th-232 and Th-228 from the Th-232 decay chain (see Figure 3-3) will be present.

Due to its long half-life, significant quantities of Th-230 by activity can remain with Th-232 in chemically processed natural thorium. However, the Th-230 to Th-232 activity ratio is highly variable and dependent on the origin of the material. Per Reference [41], thorium has been recovered as a by-product of uranium production from ores of the Blind River district in Ontario in which the Th-230 activity is 18.6 times the activity of the Th-232. Additionally, the Th-230 to Th-232 activity ratio in thorium electrodes used in tungsten inert gas (TIG) welding can reach 90%. [42]

Since Th-230 is a weak gamma emitter with its primary gamma emission being susceptible to self-attenuation (67.7 keV, yield 0.38%), it is generally not detectable by gamma spectroscopy. However, if significant quantities of aged, chemically processed natural thorium are measured by gamma spectroscopy, Ra-226 decay products from Th-230 decay can be detectable.

### *16.6.4 Th-230 to Th-232 activity ratio example*

A source containing 16 natural thorium bars totaling 358-g of Th-232 is measured using a p-type HPGe detector (60% relative efficiency). In addition, a background measurement is collected using the same HPGe detector.

***Figure 16-4. NIST traceable thorium bar source.***

Using the age provided for the source (34 years) and assuming the efficiency for the 609.3 keV (Bi-214 from the Ra-226 decay chain) and 583.2 keV (Tl-208 from the Th-232 decay chain) full-energy peaks are equal, estimate the Th-230 to Th-232 activity ratio.

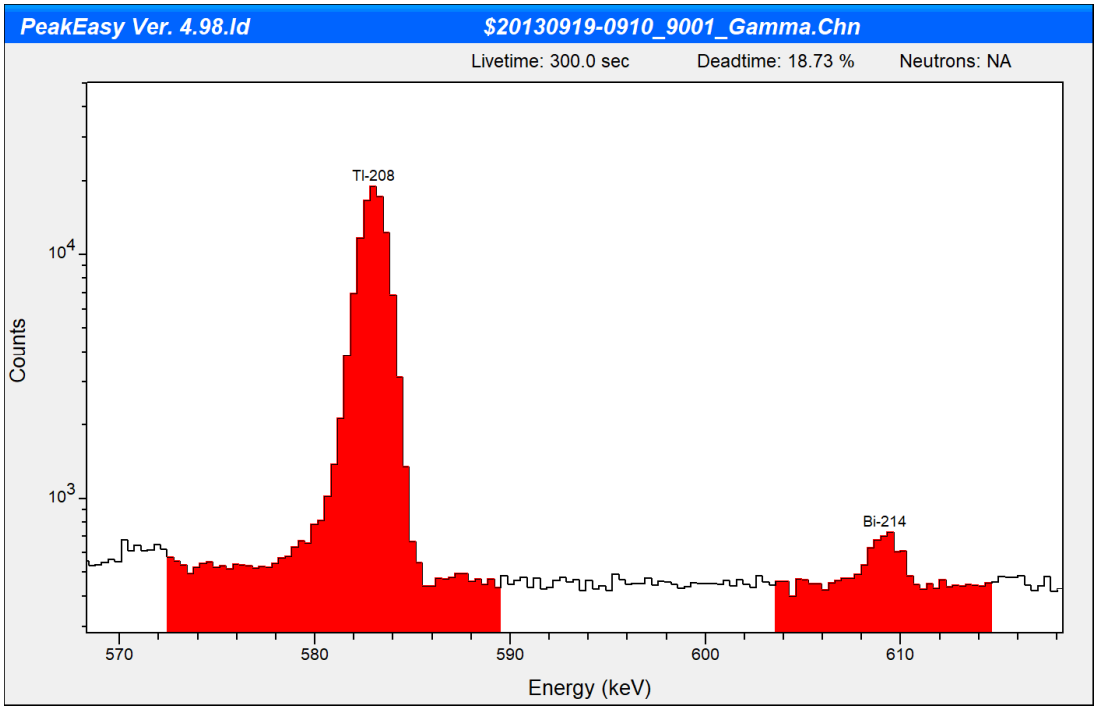


***Figure 16-5. NIST traceable thorium bar background subtracted spectrum.***

***Table 16-2. Relevant information for NIST traceable thorium bar.***

| Nuclide | Energy (keV) | Yield (gps/dps) | Net Area (counts) | Net Area / Yield |
|---|---|---|---|---|
| Th-232+ | 583.2 | 3.05E-01 | 100011 | 3.28E+05 |
| Ra-226+ | 609.3 | 4.61E-01 | 1602 | 3.48E+03 |

Ra-226+/Th-232+ activity ratio estimate = 3.48E+03 / 3.28E+05= 1.06E-02.

Thirty-four years after chemical processing, the Th-230 to Ra-226 activity ratio is 68.38 per Equation 4-1. Therefore, the estimated Th-230 to Th-232 activity ratio is 68.38 x 1.06E-02 = 0.73.

## 16.7 Doppler broadening

Reactions such as (n,n'γ), (α,nγ), (p,αγ), (n,αγ) leave the nucleus in an excited state which subsequently deexcites by gamma emission. If these reactions occur on light targets (such as B, Be, Li, etc.), the nucleus can acquire significant kinetic energy and, dependent on the mean lifetime of the excited nucleus, deexcite during flight (moving either toward or away from the detector). If deexcitation occurs while moving toward the detector, the measured photon energy will be larger than the energy measured for a photon emitted from a nucleus at rest. Alternatively, if deexcitation occurs while moving away the detector, the measured photon energy will be less than the energy measured for a photon emitted from a nucleus at rest. [43]

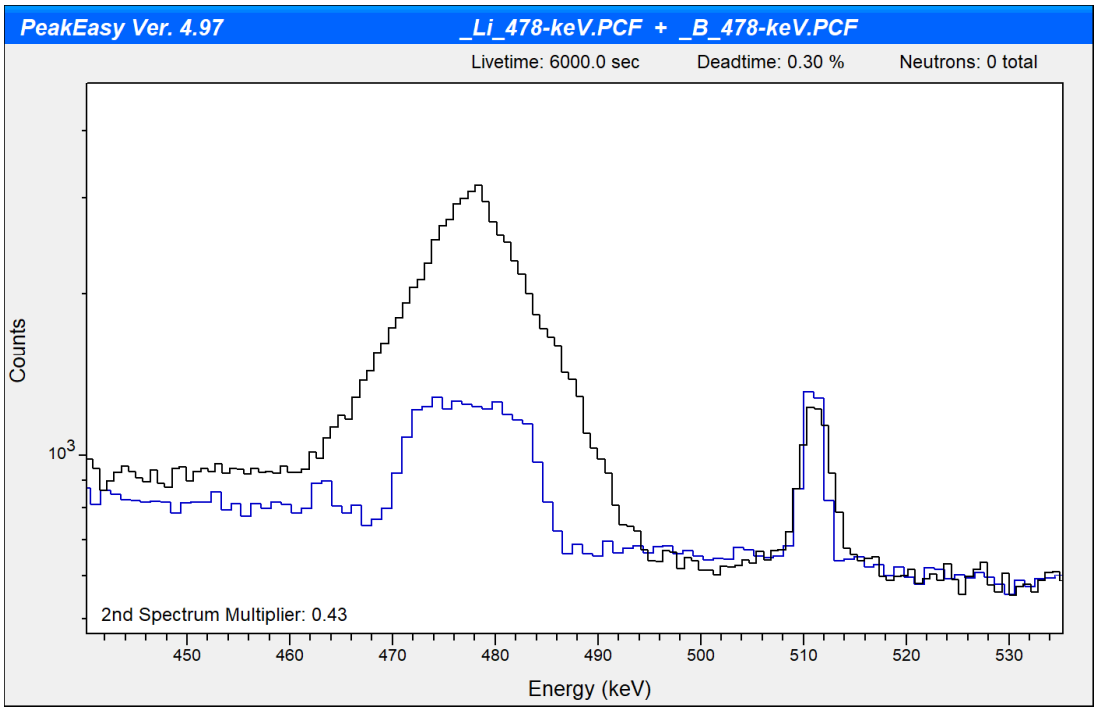


***Figure 16-6. Doppler broadening examples: Li-7(α,α'γ)Li-7 = Doppler broadened triangle (black); B-10(n,αγ)Li-7 = Doppler broadened square (blue).***

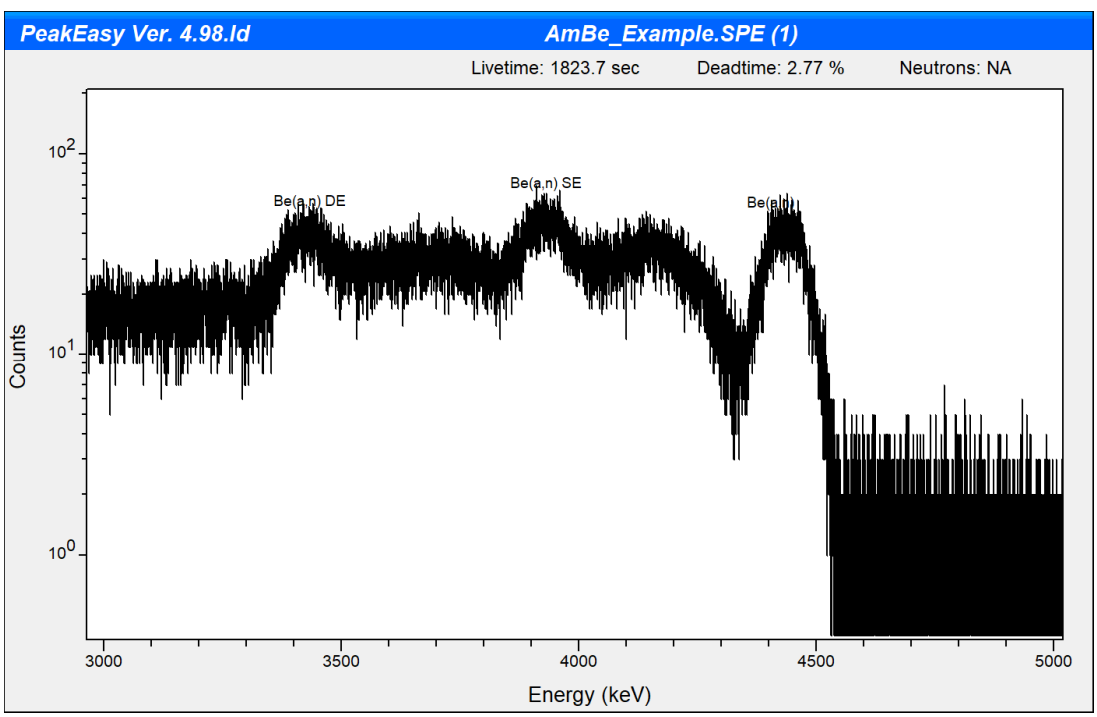


***Figure 16-7. Doppler broadened full-energy peak at 4438.9 keV from Am-241:Be-9(α,nγ)C-12 source with single and double escape peaks labeled.***

## 16.8 Common gamma signatures from neutron interactions

In addition to *Neutron interactions on germanium* discussed in SECTION 6.0, gamma rays from neutron capture (n,γ) and neutron scatter (n,n'γ) reactions on common metals and non-metals are occasionally seen in gamma ray spectra. Table 16-3 presents primary gamma emissions from neutron interactions on hydrogen, aluminum, chlorine, cadmium, and iron.

***Table 16-3. Primary gamma emissions from neutron interactions on hydrogen, aluminum, chlorine, cadmium, and iron.***

| Reaction | Energy (keV) |
|---|---|
| Cd-113(n,γ) | 558.6 |
| Al(n,n'γ) | 843.8 |
| Fe(n,n'γ) | 846.8 |
| Al(n,n'γ) | 1014.4 |
| Cl-35(n,γ) | 1164.7 |
| Al-27(n,γ) | 1779.1 |
| Cl-35(n,γ) | 1950.9 |
| H-1(n,γ) | 2223.3 |
| Fe-56(n,γ) | 7631.1 |
| Fe-56(n,γ) | 7645.5 |

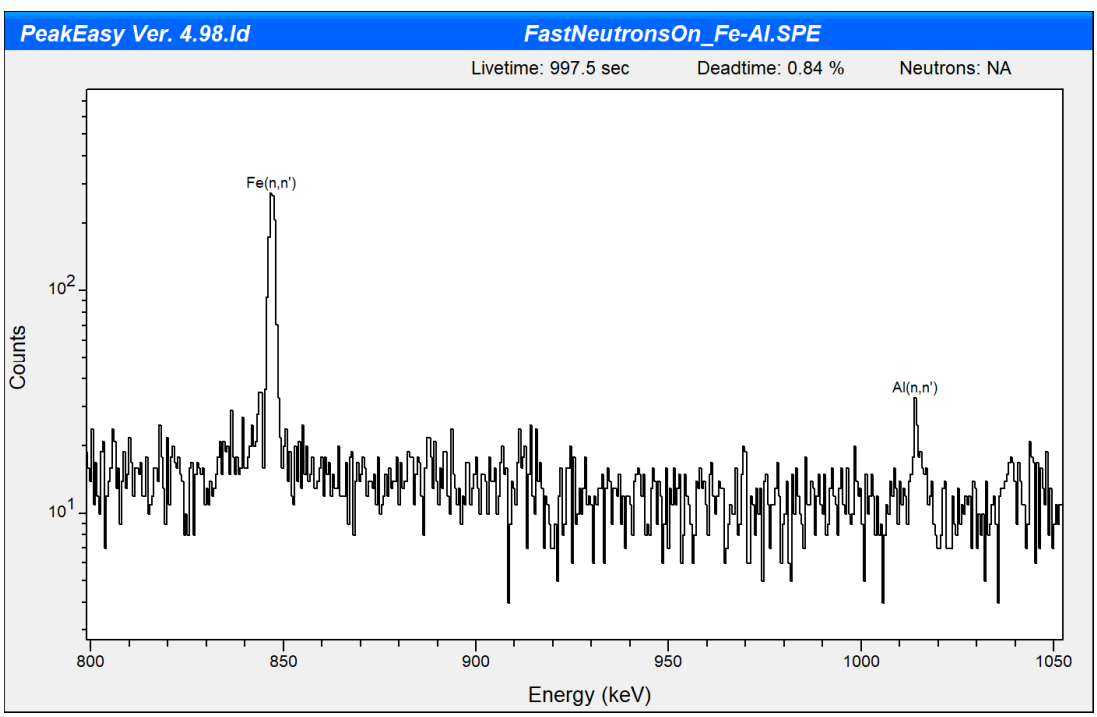


***Figure 16-8. Full-energy peaks from neutron scatter (n,n'γ) reactions on iron (846.8 keV) and aluminum (1014.4 keV).***

Lastly, elevated continuum counts above the Th-232 decay chain 2614.5 keV full-energy peak (which is generally the highest full-energy peak in a spectrum) can indicate the presence of neutron source due to neutron-capture reactions and high energy fission gamma rays. Alternatively, elevated continuum counts above 2614.5 keV may be due to a high energy gamma emitter such as Co-56, pulse pileup if high dead times are present, or true/cascade coincidence summing if sample to detector distance is small.

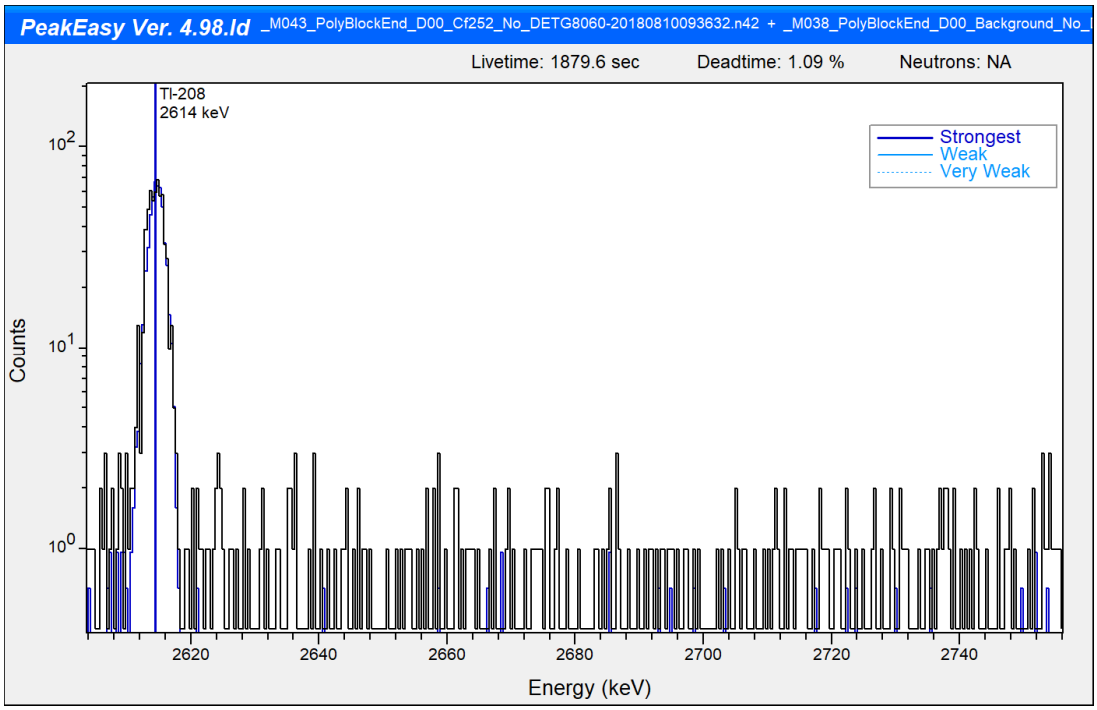


***Figure 16-9. Example of neutron source generating elevated continuum counts above 2614.5 keV. Cf-252 spectrum 0.273 cps above 2614.5 keV (black), Background spectrum 0.055 cps above 2614.5 keV (blue)***

## 16.9 Cf-252 activity and time since last chemical separation estimates [44]

For all practical purposes, Cf-252 is undetectable by gamma spectroscopy. However, Cf-252 activity and time since last chemical separation estimates can be made using gamma spectroscopy results in conjunction with the methods illustrated in the following examples.

- Note: A similar process can be used for other difficult to detect spontaneous fission emitters, such as Cm-244, to estimate activity and time since last chemical separation.

### *16.9.1 Cf-252 activity estimates*

A Cf-252 source is measured by gamma spectroscopy. Calculate the activity of the Cf-252 source using the La-140 and Cs-138 fission product full-energy peaks at 1596.2 and 1435.9 keV, respectively.

***Table 16-4. Relevant information for Cf-252 source activity determination example.***

| Nuclide | Energy (keV) | Yield (gps/dps) | Count Rate (cps) | Count Rate Unc. 1-Sigma (cps) | Efficiency (c/g) |
|---|---|---|---|---|---|
| La-140 | 1596.2 | 9.54E-01 | 0.585 | 0.047 | 3.02E-04 |
| Cs-138 | 1435.9 | 7.63E-01 | 0.559 | 0.050 | 3.26E-04 |

***Table 16-5. Cf-252 cumulative spontaneous fission product yields for mass number 140 and 138. [9]***

| Nuclide | t1/2 | Ind. Yield | Cum. Yield |
|---|---|---|---|
| 140Te | 0.894s | 8.48E-04 | 8.48E-04 |
| 140I | 0.86 s | 1.16E-01 | 1.17E-01 |
| 140Xe | 13.6 s | 2.55E+00 | 2.67E+00 |
| 140Cs | 1.06 m | 2.77E+00 | 5.44E+00 |
| 140Ba | 12.75d | 5.16E-01 | 5.95E+00 |
| 140La | 1.678d | 5.03E-03 | 5.96E+00 |

| Nuclide | t1/2 | Ind. Yield | Cum. Yield |
|---|---|---|---|
| 138Sn | | 6.66E-08 | 6.66E-08 |
| 138Sb | 0.173s | 2.03E-04 | 2.03E-04 |
| 138Te | 1.4 s | 5.41E-02 | 5.43E-02 |
| 138I | 6.5 s | 1.00E+00 | 1.06E+00 |
| 138Xe | 14.1 m | 3.63E+00 | 4.67E+00 |
| 138Cs-m | 2.9 m | 3.01E-01 | 3.01E-01 |
| 138Cs | 32.2 m | 5.73E-01 | 5.47E+00 |

***Table 16-6. Cf-252 spontaneous fission rate and multiplicity.***

| Nuclides | Spontaneous Fission Rate (sf/s-Ci) | Spontaneous Fission Multiplicity (neutrons/sf) |
|---|---|---|
| Cf-252 | 1.16E+09 | 3.76 |

- Calculate the gamma emission rate.

  Divide the measured count rate by the efficiency.

  - La-140 1596.2 keV gamma emission rate = 0.585 cps / 3.02E-04 c/g = 1.94E+03 gps
  - Cs-138 1435.9 keV gamma emission rate = 0.559 cps / 3.26E-04 c/g = 1.71E+03 gps

- Calculate the Cf-252 spontaneous fission rate.

Divide the *gamma emission rate* by the gamma yield multiplied by the cumulative spontaneous fission yield.

- Using the La-140 1596.2 keV peak: 1.94E+03 gps / (0.954 gps/dps x 0.0596) = 3.41E+04 fissions/second
- Using the Cs-138 1435.9 keV peak: 1.71E+03 gps / (0.763 gps/dps x 0.0547) = 4.10E+04 fissions/second

- Calculate the **Cf-252 activity**.

  Divide the *Cf-252 spontaneous fission rate* by the spontaneous fission rate per Ci (1.16E+09 sf/s-Ci).

  - Using the La-140 1596.2 keV peak: 8.54E+04 fissions/second / 1.16E+09 sf/s-Ci = 2.94E-05 Ci or 29.4 μCi
  - Using the Cs-138 1435.9 keV peak: 1.03E+05 fissions/second / 1.16E+09 sf/s-Ci = 3.54E-05 Ci or 35.4 μCi

- Calculate the Cf-252 spontaneous neutron emission rate.

  Multiply the *Cf-252 spontaneous fission rate* by the Cf-252 spontaneous fission multiplicity (3.76 neutrons/sf).

  - Using the La-140 1596.2 keV peak: 3.41E+04 fissions/second x 3.76 neutrons/sf = 1.28E+05 neutrons/second
  - Using the Cs-138 1435.9 keV peak: 4.10E+04 fissions/second x 3.76 neutrons/sf = 1.54E+05 neutrons/second

- Note: The methods described above are valid once La-140 and Cs-138 fission product activities have reached equilibrium (63.8 days and 2.7 hours, respectively, using 5 half-lives or 96.9% equilibrium).

- Note: The known Cf-252 source activity was 32.8 μCi.

### *16.9.2 Cf-252 time since last chemical separation estimates*

Cf-252 age estimates can be made using the measured gamma spectroscopy Cs-137 to I-132 activity ratio in conjunction with calculated Cs-137 to I-132 activity ratios as a function of time since last chemical separation. Using Equation 16-5, Cs-137 and I-132 activities from Cf-252 spontaneous fission as a function of time since last chemical separation can be calculated. Alternatively, *Appendix B. Time Since Last Chemical Separation (age) Tables* can be used in conjunction with measured gamma spectroscopy Cs-137 to I-132 activity ratios directly.

**Equation 16-5. Spontaneous fission product activity equation.**

$$A_{FP} = CY_{SF} \cdot SF_{252} \cdot A_{252_0} \cdot \left(\frac{\lambda_{FP}}{\lambda_{FP} - \lambda_{252}}\right) \cdot \left(e^{-\lambda_{252} \cdot t} - e^{-\lambda_{FP} \cdot t}\right)$$

Where:
$A_{FP}$ = Fission product activity (Bq);
$CY_{SF}$ = Fission product cumulative fission yield (Cs-137 0.0502 atoms/fission, I-132 0.0215 atoms/fission); [9]
$SF_{252}$= Cf-252 spontaneous fission rate (3.14E-02 fissions/second per Bq);
$A_{252_0}$ = Cf-252 initial activity (Bq);
$\lambda_{252}$ = Cf-252 decay constant (days$^{-1}$);
$\lambda_{FP}$ = Fission product radionuclide decay constant (days$^{-1}$);
$t$ = Time (days).

### *16.9.3 Cf-252 time since last chemical separation example*

A Cf-252 source is measured by gamma spectroscopy. Estimate the time since last chemical separation using the measured Cs-137 to I-132 activity ratio presented in Table 16-7.

***Table 16-7. Relevant information for Cf-252 age determination example.***

| Nuclide | Energy (keV) | Yield (gps/dps) | Activity (µCi) | Activity Ratio Cs-137/I-132 |
|---|---|---|---|---|
| Cs-137 | 661.7 | 8.47E-01 | 2.65E+00 | --- |
| I-132 | 667.7 | 9.87E-01 | 4.00E-02 | 66.2 |

Using the calculated Cs-137 to I-132 activity ratio of 66.2 in conjunction with *Appendix B. Time Since Last Chemical Separation (age) Tables* the time since chemical separation is approximately 23.4 years prior to gamma spectroscopy analysis.

- Note: The known Cf-252 time since last chemical separation was 21.9 years.

## 16.10 Graded shielding

Graded shielding is commonly used to eliminate lead fluorescent X-rays produced from interactions in the lead shielding used to reduce background in gamma spectroscopy measurements. To eliminate the lead fluorescent x-rays, the lead shielding is covered by cadmium which attenuates the lead fluorescent x-rays but produces cadmium fluorescent X-rays at roughly 23 and 26 keV. To eliminate the cadmium fluorescent X-rays, the cadmium shielding is subsequently covered by copper which attenuates the

cadmium fluorescent x-rays and produces copper fluorescent X-rays between 8 and 9 keV which are generally of little concern.

For a typical commercial detector shields used in laboratory gamma spectroscopy systems, the graded shield consists of 10-cm Pb, 3-mm Cd, and 0.7-mm Cu. Lastly, tin can be substituted for cadmium in the graded shield configuration as needed.

Note: The use of Cd-Cu or Sn-Cu graded shielding to eliminate/reduce Am-241 59.5 keV gamma emissions from unshielded or lightly shielded plutonium samples is discussed under *Additional information* in SECTION 13.0.

## 16.11 Use of high Z shielding to reduce detection limits

In general, additional shielding increases detection limits. However, on occasion, the use of additional shielding can be used to reduce detection limits. This opportunity can occur when a radionuclide with low energy gamma emissions (Cm-243) is present with a radionuclide with high energy gamma emissions (Cm-244) and the radionuclide with low energy gamma emissions dominates the spectrum resulting in significant dead time, large measurement distances, and non-detection of the radionuclide with high energy gamma emissions.

In these instances, shielding can sometimes be used to reduce/eliminate the contribution from the radionuclide with low energy gamma emissions allowing closer measurement distances to be used to detect the radionuclide with high energy gamma emissions. If the measurement distance reduction outweighs the additional attenuation from the shielding, then use of additional shielding is warranted.

## 16.12 Background count time

Background measurements should be recorded for a time equal to or longer than the sample measurements. Visual review should be performed to ensure that no unexpected or unwanted full-energy peaks are present. [45]

## 16.13 Background suppression

Large and/or dense objects can attenuate a portion of the background radiation during a measurement. In these instances, if the background measurement is not performed in the same location with a similar non-radioactive object, the background measurement count rates will be biased high. When analysis is performed, and background suppression is not recognized by the gamma spectroscopist, radionuclides present may not be reported as detectable and/or reported radionuclide activities will be biased low.

# SECTION 17.0 DETECTOR SYSTEMS FAMILIARITY AND AWARENESS

## Table of Contents



## Figures

## 17.1 Common commercial detector crystal nominal dimensions [47] [48]

- ORTEC Micro Detective/ORTEC Detective: 50-mm diameter x 33-mm deep (±10%), p-type HPGe, Coaxial construction.
- ORTEC Detective-100: 65-mm diameter x 50-mm deep, p-type HPGe, Coaxial construction.
- ORTEC Detective-200: 85-mm diameter x 30-mm deep, p-type HPGe, Coaxial construction.
- CANBERRA Falcon 5000: 60-mm diameter x 30-mm deep, Broad Energy Germanium (BEGe), relative efficiency of approximately 18%.


***Figure 17-1. ORTEC Detective and CANBERRA Falcon-5000, respectively.***

## 17.2 Aerial measurement systems

Aerial measurement systems are used for rapid assessment of radioactive contamination on the ground over large areas using highly sensitive radiation detection systems. In addition, aerial measurement systems can be used to search for lost radioactive sources or scattered radioactive material fragments.

Dependent on the level of detail needed for the aerial survey, aircraft altitude and speed can be adjusted. For example, an emergency response survey would generally utilize higher altitudes and faster speeds as compared to a small area, detailed survey.

### 17.2.1 Remote Sensing Laboratory (RSL) [49]

The RSL aerial measurement systems, based out of Nellis Air Force Base in Las Vegas, Nevada (RSL-Nellis) and Joint Base Andrews in Washington, D.C (RSL-Andrews), utilize NaI radiation detection systems mounted on fixed-wing aircraft and helicopters (see Figure 17-2).


***Figure 17-2. RSL fixed-wing aircraft and helicopter. [46]***

### 17.2.2 Environmental Protection Agency (EPA) Airborne Spectral Photometric Environmental Collection Technology (ASPECT) [50] [51]

Based near Dallas, Texas, EPA uses a fixed-wing aircraft (Figure 17-3) to provide real-time chemical and radiological detection, using NaI or $LaBr_3$ detectors, as well as infrared and photographic imagery.


***Figure 17-3. EPA ASPECT fixed-wing aircraft.***

## 17.3 FIDLER/Violinist [52]

When calibrated appropriately, the FIDLER (Field Instrument for the Detection of Low-Energy Radiation) NaI detector and Violinist multi-channel analyzer (MCA) can measure and determine surface contamination levels of plutonium and Am-241 (activity per unit area). The FIDLER NaI detector consists of a 5-inch by 1/16-inch-thick NaI crystal effective in detecting 10 to 100 keV X-rays and gammas. The analysis software's algorithms use the detection of Pu x-rays (17 keV x-rays) and Am-241 gamma emissions at 59.5 keV to determine surface contamination levels.

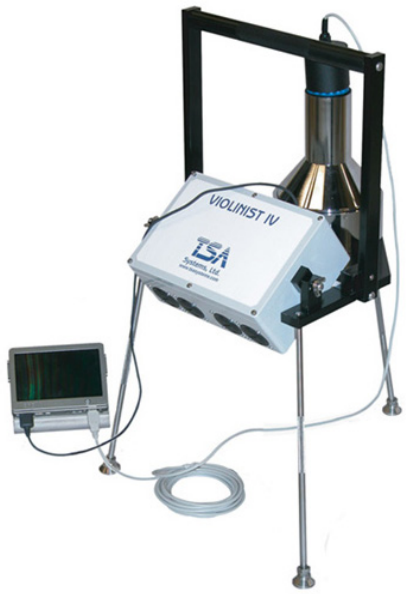


***Figure 17-4. FIDLER.***

# SECTION 18.0 REFERENCES


[1] P. Karpius and S. Myers, *LA-UR-16-25924, Gamma-Ray Interactions for Reachback Analysts,* 2016.

[2] G. Gilmore, Practical Gamma-Ray Spectrometry, 2nd Edition, John Wiley, 2008.

[3] L. Ussery, "Gamma Specialist's Handbook, DRAFT," Los Alamos National Lab, 2013.

[4] Nuclear Regulatory Commission, "Radiological Toolbox, Version 3.0.0," Nuclear Regulatory Commission, April 2013.

[5] "PeakEasy spectral library version 3.0," Los Alamos National Lab, 2018.

[6] "Radiation Information Network's - Radioactivity in Nature," Idaho State University, [Online]. Available: http://www.physics.isu.edu/radinf/natural.htm.

[7] T. Rider and B. England, "LA-UR-94-3106 / ENDF-349, Evaluation and Compilation of Fission Product Yields," Los Alamos National Lab, 1993.

[8] G. Knoll, Radiation Detection and Measurement, 4th Edition, John Wiley, 2010.

[9] "File:Marinelli beakers.png," 2014. [Online]. Available: https://en.wikipedia.org/w/index.php?curid=43709201.

[10] N. Tsoulfanidis, Measurement and Detection of Radiation, 3rd Edition, CRC Press, 2010.

[11] K. Nelson, T. Gosnell and D. Knapp, "LLNL-TR-411374, The Effect of Gamma-Ray Detector Energy Resolution on the Ability to Identify Radioactive Sources," Lawrence Livermore National Laboratory, 2009.

[12] "Passive Nondestructive Assay Manual – PANDA 2007 Addendum," Los Alamos National Lab, 2007.

[13] ANSI N42.14-1999, "American National Standard for Calibration and Use of Germanium Spectrometers for the Measurement of Gamma-Ray Emission Rates of Radionuclides," 1999.

[14] R. Gehrke and J. Davidson, "Acquisition of quality gamma-ray spectra with HPGe spectrometers," *Applied Radiation and Isotopes,* p. 479–499, 2005.

[15] R. McFarland, "Coincidence Summing Consideration in the Measurement of Radionuclides on Filter Papers using Germanium Gamma-Ray Spectroscopy," *Radioactivity and Radiochemistry,* vol. 2, no. 2, pp. 69-70, 1991.

[16] A. Seifert, W. K. Hensley, E. R. Siciliano and K. W. Pitts, "Fast Neutron Sensitivity with HPGe," in *IEEE Nuclear Science Symposium Conference* , 2007 .

[17] J.-H. Chao, "Neutron-induced gamma-rays in germanium detectors," *Applied Radiation and Isotopes,* vol. 44, no. 3, pp. 605-611, 1993.

[18] "A Summary of Error Propagation - Harvard University," [Online]. Available: http://ipl.physics.harvard.edu/wp-uploads/2013/03/PS3_Error_Propagation_sp13.pdf.

[19] International Atomic Energy Agency, "INDC(NDS)-0534, International Nuclear Data Committee Report, Handbook of Nuclear Data for Safeguards Database Extensions," 2008.

[20] M. Benedict, T. Pigford and H. W. Levi, "Chapter 8, Properties of Irradiated Fuel and Other Reactor Materials," in *Nuclear Chemical Engineering, Second Edition*, McGraw Hill Book Company, 1981, pp. 352-406.

[21] P. Frame, *Neutron Activation,* Oak Ridge Associated Universities, 1992.

[22] R. H. Meyer and J. E. Till, NUREG/CR-3332, Radiological Assessment, A Textbook on Environmental Dose Analysis, 1983.

[23] C. Lin, Radiochemistry In Nuclear Power Reactors, National Academy Press, 1996.

[24] M. Enghauser, "Environmental In-Situ Gamma Spectroscopy Training, Revision 00," August 2018.

[25] H. Beck, W. Condon and W. Lowder, "USAEC Report HASL-150, Spectometric Techniques for Measuring Environemntal Gamma Radiation," 1964.

[26] H. Beck, J. DeCampo and C. Gogolak, "USAEC Report HASL-258, In situ Ge(Li) and NaI(Tl) gamma ray Spectrometry," 1972.

[27] G. Kis-Benedek, "In-situ-gamma Spectrometry (Workshop on Understanding and Evaluating Radioanalytical Measurement Uncertainty)," in *International Atomic Energy Agency (IAEA)*, 2007.

[28] I. Helfer and K. Miller, "Calibration factors for Ge detectors used for field spectrometry," *Health Physics,* pp. 15-29, 1988.

[29] M. Enghauser, "SAND2018-3370PE, Uranium Gamma Spectroscopy Training, Revision 00," March 2018.

[30] T. Rucker and C. Johnson, " Relationship between isotopic uranium activities and total uranium at various uranium enrichments," *Journal of Radioanalytical and Nuclear Chemistry,* pp. 47-52, 1998.

[31] "World Nuclear Association," [Online]. Available: http://www.world-nuclear.org/information-library/nuclear-fuel-cycle/uranium-resources/supply-of-uranium.aspx.

[32] "NUREG/CR-5550, LA-UR-90-732, Passive Nondestructive Assay Manual," Los Alamos National Lab, 1991.

[33] M. Enghauser, "SAND2018-3369PE, Plutonium Gamma Spectroscopy Training, Revision 02," March 2018.

[34] "LA-12846-MS, Specific Activities and DOE-STD-1027-92 Hazard Category 2 Thresholds LANL Fact Sheet," Los Alamos National Lab, 1994.

[35] "DOE-STD-1128-2008, Guide of Good Practices for Occupational Radiological Protection in Plutonium Facilities," Department of Energy, 2008.

[36] M. Enghauser, "SAND2016-9912PE, Relative Efficiency Curves Demystified," July 2016.

[37] "LA-14018, Application Guide to Gamma Ray Isotopic Analysis Using the FRAM Software," Los Alamos National Lab, 2003.

[38] R. Seymour, F. Sergent, W. Clark and G. Gleason, "Quality Control and Statistical Process Control for Nuclear Analytical Measurements," *Radioactivity and Radiochemistry,* vol. 4, no. 4, pp. 24-44, 1993.

[39] "National Institute of Standards and Technology Xcom," [Online]. Available: http://physics.nist.gov/PhysRefData/Xcom/html/xcom1.html.

[40] M. Benedict, T. Pigford and H. W. Levi, "Chapter 6, Thorium," in *Nuclear Chemical Engineering, Second Edition*, McGraw Hill Book Company, 1981, pp. 283-285.

[41] T. Ludwig, D. Schwass, G. Seitz and H. Siekmann, "Intakes of thorium while using thoriated tungsten electrodes for TIG welding," *Health Physics,* vol. 77, no. 4, pp. 462-469, 1999.

[42] Z. Janout, P. S and V. M, "Observation of a Doppler broadening of the 4438 keV gamma-line of12C in processes12C(n,n′γ)12C and 9Be(α,nγ)12C," *Journal of Radioanalyttcal Chemistry,* vol. 56, no. 1-2, pp. 71-81, 1980.

[43] R. Gehrke, R. Aryaeinejad, J. Hartwell, W. Yoon, E. Reber and J. Davidson, "The γ-ray spectrum of 252Cf and the information contained within it," *Nuclear Instruments and Methods in Physics Research Section B,* vol. 213, pp. 10-21, 2004.

[44] J. Goldsmith, M. Enghauser and K. Hertz, "SAND2014-4966, DHS SEED Gamma Ray Instrument Characterization and Measurement Procedures," June 2014.

[45] "Nevada Naitonal Security Site, Remote Sensing Laboratory," [Online]. Available: https://www.nnss.gov/pages/facilities/RSL.html.

[46] "ORTEC » PRODUCTS » Nuclear Security and Safeguards » Hand-Held Radioisotope Identifiers (RIIDs)," [Online]. Available: https://www.ortec-online.com/products/nuclear-security-and-safeguards/hand-held-radioisotope-identifiers-riids.

[47] "Mirion Technologies » Products and Applications » Spectroscopy & Counting Labs » In-Situ Measurments » Falcon 5000 HPGe-Based Radionculide Identifier," [Online]. Available: https://www.mirion.com/products/falcon-portable-hpge-based-radionuclide-identifier.

[48] *Aerial Measuring System (AMS) Overview, PowerPoint Presentation.*

[49] "Environmental Protection Agency, Airborne Spectral Photometric Environmental Collection Technology, Fact Sheet," [Online]. Available: https://www.epa.gov/sites/production/files/2017-08/documents/aspect_fact_sheet_2017.pdf.

[50] "Environmental Protection Agency, Airborne Spectral Photometric Environmental Collection Technology, Webinar Slides," [Online]. Available: https://www.epa.gov/sites/production/files/2014-09/documents/aspect_webinar_slides_09-11-14.pdf.

[51] "Violinist IV, Special Purpose Multi-Channel Analyzer," [Online]. Available: http://www.laurussystems.com/products/products_pdf/Violinist_IV.pdf.

[52] E. L. Reber, R. J. Gehrke, R. Aryaeinejad and J. K. Hartwell, "Measurement of the fission yields of selected prompt and decay fission product gamma-rays of spontaneously fissioning 252Cf and 244Cm," *Journal of Radioanalytical and Nuclear Chemistry,* vol. 264, no. 1, pp. 243-253, 2005.

[53] G. Gilmore, "Decision Limits in Gamma-Ray Spectrometry," [Online].

[54] "ICRP Publication 107. Nuclear decay data for dosimetric calculations.," 2008.

[55] M. Rawool-Sullivan and J. Sullivan, *LA-UR-14-23048, Revision 1, Understanding Doppler Broadening of Gamma Rays,* Los Alamos National Lab.

[56] R. M. Lindstrom, "Dead Time, Pileup, and Accurate Gamma-Ray Spectrometry," *Radioactivity and Radiochemistry,* vol. 6, no. 2, pp. 20-27, 1995.

# APPENDIX A. GAMMA AND X-RAYS OF INTEREST

## Table of Contents

- Note: For radionuclides listed under the Plutonium section, "**bolded**" gamma emissions can be treated as interference free. For all other radionuclides, "**bolded**" gamma emissions represent the primary gamma emissions.

## A.1. Thorium

Th-232 (1.41E+10 y, 1.10E-07 Ci/g, 1.1 pCi/g typical soil concentration)

| Parent | Emitter | Energy (keV) | Yield (gps/dps) |
|---|---|---|---|
| **Th-232+** | **Pb-212** | **238.6** | **4.33E-01** |
| **Th-232+** | **Tl-208** | **2614.5** | **3.56E-01** |
| **Th-232+** | **Tl-208/Ac-228** | **583.2** | **3.05E-01** |
| **Th-232+** | **Ac-228** | **911.2** | **2.58E-01** |
| **Th-232+** | **Ac-228** | **969.0** | **1.58E-01** |
| **Th-232+** | **Ac-228** | **338.3** | **1.13E-01** |
| **Th-232+** | **Bi-212/Ac-228** | **727.3** | **7.20E-02** |
| Th-232+ | Tl-208 | 860.6 | 4.47E-02 |
| Th-232+ | Ac-228 | 794.9 | 4.25E-02 |
| Th-232+ | Ac-228 | 1588.2 | 3.22E-02 |

Th-232+ represents Th-232 in equilibrium with its decay products
Th-232+ (Tl-208): Yield includes the 35.94% branch from its parent radionuclide, Bi-212

Thorium X-rays

| Element | Shell | Energy (keV) | Intensity per vacancy |
|---|---|---|---|
| Th X-ray | Kα1 | 93.4 | 4.60E-01 |
| Th X-ray | Kα2 | 90.0 | 2.82E-01 |

## A.2. Radium

Ra-226 (1600.2 y, 0.989 Ci/g, 1.3 pCi/g typical soil concentration, 90% equilibrium at 12.7 d)

| Parent | Emitter | Energy (keV) | Yield (gps/dps) |
|---|---|---|---|
| **Ra-226+** | **Bi-214** | **609.3** | **4.61E-01** |
| **Ra-226+** | **Pb-214/Bi-214** | **351.9** | **3.77E-01** |
| Ra-226+ | Pb-214 | 295.2 | 1.93E-01 |
| **Ra-226+** | **Bi-214** | **1764.5** | **1.54E-01** |
| **Ra-226+** | **Bi-214** | **1120.3** | **1.51E-01** |
| Ra-226+ | Pb-214 | 242.0 | 7.43E-02 |
| Ra-226+ | Bi-214 | 1238.1 | 5.79E-02 |
| Ra-226+ | Bi-214 | 2204.2 | 5.08E-02 |
| Ra-226+ | Bi-214 | 768.4 | 4.94E-02 |
| Ra-226+ | Bi-214 | 1377.7 | 4.00E-02 |
| Ra-226+ | Ra-226 | 186.2 | 3.59E-02 |
| Ra-226+ | Bi-214 | 934.1 | 3.08E-02 |
| Ra-226+ | Bi-214 | 2447.9 | 1.57E-02 |

Ra-226+ represents Ra-226 in equilibrium with its decay products

## A.3. Potassium

K-40 (1.28E+09 y, 11.0 pCi/g typical soil concentration, 429 pCi/g in 100% K)

| Parent | Emitter | Energy (keV) | Yield (gps/dps) |
|---|---|---|---|
| **K-40** | **K-40** | **1460.8** | **1.07E-01** |

## A.4. Uranium

U-238 (4.70E+09 y, 3.20E-07 Ci/g, 90% equilibrium at 79.9 d)

| Parent | Emitter | Energy (keV) | Yield (gps/dps) |
|---|---|---|---|
| **U-238+** | **Th-234 x 2** | **92.6** | **5.58E-02** |
| **U-238+** | **Th-234** | **63.3** | **4.84E-02** |
| **U-238+** | **Pa-234m** | **1001.0** | **8.36E-03** |
| **U-238+** | **Pa-234m/Pa-234** | **766.4** | **2.94E-03** |
| U-238+ | Pa-234m/Pa-234 | 742.8 | 8.32E-04 |
| **U-238+** | **Pa-234m** | **258.3** | **7.27E-04** |
| U-238+ | Pa-234m/Pa-234 | 786.3 | 5.03E-04 |
| U-238+ | Pa-234/Pa-234m | 946.0 | 3.13E-04 |
| **U-238+** | **Pa-234m/Pa-234** | **1737.7** | **2.12E-04** |
| U-238+ | Pa-234 x 2 | 569.3 | 1.90E-04 |
| **U-238+** | **Pa-234m** | **1831.3** | **1.72E-04** |

U-238+ represents U-238 in equilibrium with its decay products (Th-234, Pa-234m, and Pa-234)
U-238+ (Pa-234): Yield includes the 0.16% branch from its parent radionuclide, Th-234
U-238+ (Pa-234m): Yield includes the 99.84% branch from its parent radionuclide, Th-234

U-235 (7.04E+08 y, 2.16E-06 Ci/g)

| Parent | Emitter | Energy (keV) | Yield (gps/dps) |
|---|---|---|---|
| **U-235** | **U-235** | **185.7** | **5.72E-01** |
| **U-235** | **U-235** | **143.8** | **1.10E-01** |
| **U-235** | **U-235** | **163.3** | **5.08E-02** |
| **U-235** | **U-235** | **205.3** | **5.01E-02** |

U-234 (2.48E+05 y, 6.16E-03 Ci/g)

| Parent | Emitter | Energy (keV) | Yield (gps/dps) |
|---|---|---|---|
| U-234 | U-234 | 53.2 | 1.23E-03 |
| **U-234** | **U-234** | **120.9** | **3.97E-04** |

U-232 (72.0 y, 21.4 Ci/g, 90% equilibrium at 6.3 y) → Th-228 (1.9 y)

| Parent | Emitter | Energy (keV) | Yield (gps/dps) |
|---|---|---|---|
| **U-232+** | **Pb-212** | **238.6** | **4.33E-01** |
| **U-232+** | **Tl-208** | **2614.5** | **3.56E-01** |
| **U-232+** | **Tl-208** | **583.2** | **3.04E-01** |
| **U-232+** | **Bi-212** | **727.3** | **6.58E-02** |
| **U-232+** | **Tl-208** | **860.6** | **4.47E-02** |
| **U-232+** | **Bi-212** | **1620.5** | **1.49E-02** |

U-232+ represents U-232 in equilibrium with its decay products
U-232+ (Tl-208): Yield includes the 35.94% branch from its parent radionuclide, Bi-212

Uranium X-rays

| Element | Shell | Energy (keV) | Intensity per vacancy |
|---|---|---|---|
| U X-ray | Kα1 | 98.4 | 4.52E-01 |
| U X-ray | Kα2 | 94.7 | 2.82E-01 |

## A.5. Plutonium

Pu-239 (2.41E+04 y, 0.062 Ci/g, 2.2E+01 n/s-kg, 1.89 W/kg)

| Parent | Emitter | Energy (keV) | Yield (gps/dps) |
|---|---|---|---|
| **Pu-239** | **Pu-239** | **129.3** | **6.310E-05** |
| **Pu-239** | **Pu-239** | **375.1** | **1.554E-05** |
| **Pu-239** | **Pu-239** | **413.7** | **1.466E-05** |
| **Pu-239** | **Pu-239** | **345.0** | **6.060E-06** |
| **Pu-239** | **Pu-239** | **203.6** | **5.690E-06** |
| **Pu-239** | **Pu-239** | **451.5** | **1.894E-06** |
| **Pu-239** | **Pu-239** | **255.4** | **8.000E-07** |
| **Pu-239** | **Pu-239** | **645.9** | **1.520E-07** |
| Pu-239 | Pu-239 x 2 | 769.3 | 1.190E-07 |
| **Pu-239** | **Pu-239** | **658.9** | **9.700E-08** |
| Pu-239 | Pu-239 | 640.0 | 8.700E-08 |
| **Pu-239** | **Pu-239** | **718.0** | **2.800E-08** |

Am-241 (433.2 y, 3.42 Ci/g, 112 W/kg) → Np-237 (2.14E+06 y)

| Parent | Emitter | Energy (keV) | Yield (gps/dps) |
|---|---|---|---|
| **Am-241** | **Am-241** | **59.5** | **3.590E-01** |
| Am-241 | Am-241 | 125.3 | 4.080E-05 |
| Am-241 | Am-241 | 208.0 | 7.910E-06 |
| **Am-241** | **Am-241** | **662.4** | **3.640E-06** |
| **Am-241** | **Am-241** | **722.0** | **1.960E-06** |
| **Am-241** | **Am-241** | **419.3** | **2.870E-07** |

Pu-241 (14.35 y, BR = 0.99998) → Am-241 (433.2 y) → Np-237 (2.14E+06 y) → Pa-233 (27.0 d)
Pu-241 (14.35 y, BR = 0.0000245) → U-237 (6.8 d) → Np-237 (2.14E+06 y) → Pa-233 (27.0 d)

| Parent | Emitter | Energy (keV) | Yield (gps/dps) |
|---|---|---|---|
| Pu-241+ | U-237 | 208.0 | 5.194E-06 |
| **Pu-241+** | **Pu-241** | **148.6** | **1.855E-06** |

Pu-241+ represents Pu-241 in equilibrium with U-237
Pu-241+ (U-237): Yield includes the 2.45E-03% branch from its parent radionuclide, Pu-241
Pu-241 specific activity = 103.3 Ci/g

Pu-240 (6537.3 y, 0.228 Ci/g, 1.0E+06 n/s-kg, 6.94 W/kg)

| Parent | Emitter | Energy (keV) | Yield (gps/dps) |
|---|---|---|---|
| Pu-240 | Pu-240 | 160.3 | 4.020E-06 |
| Pu-240 | Pu-240 | 642.4 | 1.300E-07 |

Np-237 (2.14E+06 y, 7.05E-04 Ci/g, 1.1E-01 n/s-kg) → Pa-233 (27.4 d): 90% equilibrium at 91.3 d

| Parent | Emitter | Energy (keV) | Yield (gps/dps) |
|---|---|---|---|
| Np-237+ | Pa-233 | 312.2 | 3.860E-01 |
| **Np-237+** | **Pa-233** | **300.3** | **6.620E-02** |
| Np-237+ | Pa-233 | 340.8 | 4.470E-02 |

Np-237+ represents Np-237 in equilibrium with Pa-233

Pu-238 (87.7 y, 17.2 Ci/g, 2.6E+06 n/s-kg, 557 W/kg)

| Parent | Emitter | Energy (keV) | Yield (gps/dps) |
|---|---|---|---|
| **Pu-238** | **Pu-238** | **152.7** | **9.370E-06** |
| Pu-238 | Pu-238 | 766.4 | 2.200E-07 |
| Pu-238 | Pu-238 | 742.8 | 5.200E-08 |
| Pu-238 | Pu-238 | 201.0 | 3.900E-08 |
| Pu-238 | Pu-238 | 786.3 | 3.250E-08 |
| Pu-238 | Pu-238 | 851.7 | 1.250E-08 |
| **Pu-238** | **Pu-238** | **1001.0** | **9.900E-09** |

Pu-236 (2.9 y) → U-232 (72.0 y) → Th-228 (1.9 y)

| Parent | Emitter | Energy (keV) | Yield (gps/dps) |
|---|---|---|---|
| **Th-228+** | **Pb-212** | **238.6** | **4.330E-01** |
| **Th-228+** | **Tl-208** | **2614.5** | **3.564E-01** |
| **Th-228+** | **Tl-208** | **583.2** | **3.036E-01** |
| Th-228+ | Bi-212 | 727.3 | 6.579E-02 |
| Th-228+ | Tl-208 | 860.6 | 4.465E-02 |

Th-228+ represents Th-228 in equilibrium with its decay products
Th-228+ (Tl-208): Yield includes the 35.94% branch from its parent radionuclide, Bi-212

## A.6. Long lived fission products

Cs-137 (30.1 y, 86.6 Ci/g, 0.645 R/h per Ci @ 1-m, 6.19 FP-yield)

| Parent | Emitter | Energy (keV) | Yield (gps/dps) |
|---|---|---|---|
| **Cs-137** | **Ba-137m** | **661.7** | **8.47E-01** |

Cs-137: Yield includes the 94.4% branch from its parent radionuclide, Ba-137m

Sr-90 (28.5 y, 139.5 Ci/g, 5.78 FP-yield)

| Parent | Emitter | Energy (keV) | Yield (gps/dps) |
|---|---|---|---|
| Sr-90 | Sr-90/Y-90 | β- max 546/2284 | 1.00E+00/1.00E+00 |

Sr-90 and Y-90 are pure beta emitters

Cs-134 (2.1 y) = FP-133 → Xe-133 (5.2 d, 6.70 FP-yield) → Cs-133(n,γ)Cs-134

| Parent | Emitter | Energy (keV) | Yield (gps/dps) |
|---|---|---|---|
| **Cs-134** | **Cs-134** | **604.7** | **9.76E-01** |
| **Cs-134** | **Cs-134** | **795.9** | **8.55E-01** |
| Cs-134 | Cs-134 | 569.3 | 1.54E-01 |
| Cs-134 | Cs-134 | 802.0 | 8.69E-02 |
| Cs-134 | Cs-134 | 563.2 | 8.35E-02 |
| **Cs-134** | **Cs-134** | **1365.2** | **3.01E-02** |

Zr-95 (64.0 d, 6.50 FP-yield) → Nb-95 (35.0 d)

| Parent | Emitter | Energy (keV) | Yield (gps/dps) |
|---|---|---|---|
| **Zr-95** | **Zr-95** | **756.7** | **5.44E-01** |
| **Zr-95** | **Zr-95** | **724.2** | **4.43E-01** |
| **Nb-95** | **Nb-95** | **765.8** | **9.98E-01** |

Nb-95/Zr-95 transient equilibrium activity ratio = 2.205

Ce-141 (32.5 d, 5.85 FP-yield)

| Parent | Emitter | Energy (keV) | Yield (gps/dps) |
|---|---|---|---|
| **Ce-141** | **Ce-141** | **145.4** | **4.83E-01** |

Ce-144 (28.9 d, 5.50 FP-yield)

| Parent | Emitter | Energy (keV) | Yield (gps/dps) |
|---|---|---|---|
| **Ce-144+** | **Ce-144** | **133.5** | **1.11E-01** |
| Ce-144+ | Ce-144 | 80.1 | 1.36E-02 |
| **Ce-144+** | **Pr-144** | **696.5** | **1.34E-02** |

Ce-144+ represents Ce-144 in equilibrium with Pr-144

Ru-103 (39.3 d, 3.03 FP-yield)

| Parent | Emitter | Energy (keV) | Yield (gps/dps) |
|---|---|---|---|
| **Ru-103** | **Ru-103** | **497.1** | **9.1E-01** |
| **Ru-103** | **Ru-103** | **610.3** | **5.8E-02** |

Ru-106 (373.6 d, 0.40 FP-yield)

| Parent | Emitter | Energy (keV) | Yield (gps/dps) |
|---|---|---|---|
| **Ru-106+** | **Rh-106** | **511.9** | **2.0E-01** |
| **Ru-106+** | **Rh-106** | **621.9** | **9.9E-02** |
| **Ru-106+** | **Rh-106** | **1050.4** | **1.6E-02** |

Ru-106+ represents Ru-106 in equilibrium with Rh-106

## A.7. Long lived activation products

Co-60 (5.3 y, 1131.6 Ci/g, 12.9 R/h per Ci @ 1-m, Co-59 (n,γ) 100.0% 37.5 $barns_{thermal}$)

| Parent | Emitter | Energy (keV) | Yield (gps/dps) |
|---|---|---|---|
| **Co-60** | **Co-60** | **1332.5** | **1.00E+00** |
| **Co-60** | **Co-60** | **1173.2** | **9.99E-01** |

Zn-65 (243.8 d, Zn-64(n,γ) 48.9% 0.76 $barns_{thermal}$)

| Parent | Emitter | Energy (keV) | Yield (gps/dps) |
|---|---|---|---|
| **Zn-65** | **Zn-65** | **1115.5** | **5.06E-01** |

Mn-54 (312.2 d, Fe-54(n,p) 5.8% 0.082 $barns_{thermal}$)

| Parent | Emitter | Energy (keV) | Yield (gps/dps) |
|---|---|---|---|
| **Mn-54** | **Mn-54** | **834.8** | **1.00E+00** |

## A.8. X-rays of interest

| Element | Shell | Energy (keV) | Intensity per vacancy |
|---|---|---|---|
| Pb | Kα1 | 75.0 | 4.68E-01 |
| Pb | Kα2 | 72.8 | 2.78E-01 |

| Element | Shell | Energy (keV) | Intensity per vacancy |
|---|---|---|---|
| Au | Kα1 | 68.8 | 4.70E-01 |
| Au | Kα2 | 67.0 | 2.76E-01 |

| Element | Shell | Energy (keV) | Intensity per vacancy |
|---|---|---|---|
| Ag | Kα1 | 22.2 | 4.56E-01 |
| Ag | Kα2 | 22.0 | 2.42E-01 |

## A.9. X-rays from graded shielding

| Element | Shell | Energy (keV) | Intensity per vacancy |
|---|---|---|---|
| Sn | Kα1/Kα2 | 25.3/25.0 | 4.6E-01/2.5E-01 |
| Sn | Kβ1/Kβ3 | 28.5/28.4 | 8.0E-02/4.2E-02 |

| Element | Shell | Energy (keV) | Intensity per vacancy |
|---|---|---|---|
| Cd | Kα1/Kα2 | 23.2/23.0 | 4.6E-01/2.5E-01 |
| Cd | Kβ1/Kβ3 | 26.1/26.1 | 7.7E-02/4.0E-02 |

| Element | Shell | Energy (keV) | Intensity per vacancy |
|---|---|---|---|
| Cu | Kα1/Kα2 | 8.1/8.0 | 2.6E-01/1.3E-01 |
| Cu | Kβ1/Kβ3 | 8.9/8.9 | 3.1E-02/1.6E-02 |

# APPENDIX B. TIME SINCE LAST CHEMICAL SEPARATION (AGE) TABLES

## Table of Contents

## B.1. Plutonium-241

**Pu-241 (14.35 y, BR = 0.99998) → Am-241 (433.2 y) → Np-237 (2.14E+06 y) → Pa-233 (27.0 d)**
**Pu-241 (14.35 y, BR = 0.0000245) → U-237 (6.8 d) → Np-237 (2.14E+06 y) → Pa-233 (27.0 d)**

| Time (years) | Activity Ratio Pa233/Pu-241 | Activity Ratio Np237/Pu241 | Activity Ratio Am241/Pu241 |
|---|---|---|---|
| 0.5 | 4.68E-11 | 6.97E-11 | 8.11E-04 |
| 1.0 | 2.24E-10 | 2.75E-10 | 1.64E-03 |
| 1.5 | 5.43E-10 | 6.24E-10 | 2.49E-03 |
| 2.0 | 1.01E-09 | 1.12E-09 | 3.36E-03 |
| 2.5 | 1.64E-09 | 1.77E-09 | 4.25E-03 |
| 3.0 | 2.42E-09 | 2.59E-09 | 5.16E-03 |
| 3.5 | 3.38E-09 | 3.58E-09 | 6.10E-03 |
| 4.0 | 4.50E-09 | 4.75E-09 | 7.05E-03 |
| 4.5 | 5.83E-09 | 6.10E-09 | 8.03E-03 |
| 5.0 | 7.34E-09 | 7.65E-09 | 9.03E-03 |
| 6.0 | 1.10E-08 | 1.14E-08 | 1.11E-02 |
| 7.0 | 1.56E-08 | 1.60E-08 | 1.33E-02 |
| 8.0 | 2.11E-08 | 2.15E-08 | 1.56E-02 |
| 9.0 | 2.75E-08 | 2.82E-08 | 1.79E-02 |
| 10.0 | 3.52E-08 | 3.59E-08 | 2.04E-02 |
| 12.0 | 5.44E-08 | 5.52E-08 | 2.58E-02 |
| 14.0 | 7.93E-08 | 8.04E-08 | 3.17E-02 |
| 16.0 | 1.11E-07 | 1.12E-07 | 3.82E-02 |
| 18.0 | 1.50E-07 | 1.52E-07 | 4.53E-02 |
| 20.0 | 1.99E-07 | 2.01E-07 | 5.31E-02 |
| 22.0 | 2.58E-07 | 2.60E-07 | 6.17E-02 |
| 24.0 | 3.30E-07 | 3.32E-07 | 7.11E-02 |
| 26.0 | 4.13E-07 | 4.17E-07 | 8.15E-02 |
| 28.0 | 5.17E-07 | 5.19E-07 | 9.29E-02 |
| 30.0 | 6.34E-07 | 6.39E-07 | 1.05E-01 |

Assumes no Pu-241 decay products present at t=0

| Time (years) | Activity Ratio Pa233/Pu241 | Activity Ratio Np237/Pu241 | Activity Ratio Am241/Pu241 |
|---|---|---|---|
| 32.0 | 7.74E-07 | 7.80E-07 | 1.19E-01 |
| 34.0 | 9.42E-07 | 9.45E-07 | 1.34E-01 |
| 36.0 | 1.14E-06 | 1.14E-06 | 1.51E-01 |
| 38.0 | 1.36E-06 | 1.36E-06 | 1.69E-01 |
| 40.0 | 1.61E-06 | 1.62E-06 | 1.89E-01 |
| 42.0 | 1.92E-06 | 1.92E-06 | 2.11E-01 |
| 44.0 | 2.26E-06 | 2.27E-06 | 2.35E-01 |
| 46.0 | 2.66E-06 | 2.67E-06 | 2.61E-01 |
| 48.0 | 3.12E-06 | 3.13E-06 | 2.90E-01 |
| 50.0 | 3.64E-06 | 3.65E-06 | 3.22E-01 |
| 52.0 | 4.25E-06 | 4.26E-06 | 3.57E-01 |
| 54.0 | 4.92E-06 | 4.95E-06 | 3.96E-01 |
| 56.0 | 5.72E-06 | 5.73E-06 | 4.38E-01 |
| 58.0 | 6.62E-06 | 6.63E-06 | 4.85E-01 |
| 60.0 | 7.63E-06 | 7.65E-06 | 5.36E-01 |
| 62.0 | 8.81E-06 | 8.81E-06 | 5.92E-01 |
| 64.0 | 1.01E-05 | 1.01E-05 | 6.53E-01 |
| 66.0 | 1.16E-05 | 1.16E-05 | 7.21E-01 |
| 68.0 | 1.33E-05 | 1.33E-05 | 7.95E-01 |
| 70.0 | 1.52E-05 | 1.53E-05 | 8.77E-01 |
| 72.0 | 1.74E-05 | 1.74E-05 | 9.66E-01 |
| 74.0 | 1.99E-05 | 1.99E-05 | 1.06E+00 |
| 76.0 | 2.26E-05 | 2.27E-05 | 1.17E+00 |
| 78.0 | 2.58E-05 | 2.58E-05 | 1.29E+00 |
| 80.0 | 2.94E-05 | 2.94E-05 | 1.42E+00 |

## B.2. Americium-241

**Am-241 (433.2 y) → Np-237 (2.14E+06 y) → Pa-233 (27.0 d)**

| Time (years) | Activity Ratio Pa-233/Am-241 | Activity Ratio Np-237/Am-241 |
|---|---|---|
| 0.5 | 1.28E-07 | 1.62E-07 |
| 1.0 | 2.89E-07 | 3.24E-07 |
| 1.5 | 4.51E-07 | 4.86E-07 |
| 2.0 | 6.13E-07 | 6.48E-07 |
| 2.5 | 7.75E-07 | 8.10E-07 |
| 3.0 | 9.38E-07 | 9.72E-07 |
| 3.5 | 1.10E-06 | 1.13E-06 |
| 4.0 | 1.26E-06 | 1.30E-06 |
| 4.5 | 1.43E-06 | 1.46E-06 |
| 5.0 | 1.59E-06 | 1.62E-06 |
| 6.0 | 1.91E-06 | 1.95E-06 |
| 7.0 | 2.24E-06 | 2.28E-06 |
| 8.0 | 2.57E-06 | 2.60E-06 |
| 9.0 | 2.90E-06 | 2.93E-06 |
| 10.0 | 3.22E-06 | 3.26E-06 |
| 12.0 | 3.88E-06 | 3.92E-06 |
| 14.0 | 4.54E-06 | 4.58E-06 |
| 16.0 | 5.21E-06 | 5.24E-06 |
| 18.0 | 5.87E-06 | 5.90E-06 |
| 20.0 | 6.54E-06 | 6.57E-06 |
| 22.0 | 7.20E-06 | 7.24E-06 |
| 24.0 | 7.88E-06 | 7.91E-06 |
| 26.0 | 8.55E-06 | 8.58E-06 |
| 28.0 | 9.22E-06 | 9.26E-06 |
| 30.0 | 9.90E-06 | 9.94E-06 |

| Time (years) | Activity Ratio Pa-233/Am-241 | Activity Ratio Np-237/Am-241 |
|---|---|---|
| 32.0 | 1.06E-05 | 1.06E-05 |
| 34.0 | 1.13E-05 | 1.13E-05 |
| 36.0 | 1.19E-05 | 1.20E-05 |
| 38.0 | 1.26E-05 | 1.27E-05 |
| 40.0 | 1.33E-05 | 1.34E-05 |
| 42.0 | 1.40E-05 | 1.40E-05 |
| 44.0 | 1.47E-05 | 1.47E-05 |
| 46.0 | 1.54E-05 | 1.54E-05 |
| 48.0 | 1.61E-05 | 1.61E-05 |
| 50.0 | 1.68E-05 | 1.68E-05 |
| 52.0 | 1.75E-05 | 1.75E-05 |
| 54.0 | 1.82E-05 | 1.82E-05 |
| 56.0 | 1.89E-05 | 1.89E-05 |
| 58.0 | 1.96E-05 | 1.96E-05 |
| 60.0 | 2.03E-05 | 2.04E-05 |
| 62.0 | 2.10E-05 | 2.11E-05 |
| 64.0 | 2.18E-05 | 2.18E-05 |
| 66.0 | 2.25E-05 | 2.25E-05 |
| 68.0 | 2.32E-05 | 2.32E-05 |
| 70.0 | 2.39E-05 | 2.39E-05 |
| 72.0 | 2.46E-05 | 2.47E-05 |
| 74.0 | 2.54E-05 | 2.54E-05 |
| 76.0 | 2.61E-05 | 2.61E-05 |
| 78.0 | 2.68E-05 | 2.69E-05 |
| 80.0 | 2.76E-05 | 2.76E-05 |

Assumes no Am-241 decay products present at t=0

## B.3. Uranium-233

**U-233 (1.58E+05 y) → Th-229 (7342 y) → Ra-225 (14.9 d) → Ac-225 (10.0 d) → Fr-221 (4.9 m) → At-217 (32.3 ms) → Bi-213 (45.6 m, BR = 0.0209) → Tl-209 (2.2 m) → Pb-209 (3.25 h) → Bi-209 (Stable)**

**U-233 (1.58E+05 y) → Th-229 (7342 y) → Ra-225 (14.9 d) → Ac-225 (10.0 d) → Fr-221 (4.9 m) → At-217 (32.3 ms) → Bi-213 (45.6 m, BR = 0.9781) → Po-213 (4.2 µs) → Pb-209 (3.25 h) → Bi-209 (Stable)**

| Time (years) | Activity Ratio Bi-213/U-233 | Activity Ratio Th-229/U-233 |
|---|---|---|
| 0.5 | 3.79E-05 | 4.72E-05 |
| 1.0 | 8.51E-05 | 9.44E-05 |
| 1.5 | 1.32E-04 | 1.42E-04 |
| 2.0 | 1.80E-04 | 1.89E-04 |
| 2.5 | 2.27E-04 | 2.36E-04 |
| 3.0 | 2.74E-04 | 2.83E-04 |
| 3.5 | 3.21E-04 | 3.31E-04 |
| 4.0 | 3.68E-04 | 3.78E-04 |
| 4.5 | 4.16E-04 | 4.25E-04 |
| 5.0 | 4.63E-04 | 4.72E-04 |
| 6.0 | 5.57E-04 | 5.67E-04 |
| 7.0 | 6.51E-04 | 6.61E-04 |
| 8.0 | 7.46E-04 | 7.55E-04 |
| 9.0 | 8.40E-04 | 8.50E-04 |
| 10.0 | 9.35E-04 | 9.44E-04 |
| 12.0 | 1.12E-03 | 1.13E-03 |
| 14.0 | 1.31E-03 | 1.32E-03 |
| 16.0 | 1.50E-03 | 1.51E-03 |
| 18.0 | 1.69E-03 | 1.70E-03 |
| 20.0 | 1.88E-03 | 1.89E-03 |
| 22.0 | 2.07E-03 | 2.08E-03 |
| 24.0 | 2.25E-03 | 2.26E-03 |
| 26.0 | 2.44E-03 | 2.45E-03 |
| 28.0 | 2.63E-03 | 2.64E-03 |
| 30.0 | 2.82E-03 | 2.83E-03 |

| Time (years) | Activity Ratio Bi-213/U-233 | Activity Ratio Th-229/U-233 |
|---|---|---|
| 32.0 | 3.01E-03 | 3.02E-03 |
| 34.0 | 3.20E-03 | 3.21E-03 |
| 36.0 | 3.38E-03 | 3.39E-03 |
| 38.0 | 3.57E-03 | 3.58E-03 |
| 40.0 | 3.76E-03 | 3.77E-03 |
| 42.0 | 3.95E-03 | 3.96E-03 |
| 44.0 | 4.14E-03 | 4.15E-03 |
| 46.0 | 4.33E-03 | 4.34E-03 |
| 48.0 | 4.51E-03 | 4.52E-03 |
| 50.0 | 4.70E-03 | 4.71E-03 |
| 52.0 | 4.89E-03 | 4.90E-03 |
| 54.0 | 5.08E-03 | 5.09E-03 |
| 56.0 | 5.27E-03 | 5.28E-03 |
| 58.0 | 5.45E-03 | 5.46E-03 |
| 60.0 | 5.64E-03 | 5.65E-03 |
| 62.0 | 5.83E-03 | 5.84E-03 |
| 64.0 | 6.02E-03 | 6.03E-03 |
| 66.0 | 6.20E-03 | 6.21E-03 |
| 68.0 | 6.39E-03 | 6.40E-03 |
| 70.0 | 6.58E-03 | 6.59E-03 |
| 72.0 | 6.77E-03 | 6.78E-03 |
| 74.0 | 6.96E-03 | 6.97E-03 |
| 76.0 | 7.14E-03 | 7.15E-03 |
| 78.0 | 7.33E-03 | 7.34E-03 |
| 80.0 | 7.52E-03 | 7.53E-03 |

Assumes no U-233 decay products present at t=0

## B.4. Zirconium-95

**Zr-95 (64.0 d, BR 0.9892) -> Nb-95 (35.0 d)**
**Zr-95 (64.0 d, BR 0.0108) -> Nb-95m (3.6 d, BR 0.944) → Nb-95 (35.0 d)**

| Time (days) | Activity Ratio Nb-95/Zr-95 | Time (days) | Activity Ratio Nb-95/Zr-95 | Time (days) | Activity Ratio Nb-95/Zr-95 |
|---|---|---|---|---|---|
| 0.5 | 0.0098 | 22.0 | 0.3944 | 110.0 | 1.3833 |
| 1.0 | 0.0195 | 24.0 | 0.4266 | 120.0 | 1.4538 |
| 1.5 | 0.0292 | 26.0 | 0.4583 | 130.0 | 1.5182 |
| 2.0 | 0.0389 | 28.0 | 0.4894 | 140.0 | 1.5771 |
| 2.5 | 0.0485 | 30.0 | 0.5199 | 150.0 | 1.6310 |
| 3.0 | 0.0581 | 32.0 | 0.5499 | 160.0 | 1.6802 |
| 3.5 | 0.0677 | 34.0 | 0.5794 | 170.0 | 1.7251 |
| 4.0 | 0.0772 | 36.0 | 0.6084 | 180.0 | 1.7662 |
| 4.5 | 0.0867 | 38.0 | 0.6368 | 190.0 | 1.8038 |
| 5.0 | 0.0961 | 40.0 | 0.6647 | 200.0 | 1.8382 |
| 5.5 | 0.1055 | 42.0 | 0.6921 | 220.0 | 1.8983 |
| 6.0 | 0.1149 | 44.0 | 0.7191 | 240.0 | 1.9485 |
| 6.5 | 0.1242 | 46.0 | 0.7455 | 260.0 | 1.9904 |
| 7.0 | 0.1335 | 48.0 | 0.7715 | 280.0 | 2.0255 |
| 7.5 | 0.1428 | 50.0 | 0.7971 | 300.0 | 2.0548 |
| 8.0 | 0.1520 | 55.0 | 0.8589 | 320.0 | 2.0792 |
| 8.5 | 0.1612 | 60.0 | 0.9180 | 340.0 | 2.0997 |
| 9.0 | 0.1703 | 65.0 | 0.9746 | 360.0 | 2.1168 |
| 9.5 | 0.1794 | 70.0 | 1.0286 | 380.0 | 2.1310 |
| 10.0 | 0.1885 | 75.0 | 1.0803 | 400.0 | 2.1430 |
| 12.0 | 0.2243 | 80.0 | 1.1297 | 420.0 | 2.1529 |
| 14.0 | 0.2596 | 85.0 | 1.1769 | 440.0 | 2.1613 |
| 16.0 | 0.2942 | 90.0 | 1.2221 | 460.0 | 2.1682 |
| 18.0 | 0.3282 | 95.0 | 1.2652 | 480.0 | 2.1740 |
| 20.0 | 0.3616 | 100.0 | 1.3065 | 500.0 | 2.1789 |

Assumes no Nb-95 present at t=0
Nb-95/Zr-95 activity ratio at transient equilibrium = 2.205

## B.5. Californium-252

| Time (years) | Activity Ratio Cs-137/I-132 | Time (years) | Activity Ratio Cs-137/I-132 |
|---|---|---|---|
| 0.5 | 2.85E-02 | 32.0 | 4.71E+02 |
| 1.0 | 6.06E-02 | 34.0 | 7.61E+02 |
| 1.5 | 9.68E-02 | 36.0 | 1.23E+03 |
| 2.0 | 1.38E-01 | 38.0 | 1.98E+03 |
| 2.5 | 1.84E-01 | 40.0 | 3.19E+03 |
| 3.0 | 2.35E-01 | 42.0 | 5.15E+03 |
| 3.5 | 2.94E-01 | 44.0 | 8.31E+03 |
| 4.0 | 3.59E-01 | 46.0 | 1.34E+04 |
| 4.5 | 4.34E-01 | 48.0 | 2.16E+04 |
| 5.0 | 5.17E-01 | 50.0 | 3.49E+04 |
| 6.0 | 7.17E-01 | 52.0 | 5.63E+04 |
| 7.0 | 9.72E-01 | 54.0 | 9.08E+04 |
| 8.0 | 1.29E+00 | 56.0 | 1.46E+05 |
| 9.0 | 1.71E+00 | 58.0 | 2.36E+05 |
| 10.0 | 2.23E+00 | 60.0 | 3.81E+05 |
| 12.0 | 3.73E+00 | 62.0 | 6.15E+05 |
| 14.0 | 6.15E+00 | 64.0 | 9.91E+05 |
| 16.0 | 1.01E+01 | 66.0 | 1.60E+06 |
| 18.0 | 1.64E+01 | 68.0 | 2.58E+06 |
| 20.0 | 2.65E+01 | 70.0 | 4.16E+06 |
| 22.0 | 4.30E+01 | 72.0 | 6.71E+06 |
| 24.0 | 6.94E+01 | 74.0 | 1.08E+07 |
| 26.0 | 1.12E+02 | 76.0 | 1.75E+07 |
| 28.0 | 1.81E+02 | 78.0 | 2.82E+07 |
| 30.0 | 2.92E+02 | 80.0 | 4.55E+07 |

Assumes no Cs-137 or I-132 present at t=0

# APPENDIX C. SOFTWARE/APPLICATIONS OF POTENTIAL INTEREST

## Table of Contents

## C.1. Spectral file translation and conversion

- Cambio, SNL, https://hekili.ca.sandia.gov/cambio/

## C.2. Spectral file translation, conversion, spectral analysis / radionuclide identification

- PeakEasy, LANL, https://peakeasy.lanl.gov/

## C.3. Spectral analysis / radionuclide identification

- SNL_GammaMatch.xlsb, SNL EXCEL application

Note: SNL_GammaMatch.xlsb is also useful for plutonium, Am-241, U-233, and Cf-252 "age" determinations.

## C.4. Source modeling and quantitative spectral analysis

- LabSOCS (Laboratory Source-less Calibration Software) / ISOCS (In-Situ Object Calibration Software), CANBERRA Industries
- ANGLE Advanced Gamma Spectroscopy Efficiency Calibration / ISOTOPIC Gamma Spectrometry Waste Assay Measurement, AMETEK ORTEC
- GADRAS (Gamma Detector Response and Analysis Software), SNL
- GammaDesigner, LLNL
- Interspec, SNL, https://github.com/sandialabs/interspec
- GAMMANAL, LLNL
- SNL_GammaQuant.xlsb, SNL EXCEL application

## C.5. Relative efficiency

- FRAM (Fixed-Energy Response-Function Analysis with Multiple Efficiency), LANL
- MGA (Multi-Group Analysis), LLNL
- SNL_RelativeEff_Uiso.xlsb, SNL EXCEL application for uranium isotopic assessments
- SNL_RelativeEfficiency.xlsb, SNL EXCEL application for general relative efficiency assessments

## C.6. Environmental in-situ gamma spectroscopy

- ISOCS, CANBERRA Industries
- ANGLE, AMETEK ORTEC
- HPGe in situ soil.xlsx, NV Remote Sensing Laboratory (RSL) EXCEL application
- SNL_InSituSoil-GS.xlsb, SNL EXCEL application

## C.7. True coincidence correction

- Genie 2000, CANBERRA Industries
- GammaVision, AMETEK ORTEC
- TrueCoinc, http://kisfiz.phys.klte.hu/kisfiz/sudar/truecoinc.htm
- EFFTRAN, http://efftran.com/
- ETNA (Efficiency Transfer for radionuclide Activity)

## C.8. Curve fitting / efficiency curve generation

- SNL_PolynomialCurveFitting.xlsb, SNL EXCEL application
- SNL_EffAbsCal.xlsb, SNL EXCEL application

## C.9. Fission product activity calculator

- SNL_ FissionProduct_ActivityCalculator.xlsb, SNL EXCEL application

## C.10. General health physics applications including decay chain calculations

- NRC Rad Toolbox, Nuclear Regulatory Commission, https://www.ornl.gov/crpk/software
- Rad Pro Calculator, http://www.radprocalculator.com/

## C.11. Photon shielding / dose assessment program

- MicroShield, Grove Engineering

## C.12. Spectral pattern recognition / radionuclide identification

- SpectraTester.xlsb, SNL EXCEL application

## C.13. Solid angle calculator for complex detector/sample geometries

- SACALC, RSICC

## C.14. Predictive plotter for plutonium gamma spectroscopy region of interests

- SNL_GS-Pu-PredictivePlotter.xlsb, SNL EXCEL application

## C.15. Quality control / performance check evaluation and chart generation

- SNL_QC_Chart.xlsb, SNL EXCEL application

## C.16. SpecFIDLER surface contamination level calculator for plutonium isotopes and Am-241

- SNL_SpecFIDLER.xlsb, SNL EXCEL application

## C.17. Internet gamma emission databases

- Decay Radiation Search - NuDat Database (Includes gamma coincidence information), http://www.nndc.bnl.gov/nudat2/indx_dec.jsp
- Nucléide - Lara - Library for gamma and alpha emissions (Includes general gamma-gamma coincidence and decay scheme information), http://www.nucleide.org/Laraweb/
- The Lund/LBNL Nuclear Data Search, Version 2.0, February 1999, S.Y.F. Chu, L.P. Ekström and R.B. Firestone, http://nucleardata.nuclear.lu.se/toi/

# APPENDIX D. TRUE COINCIDENCE CORRECTION FACTORS FOR AN ON-CONTACT POINT SOURCE

True coincidence correction factors for an on-contact point source were calculated using CANBERRA Industries LabSOCS for a **standard coaxial (59.0-mm x 63.0-mm deep, relative efficiency 39%)** and an **extended range coaxial (62.2 mm x 58.0-mm deep, relative efficiency 47%)**. Values below 1 represent "summing out" and values above 1 represent "summing in."

| Parent Nuclide | Emitter Nuclide | Energy (keV) | Yield (gps/dps) | True Coin. Correct. Factor Standard coaxial | True Coin. Correct. Factor Extended range coaxial |
|---|---|---|---|---|---|
| Ag-108m | Ag-108m | 433.9 | 9.05E-01 | 0.59 | 0.54 |
| Ag-108m | Ag-108m | 722.9 | 9.08E-01 | 0.57 | 0.27 |
| Ag-110m | Ag-110m | 657.8 | 9.43E-01 | 0.58 | 0.53 |
| Ag-110m | Ag-110m | 884.7 | 7.27E-01 | 0.57 | 0.52 |
| Am-241 | Am-241 | 59.5 | 3.59E-01 | free | free |
| Am-243 | Np-239 | 228.2 | 1.08E-01 | 0.93 | 0.90 |
| Am-243 | Np-239 | 277.6 | 1.44E-01 | 0.91 | 0.86 |
| Ba-133 | Ba-133 | 81.0 | 3.41E-01 | 0.72 | 0.34 |
| Ba-133 | Ba-133 | 356.0 | 6.21E-01 | 0.93 | 0.47 |
| Ba-140 | Ba-140 | 162.7 | 6.22E-02 | 0.86 | 0.83 |
| Ba-140 | Ba-140 | 537.3 | 2.44E-01 | 1.00 | 0.94 |
| Cd-109 | Cd-109 | 88.0 | 3.59E-02 | free | free |
| Cd-115+ | In-115m | 336.2 | 4.58E-01 | 0.90 | 0.89 |
| Cd-115+ | Cd-115 | 527.9 | 2.75E-01 | 0.87 | 0.71 |
| Ce-139 | Ce-139 | 165.9 | 7.89E-01 | 1.00 | 0.75 |
| Ce-141 | Ce-141 | 145.4 | 4.83E-01 | free | free |
| Ce-143 | Ce-143 | 57.4 | 1.17E-01 | 0.85 | 0.81 |
| Ce-143 | Ce-143 | 293.3 | 4.28E-01 | 0.98 | 0.69 |
| Ce-144+ | Ce-144 | 80.1 | 1.36E-02 | free | free |
| Ce-144+ | Ce-144 | 133.5 | 1.11E-01 | free | free |
| Ce-144+ | Pr-144 | 696.5 | 1.34E-02 | 0.96 | 0.95 |
| Ce-144+ | Pr-144 | 2185.7 | 6.94E-03 | 1.04 | 1.05 |
| Co-56 | Co-56 | 846.8 | 9.99E-01 | 0.76 | 0.73 |
| Co-56 | Co-56 | 1238.3 | 6.69E-01 | 0.71 | 0.67 |
| Co-57 | Co-57 | 122.1 | 8.56E-01 | 1.00 | 0.97 |
| Co-57 | Co-57 | 136.5 | 1.07E-01 | 1.00 | 1.17 |
| Co-58 | Co-58 | 810.8 | 9.95E-01 | 1.00 | 1.00 |
| Co-60 | Co-60 | 1173.2 | 9.99E-01 | 0.80 | 0.78 |
| Co-60 | Co-60 | 1332.5 | 1.00E+00 | 0.79 | 0.77 |
| Cr-51 | Cr-51 | 320.1 | 9.92E-02 | free | free |
| Cs-134 | Cs-134 | 604.7 | 9.76E-01 | 0.73 | 0.70 |

| Parent Nuclide | Emitter Nuclide | Energy (keV) | Yield (gps/dps) | True Coin. Correct. Factor Standard coaxial | True Coin. Correct. Factor Extended range coaxial |
|---|---|---|---|---|---|
| Cs-134 | Cs-134 | 795.9 | 8.55E-01 | 0.73 | 0.69 |
| Cs-137 | Ba-137m | 661.7 | 8.47E-01 | free | free |
| Eu-152 | Eu-152 | 121.8 | 2.87E-01 | 0.76 | 0.48 |
| Eu-152 | Eu-152 | 1408.0 | 2.11E-01 | 0.87 | 0.42 |
| Eu-154 | Eu-154 | 123.1 | 4.06E-01 | 0.77 | 0.74 |
| Eu-154 | Eu-154 | 1274.4 | 3.50E-01 | 0.87 | 0.72 |
| Eu-155 | Eu-155 | 86.5 | 3.07E-01 | free | free |
| Eu-155 | Eu-155 | 105.3 | 2.12E-01 | 1.00 | 1.00 |
| Fe-59 | Fe-59 | 1099.3 | 5.65E-01 | 0.98 | Not calculated |
| Fe-59 | Fe-59 | 1291.6 | 4.32E-01 | 1.02 | Not calculated |
| Gd-153 | Gd-153 | 97.4 | 2.90E-01 | 0.99 | 0.70 |
| Gd-153 | Gd-153 | 103.2 | 2.11E-01 | 0.98 | 0.64 |
| Hg-203 | Hg-203 | 279.2 | 8.15E-01 | free | free |
| I-131 | I-131 | 364.5 | 8.17E-01 | 1.01 | 1.01 |
| I-131 | I-131 | 637.0 | 7.17E-02 | free | free |
| I-132 | I-132 | 667.7 | 9.87E-01 | 0.64 | 0.59 |
| I-132 | I-132 | 772.6 | 7.56E-01 | 0.63 | 0.58 |
| I-133 | I-133 | 529.9 | 8.70E-01 | 0.99 | 0.99 |
| I-133 | I-133 | 875.3 | 4.51E-02 | free | free |
| Kr-85 | Kr-85 | 514.0 | 4.34E-03 | 1.00 | 0.86 |
| La-140 | La-140 | 487.0 | 4.55E-01 | 0.70 | 0.66 |
| La-140 | La-140 | 1596.2 | 9.54E-01 | 0.73 | 0.69 |
| Mn-52 | Mn-52 | 935.5 | 9.45E-01 | 0.62 | 0.58 |
| Mn-52 | Mn-52 | 1434.1 | 1.00E+00 | 0.61 | 0.56 |
| Mo-99 | Mo-99 | 181.1 | 5.99E-02 | 0.65 | 0.64 |
| Mo-99 | Mo-99 | 739.5 | 1.21E-01 | 0.75 | 0.63 |
| Na-22 | Na-22 | 1274.5 | 9.99E-01 | 0.55 | 0.48 |
| Na-24 | Na-24 | 1368.6 | 1.00E+00 | 0.83 | 0.82 |
| Na-24 | Na-24 | 2754.0 | 9.99E-01 | 0.80 | 0.78 |
| Nb-95 | Nb-95 | 765.8 | 9.98E-01 | free | free |
| Nd-147 | Nd-147 | 91.1 | 2.79E-01 | 0.99 | 0.98 |
| Nd-147 | Nd-147 | 531.0 | 1.31E-01 | 1.01 | 1.01 |
| Nd-149 | Nd-149 | 114.3 | 1.92E-01 | 0.81 | 0.72 |
| Nd-149 | Nd-149 | 211.3 | 2.59E-01 | 0.95 | 0.92 |
| Np-237+ | Pa-233 | 300.3 | 6.62E-02 | 0.99 | 0.97 |
| Np-237+ | Pa-233 | 312.2 | 3.86E-01 | 0.99 | 0.98 |
| Pa-231 | Pa-231 | 300.1 | 2.47E-02 | 1.00 | 1.01 |
| Pa-231 | Pa-231 | 302.7 | 2.87E-02 | 1.00 | 0.93 |

| Parent Nuclide | Emitter Nuclide | Energy (keV) | Yield (gps/dps) | True Coin. Correct. Factor Standard coaxial | True Coin. Correct. Factor Extended range coaxial |
|---|---|---|---|---|---|
| Pb-210 | Pb-210 | 46.5 | 4.25E-02 | free | free |
| Pu-239 | Pu-239 | 129.3 | 6.31E-05 | free | free |
| Pu-239 | Pu-239 | 375.1 | 1.55E-05 | 1.00 | 1.00 |
| Pu-239 | Pu-239 | 413.7 | 1.47E-05 | 1.00 | 1.00 |
| Ra-226+ | Ra-226 | 186.2 | 3.59E-02 | free | free |
| Ra-226+ | Pb-214 | 295.2 | 1.93E-01 | 1.00 | 1.01 |
| Ra-226+ | Pb-214 | 351.9 | 3.77E-01 | free | free |
| Ra-226+ | Bi-214 | 609.3 | 4.61E-01 | 0.80 | 0.77 |
| Ra-226+ | Bi-214 | 1764.5 | 1.54E-01 | 1.01 | 1.01 |
| Ru-103 | Ru-103 | 497.1 | 9.10E-01 | free | free |
| Ru-103 | Ru-103 | 610.3 | 5.76E-02 | free | free |
| Ru-106 | Ru-106 | 511.9 | 2.04E-01 | 0.86 | 0.84 |
| Ru-106 | Ru-106 | 621.9 | 9.93E-02 | 0.75 | 0.71 |
| Sb-124 | Sb-124 | 602.7 | 9.83E-01 | 0.83 | 0.81 |
| Sb-124 | Sb-124 | 1691.0 | 4.78E-01 | 0.77 | 0.73 |
| Sb-125 | Sb-125 | 427.9 | 2.98E-01 | 1.00 | 0.71 |
| Sb-125 | Sb-125 | 600.6 | 1.78E-01 | 1.00 | 0.71 |
| Sn-113 | Sn-113 | 255.1 | 2.11E-02 | free | free |
| Sn-113 | Sn-113 | 391.7 | 6.49E-01 | free | free |
| Ta-182 | Ta-182 | 67.8 | 4.13E-01 | 0.72 | 0.67 |
| Ta-182 | Ta-182 | 1121.3 | 3.49E-01 | 0.76 | 0.50 |
| Tc-99m | Tc-99m | 140.5 | 8.91E-01 | free | free |
| Te-131m | Te-131m | 773.7 | 3.89E-01 | 0.67 | 0.57 |
| Te-131m | Te-131m | 852.2 | 2.14E-01 | 0.65 | 0.59 |
| Te-132 | Te-132 | 49.7 | 1.50E-01 | 0.75 | 0.68 |
| Te-132 | Te-132 | 228.2 | 8.80E-01 | 0.99 | 0.70 |
| Th-232+ | Pb-212 | 238.6 | 4.33E-01 | free | free |
| Th-232+ | Ra-224 | 241.0 | 4.10E-02 | free | free |
| Th-232+ | Tl-208 | 583.2 | 3.05E-01 | 0.75 | 0.71 |
| Th-232+ | Bi-212 | 727.3 | 7.20E-02 | 0.93 | 0.92 |
| Th-232+ | Tl-208 | 860.6 | 4.47E-02 | 0.92 | 0.92 |
| Th-232+ | Ac-228 | 911.2 | 2.58E-01 | 0.95 | 0.94 |
| Th-232+ | Ac-228 | 964.8 | 4.99E-02 | 0.91 | 0.89 |
| Th-232+ | Bi-212 | 1620.5 | 1.49E-02 | 1.03 | 1.03 |
| Tl-201 | Tl-201 | 71.1 | 4.64E-01 | 1.00 | 1.00 |
| Tl-201 | Tl-201 | 167.4 | 1.00E-01 | 0.89 | 0.72 |
| U-235+ | U-235 | 143.8 | 1.10E-01 | free | free |
| U-235+ | U-235 | 185.7 | 5.72E-01 | free | free |

| Parent Nuclide | Emitter Nuclide | Energy (keV) | Yield (gps/dps) | True Coin. Correct. Factor Standard coaxial | True Coin. Correct. Factor Extended range coaxial |
|---|---|---|---|---|---|
| U-238+ | U-235 | 92.6 | 5.58E-02 | 1.00 | 1.00 |
| Y-88 | Y-88 | 898.0 | 9.37E-01 | 0.82 | 0.64 |
| Y-88 | Y-88 | 1836.1 | 9.92E-01 | 0.79 | 0.65 |
| Zn-65 | Zn-65 | 1115.5 | 5.06E-01 | free | free |
| Zr-95 | Zr-95 | 724.2 | 4.43E-01 | free | free |
| Zr-95 | Zr-95 | 756.7 | 5.44E-01 | free | free |

# APPENDIX E. NF / NO, PRE-CALCULATED TABLES FOR DOWNWARD FACING HPGE DETECTOR AT 1-METER [28]

Downward facing detector at 1-meter, uniform radionuclide depth distribution

| | L/D | L/D | L/D | L/D | L/D | L/D | L/D | L/D | L/D |
|---|---|---|---|---|---|---|---|---|---|
| | 0.5 | 0.6 | 0.7 | 0.8 | 0.9 | 1 | 1.1 | 1.2 | 1.3 |
| Energy (keV) | $N_f$ / $N_o$ | $N_f$ / $N_o$ | $N_f$ / $N_o$ | $N_f$ / $N_o$ | $N_f$ / $N_o$ | $N_f$ / $N_o$ | $N_f$ / $N_o$ | $N_f$ / $N_o$ | $N_f$ / $N_o$ |
| 300 | 0.80 | 0.80 | 0.81 | 0.83 | 0.88 | 0.97 | 1.07 | 1.19 | 1.35 |
| 500 | 0.82 | 0.82 | 0.83 | 0.85 | 0.90 | 0.97 | 1.06 | 1.16 | 1.29 |
| 700 | 0.83 | 0.84 | 0.85 | 0.87 | 0.91 | 0.97 | 1.05 | 1.14 | 1.25 |
| 1000 | 0.85 | 0.85 | 0.86 | 0.88 | 0.92 | 0.97 | 1.04 | 1.12 | 1.22 |
| 1500 | 0.86 | 0.87 | 0.88 | 0.90 | 0.93 | 0.97 | 1.03 | 1.10 | 1.17 |
| 2000 | 0.88 | 0.89 | 0.90 | 0.91 | 0.93 | 0.97 | 1.02 | 1.08 | 1.14 |
| 2500 | 0.89 | 0.90 | 0.91 | 0.92 | 0.94 | 0.97 | 1.01 | 1.07 | 1.12 |

Downward facing detector at 1-meter, surface radionuclide source distribution

| | L/D | L/D | L/D | L/D | L/D | L/D | L/D | L/D | L/D |
|---|---|---|---|---|---|---|---|---|---|
| | 0.5 | 0.6 | 0.7 | 0.8 | 0.9 | 1 | 1.1 | 1.2 | 1.3 |
| Energy (keV) | Nf / No | Nf / No | Nf / No | Nf / No | Nf / No | Nf / No | Nf / No | Nf / No | Nf / No |
| 300 | 0.81 | 0.82 | 0.83 | 0.86 | 0.91 | 0.99 | 1.08 | 1.18 | 1.31 |
| 500 | 0.84 | 0.85 | 0.85 | 0.88 | 0.93 | 0.99 | 1.06 | 1.14 | 1.25 |
| 700 | 0.86 | 0.86 | 0.87 | 0.90 | 0.93 | 0.98 | 1.05 | 1.12 | 1.21 |
| 1000 | 0.88 | 0.88 | 0.89 | 0.91 | 0.94 | 0.98 | 1.03 | 1.10 | 1.18 |
| 1500 | 0.91 | 0.91 | 0.91 | 0.92 | 0.94 | 0.97 | 1.02 | 1.07 | 1.13 |
| 2000 | 0.92 | 0.92 | 0.93 | 0.93 | 0.94 | 0.96 | 1.00 | 1.05 | 1.10 |
| 2500 | 0.94 | 0.94 | 0.94 | 0.94 | 0.95 | 0.96 | 0.99 | 1.03 | 1.07 |

# APPENDIX F. DECAY DURING THE COUNT CORRECTION FACTORS

| Count Time / Half-Life | Correction Factor |
|---|---|
| 0.025 | 1.009 |
| 0.050 | 1.017 |
| 0.075 | 1.026 |
| 0.100 | 1.035 |
| 0.150 | 1.053 |
| 0.200 | 1.071 |
| 0.250 | 1.089 |
| 0.300 | 1.108 |
| 0.350 | 1.126 |
| 0.400 | 1.145 |
| 0.450 | 1.164 |
| 0.500 | 1.183 |
| 0.600 | 1.222 |
| 0.700 | 1.262 |
| 0.800 | 1.303 |
| 0.900 | 1.344 |
| 1.000 | 1.386 |
| 1.100 | 1.429 |
| 1.200 | 1.473 |
| 1.300 | 1.517 |
| 1.400 | 1.562 |
| 1.500 | 1.608 |
| 1.600 | 1.655 |
| 1.700 | 1.702 |
| 1.800 | 1.750 |
| 1.900 | 1.799 |
| 2.000 | 1.848 |
| 2.100 | 1.898 |
| 2.200 | 1.949 |
| 2.300 | 2.000 |
| 2.400 | 2.052 |
| 2.500 | 2.105 |

| Count Time / Half-Life | Correction Factor |
|---|---|
| 2.6 | 2.158 |
| 2.7 | 2.212 |
| 2.8 | 2.266 |
| 2.9 | 2.321 |
| 3.0 | 2.377 |
| 3.5 | 2.661 |
| 4.0 | 2.957 |
| 4.5 | 3.263 |
| 5.0 | 3.578 |
| 6.0 | 4.225 |
| 7.0 | 4.890 |
| 8.0 | 5.567 |
| 9.0 | 6.251 |
| 10.0 | 6.938 |
| 12.0 | 8.320 |
| 14.0 | 9.705 |
| 16.0 | 11.091 |
| 18.0 | 12.477 |
| 20.0 | 13.863 |
| 22.0 | 15.249 |
| 24.0 | 16.636 |
| 26.0 | 18.022 |
| 28.0 | 19.408 |
| 30.0 | 20.794 |
| 35.0 | 24.260 |
| 40.0 | 27.726 |
| 50.0 | 34.657 |
| 60.0 | 41.589 |
| 70.0 | 48.520 |
| 80.0 | 55.452 |
| 90.0 | 62.383 |
| 100.0 | 69.315 |

# APPENDIX G. EXAMPLE HPGE SPECTRAL PEAK IDENTIFICATION PROCESS

1. Perform a high-quality energy calibration to narrow down the energy match tolerance for peak ID.
2. Perform an automated peak search/nuclide ID using an appropriate software/application.
3. Use the automated peak search/nuclide ID results as a starting point and ID peaks you know then IDs peaks from large area peaks to small area peaks and/or from high energy peaks to low energy peaks.
4. Determine whether the radionuclide is plausible considering **peak centroid, detector efficiency, shielding, continuum, yield, and half-life**.
   - Centroid: If a high-quality energy calibration is performed, the energy match tolerance for peak ID can be small (< 0.5 keV and likely within 0.3 keV).
   - Detector efficiency: Consider the shape of the detector efficiency curve for an unattenuated source when performing radionuclide ID. For example, the detector efficiency of a p-type HPGe at 100 keV is greater than the detector efficiency at 1000 keV.
   - Shielding: In general, check for presence of x-ray and low energy gamma emissions. For a single radionuclide with multiple gamma emissions, if high yield, high energy gamma emissions are detected but high yield, low energy gamma emissions are not detected then the item is shielded. Remember the presence of x-ray emissions may provide information on the type of shielding (material) present.
   - Continuum: When scattering occurs, elevated continuum may limit the ability to detect low and middle energy gamma emissions. For example, high yield, low energy gamma emissions may not be detected when significant continuum is present.
   - Self-attenuation: Consider that radioactive dense materials are very good at self-attenuating their own gamma emissions. Therefore, high yield, low energy gamma emissions may be significantly reduced or not detected from dense materials.
   - Half-life: Check whether the radionuclide is plausible based on the half-life and/or whether its presence is possibly due to equilibrium with a longer-lived parent radionuclide (e.g., Te-132/I-132).
   - Yield: If peak area counts/yield for gamma emissions with similar energies are vastly different then the gamma emissions are not from a single radionuclide.
5. If **high dead time**, check for random/chance coincidence sum, Compton edge, and backscatter peaks, peak shifts, distortion/broadening, and high-side tailing.
6. If the **sample to detector distance is small** (generally within a few diameters of the detector), check for true/cascade coincidence summing. Common radionuclides susceptible to true/cascade coincidence are Co-60, Y-88, Eu-152, Eu-154, Sb-125, Cs-134, and Ba-133.
7. Check for **guilt by association**.
   - Uranium detected: Check for additional uranium isotopes. Example: If U-235 is detected, check for U-238 (1001.0 keV) and/or U-234 (120.9 keV).

- Plutonium detected: Check for additional plutonium isotopes, Am-241, and Np-237/Pa-233.
- Long-lived activation product(s) detected: Check for Co-60, Mn-54, Zn-65, and Ag-110m. Also, see Table 8-3.
- Short-lived activation product(s) detected: Check for Na-24, Cr-51, Co-58, Fe-59, and Np-239. Also, see Table 8-3.
- Short-lived fission product(s) detected: Check for Zr-95/Nb-95, Zr-97/Nb-97, Mo-99/Tc-99m, Ru-103/Rh-103, Ru-106/Rh-106, Sb-125/Te-125m, Te-127m, Te-129m, I-131/Xe-131, Te-132/I-132, I-133, Cs-134, Cs-137, Ba-140/La-140, Ce-141, Ce-143/Pr-143, Ce-144/Pr-144, Nd-147/Pm-147, Pm-151/Sm-151, Eu-154, and Eu-155. Also, see Table 8-1.
- Short-lived radionuclide detected in the presence of other long-lived radionuclides: Check for short-lived radionuclide's long-lived parent (Te-132/I-132).
- Gaseous or volatile fission product(s) detected: Check for krypton, xenon, and iodine isotopes such as Kr-85, Xe-133, I-131, and I-132. Also, see Table 8-2.
- Common radionuclide pairs: Check for Zr-95/Nb-95, Mo-99/Tc-99m, I-131/Xe-131m, Ba-140/La-140, Ce-144/Pr-144, and Nd-147/Pm-147.
- Neutron emitters/sources: Check for peaks from (n,γ) and (n,n'γ) neutron reactions on common metals (such as iron, aluminum, and cadmium) and non-metals (such as hydrogen, nitrogen, and chlorine). In addition, check for a Doppler broadened "square" peak at 477.6 keV from B-10(n,α)Li-7.
  - Am-241:Be (432.2 y): Check for a Doppler broadened peak at 4438.9 keV from Be-9(α,n)C-12. Check for Mn-56 (2.6 h) from neutron activation of minor/trace amounts of Mn in alloys.
  - Am-241:Li (432.2 y): Check for a Doppler broadened "triangular" peak at 477.6 keV from Li-7(α,α')Li-7. Check for Eu-154 (8.6 y) + Eu-152 (13.5 y) from neutron activation of minor/trace amounts of Eu in alloys.
  - Cf-252 (2.6 y): Check for Cf-249 (351.0 y) + Cf-251 (900.0 y) + Spontaneous fission products (For common Cf-252 fission products, see Reference *[53]*)
  - Cm-244 (18.1 y): Check for Cm-243 (29.1 y) + Cm-245 (8.5 ky) + Spontaneous fission products (For common Cm-244 fission products, see Reference *[53]*)
- Possible impurities:
  - Am-241 (432.2 y) + Am-243 (7.4 ky) / Np-239 (2.4 d)
  - Co-56 (77.2 d) + Co-57 (217.7 d) + Co-58 (70.9 d) + Mn-52 (5.6 d) + Mn-54 (312.0 d) + V-48 (16.0 d) + Re-183 (70.0 d) + Re-184 (38.0 d)
  - Co-57 (217.7 d) + Co-56 (77.2 d) + Co-58 (70.9 d)
  - Co-58 (70.9 d) + Co-57 (217.7 d) + Co-60 (5.3 y)
  - Cs-131 (9.7 d) + Cs-132 (6.5 d) + Cs-136 (13.2 d) + Zn-65 (244.1 d)
  - Eu-154 (8.6 y) + Eu-152 (13.5 y) + Eu-155 (4.8 y)
  - Ho-166m (1.2 ky) + Eu-154 (8.6 y)
  - I-123 (13.2 h) + Te-121 (19.2 d) + I-124 (4.2 d) + I-125 (59.4 d) + I-121? (2.1 h)

- I-125 (59.4 d) + I-126 (12.9 d)
- In-111 (2.8 d) + In-114m (49.5 d)
- Ir-192 (73.8 d) + Ir-194m2 (171.0 d)
- Lu-177 (6.6 d) + Lu-177m (160.4 d)
- Rb-86 (18.6 d) + Cs-134 (2.1 y)
- Sm-153 (46.3 h) + Eu-152 (13.5 y) + Eu-154 (8.6 y) + Eu-156 (15.2 d)
- Sn-113 (115.1 d) + Sn-117m (13.8 d)
- Sr-82 (25.0 d) / Rb-82 (1.3 m) + Sr-85 (64.9 d)
- Tl-201 (72.9 h) + Tl-202 (12.2 d) + Tl-200 (26.1 h)
- Xe-133 (5.2 d) + Xe-133m (2.2 d) + Xe-131m (11.8 d)
- Y-90 (64.0 h) + Y-88 (106.7 d) + Eu-152 (13.5 y) + Eu-154 (8.6 y) + Co-57 (217.7 d) + Co-60 (5.3 y)
- Zr-95 (64.0 d) + Nb-95 (35.0 d) + Hf-181 (42.4 d)

8. For spectrums with **high energy gamma rays** (> 1022 keV), check for **single and double escape peaks**.
   - Single escape and double escape peaks associated with true/cascade summing of gamma rays > 1022 keV may be seen in the spectrum (e.g., Na-24 single escape peak at 3611 keV = 1368 + 2754 - 511 keV).
   - Single escape and double escape peaks may be seen in the spectrum without the full-energy peak spectrum energy range does not extend high enough (e.g., For a spectrum with a 3500 keV energy range, the Be-9(α,n) double escape peak at 3416.9 keV may be seen without the full-energy peak at 4438.9 keV).
   - Single and double escape peaks are wider than a gamma ray of the same energy due to the Doppler broadening that can occur during the annihilation process.
   - Single and double escape peaks may exhibit a high-energy step due to annihilation photons that deposit a portion of their energy as they escape from the detector.
9. Consider energy **line widths of x-rays are larger than gamma rays** of the same energy and can have long tails due to Lorentzian broadening.
10. Check for **characteristic x-ray peaks from induced x-ray fluorescence**, which are characteristic of the element that was ionized, considering the **materials potentially present**.
11. Check for **characteristic x-ray peaks from internal conversion** which are characteristic of the decay product element.
12. Check for **germanium (Ge) and characteristic x-ray escape peaks if low energy gamma rays (generally < 80 keV) are present** and the detector has a large surface-to-volume ratio.
13. Check the peak shape and width to determine **if the peak is possibly broadened** and due to (n,n'), (α,α'), (n,α), or (α,n) reactions or something else.